1-1-2019

Synthesis, Characterization, and Reactivity of Chelating Ligand Complexes of Group 13-15 Elements

Ala'aeddeen Swidan
University of Windsor

Synthesis, Characterization, and Reactivity of Chelating Ligand Complexes of Group 13-15 Elements

By

Ala'aeddeen Swidan

A Dissertation
Submitted to the Faculty of Graduate Studies
through the Department of Chemistry and Biochemistry
in Partial Fulfillment of the Requirements for
the Degree of Doctor of Philosophy
at the University of Windsor

Windsor, Ontario, Canada

2019

Synthesis, Characterization, and Reactivity of Chelating Ligand Complexes of Group 13-15 Elements

by

Ala'aeddeen Swidan

APPROVED BY:

_____
D. Richeson, External Examiner
University of Ottawa

_____
J. Gagnon
Earth and Environmental Sciences

_____
J.R. Green
Department of Chemistry and Biochemistry

_____
S. Johnson
Department of Chemistry and Biochemistry

_____
C. Macdonald, Advisor
Department of Chemistry and Biochemistry

June 17, 2019

DECLARATION OF CO-AUTHORSHIP AND PREVIOUS PUBLICATION

Co-Authorship

I hereby declare that this dissertation incorporates material that is a result of joint research, as follows:

Chapter 2 of the dissertation contains results published in the original research communication "2,6-Bis(benzimidazol-2-yl)pyridines as more electron-rich and sterically accessible alternatives to 2,6-bis(imino)pyridine for group 13 coordination chemistry" (Swidan, A.; Binder, J. F.; St. Onge, P. B.; Suter, R.; Burford, N.; Macdonald, C. *Dalton Trans.* **2019**, 1284–1291). Mr. St. Onge contributed to the synthesis and characterization of some of the reported compounds, Mr. Binder contributed to the computational studies, Dr. Macdonald and Dr. Suter helped in the writing and editing of the manuscript.

Chapter 3 of the dissertation contains results published in the original research article "2,6-Bis(benzimidazol-2-yl)pyridine Complexes of Group 14 Elements" (Swidan, A.; St. Onge, P. B.; Binder, J. F.; Suter, R.; Burford, N.; Macdonald, C. *Dalton Trans.* **2019**, *48*, 7835-7843). Mr. St. Onge contributed to the synthesis and characterization of some the reported compounds, Mr. Binder contributed to the computational studies, Dr. Macdonald helped in the writing, editing and provided ideas to investigate and include in the manuscript.

Chapter 5 of the dissertation contains results published in the original research article "Tris(benzoimidazol)amine (L) complexes of pnictogen(III) and pnictogen(V) cations and assessment of the $[LP]^{3+}/[LPF_2]^{3+}$ redox couple" (Swidan, A.; Suter, R.; Macdonald, C. L. B.; Burford, N. **2018**, 5837–5841). Dr. Suter contributed to the synthesis and characterization of some of the reported compounds as well as in the computational studies, writing, and editing of the manuscript. Dr. Macdonald contributed to the computational studies, writing, and editing of the manuscript.

I am aware of the University of Windsor Senate Policy on Authorship and I certify that I have properly acknowledged the contribution of other researchers to my dissertation and have obtained written permission from each of the co-author(s) to include the above material(s) in my dissertation. I certify that, with the above qualification, this dissertation, and the research to which it refers, is the product of my own work.

Previous Publication

This dissertation includes 3 original papers that have been previously published/submitted for publication in peer-reviewed journals, as follows:

Dissertation Chapter	Publication title/full citation	Publication status
Chapter 2	"2,6-Bis(benzimidazol-2-yl)pyridines as more electron-rich and sterically accessible alternatives to 2,6-bis(imino)pyridine for group 13 coordination chemistry" Swidan, A.; Binder, J. F.; St. Onge, P. B.; Suter, R.; Burford, N.; Macdonald, C. *Dalton Trans.* **2019**, 1284–1291.	Published
Chapter 3	"2,6-Bis(benzimidazol-2-yl)pyridine Complexes of Group 14 Elements" Swidan, A.; St. Onge, P. B.; Binder, J. F.; Suter, R.; Burford, N.; Macdonald, C. *Dalton Trans.* **2019**, *48*, 7835-7843.	Published
Chapter 5	"Tris(benzoimidazol)amine (L) complexes of pnictogen(III) and pnictogen(V) cations and assessment of the [LP]3+/[LPF2]3+ redox couple" Swidan, A.; Suter, R.; Macdonald, C. L. B.; Burford, N. **2018**, 5837–5841.	Published

I certify that I have obtained written permission from the copyright owner(s) to include the above published material(s) in my dissertation. I certify that the above material describes work completed during my registration as a graduate student at the University of Windsor.

General

I declare that, to the best of my knowledge, my dissertation does not infringe upon anyone's copyright nor violate any proprietary rights and that any ideas, techniques, quotations, or any other material from the work of other people included

in my dissertation, published or otherwise, are fully acknowledged in accordance with the standard referencing practices. Furthermore, to the extent that I have included copyrighted material that surpasses the bounds of fair dealing within the meaning of the Canada Copyright Act, I certify that I have obtained written permission from the copyright owner(s) to include such material(s) in my dissertation.

I declare that this is a true copy of my dissertation, including any final revisions, as approved by my dissertation committee and the Graduate Studies office and that this dissertation has not been submitted for a higher degree to any other University or Institution.

ABSTRACT

2,6-bis(benzimidazol-2-yl)pyridine derivative (G-BZIMPY, G = NBn, N(3,5-CF3)Bn, N-allyl and O) have been used as pincer ligands to coordinate and isolate various group 13-15 complexes. For Group 13, treatment of G-BZIMPY with two equivalents of $GaCl_3$ results in the self-ionization products [G-BZIMPYGaCl$_2$][GaCl$_4$]. This Ga(III) complex can be reduced to a Ga(I) centre using K$_2$[Fe(CO)$_4$] as a reducing agent to result in the Ga(I) complex [(NBn-BZIMPY)(Cl)Ga–Fe(CO)$_4$] (Chapter 2).

Group 14 complexes of G-BZIMPY have been synthesized in a similar fashion through the self-ionization reactions of G-BZIMPY with two equivalents of MCl$_2$ (M = Ge, Sn) to yield [G-BZIMPYMCl][MCl$_3$]. Attempts to reduce these complexes into the M(0) centre were not successful. Other reactivities and UV-vis studies are detailed in this dissertation (Chapter 3). Comparison of group 13 and 14 complexes of G-BZIMPY to complexes of the structurally similar bis(imino)pyridine (DIMPY) are studied and reveal G-BZIMPY as a stronger donor than DIMPY for group 13 coordination. For group 15 elements, treatment of PnCl$_3$ (Pn = P, As, Sb) with G-BZIMPY does not yield any reactivity, however, the addition of TMS-OTf (Trimethylsilyl trifluoromethanesulfonate) results in the isolation of [G-BZIMPYPnCl][OTf]$_2$ (Chapter 4).

In-addition, a tetradentate ligand tris((1-ethyl-benzoimidazol-2-yl)methyl)amine (BIMEt$_3$) has been investigated. A series of cationic complexes involving a pnictogen(III) (Pn = P, As, Sb) centre coordinated to BIMEt$_3$ have been synthesized and comprehensively characterized. Oxidation of [P(BIMEt$_3$)]$^{3+}$ with

XeF$_2$ provides access to [PF$_2$(BIMEt$_3$)]$^{3+}$ representing the first structurally characterized example of a phosphorus(V) centred trication (Chapter 5).

Attempts to synthesize an anionic carbon(0) are detailed in chapter 6. Although obtaining an anionic carbon(0) was not successful, it lead to a series of interesting compounds and results. Compounds containing carbon centre behave differently than their heavier group-14 analogues of the same bidentate anionic bisphosphine ligand.

DEDICATION

To Family and Science!

ACKNOWLEDGEMENTS

My academic journey would not have been possible if it wasn't for the support of my community. My community has provided me with the necessary environment and tools to be successful and for that, I am eternally gratefully and will always be indebted to this loving and caring community.

My supervisor, Dr. Charles L. B. Macdonald, has been very supportive throughout the years and I am very thankful to have him as my mentor and for giving me the opportunity to join his research group. Despite his busy schedule, Chuck is always available, even after moving to Carleton, Chuck is available to answer questions and would free-up time to be there for the group. Working with Chuck allowed me opportunities that helped me improve by building on my experiences and skills. Different collaborations and taking part in developing a course are among the many opportunities that were made available to me by Chuck, and for that, I am very thankful.

The Macdonald group members have made this journey an enjoyable one and for that, I would like to thank all the past and present group members. Special thanks to Blake whom I mentored in his 410 project and by having him on-board, he helped make significant advances. Although I was mentoring and training Blake, I myself have learned a lot from Blake. I would like to thank Justin for the continued collaborations we had over the years and for all the good times spent together in and out of the lab. When it comes to chemistry discussions between Justin and myself, if there is one thing we agree on, it is to disagree! I would also like to thank Brad for the

numerous conversations and hangouts we had. Lastly, I would like to thank Steph, Max and Loue for making the lab a fun place to be in and for the amazing memories that I will cherish forever.

I would like to thank our collaborators, Dr. Neil Burford and Dr. Riccardo Suter for the amazing collaborations we had over the last two years. Meeting Dr. Suter at the Toronto CSC conference in 2017, little did I know the extent this collaboration will have, and I am very pleased in the turnout of this fruitful collaboration between the two groups.

In the chemistry department, I would like to thank Dr. Matthew Revington for his help and training in the NMR instruments. Dr. Janeen Auld for her help in the set-up of elemental analysis instruments, making it always available and ready to go. A special thanks to Marlene Bezaire, our graduate secretary, for keeping me on track to graduate and for all the love and support she shows to graduate students. She is very caring and wants all students to be successful, she tries her best to make this happen. In addition, I would like to thank our undergraduate laboratory coordinators, Una Lee and Nedhal Al-Nidawy, for the opportunity to teach and mentor undergraduate students over the years.

I would like to thank my committee members, not only for agreeing to be on my committee but also for providing guidance and assistance throughout my degree. Dr. Green is always my go to when I have any questions or problems with synthesis or any organic related problems. Whenever I have any questions regarding transition metals or coordination chemistry, Dr. Johnson is always there to help, guide and

clarify. Working with Dr. Johnson on the inorganic chemistry tutorials is something I really enjoyed, and I looked forward to GAing the course year after year. I would like to thank Dr. Maeva for agreeing to be my outside-of-department reader at the beginning of my PhD. I would like to thank Dr. Joel Gagnon for agreeing to fill-in for Dr. Maeva and really appreciate his time and willingness to be on my committee. I would like to thank Dr. Richeson for agreeing to be my external examiner and really appreciate his time and the trouble of travel. Dr. Richeson's research has been of great interest to me and some of the research results in this dissertation were a direct inspiration of work reported by Dr. Richeson. Additionally, I would like to thank Dr. Peter T. Wolczanski for being a great mentor during time at Cornell University as a graduate student. Pete is very supportive, and I have learned a lot in the short span of time I spent with Pete.

Last but not least, I would like to thank my wife who has been supportive and understanding. Having to leave in the middle of the night to mount the next crystal when it's our turn on the diffractometer is something I had to do frequently, and my wife has been very supportive throughout my PhD journey and I would like to thank her for that.

TABLE OF CONTENTS

LIST OF TABLES

LIST OF FIGURES

LIST OF SCHEMES

LIST OF ABBREVIATIONS, SYMBOLS, AND UNITS

Å	ångström
ADPnO	5-aza-2,8-dioxa-3,7-di-tert-butyl-1-[Pn]bicyclo[3.3.0]octa 3,6-diene *Pn = Pnictogen
AIM	Atoms in Molecules
Anal.	Analytical
Ar	aryl
^{11}B	boron-11
BDE	bond dissociation energy
Bn	benzyl
Bn	Benzyl (CH_2-C_6H_5)
b	broad
^nBu	*n*-butyl
^tBu	*tert*-butyl
BZIMPY	2,6-Bis(benzimidazol-2-yl)pyridine
^{13}C	carbon-13
C_6D_6	deuterated benzene
°C	degree(s) Celsius
cal	calorie(s)
calc.	calculated
CDC	carbodicarbene
CDP	carbodiphosphorane
CHN	carbon hydrogen nitrogen
cm^{-1}	wavenumber(s)
cryst	crystal
COD	1,5-cyclooctadiene
CSD	Cambridge Structural Database
d	doublet
DCM	dichloromethane

deg (or °)	degree(s)
DFT	density functional theory
DIMPY	bis(imino)pyridine
dppe	bis(diphenylphosphino)ethane
Et	ethyl
Et_2O	diethyl ether
eV	electronvolt
^{19}F	fluorine-19
F	structure factors (X-ray crystallography)
fac-	facial
FT	Fourier transform
g	gram(s)
^{1}H	hydrogen-1
$\{^{1}H\}$	hydrogen-1 decoupled
HOMO	highest occupied molecular orbital
HR-ESI-MS	high-resolution electrospray ionization mass spectrometry
Hz	hertz
IR	infrared
J	joule(s)
$^{n}J_{AB}$	n-bond scalar coupling constant between nuclei A and B
K	kelvin
kcal	kilocalorie(s)
kJ	kilojoule(s)
L	liter
LCD	Liquid-Crystal Display
LED	Light-Emitting Diode
LUMO	lowest unoccupied molecular orbital
m	multiplet
Me	methyl
MeCN	acetonitrile
mer-	meridional

Mes	mesityl, 2,4,6-trimethylphenyl
MG	main group
mg	milligram
MHz	megahertz
mL	milliliter
mmol	millimole
MO	molecular orbital
mol	mole
Mp	melting point
mV	millivolt
MW	molecular weight
m/z	mass/charge
NacNac	1,3-Diketimines derivatives
NBO	natural bond orbital
NHC	*N*-heterocyclic carbene
NMR	nuclear magnetic resonance
NRT	natural resonance theory
OAc	acetoxy
ORTEP	Oakridge Thermal Ellipsoid Plotting Program
[OTf]$^-$	triflate, trifluoromethanesulfonate, $[CF_3SO_3]^-$
p	pentet
^{31}P	phosphorus-31
Ph	phenyl
Pn	pnictogen
ppm	parts per million
^iPr	isopropyl
PYBOX	bis(oxazoline)pyridine
q	quartet
R	hydrocarbyl
R	reliability factor (X-ray crystallography)
R^2	coefficient of determination for a linear regression

Reflns	reflections (X-ray crystallography)
s	singlet
SCXRD	single crystal X-ray diffraction
SIMes	1,3-bis(2,4,6-trimethylphenyl)-4,5-dihydroimidazol-2-ylidene
SNHC	*S,N*-heterocyclic carbene
t	triplet
TD-DFT	time-dependant density functional theory
tmeda	tetramethylethylenediamine
TMS	trimethylsilyl
UV-Vis	ultraviolet-visible
THF	tetrahydrofuran
V	volt
vt	virtual triplet
$[X]^-$	halide anion
Z	asymmetric units per unit cell (X-ray crystallography) or trans (opposite side)
α	atom in the alpha position or angle label (X-ray crystallography)
β	atom in the beta position or angle label (X-ray crystallography)
γ	angle label (X-ray crystallography)
ε	molar absorptivity
δ	chemical shift in ppm
θ	degrees (X-ray crystallography)
ν	vibrational frequency
η^n	n-hapto
μA	microampere
λ	wavelength
μ	bridging or absorption coefficient (X-ray crystallography)
π	pi-bonding
ρ	density
σ	estimated standard deviation (X-ray crystallography) or sigmabonding

%   percent

CHAPTER 1:
Introduction

1.1 General Introduction

The renaissance of Main Group Chemistry was born in the mid-1980s with the October issue of *Chemical Reviews* in 1985 entitled "Main Group Chemistry".[1] Main group chemistry is made up of both s- and p- block elements. s- and p- block elements make up more than 90% of the elemental composition of the Earth's crust.[2] Additionally, elements like carbon, hydrogen, nitrogen, oxygen, phosphorus, and sulfur are the most common elements found in biological organisms.[3] The periodic table is organized in different groups (columns) labeled 1-18 (using Arabic numerals) or IA-VIIIA (using Roman numerals). Our group is mainly interested in p-block elements, more specifically, groups 13-15 elements in lower than usual oxidation states.

Group 13 elements, also known as the boron group or triels, contain boron (B), aluminium (Al), gallium (Ga), indium (In) and thallium (Tl) with more attention given to boron through indium due to the high toxicity of thallium. Triels contain three valence electrons and have many industrial applications. For example, boron is commonly used in fiberglass, ceramics, and bleach. Aluminium is used in various electrical devices, construction materials and is widely used for food storage for its inertness towards food products.[4] Gallium arsenides are used in semiconductors, solar cells and make up a major component of LEDs (Light Emitting Diodes).[5] Indium

is usually used as an alloy with other metals for various applications, mainly conductive coating for displays like LCDs (liquid crystal displays).[6]
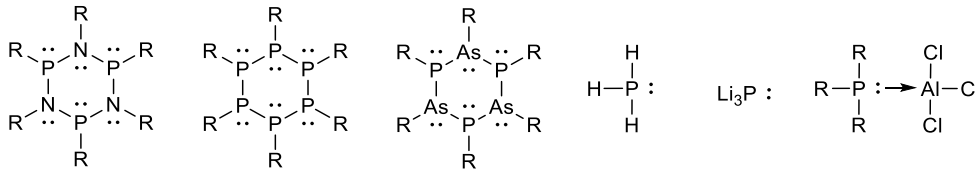
Group 14 elements, also known as the carbon group or tetrels, contain carbon (C), silicon (Si), germanium (Ge), tin (Sn) and lead (Pb). Tetrels contain four valence electrons with +4 as the most common oxidation state found (for C, Si, and Ge). Carbon exists in various allotropes that include amorphous carbon, graphite, diamond, fullerenes, buckyballs, nanotubes, nanobuds and nanofibers.[7] Carbon is of particular interest in organic chemistry because it's the backbone for organic compounds and living organisms in general. Carbon is smaller than its group 14 analogs and can have a more effective overlap of p-orbitals making it possible for carbon to obtain double and triple bonds. Uses of carbon vary depending on the form used, for example, crude oil containing hydrocarbon chains and charcoal are used as fuel sources, while diamond is considered very precious and expensive. Silicon is the second most abundant element in earth's crust with various applications that range from use in toothpaste to being a major component of glass.[8] Germanium oxide is mainly used in fiber optics (microscopes, camera lenses, etc.) due to its high index of refraction and low optical dispersion.[9] Tin's most common use is in soldering where solder is used to create a permanent bond between metal pieces like copper pipes or binding a wire to a circuit board.[8] When it comes to lead, most of the lead produced is used in the creation of lead-acid batteries. Just like thallium, lead is toxic and the use of lead decreased over time due to concerns of its toxicity.

Group 15 elements, also known as the nitrogen family or pnictogens, contain nitrogen (N), phosphorus (P), arsenic (As), antimony (Sb) and bismuth (Bi). Pnictogens contain 5 valence electrons and exist mainly in +3 and +5 oxidation states. In their elemental forms, the physical and chemical properties of these pnictogens vary considerably. Nitrogen is found as a non-metal diatomic gas, phosphorus exists as different allotropes and is a non-metal solid in most of these allotropes, arsenic and antimony are metalloids and bismuth is considered a metal. Nitrogen (N_2) makes up most of the atmosphere on Earth and can be isolated by fractional distillation of air. With a boiling point of –196 °C, nitrogen is commonly used as a cryogenic liquid.[10] Both nitrogen and phosphate are used in fertilizers and elemental phosphorus is used in the making of matches.[10] Arsenic is highly toxic, as a result, one of its uses is as an insecticide. Another use is in the form of an alloy with gallium in the making of LEDs as mentioned above.

1.2 Oxidation States

Oxidation state is an integer number assigned to an atom which provides a charge indicating the degree of oxidation. The degree of oxidation refers to the number of electrons that have been removed from a neutral atom. French chemist, Antoine Lavoisier was the first to use the term oxidation in reference to a reaction of a substance with oxygen. The definition has been extended to include all reactions in which electrons are lost.[11]

An oxidation state is used to assign electrons to individual atoms within a molecule and thus can give an insight into the electron rich, poor and neutral sites within a molecule. There are numerous ways of assigning oxidation states, but most commonly, oxidation state is determined by disregarding the concept of shared electrons (in covalent bonds) and assigning those electrons merely on the basis of electronegativity where the more electronegative atom is assigned the electrons in a chemical bond.[12] Another term used, valence state, is based on the number of electrons involved in bonding while taking charges into consideration. Both terms are sometimes used interchangeably to describe the same thing which can be confusing in many cases.

Oxidation State	+3	+1	−1	−3	−3	±3
Valence State	3	3	3	3	3	5

Figure 1.1. *Oxidation states of phosphorus in different molecules showing how oxidation state is not always consistent with valence state.*

By examining the different phosphorus compounds shown in **Figure 1.1**, one can see how oxidation state is not always in agreement with valence state. Oxidation state itself is not always consistent and/or representative of the reactivity of a compound. Comparing the first three compounds that contain pnictogens in a cyclohexyl arrangement, one can observe that the phosphorus centres are assigned

very different oxidation states when they are similar in nature and bonding. Comparing phosphine (PH_3) and phosphide (Li_3P), based on oxidation state rules, they are assigned the same oxidation state (-3) when they are very different compounds.

In the Macdonald group, we like using a more convenient model that is based on the number of lone pairs in a given atom.[13,14] In the case of phosphorus, phosphorus with no lone pairs is in the +5 oxidation state (P^V), phosphorus with one lone pair is in the +3 oxidation state (P^{III}) and phosphorus with two lone pairs is in the +1 oxidation state (P^I). This model can be extended to other main group elements and is particularly useful for group 13-15 main group elements. **Figure 1.2** shows the assignment of oxidation state for carbon using this model where carbon with no lone pairs, one lone pair, two lone pairs, three lone pairs and four lone pairs are assigned as carbon(+4), carbon(+2), carbon(0), carbon(-2) and carbon(-4), respectively.

+4	+2	0	−2	−4
Oxidation State				
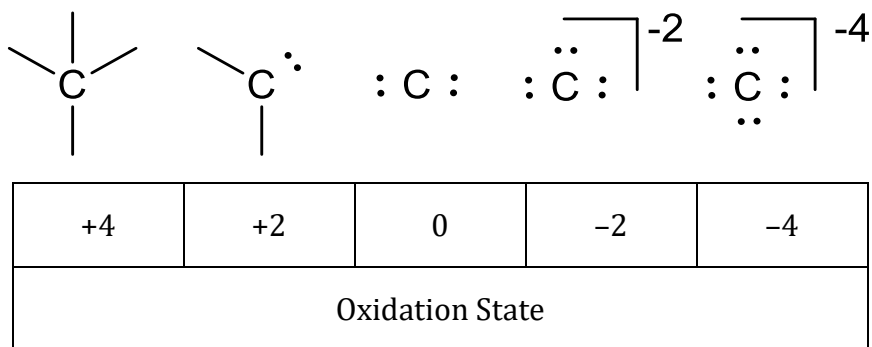
Figure 1.2. *A more convenient model to assigning an oxidation state based on the number of lone pairs present on a given atom.*

Every system has its shortcomings, and in this case, as the assignment depends on the number of lone pairs present, it'll heavily depend on the structure drawn. A

Lewis structure can be ambiguous as it's possible to draw more than one plausible

structure for a given system. In the case of a carbodiphosphorane for example, two

phosphines are bound to a carbon centre as shown in **Figure 1.3**. The oxidation state

assignment can vary greatly depending on the way the structure is drawn. Lewis

structure is a tool to help illustrate basic connectivity of a given molecule, but to be

able to obtain more accurate electron density delocalization, computational methods

would be an ideal way of figuring out and assigning the presence or absence of lone

pairs on a given atom.[15]

+4	+2	0
Oxidation State		
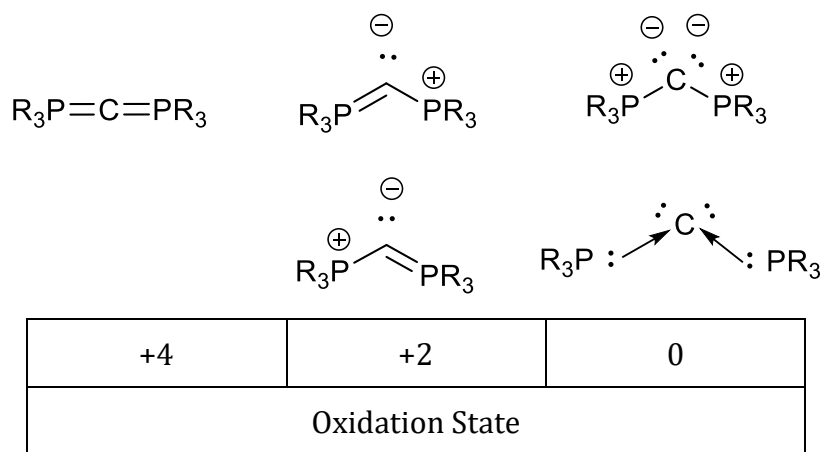
Figure 1.3. *Different Lewis drawings of carbodiphosphorane showing how the assignment of oxidation state on the carbon centre can be different depending on the way the Lewis structure is drawn.*

1.3 Chemical Bonding: The Covalent Bond

The concept of a molecule dates to the seventeenth century, but it wasn't until

the twentieth century that chemists got a better understanding of the structure of a

molecule. Gilbert Newton Lewis (1875–1946), was an American chemist that

discovered the covalent bond and the concept of an electron pair. He postulated the

idea of atoms sharing one or more electrons and developed a dot system to help keep

track of electrons. Lewis also devised the octet rule which states that any non-hydrogen atom will tend to form bonds until the octet rule is satisfied meaning it'll be surrounded by eight valence electrons.[16,17]

The Lewis model gave chemists a rationale for molecule formation, covalent bonding and a way to help predict molecular geometries, but it didn't answer the question as to why molecules come together. Likewise, the octet rule was believed to only work for the first two rows of the periodic table with the reasoning that atoms in third shell or higher have access to d-orbitals, allowing for hybridization (orbital mixing) yielding new orbitals capable of expanding beyond the octet rule. Firstly, d-orbitals are high in energy and inaccessible to an atom like phosphorus and secondly, there are examples of first and second row elements breaking the octet rule and forming hypervalent compounds.[18] Another downside to the Lewis model is the fact that a Lewis structure of O_2 (**Figure 1.4**) does not explain the paramagnetic properties observed in liquid oxygen. This was the case until the introduction of quantum mechanics.
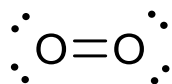
Figure 1.4. A Lewis structure of a dioxygen atom (O_2).

Molecular Orbital Theory (MO theory) is a method that describes a molecular structure by combining atomic orbitals into orbitals that describe the bonding in a molecule as a whole rather than assigning electrons to individual bonds between atoms. By considering two overlapping 1s atomic orbitals (H_2 molecule), MO theory

dictates that the combination of these two orbitals would result in two molecular orbitals, one bonding, and one anti-bonding. This is in accordance with Pauli exclusion principle where no two electrons in a molecule can have the same set of quantum numbers. Therefore, it's necessary that the two originating atomic orbitals be split into two molecular orbitals as shown in **Figure 1.5.**
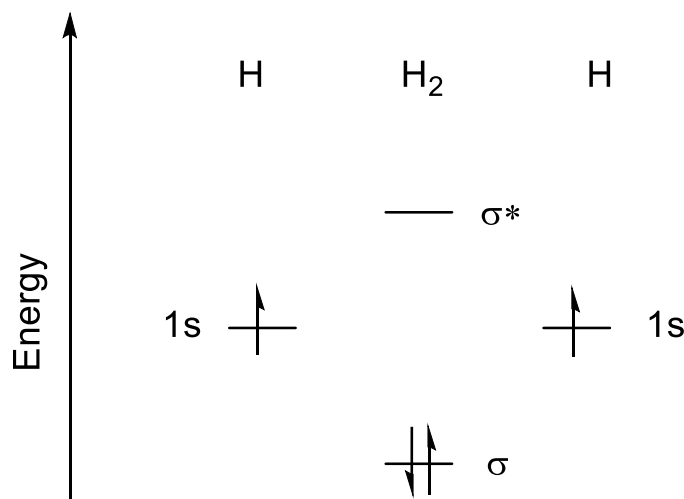
Figure 1.5. Molecular orbital diagram of dihydrogen.

MO theory not only helps in rationalizing bonding but also explains why bonding happens. Sharing of electrons can help stabilize a given molecule by bringing down the energy of electrons as shown in **Figure 1.5**. Going back to the O_2 example, sketching the MO diagram (**Figure 1.6**) will make it clear why dioxygen is paramagnetic. According to Hund's rule, every orbital within a subshell is singly occupied before an orbital is doubly occupied, thus, with two electrons to fill the doubly degenerate π^* orbital, each orbital must be filled with an electron before pairing electrons and this is why dioxygen is paramagnetic.

O O_2 O
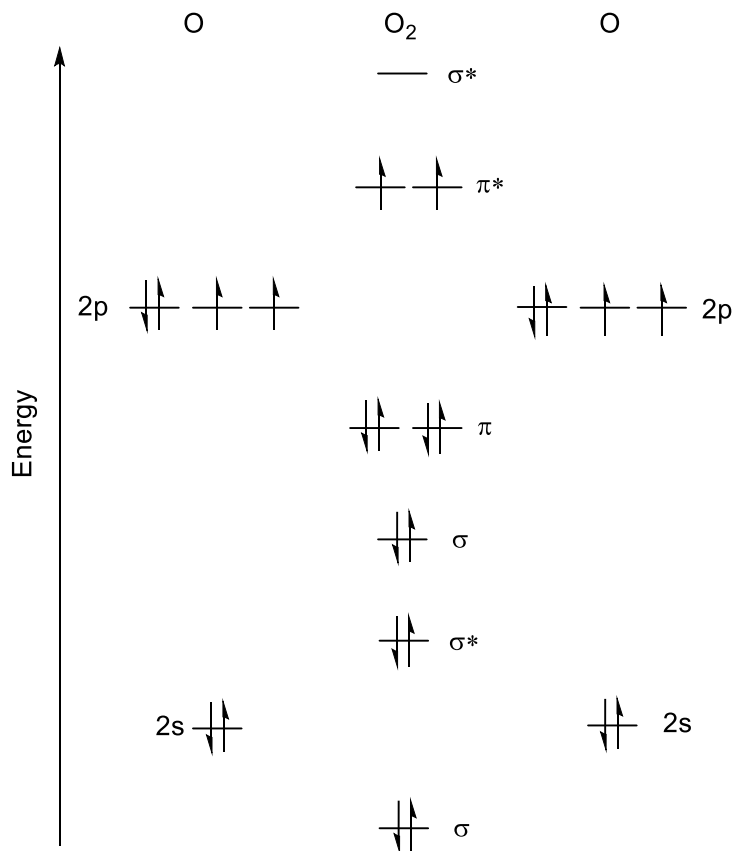
Figure 1.6. *Molecular orbital diagram of an O₂.*

1.4 Pincer Ligands

Early work in organometallic chemistry focused on monodentate and chelate ligands; recent work, however, showed a lot of interest in pincer ligands due to their versatility and ease of use. The term 'pincer' dates back to 1989 in which van Koten used the term to describe tridentate ligands with an anionic carbon centre.[19] Over the past 15 years, the term pincer broadened to generally refer to any tridentate (three-coordinate) ligand with adjacent binding sites that usually adopt a meridional (*mer*-) geometry but can also be found with facial (*fac*-) geometry (butterfly-like) in some cases. There are examples of pincer complexes adapting a fluxional process between

the two geometries.[20] **Figure 1.7** illustrates an [ONO] type ligand that is fluxional in the sense that it can be present in a T-shaped geometry or a bent geometry, more details to follow in section **1.5**.[21]
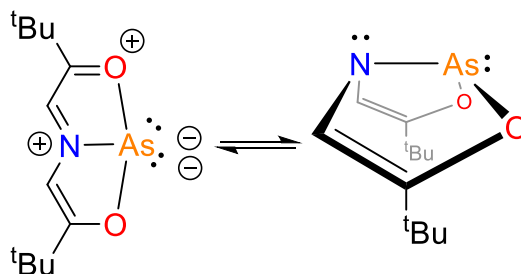
Figure 1.7. *Arduengo's 10–As–3 T–shaped complex (mer-, left) and in the bent shape (fac-, right).*

Due to their broadened definition, there is ambiguity regarding the classification and nomenclature of pincer ligands. In a recent review, Peris and Crabtree[20] classify pincer ligands based on the charge and symmetry of the pincer ligand. The term palindromic is used to describe symmetric donor arms (regardless of the central donor), thus, coordinating atoms like [N,N,N], [O,N,O] and [P,C,P] are all considered to be palindromic, as long as the substituents on terminal donors are the same. In cases where the two terminal arms have differing donor atoms like [N,N,P], or different substituents like [LN,N,NL'], the ligand is considered to be non-palindromic. Regardless of the palindromicity of the pincer ligand, it can also be further classified based on the overall charge of the ligand. It can be neutral (L_3), anionic (XL_2), dianionic (X_2L) or trianionic (X_3) as illustrated in **Figure 1.8**.

| L₃ | XL₂ | X₂L | X₃ |
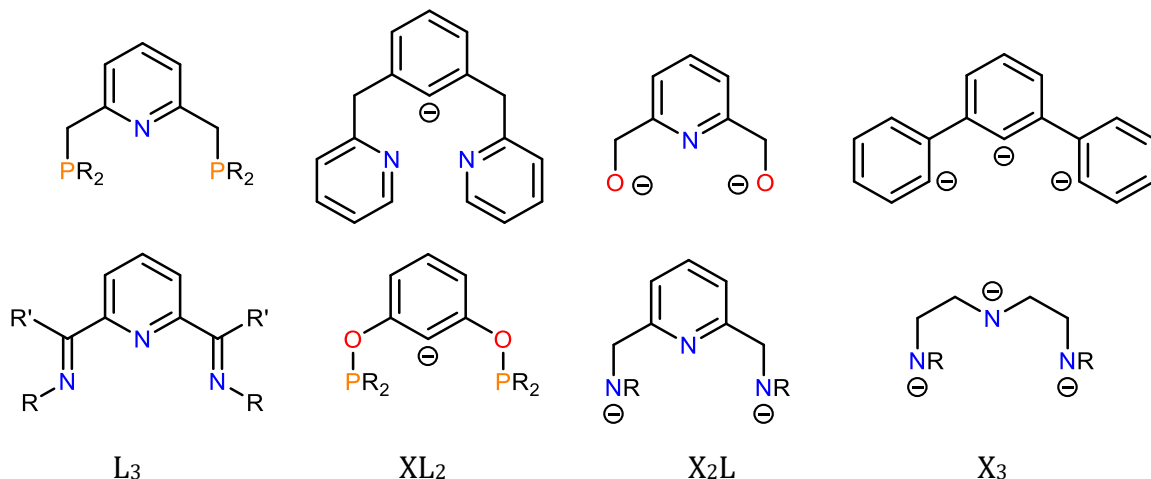
Figure 1.8. *Classification of pincer ligands based on the overall charge of the pincer ligand, neutral (L₃), anionic (XL₂), dianionic (X₂L) or trianionic (X₃).*

The use of pincer ligands with transition metals gained a lot of interest due to the stability pincer ligands, the ease of tunability and cooperativity (through non-innocent pincer ligands). Non-innocent ligands are redox active ligands that can accept or lose electrons in its π-system resulting in significant change in the internal bond distances of the ligand. This allows for the coordinated metal to maintain its starting oxidation state or undergo reactivity that otherwise would not be possible. Pincer ligands are very robust, which makes them a great choice in reactions that require harsh conditions. Goldman and Brookhart[22] reported the production of *n*-alkanes using an iridium pincer catalyst (**Figure 1.9**) that can undergo extreme reaction conditions, such as in the metathesis of *n*-decane that requires heating at 175 °C for nine days. Another example of the robustness of such systems is the Ni(II) complex, **Figure 1.9** (right), that is very thermally stable to the point that it can be sublimed in air at 240 °C in air without decomposition.[23]
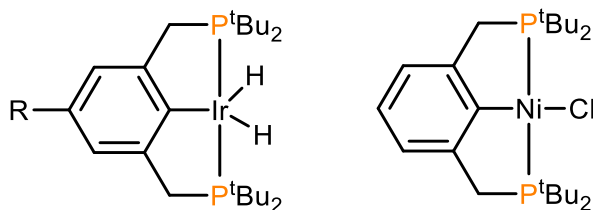
Figure 1.9. *Goldman and Brookhart's Iridium(III) catalyst (left) and Moulton's Nickel(II) (right) are examples of robust metal pincer catalysts.*

Pincer ligands also allow for tunability of the ligand framework, which gives chemists a handle to manipulate the reactivity of the overall catalyst by modifying the pincer ligand. The importance of pincer ligand design is illustrated in the Ni(II) catalyst shown in **Figure 1.10** that is used in the Sonogashia coupling between terminal alkynes and alkyl halides. Dissociation of an amine sidearm is the rate determining step of the reaction, a more labile amine (right) results in the catalyst being active at room temperature, while a more rigid amine group (left) results in the catalyst requiring temperatures exceeding 100 °C for the dissociation of the amine to occur and for the catalyst to become active.[24]
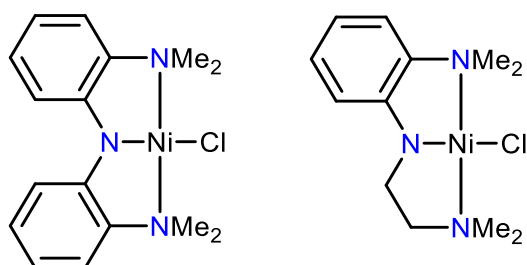
Figure 1.10. *An example of how the tuning of pincer ligand can affect the reactivity of the catalyst.*

Another interesting aspect of pincer ligands is the possibility of introducing chirality into the ligand design, allowing for enantioselective catalysis. Anionic [N,N,N] pincer ligands like the ones depicted in **Figure 1.11** have shown to yield

highly enantioselective transformations. The high kinetic stability of the resulting catalysts allow for reduced catalyst loadings.[25]
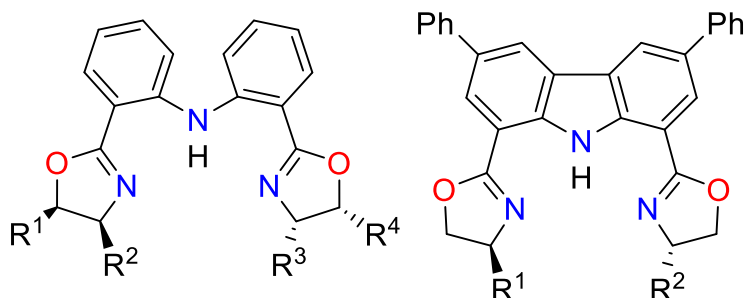
Figure 1.11. *Examples of chiral [N,N,N] pincer ligands.*

Although pincer complexes are generally viewed as stable compounds, where the ligand framework remains unchanged under harsh reaction conditions, there are cases where the pincer ligand itself undergoes transformations resulting in unusual reactivities. This occurs in cases where there is a great delocalization of electron density over multiple aromatic rings resulting in a lowered HOMO–LUMO gap, that is ligand based, allowing it to participate in electron transfer reactions.[20] In such cases, the ligand is considered to be "non-innocent" and is redox active. **Figure 1.12** illustrates the reaction of a Ta(V) complex with a phenyl azide yielding in a nitrene transfer onto the metal centre. The oxidation state of the tantalum centre does not change, where tantalum maintains its preferred +5 oxidation state; however, the pincer ligand goes from being a trianionic (X_3) ligand to a monoanionic (XL_2) ligand, meaning, the ligand underwent a two-electron oxidation.[26]
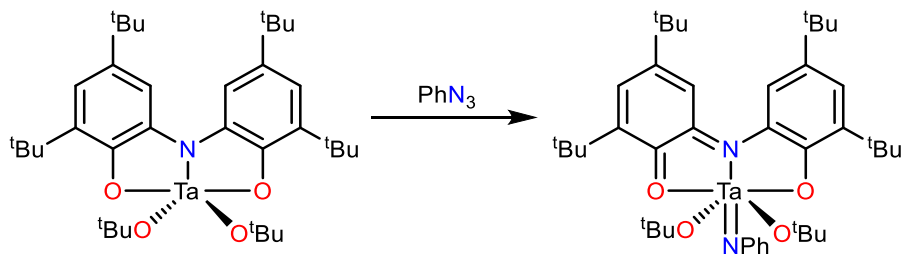
Figure 1.12. *An example of a redox non-innocent ligand that allows Ta(V) undergo reaction with nitrene without changing the preferred oxidation state of the metal centre.*

1.5 Pincer Complexes of Group 15 Elements and Their Role in Modern Main Group Chemistry

Main group elements combined with various types of pincer ligands resulted in some of the most interesting complexes to appear in the literature over the past decade.[25,27] In the 1980s, Arduengo was a pioneer in multidentate pnictogen complexes.[21,28–31] In the 1990s, he went on to synthesize the first stable carbene that will be further discussed in Chapter 6 of this dissertation.[32] Arduengo reported the phosphorus complex of 5-aza-2,8-dioxa-3,7-di-tert-butyl-1-phosphabicy-clo[3.3.0]octa-3,6-diene (ADPO), which is referred to as a 10–P–3 complex if it assumes T–shaped geometry (**Figure 1.13**, left).[30] The 10 denotes the number of π–electrons in the system and the 3 refers to the number of coordination sites. If the complex assumes a bent geometry, then there are 8 π–electrons in the system and the system is referred to as an 8–P–3 complex (**Figure 1.13**, right).
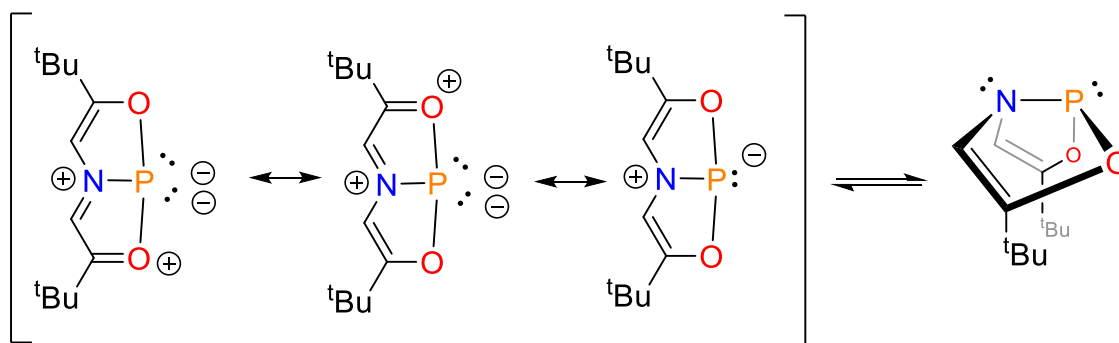
Figure 1.13. *Arduengo's 10–P–3 T–shaped complex and its different resonance structures (left), and 8–P–3 bent complex (right).*

Arduengo additionally reported the complexation of other pnictogens to the same ligand (ADPnO). Arsenic and antimony both adapted the 10–Pn–3 T–shape geometry[21,28] while bismuth reacted with three equivalents of the ligand to yield a 20–Bi–9 complex (**Figure 1.14**, right).[31] Upon treatment of ADPnO with silver, Arduengo observed that, in the cases of arsenic and antinomy, the ligand system maintained the T–shaped geometry resulting in a 10–Pn–4 complex, while in the case of phosphorus, the coordination resulted in bent structure yielding an 8–Pn–4 system.[33]
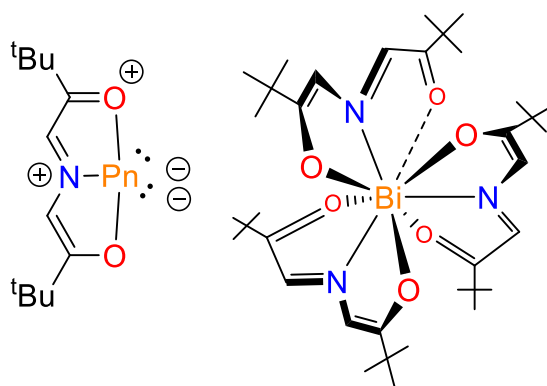
Figure 1.14. *Pnictogens with 10–Pn–3 system, P, As and Sb (left), and 20–Bi–9 system (right).*

ADPnO complexes have interesting reactivities, starting with the ADSbO, as treatment with hexafluoro-2-butyne afforded an unprecedented addition of a substrate to hypervalent species as shown in **Scheme 1.1**, where two acetylenes add across the antimony and carbon backbone. The reaction of ADSbO with hexafluorobiacetyl results in the 4–coordinate adduct shown in the scheme below (10–Sb–4) where two oxygens add across the antimony centre with an appended arm of the tridentate ligand. In the case of arsenic, ADAsO reacts with bis(trifluoromethyl)dithiete in a similar manner to that of the hexafluorobiacetyl (with ADSbO) where the two sulfurs add across the arsenic centre; except that the resulting complex is 5–coordinate (12–As–5).
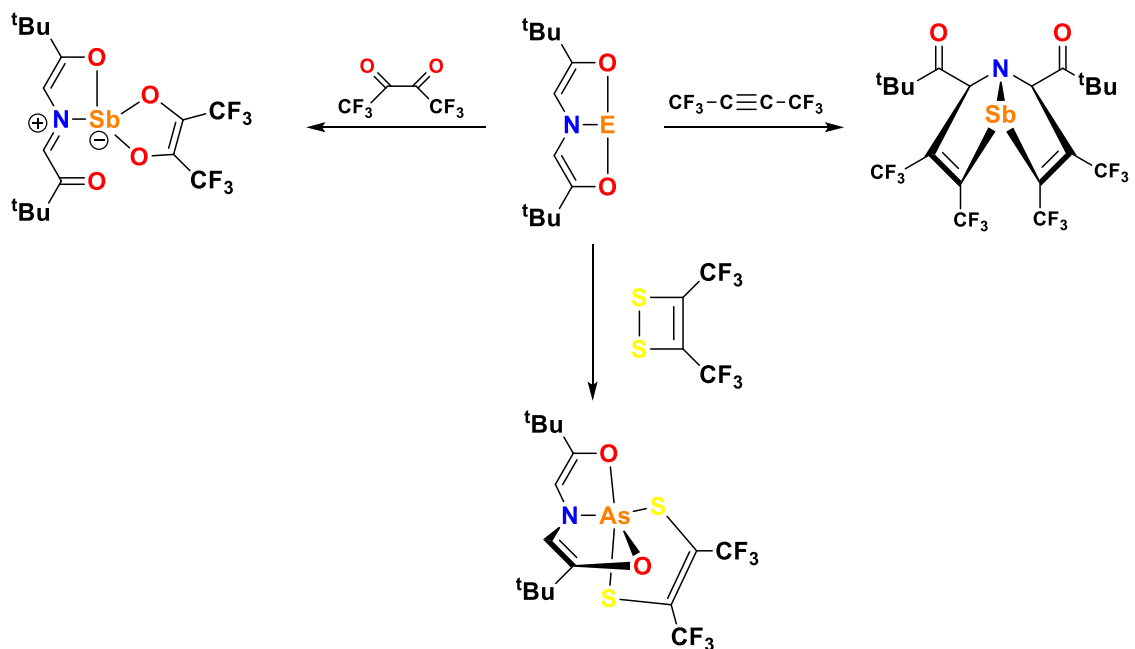
Scheme 1.1. *The Reaction of ADSbO with hexafluoro-2-butyne (right) and with hexafluorobiacetyl (left). The reaction of bis(trifluoromethyl)dithiete with ADAsO (bottom).*

In light of recent advancements in main group chemistry in the activation of dihydrogen and other small molecules using Frustrated Lewis Pairs (FLPs),[34]

chemists have been searching for other ways to activate small molecules using main group elements. The ADPO complex that was first synthesized by Arduengo has been recently investigated by Radosevich for possible catalytic activity.[30,35,36] Practically, tricoordinate P(III) compounds will tend to adopt a pyramidal geometry (**Figure 1.15**, left); however, through appropriate ligand design, it's possible to deviate from such geometry and by doing so, change the reactivity at the phosphorus centre. Lowering the symmetry of a phosphine results in a smaller HOMO–LUMO gap that results from destabilization of the HOMO and the stabilization of the LUMO. This gives rise to a biphilic phosphorus centre capable of behaving as an electron donor and an electron acceptor at the same site.[35,36]
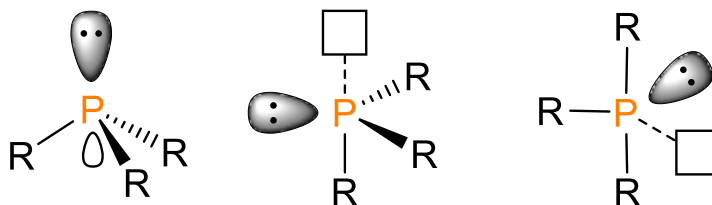
Figure 1.15. *Different geometries adapted by tricoordinate phosphorus: C_{3V}, Cs and C_{2V} respectively.*

Radosevich demonstrated that Arduengo's phosphine (ADPO) is capable of activating N–H and O–H bonds of small molecules across the phosphorus centre. Calculations show that this reaction does not undergo a concerted oxidative addition via a three-centre transition; rather, an amine molecule would bind first to the electrophilic phosphorus followed by a heterolytic cleavage of the N–H bond and a proton transfer from N to P.[36] ADPO is also capable dehydrogenating an ammonia–borane complex (**Scheme 1.2**) to yield a P(V)–H_2 complex, which can also be accessed via the treatment of a P(V)–Cl_2 complex with sodium cyanoborohydride.
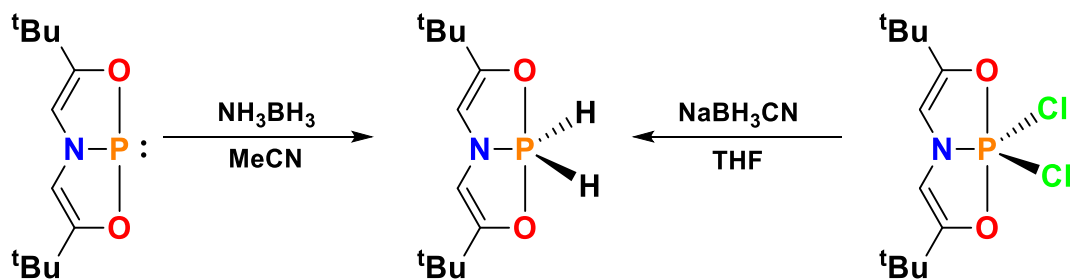
Scheme 1.2. *Radosevich's synthesis of P(V)–H₂ complex.*

The resulting pentacoordinate P(V)–H$_2$ complex can transfer hydrogens onto an unsaturated organic substrate. The reaction was shown to be catalytic in the presence of both ammonia–borane and azobenzene. A 10 mol% catalyst loading of P(V)–H$_2$ can transfer hydrogenate onto azobenzene substrate in yields exceeding 80% at room temperature. The difference between this method of transfer hydrogenation and FLPs is that in the case of an FLP, the phosphorus acts as an electron donor and requires the presence of a Lewis acid to act as an electron acceptor. In the case of ADPO, however, both the electron donor and acceptor are on the same site making it possible to perform two-electron redox transformations that are observed in transition metal catalysts.[35] The proposed mechanism for this transformation is shown in **Scheme 1.3** with an equilibrium between P(III) and P(V) that illustrates the redox capability of the phosphorus centre. Other recent work by Radosevich showed evidence of the formation of pentacoordinate phosphorus via a concerted cyclic transition suggesting the potential of organophosphorus catalysis via it's biphilic centre.[37]
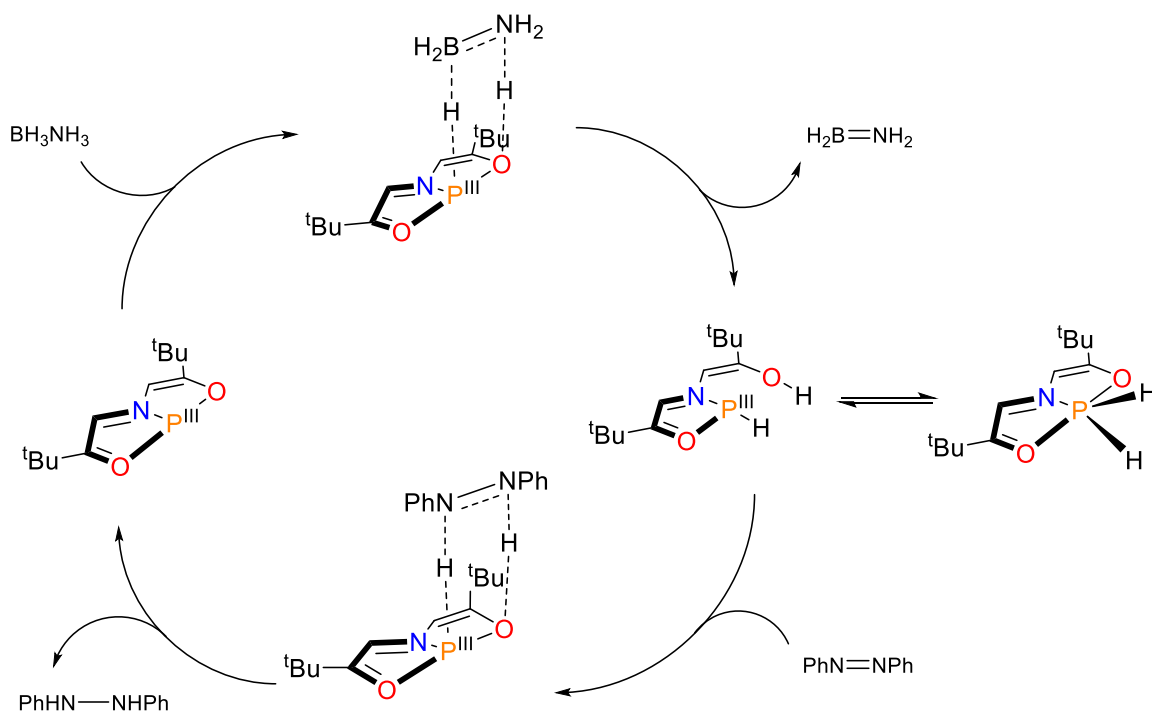
Scheme 1.3. *Proposed mechanism of transfer hydrogenation catalysis of ADPO catalyst.*

Pincer ligands have been used in the isolation of other various low valent main group elements. In 2006, Cowley demonstrated that upon treating $AsCl_3$ with $SnCl_2$, the arsenic is reduced to the arsenic(I) species ("AsCl") that can be isolated by treatment of the resulting suspension with an α,α′–diiminopyridine ligand (also known as diiminopyridine, DIMPY and DIP), resulting in the arsenic(I) salt as shown in **Scheme 1.4**.[38] Ragogna later illustrated that the same ligand can be used in the isolation of a phosphorus(I) salt by treatment of DIMPY ligand with PI_3 resulting in a P(I) centre and an I_3^- as the counterion (^{31}P δ = 169 ppm). Ragogna reported that the use of PCl_3 and PBr_3 resulted in either no reaction or in indiscernible mixtures. Including a halide abstracting agent like cyclohexene in the presence of PCl_3 didn't show any reactivity; however, there was conversion into product in the case of PBr_3

with cyclohexene with much smaller yields (28% compared to >80% in the case of

PI_3).[39]
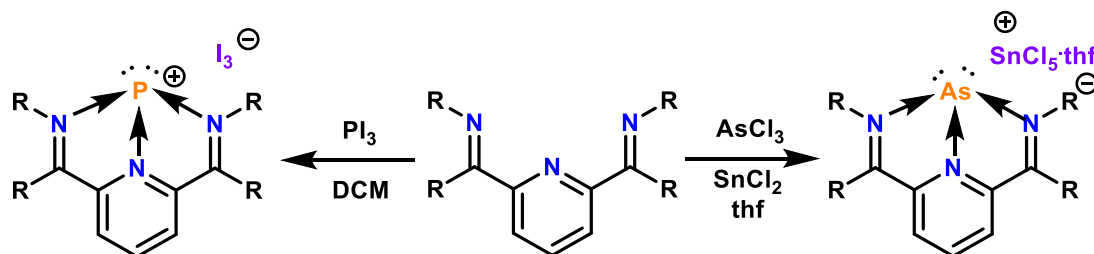
Scheme 1.4. *Examples of Group 15 low valent pincer complexes.*

1.6 Pincer Complexes of Group 14 Elements and Their Role in Modern Main Group Chemistry

The use of pincer ligands with group 14 elements dates back to 1985, before the term pincer was even adopted, where Archer and co-workers reported the synthesis of a tripyridine tin(II)chloride (**Figure 1.16**).[39] Reid and co-workers reported the synthesis of a germanium(II) salt of a triamine, pmdta ($MeN(CH_2CH_2NMe_2)_2$) (**Figure 1.16**) by treatment of pmdta with 2 equivalents of GeX_2 (X = Cl, Br) yielding to the self-ionization of the GeX_2 centre into a GeX^+ and GeX_3^- fragments.[40] Although this is a more flexible ligand and is capable of adopting a facial geometry, it rather adopts a planar meridional geometry.
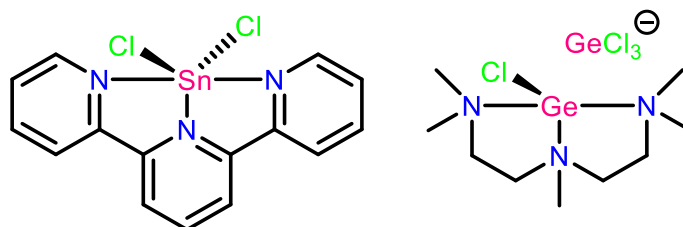
Figure 1.16. *Early examples of pincer-type complexes of group 14 main group elements.*

As mentioned earlier, one of the reasons pincer ligands are attractive ligands is the possibility to tune the ligand, thus, asymmetry can be introduced into the ligand yielding a chiral metal centre. Evans and co-workers demonstrated this via the use of a chiral ligand PYBOX (bis(oxazoline)pyridine) in the isolation of a chiral tin(II) Lewis acid (**Figure 1.17**) that is capable of catalyzing aldol condensation reactions.[42] With 10 mol% loading, aldol reactions can be performed between ethyl glyoxylate and silylketene acetals to yield respective products in good yields in greater than 90% ee.
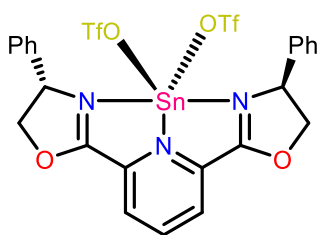
Figure 1.17. *Evans' tin(II) chiral Lewis acid complex.*

DIMPY ligands have been important in development of group 14 low-valent main group chemistry, Roesky reported that using such ligands, one is able to isolate the self-ionization product of germanium(II) and tin(II) (**Scheme 1.5**).[43] Nikonov later reported that the treatment of a DIMPY-Ge(II) complex with two equivalents of potassium graphite (KC_8) in benzene results in a germanium(0) complex as illustrated in **Scheme 1.5**.[44] Other variants of the M(II) DIMPY (M = Ge, Sn) have also been reported.[45,46]
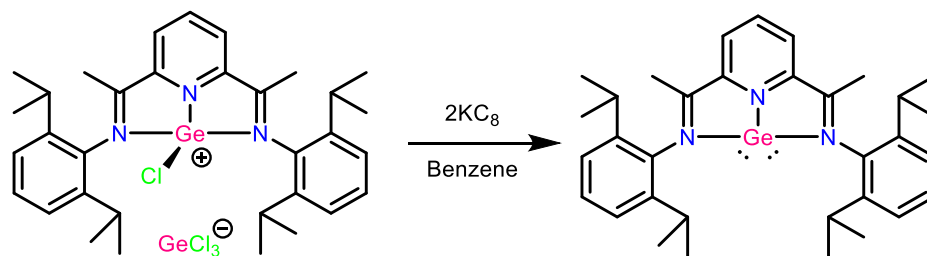
Scheme 1.5. *Roesky's DIMPY-M(II) complex (M = Ge, Sn) and Nikonov's reduced Ge(0) complex.*

Although Sn(0) has not been synthesized in the same manner (reduction from Sn(II) to Sn(0)) as in the case of germanium, Flock and co-workers were successful using a different variant of DIMPY ligand with $Sn[N(SiMe_3)_2]_2$ resulting in a transamination reaction that yields a Sn(0) complex by eliminating two amine equivalents (**Scheme 1.6**).[47]
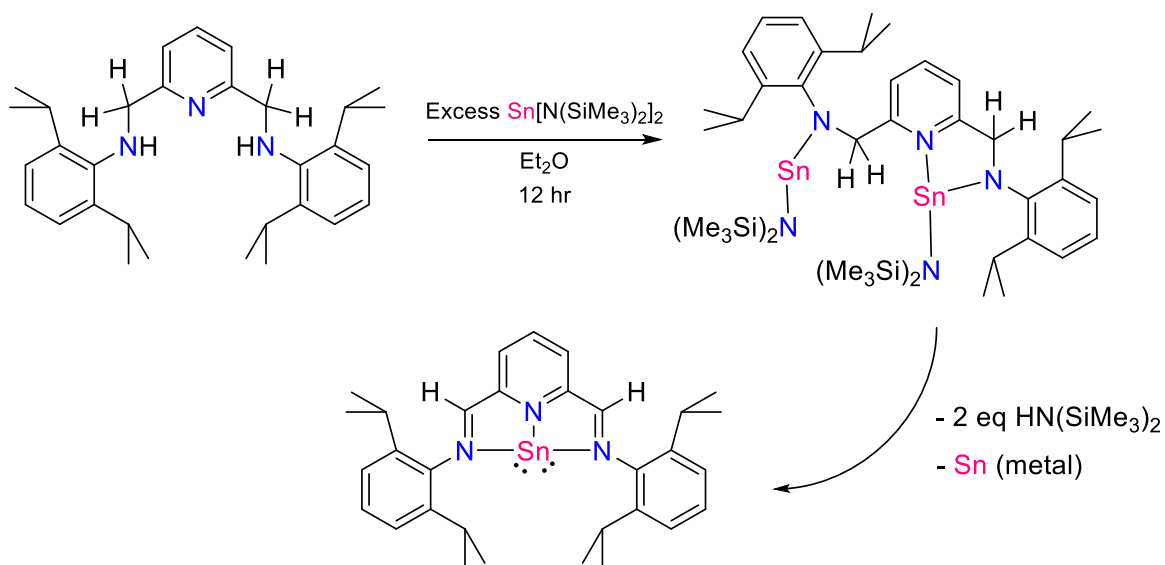
Scheme 1.6. *Mechanism of the transamination reaction of DIMPY ligand with $Sn[N(SiMe_3)_2]_2$ to yield a Sn(0) complex.*

Zaitsev's group reported a different variant of dianionic tridentate complexes of group 14 elements and have demonstrated that the main group element centre is

reactive and can undergo reactions like oxidative addition and transition metal coordination (**Scheme 1.7**).[48–50] Coordination of germanium and tin complexes to tungsten and molybdenum carbonyl compounds have been successful. In addition, both germanium and tin complexes are capable of oxidatively adding small molecules like MeI, Br$_2$, and Ph$_2$S$_2$. Furthermore, DIMPY-Sn(II) complexes have been employed in various transition metal coordination as a result of the work of Jambor and co-workers.[51,52]
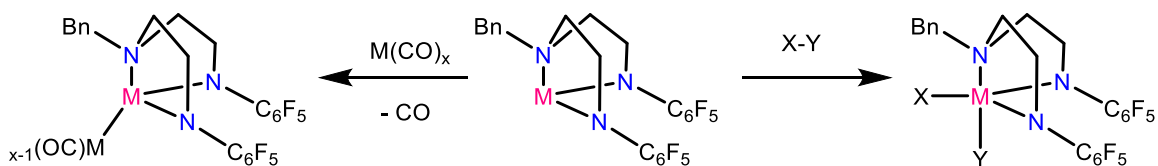
Scheme 1.7. *Zaitsev's tridentate complexes and reactivity.*

1.7 Pincer Complexes of Group 13 Elements and Their Role in Modern Main Group Chemistry

Pincer complexes of group 13 main group elements are more prominent in literature in comparison to either group 14 and 15, particularly, after their recent advancement as supporting ligands (metalloligand scaffold) for transition metal catalysts.[53] An example of this is the use of metalloligand pincer scaffolds' of group 13 elements that forms an overall pincer ligand with a group 13 element as the central atom (**Scheme 1.8**).[54–56]
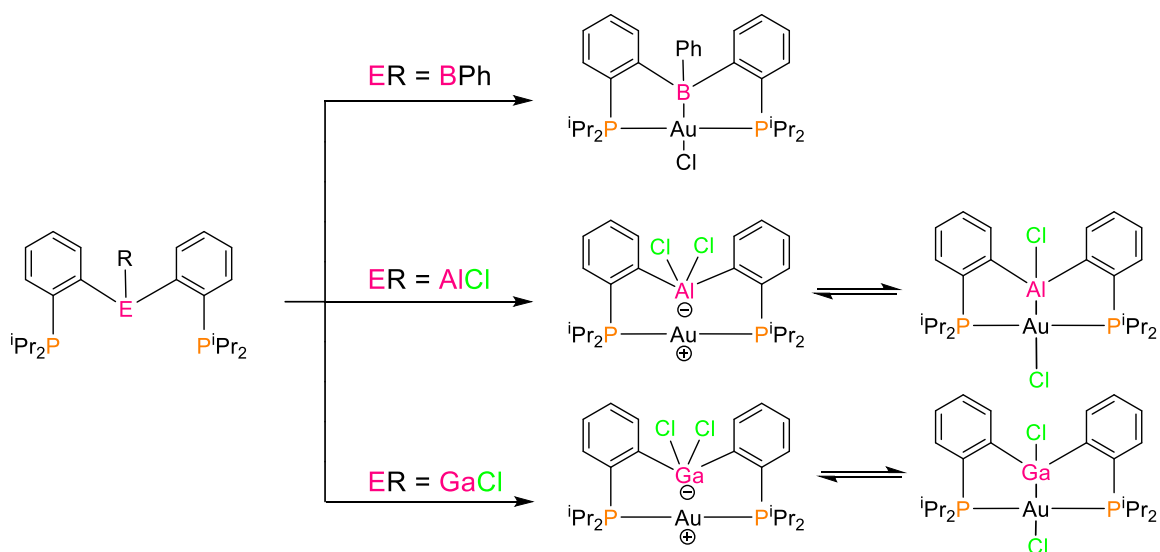
Scheme 1.8. *Zwitterionic complexes containing ambiphilic pincer ligands.*

The presence of a Lewis acid (e.g. boron or aluminium containing compounds) at or near transition metals results in altered reactivity of the metal centre.[57] Lewis acids have been used in conjunction with transition metal catalysts as external activators or co-catalysts. Only recently have Lewis acids been incorporated within ligand motif resulting in ambiphilic ligands where the Lewis acid acts as a σ-acceptor (Z-type) ligand. The different donor types can be described as L (2-electron donor), X (1 electron donor) and Z (2-electron acceptor) type ligands. σ-acceptors can have different goals in coordinating transition metals, they can be used to generate a reactive electron-deficient metal centre and can also be used in cooperative metal-ligand activation of small molecules.[57–59] Having a group 13 element acting as a σ–acceptor have mostly been investigated in use as an external activator or a co-catalyst, but not until recently has it been investigated as part of a ligand scaffold to yield a Z–type ligand (**Figure 1.17**).[60] Z–type ligands are considered Lewis acids and when coordinated to a metal centre, both electrons come from the metal centre. Recent

studies show that the use of Lewis acids or Z-type donors in general at or near

transition metals result in increased reactivity of the metal centre.[34,53,60,61]
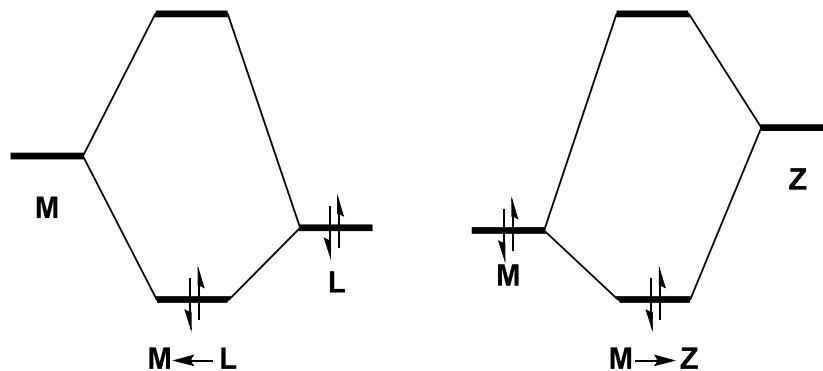
Figure 1.18. *MO diagram depicting the difference between an L- and a Z-type ligand coordinating to a transition metal.*

One example that illustrates this altered reactivity by incorporating a group

13 element is the work of Takaya and Iwasawa.[53] The palladium(II) complex

proposed contains a group 13 main group element (E) within the ligand scaffold that's

directly coordinated to palladium as illustrated in **Figure 1.19**. This catalyst is used

towards the hydrosilylation of CO_2 and depending on the main group element

incorporated, the resulting reactivity of the catalyst was altered. Aluminium showed

the highest reactivity in the group 13 series and was much more reactive in

comparison to either gallium or indium. The aluminium containing catalyst exhibited

the highest catalyst activity reported for hydrosilylation of CO_2 to be reported at the

time. This result shows a promising future for the development of new catalysts with

various tunable metalloligands.
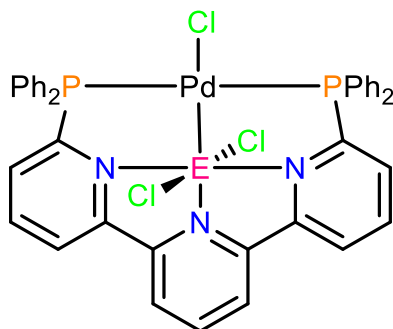
Figure 1.19. *Takaya and Iwasawa's palladium(II) catalyst with E = Al, Ga and In.*

Although pincer metalloligands have gained popularity over the past decade due to the altered reactivity, the use of pincer ligands with group 13 elements have been useful in the isolation of various +1 and +3 group 13 elements. Diiminopyridine (DIMPY) ligands that were introduced earlier have been used in the isolation of group 14 and 15 main group elements in various oxidation states. Attempts to isolate gallium(I) using DIMPY ligand by employing "GaI" as a gallium(I) source by Mills and Richeson yielded mixtures of gallium(III) and gallium(II) radical species as shown in **Scheme 1.9**.[62,63] Initially it wasn't clear as to why this was the case, however, solid-state analysis by Ragogna's group presented that the simple mixing of gallium metal with half an equivalent of iodine does not yield the anticipated "GaI", rather, a mixture with an overall formula of $[Ga^0]_2[Ga^+]_2[Ga_2I_6^{2-}]$ was observed. Varying the reaction time would result in a different mixture; for example, a shorter reaction time (40 minutes) yields the overall formula: $[Ga^0]_2[Ga^+][GaI_4^-]$.[64] Treatment of DIMPY with two equivalents of GaI_3 or $AlCl_3$ results in the clean isolation of self-ionized products [DIMPY-MX][MX$_4$] (**Scheme 1.9**).
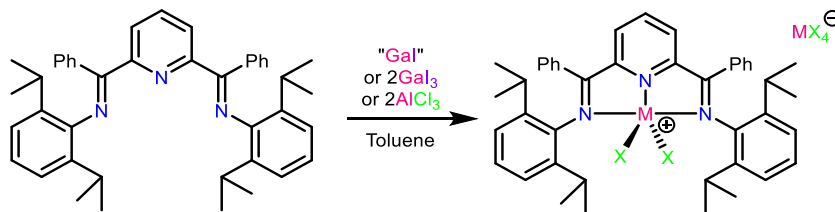
Scheme 1.9. *Reaction of DIMPY ligand with GaI, 2GaI$_3$ or 2AlCl$_3$.*

Mills reported that the treatment of two equivalents of InCl with DIMPY ligand results in the deposition of indium metal and the coordination of InCl$_3$ to DIMPY.[63] Later work by Richeson demonstrated that using a more appropriate In(I) source (InOTf) with DIMPY ligand results in the isolation of [In-DIMPY][OTf] as shown in **Scheme 1.10**.[65] Additionally, Richeson showed that the indium(III) complex of DIMPY can be conveniently prepared by treatment of DIMPY with two equivalents of InCl$_3$ to yield the self-ionized product shown in the scheme below.
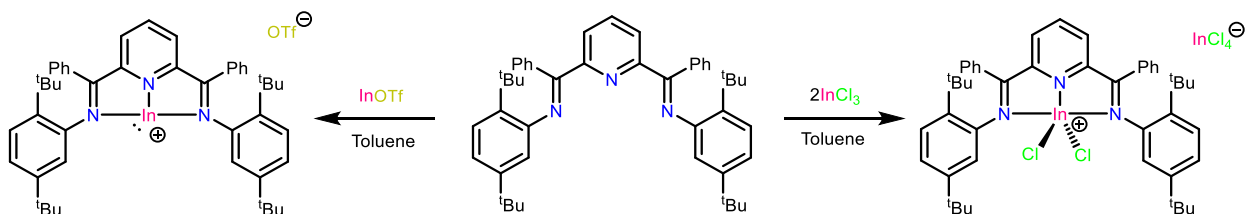
Scheme 1.10. *Reaction of DIMPY ligand with InOTf (left) and two equivalents of InCl$_3$ (right).*

DIMPY complexes of aluminium are more common than either indium or gallium, which is due to the fact that DIMPY-Al complexes have been useful in the activation of small molecules and play an important role in studies of catalytic reactions like Ziegler–Natta catalysis.[66–68] Among the very first examples of DIMPY-Al complexes was the work of Gambarotta and co-workers where they isolated paramagnetic Al complexes of DIMPY via treatment of DIMPY–FeCl$_2$ with either AlMe$_3$

or AlEt$_3$ in an attempt to study the mechanism involved in this Ziegler-Natta catalyst where aluminium is used as a cocatalyst (**Scheme 1.11**).[69]
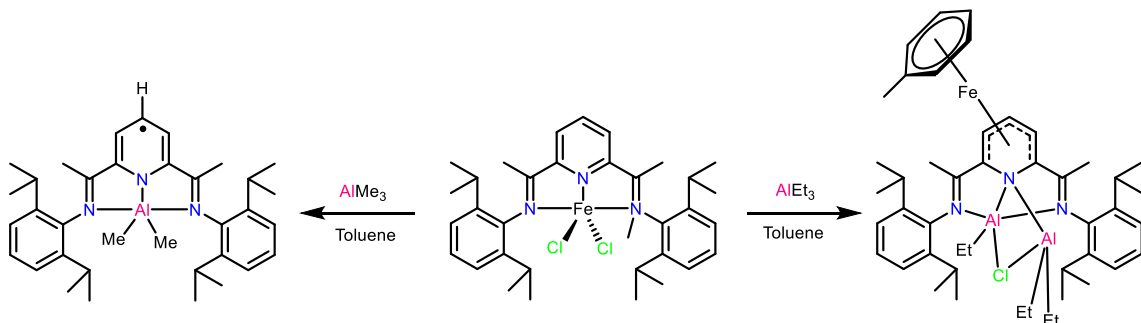
Scheme 1.11. *Reaction of DIMPY–FeCl$_2$ with AlMe$_3$ and AlEt$_3$.*

Berben et. al. reported the synthesis of two square planar complexes of DIMPY-AlX (X = Cl, H).[68] These complexes were synthesized by initially reducing the ligand by 2 electrons using sodium metal, followed by the introduction of aluminium trichloride or dichloroalumane, respectively, to yield the square planar complexes shown in **Scheme 1.12**. The hydride complex is capable of activating N−H bonds via a metal–ligand cooperative mechanism.[67] In-addition, Berben demonstrated that the same aluminium hydride catalyst can promote selective dehydrogenation of formic acid to H$_2$ and CO$_2$ via an aluminium–ligand cooperative mechanism (**Scheme 1.12**).[66]
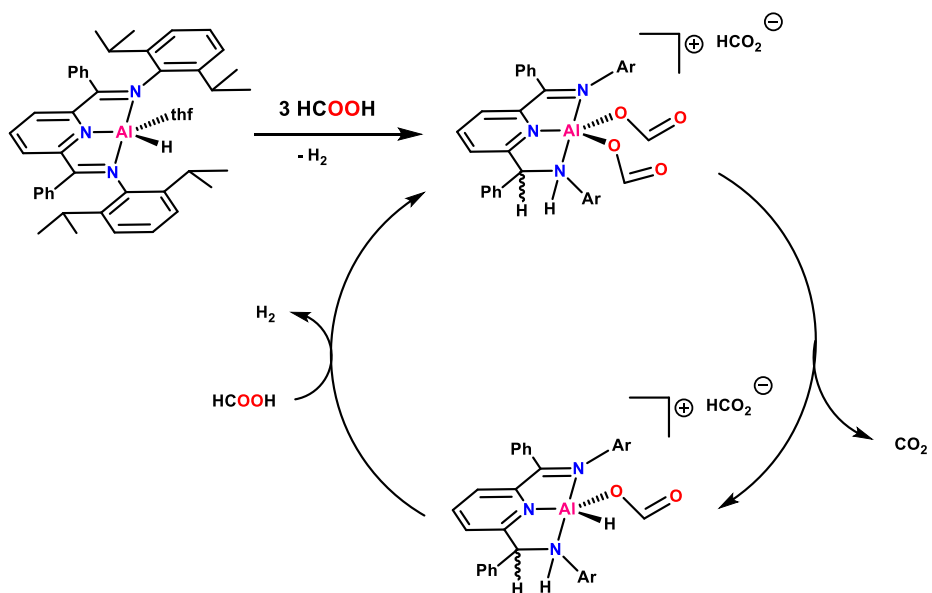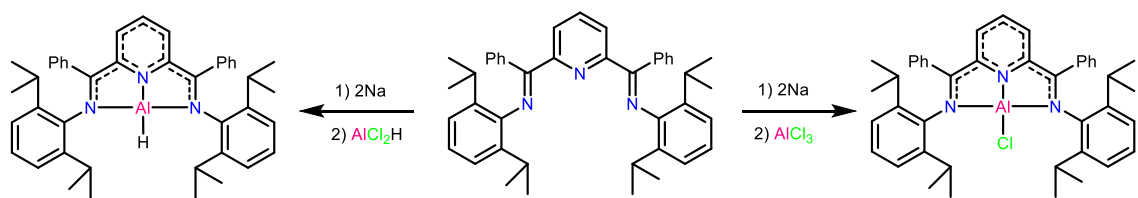
Scheme 1.12. *Reaction of DIMPY with AlCl₃ and AlCl₂H.*

1.8 References

(1)   Bertrand, G. *Chem. Rev.* **2010**, *110* (7), 3851.

(2)   Lutgens, F. K.; Tarbuck, E. J. *Essentials of Geology*; Upper Saddle River, NJ, 2000.

(3)   Audesirk, T.; Audesirk, G.; Byers, B. E. *Biology : Life on Earth With Physiology*;
       Pearson Education Limited: Harlow, 2014.

(4)   Peter H. M. Budzelaar, G. T. *Group 13 Chemistry III*. 2006, pp 141–165.

(5)   Hermann, F. *Angew. Chem.* **2006**, *100* (6), 892.

(6)   Du, J.; Chen, X.; Liu, C.; Ni, J.; Hou, G.; Zhao, Y.; Zhang, X. *Appl. Phys. A* **2014**, *117*
       (2), 815–822.

(7)   Hoffmann, R.; Kabanov, A. A.; Golov, A. A.; Proserpio, D. M. *Angew. Chem. - Int.*
       Ed. **2016**, *55* (37), 10962–10976.

(8)   Emsley, J. *Nature's Building Blocks: An A-Z Guide to the Elements*; OUP Oxford,
       2011.

(9)   Rieke, G. H. *Annu. Rev. Astron. Astrophys.* **2007**, *45* (1), 77–115.

(10)   Gray, T. *The Elements*; 2010.

(11)   Jensen, W. B. *J. Chem. Educ.* **2007**, *84* (9), 1418.

(12)   Parkin, G. *J. Chem. Educ.* **2006**, *83* (5), 791.

(13)   T., C. B. F.; B., M. C. L. *The Group 13 Metals Aluminium, Gallium, Indium and*
       Thallium: Chemical Patterns and Peculiarities. March 30, 2011.

(14)   Macdonald, C. L. B.; Ellis, B. D.; Swidan, A. *Encycl. Inorg. Bioinorg. Chem. Scott, R.*

A., Ed.; John Wiley & Sons, Ltd: Hoboken. **2012**.

(15)   Macdonald, C. L. B.; Ellis, B. D., *Encycl. Inorg. Chem. (2nd Ed.) R. B. King, editor,*
        John Wiley & Sons. Inc.: New York, ***2005****.*

(16)   Lewis, G. N. *J. Am. Chem. Soc.* **1916**, *38* (4), 762–785.

(17)   Langmuir, I. *J. Am. Chem. Soc.* **1919**, *41* (6), 868–934.

(18)   Magnusson, E. *J. Am. Chem. Soc.* **1990**, *112* (22), 7940–7951.

(19)   Koten, G. Van, *Pure Appl. Chem.* **1989**, *61* (10), 1681–1694.

(20)   Peris, E.; Crabtree, R. H. *Chem. Soc. Rev.* **2018**, *47*, 1959–1968.

(21)   Arduengo, A. J.; Culley, S. A. *J. Am. Chem. Soc.* **1985**, *107* (4), 1089–1090.

(22)   Choi, J.; MacArthur, A. H. R.; Brookhart, M.; Goldman, A. S. *Chem. Rev.* **2011**, *111*
        (3), 1761–1779.

(23)   Moulton, B. C. J.; Shaw, B. L., *J. Chem. Soc., Dalton Trans.* **1975**, 1020–1024.

(24)   Pérez García, P. M.; Ren, P.; Scopelliti, R.; Hu, X. *ACS Catal.* **2015**, *5* (2), 1164–
        1171.

(25)   Deng, Q. H.; Melen, R. L.; Gade, L. H. *Acc. Chem. Res.* **2014**, *47* (10), 3162–3173.

(26)   Heyduk, A. F.; Zarkesh, R. A.; Nguyen, A. I. *Inorg. Chem.* **2011**, *50* (20), 9849–
        9863.

(27)   O'Reilly, M. E.; Veige, A. S. *Chem. Soc. Rev.* **2014**, *43* (17), 6325–6369.

(28)   Stewart, C. A.; Harlow, R. L.; Arduengo, A. J. *J. Am. Chem. Soc.* **1985**, *107* (19),
        5543–5544.

(29)   Arduengo, A. J.; Dias, H. V. R.; Calabrese, J. C. *Inorg. Chem.* **1991**, *30* (26), 4880–
        4882.

(30)   Culley, S. A.; Arduengo, A. J. *J. Am. Chem. Soc.* **1984**, *106* (4), 1164–1165.

(31)   Stewart, C. A.; Calabrese, J. C.; Arduengo, A. J. *J. Am. Chem. Soc.* **1985**, *107* (11),
        3397–3398.

(32)   Arduengo, A. J.; Harlow, R. L.; Kline, M. *J. Am. Chem. Soc.* **1991**, *113* (1), 361–363.

(33)   Arduengo, A. J.; Dias, H. V. R.; Calabrese, J. C. *J. Am. Chem. Soc.* **1991**, *113* (18),
        7071–7072.

(34)   Stephan, D. W.; Erker, G. *Angew. Chem. - Int. Ed.* **2015**, *54* (22), 6400–6441.

(35)   Dunn, N. L.; Ha, M.; Radosevich, A. T. *J. Am. Chem. Soc.* **2012**, *134* (28), 11330–
        11333.

(36)   McCarthy, S. M.; Lin, Y. C.; Devarajan, D.; Chang, J. W.; Yennawar, H. P.; Rioux, R.
        M.; Ess, D. H.; Radosevich, A. T. *J. Am. Chem. Soc.* **2014**, *136* (12), 4640–4650.

(37)   Reichl, K. D.; Dunn, N. L.; Fastuca, N. J.; Radosevich, A. T. *J. Am. Chem. Soc.* **2015**,
        137 (16), 5292–5295.

(38)   Reeske, G.; Cowley, A. H. *Chem. Commun.* **2006**, No. 16, 1784–1786.

(39)   Martin, C. D.; Ragogna, P. J. *Dalton Trans.* **2011**, *40* (44), 11976.

(40)   Archer, S. J.; Koch, K. R.; Nassimbeni, L. R. *J. Crystallogr. Spectrosc. Res.* **1986**, *16*
        (4), 449–458.

(41)   Cheng, F.; Dyke, J. M.; Ferrante, F.; Hector, A. L.; Levason, W.; Reid, G.; Webster,

M.; Zhang, W. *Dalton Trans.* **2010**, *39* (3), 847–856.

(42)   Evans, D. A.; MacMillan, D. W. C.; Campos, K. R. *J. Am. Chem. Soc.* **1997**, *119* (44), 10859–10860.

(43)   Singh, A. P.; Roesky, H. W.; Carl, E.; Stalke, D.; Demers, J. P.; Lange, A. *J. Am. Chem. Soc.* **2012**, *134* (10), 4998–5003.

(44)   Chu, T.; Belding, L.; van der Est, A.; Dudding, T.; Korobkov, I.; Nikonov, G. I. *Angew. Chem. - Int. Ed.* **2014**, *53* (10), 2711–2715.

(45)   Jurca, T.; Hiscock, L. K.; Korobkov, I.; Rowley, C. N.; Richeson, D. S. *Dalton Trans.* **2014**, *43* (2), 690–697.

(46)   Magdzinski, E.; Gobbo, P.; Workentin, M. S.; Ragogna, P. J. *Inorg. Chem.* **2013**, *52* (19), 11311–11319.

(47)   Flock, J.; Suljanovic, A.; Torvisco, A.; Schoefberger, W.; Gerke, B.; Pöttgen, R.; Fischer, R. C.; Flock, M. *Chem. Eur. J.* **2013**, *19* (46), 15504–15517.

(48)   Huang, M.; Kireenko, M. M.; Zaitsev, K. V.; Oprunenko, Y. F.; Churakov, A. V.; Howard, J. A. K.; Lermontova, E. K.; Sorokin, D.; Linder, T.; Sundermeyer, J.; Karlov, S. S.; Zaitseva, G. S. *Eur. J. Inorg. Chem.* **2012**, (23) 3712–3724.

(49)   Huang, M.; Kireenko, M. M.; Lermontova, E. K.; Churakov, A. V.; Oprunenko, Y. F.; Zaitsev, K. V.; Sorokin, D.; Harms, K.; Sundermeyer, J.; Zaitseva, G. S.; Karlov, S. S. *Z. Anorg. Allg. Chem.* **2013**, *639* (3–4), 502–511.

(50)   Huang, M.; Kireenko, M. M.; Djevakov, P. B.; Zaitsev, K. V.; Oprunenko, Y. F.; Churakov, A. V.; Tyurin, D. A.; Karlov, S. S.; Zaitseva, G. S. *J. Organomet. Chem.*

2013, *735*, 15–25.

(51)   Bouska, M.; Dostál, L.; Lutter, M.; Glowacki, B.; Ruzickova, Z.; Beck, D.; Jambor, R.; Jurkschat, K. *Inorg. Chem.* **2015**, *54* (14), 6792–6800.

(52)   Novák, M.; Bouška, M.; Dostál, L.; Lutter, M.; Jurkschat, K.; Turek, J.; De Proft, Frank, Růžičková, Z.; Jambor, R. *Eur. J. Inorg. Chem.* **2017**, *2017* (9), 1292–1300.

(53)   Takaya, J.; Iwasawa, N. *J. Am. Chem. Soc.* **2017**, *139* (17), 6074–6077.

(54)   Sircoglou, M.; Bontemps, S.; Mercy, M.; Miqueu, K.; Ladeira, S.; Saffon, N.; Maron, L.; Bouhadir, G.; Bourissou, D. *Inorg. Chem.* **2010**, *49* (9), 3983–3990.

(55)   Sircoglou, M.; Bouhadir, G.; Saffon, N.; Miqueu, K.; Bourissou, D. *Organometallics* **2008**, *27* (8), 1675–1678.

(56)   Sircoglou, M.; Mercy, M.; Saffon, N.; Coppel, Y.; Bouhadir, G.; Maron, L.; Bourissou, D. *Angew. Chem. - Int. Ed.* **2009**, *48* (19), 3454–3457.

(57)   Parkin, G. *Organometallics* **2006**, *25* (20), 4744–4747.

(58)   Braunschweig, H.; Kollann, C.; Rais, D. *Angew. Chem. - Int. Ed.* **2006**, *45* (32), 5254–5274.

(59)   Braunschweig, H.; Radacki, K.; Rais, D.; Whittell, G. R. *Angew. Chem. - Int. Ed.* **2005**, *44* (8), 1192–1194.

(60)   Bouhadir, G.; Bourissou, D. *Chem. Soc. Rev.* **2016**, *45* (4), 1065–1079.

(61)   Fontaine, F. G.; Zargarian, D. *J. Am. Chem. Soc.* **2004**, *126* (28), 8786–8794.

(62)   Jurca, T.; Dawson, K.; Mallov, I.; Burchell, T.; Yap, G. P. A.; Richeson, D. S. *Dalton*

Trans. **2010**, *39* (5), 1266–1272.

(63)   Baker, R. J.; Jones, C.; Kloth, M.; Mills, D. P., *New. J. Chem.* , **2004** , 28, 207–213.

(64)   Malbrecht, B. J.; Dube, J. W.; Willans, M. J.; Ragogna, P. J. *Inorg. Chem.* **2014**, *53* (18), 9644–9656.

(65)   Jurca, T.; Lummiss, J.; Burchell, T. J.; Gorelsky, S. I.; Richeson, D. S. *J. Am. Chem. Soc.* **2009**, *131* (13), 4608–4609.

(66)   Myers, T. W.; Berben, L. A. *Chem. Sci.* **2014**, *5* (7), 2771–2777.

(67)   Myers, T. W.; Berben, L. A. *J. Am. Chem. Soc.* **2013**, *135* (27), 9988–9990.

(68)   Thompson, E. J.; Myers, T. W.; Berben, L. A. *Angew. Chem. - Int. Ed.* **2014**, *53* (51), 14132–14134.

(69)   Scott, J.; Gambarotta, S.; Korobkov, I.; Knijnenburg, Q.; De Bruin, B.; Budzelaar, P. H. M. *J. Am. Chem. Soc.* **2005**, *127* (49), 17204–17206.

CHAPTER 2:
2,6-Bis(benzimidazol-2-yl)pyridine as More Electron-Rich and Sterically Accessible Alternatives to 2,6-bis(imino)pyridine for Group 13 Coordination Chemistry

2.1 Introduction

Pincer ligands have proven to be vital in transition metal chemistry and have been studied to a great extent.[1] The use of a neutral trinitrogen donor ligand such as bis(imino)pyridine (DIMPY) with iron and cobalt resulted in highly active catalysts for ethylene polymerization.[2] This ligand has proven to be redox active, which is useful for metal-ligand cooperative catalysis.[3,4] The use of pincer ligands with main group (MG) elements has not been exploited to the same extent as with transition metals but there are some noteworthy reports. In particular, DIMPY ligand (**A**) has been used to isolate different low valent MG species including In(I)[5], As(I)[6], P(I)[7], Ge(0)[8] and Sn(0)[9].
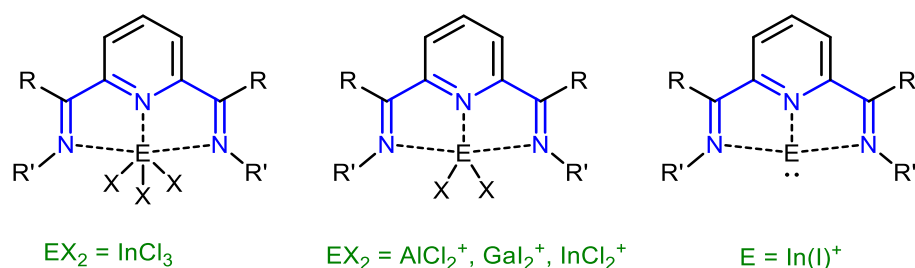
Scheme 2.1. *DIMPY complexes of group 13 elements.*

Reports of 'Ga(I)' with DIMPY ligands yielded mixtures of Ga(III) ([DIMPYGaI$_2$][GaI$_4$]) and radical Ga(II) species ([^{iPr}DIMPYGaI$_2$]$^•$); similarly with AlCl$_3$ the corresponding [DIMPYAlCl$_2$][AlCl$_4$] is formed.[10,11] Richeson however,

showed that using an appropriate In(I) source like InOTf yielded the complex [DIMPYIn(I)][OTf].[5] In the case of aluminium, the two square planar complexes of DIMPY-AlX (X = Cl, H) are formed by first reducing the ligand with two electrons, followed by the treatment with aluminium trichloride or dichloroalumane as shown in **Scheme 2.2**.[12] The hydride complex was shown to activate N−H bonds via a metal−ligand cooperative mechanism[13] and is capable of promoting selective dehydrogenation of formic acid to H_2 and CO_2.[14]
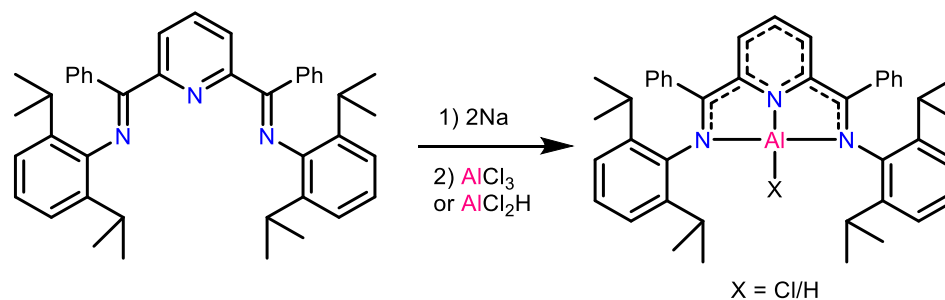
Scheme 2.2. The synthesis of square planar Al(III) complexes.

Aluminium cocatalysts are used to activate late transition metal DIMPY complexes in polymerization reactions. To that end, Gambarotta and co-workers studied the reaction of [iPrDIMPYFeCl$_2$] with AlMe$_3$ and AlEt$_3$ as shown in **Scheme 2.3**.[15] Both resulting complexes are paramagnetic and contain trivalent aluminium centres.
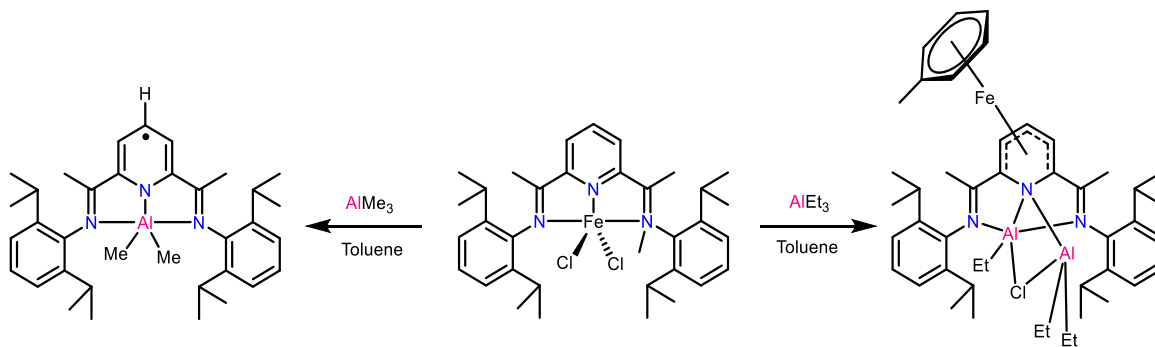
Scheme 2.3. *Reaction of [^{iPr}DIMPYFeCl$_2$] with AlMe$_3$ and AlEt$_3$.*

In this work, we explore the coordination of group 13 elements to bisbenzimidazole ligands **B** shown in **Figure 2.1** with G = NH, NMe, NEt, NBn, N(3,5-CF$_3$)Bn, N-Allyl and O. These ligands are more rigid than their DIMPY counterparts and they have been used in transition metal chemistry for supramolecular self-assembly,[16] photoinduced CO release in biological systems,[17] anti-cancer agents,[18] and catalysts for transfer hydrogenation of ketones.[19] Coordination of BZIMPY ligand to indium have been previously reported,[20,21] among other group 14 complexes.[22–29] This work presented herein represents its first application to gallium. Similar imidazole and benzimidazole tripodal ligand coordination to MG elements have been previously investigated.[30–32]
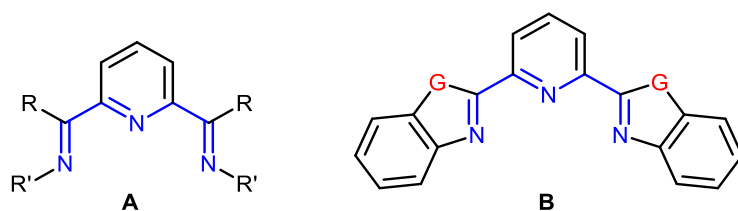
Figure 2.1. *DIMPY ligand, B: BZIMPY ligand (G = NH, NBn, N(3,5-CF$_3$)Bn, N-Allyl and O).*

CHAPTER 2
2,6-Bis(benzimidazol-2-yl)pyridine as More Electron-Rich and Sterically Accessible Alternatives to 2,6-
bis(imino)pyridine for Group 13 Coordination Chemistry

2.2 Results and Discussion

2.2.1 Synthesis and Characterization

Initial attempts to coordinate group 13 halides, MCl_3 (M = Al, Ga, In) to NH-BZIMPY (Compound **B** with G = NH) resulted in the precipitation of coloured materials that were insoluble in common organic solvents. These reactions were carried out in dichloromethane, acetonitrile and tetrahydrofuran with one or two equivalents of MCl_3. In all cases, the resulting materials could not be characterized by NMR spectroscopy or X-ray crystallography. To increase the solubility of the resulting complexes, the NH nitrogen sites were substituted using different alkylating agents to introduce Me, Et, Allyl, Bn and $(3,5-CF_3)$Bn derivatives. While the methyl and ethyl substituted ligands exhibit increased solubility compared to the free NH ligand, the resultant coordination complexes remained poorly soluble in common organic solvents. Fortunately, the use of allyl and benzyl (Bn) substituents allowed for the isolation of soluble materials that could be characterized by heteronuclear NMR spectroscopy and grown into single crystals suitable for X-ray diffraction analysis (**Figure 2.2**).
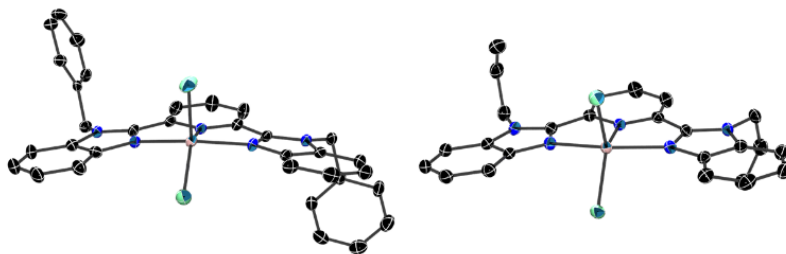
Figure 2.2. *Solid state structure of the cations in [NBn-BZIMPYGaCl$_2$][GaCl$_4$] (**1**, left) and [NAllyl-BZIMPYGaCl$_2$][GaCl$_4$] (**3**, right). Thermal ellipsoids are shown at 50% probability level. Hydrogen atoms, solvent molecules and counter anions are omitted for clarity. Selected bond distances and angles are given in **Table 2.1**.*

First we studied the known self-ionization process (L + MCl$_3$ → [LMCl$_2$][MCl$_4$]) which is evident and well-studied in combination with the structurally related DIMPY ligands.[11,33] These reactions went to completion by using two equivalents of metal halide, the halide displacement at the coordinated MG element was always observed regardless of the stoichiometry added (**Scheme 2.4**). The products (**1**, **2** and **3**) ([G-BZIMPYGaCl$_2$][GaCl$_4$] were obtained by treating G-BZIMPY with two equivalents of GaCl$_3$ in dichloromethane (DCM), resulting in an immediate clear yellow solution. DCM was removed under reduced pressure and the resulting solid is suspended in toluene, filtered, dried under vacuum and collected to yield yellow solid in almost quantitative yields. Slow evaporation from a DCM solution yields yellow crystals of (**1**, **2** and **3**) suitable for X-ray diffraction.
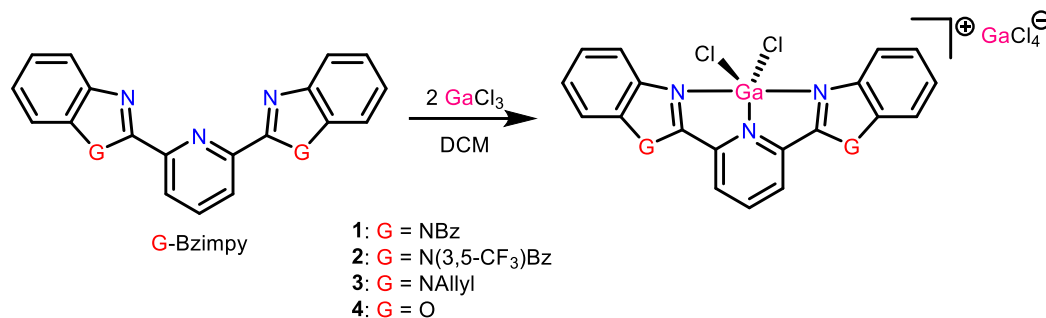
Scheme 2.4. *Self-ionization reactions of GaCl$_3$ with G-BZIMPY ligands.*

The uncoordinated 2,6-bis(benzoxazol-2-yl)pyridine (O-BZIMPY) is very poorly soluble in common organic solvents; however, treating the ligand with two equivalents of GaCl$_3$ in DCM and sonicating for 24 hours yielded a yellow/green insoluble material with yellow microcrystals of complex **4**, [O-BZIMPYGaCl$_2$][GaCl$_4$] (**Figure 2.3**). A dilute solution in CD$_3$CN allowed for NMR spectral analysis of the compound.
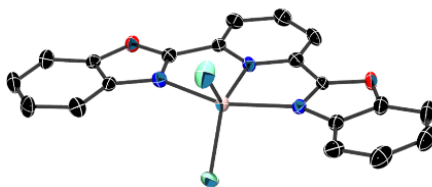
Figure 2.3. *Solid state structure of the cation in [O-BZIMPYGaCl$_2$][GaCl$_4$] (**4**). Thermal ellipsoids are shown at 50% probability level. Hydrogen atoms, solvent molecules and counter anion are omitted for clarity. Selected bond distances and angles are given in **Table 2.1**.*

Next, we were interested in comparing the coordination of Ga halides to G-BZIMPY to that of DIMPY. [^{iPr}DIMPYGaI$_2$][GaI$_4$] (^{iPr}DIMPY = 2,6-Bis-[1-(2,6-diisopropylphenylimino)ethyl]pyridine) has already been reported by Mills as a disproportionation product from GaI treated with ^{iPr}DIMPY.[11] To our knowledge, there are no reports of the chloride equivalent of gallium complex

CHAPTER 2
2,6-Bis(benzimidazol-2-yl)pyridine as More Electron-Rich and Sterically Accessible Alternatives to 2,6-
bis(imino)pyridine for Group 13 Coordination Chemistry

of ^{iPr}DIMPY, therefore, the ligand was treated with two equivalents of GaCl$_3$.

This resulted in the clean and quantitative formation of [^{iPr}DIMPYGaCl$_2$][GaCl$_4$]

(**5**) (**Figure 2.4**, left). [^{iPr}DIMPYAlCl$_2$][AlCl$_4$] has been reported by Budzelaar as

a 1:1 mixture with the free ligand ^{iPr}DIMPY.[33] Treatment of ^{iPr}DIMPY with two

equivalents of AlCl$_3$ resulted in the clean and quantitative formation of

[^{iPr}DIMPYAlCl$_2$][AlCl$_4$] (**6**) (**Figure 2.4**, right), which upon crystallizing from

DCM yielded crystals that were solvomorphic to the structure reported by

Budzelaar.
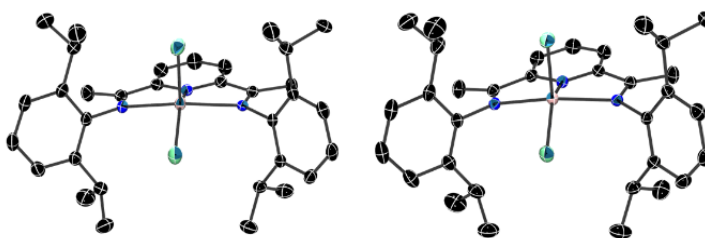
Figure 2.4. *Solid state structure of the cations in [^{iPr}DIMPYGaCl$_2$][GaCl$_4$] (**5**, left) and*
*[^{iPr}DIMPYAlCl$_2$][AlCl$_4$] (**6**, right). Thermal ellipsoids are shown at 50% probability level.*
Hydrogen atoms, solvent molecules and counter anions are omitted for clarity. Selected bond
*distances and angles are given in **Table 2.1**.*
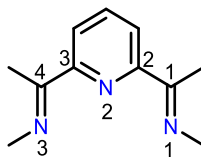
	1	2	3	4	5	6	7
M-N1	2.051(3)	2.055(2)	2.0543(13)	2.116(3)	2.1711(15)	2.0985(16)	2.174(3)
M-N2	2.051(3)	2.074(2)	2.0640(12)	2.058(3)	1.9940(16)	1.9481(15)	2.148(3)
M-N3	2.063(3)	2.029(2)	2.0458(13)	2.099(3)	2.1751(16)	2.0961(16)	2.172(3)
M-Cl	2.1905(11); 2.1771(12)	2.1831(8); 2.1545(8)	2.1893(4); 2.1809(4)	2.1517(9); 2.1436(10)	2.1574(6); 2.1569(6)	2.1121(7); 2.1174(7)	Ga-Cl 2.2477(10) Ga-Fe 2.3861(7)
N1-C1	1.330(5)	1.327(3)	1.3312(19)	1.301(4)	1.281(3)	1.287(2)	1.316(4)
C1-C2	1.476(5)	1.466(4)	1.464(2)	1.447(5)	1.486(3)	1.483(2)	1.463(5)
C2-N2	1.342(5)	1.342(3)	1.3434(19)	1.337(4)	1.330(2)	1.337(2)	1.347(4)
N2-C3	1.339(5)	1.343(3)	1.3421(18)	1.344(4)	1.336(2)	1.339(5)	1.349(4)
C3-C4	1.467(5)	1.467(4)	1.466(2)	1.454(5)	1.483(3)	1.488(5)	1.467(5)
C4-N3	1.332(5)	1.326(4)	1.3312(19)	1.302(4)	1.285(2)	1.287(2)	1.313(4)
N1-M-N2	76.47	76.06(9)	76.43(5)	75.93(11)	76.35(6)	76.98(6)	72.75(10)
N2-M-N3	76.76	76.29(9)	76.66(5)	76.22(11)	76.31(6)	77.37(6)	71.88(10)
N2-M-N3	151.49	152.22(10)	152.35(5)	152.05(11)	150.25(7)	150.69(13)	137.28(11)

Table 2.1. *Selected bond distances (Å) and angles (°) of complexes **1**-**7**.*

The M-N bond distances in the DIMPY complexes are significantly shorter for the pyridine interaction M-N2 (M = Ga, Al) than the ones to the imine side arms (M-N1 and M-N3) (**Table 2.1**). This is probably attributable to the steric hindrance of the bulky imine donors. In the case of G-BZIMPY, the bond distances for the pyridine interaction and the side arms are similar with slight asymmetry of the side arms due to the more rigid nature of the ligand forcing the gallium to be slightly off-centre. Although the M-N2 interaction with pyridine is shorter in DIMPY (**5**) than G-BZIMPY (**1**-**4**), the imidazole donors feature shorter distances to the gallium centre than the imine donors of DIMPY. This suggests that G-BZIMPY is a better donor ligand than DIMPY; this postulate is corroborated by the snapping energy calculations detailed below.

2.2.2 Reduction of Ga(III) to Ga(I)

Germanium(0) and tin(0) complexes of DIMPY ligand have been isolated, but there have been no reports of DIMPY stabilized group 13 metals in the +1 oxidation state apart from the unique example prepared by Richeson described earlier.[5,8,9] To this end, we were interested in reducing the [G-BZIMPYGaCl$_2$][GaCl$_4$] to Ga(II), Ga(I) or even Ga(0). Treatment of [NBn-BZIMPYGaCl$_2$][GaCl$_4$] with 1, 2 or 3 equivalents of KC$_8$, potassium or sodium naphthalide in THF have all resulted in reduction of the gallium centre to gallium metal and the release of the free NBn-BZIMPY ligand. This is likely attributable to the relative absence of steric protection on the front end of the BZIMPY ligand; however, we reasoned that the lack of steric bulk could allow for a nucleophilic attack with a redox active nucleophile. In this context K$_2$[Fe(CO)$_4$] was added stoichiometrically to a solution of **1** in THF at −50 °C, which resulted in an immediate colour change to a red/purple solution with the formation of a precipitate. Single crystals grown from the filtered reaction mixture identified the product as a reduced gallium species with a direct gallium iron bond (**Scheme 2.5**).
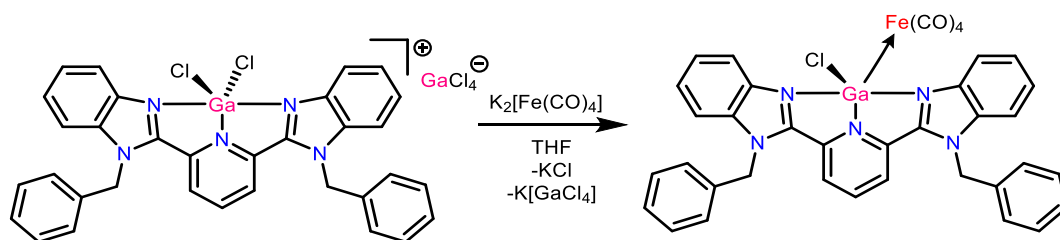
Scheme 2.5. *Reaction of [NBn-BZIMPYGaCl$_2$][GaCl$_4$] with K$_2$[Fe(CO)$_4$] in THF to yield [(NBn-BZIMPY)(Cl)Ga—Fe(CO)$_4$] (**7**).*

The two metal centres in [(NBn-BZIMPY)(Cl)Ga—Fe(CO)$_4$] (**7**, **Figure 2.5**) are best described as a Ga(I) centre coordinated to an Fe(0) centre (LGa^I→Fe(CO)$_4$). This structure is reminiscent to that of a gallium complex reported by Driess featuring a biscarbene ligand.[34] The Ga(I)-Fe bond distance reported by Driess (2.4010(12) Å) is slightly longer than that observed in complex **7** (2.3861(7) Å). Complex **7** has a trigonal bipyramid geometry at the iron centre with an $_{ax}$CO-Fe-Ga angle of 179.09(13)°. The gallium centre sits 0.610 Å above the plane of the ligand with Ga-N bond distances significantly longer than in the parent compound **1** and has a distorted trigonal bipyramid geometry with N1-Ga-N2 angle being 137.29(11)°. The Ga-Cl distance of 2.2477(10) Å is significantly longer than any of those observed for the gallium(III) complexes and is consistent with the 2.2463(6) Å value reported by Driess for their analogous complex[34] and that of 2.269(2) Å reported by Fischer for the complex [(tmeda)(Cl)Ga—Co(CO)$_5$].[35]

Reduction of **1** to **7** resulted in an increase of the Ga–N bond distances by approximately 0.11 Å (**Table 2.2**). No significant change was observed in the bond distances within the ligand framework suggesting in innocent BZIMPY ligand with the electron pair of the monovalent gallium delocalized in the dative Ga^I→Fe bond. DIMPY's square planar aluminium (^{iPr}DIMPY-AlCl) complex reported by Berben[12] involves an initial reduction of DIMPY ligand with sodium metal followed by the introduction of aluminium trichloride. Comparing bond distances of the two complexes shows a decrease in the Al-N bond distances (opposite to that observed in NBn-BZIMPY) and a significant

change in the bond distances within the ligand. The changes observed in the ligand are reflective of the redox non-innocent nature of DIMPY resulting in a dianionic ligand making the aluminium centre more appropriately described as an Al^{III} centre. Finally, the Ga–Cl distance is also consistent with the assignment of a +1 oxidation state to gallium.
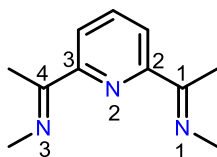
	1	**7**	**[DIMPY-AlCl$_2$]$^+$ (6)**	**[DIMPY-AlCl]^{12}**
M-N1	2.051(3)	2.174(3)	2.0985(16)	1.936(1)
M-N2	2.051(3)	2.148(3)	1.9481(15)	1.820(1)
M-N3	2.063(3)	2.172(3)	2.0961(16)	1.930(1)
M-Cl	2.1905(11); 2.1771(12)	Ga-Cl, 2.2477(10)	2.1121(7); 2.1174(7)	2.1453(8)
N1-C1	1.330(5)	1.316(4)	1.287(2)	1.362(2)
C1-C2	1.476(5)	1.463(5)	1.483(2)	1.426(2)
C2-N2	1.342(5)	1.347(4)	1.337(2)	1.386(2)
N2-C3	1.339(5)	1.349(4)	1.339(5)	1.387(2)
C3-C4	1.467(5)	1.467(5)	1.488(5)	1.413(2)
C4-N3	1.332(5)	1.313(4)	1.287(2)	1.366(2)

Table 2.2. *Selected bond distances (Å) of [NBn-BZIMPYGaCl$_2$][GaCl$_4$] (**1**), [(NBn-BZIMPY)(Cl)Ga—Fe(CO)$_4$] (**7**), [^{iPr}PDIAlCl$_2$][AlCl$_4$] (**6**) and Berben's [^{iPr}PDIAlCl].*
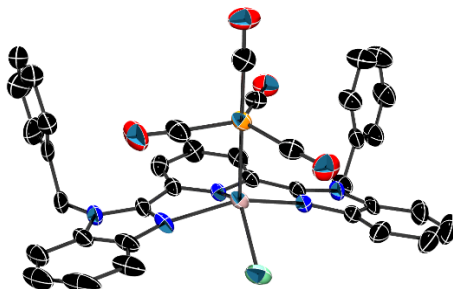
Figure 2.5. *Solid state structure of [(NBn-BZIMPY)(Cl)Ga—Fe(CO)$_4$] (**7**). Thermal ellipsoids are shown at 50% probability level. Hydrogen atoms and solvent molecules are omitted for clarity. Selected bond distances (Å) of **7**: Ga-Fe 2.3861(7), Ga-Cl 2.2477(10), $_{ax}$C-O 1.148(5), $_{eq}$C-O 1.160(4), 1.152(5), 1.162(5). Selected bond distances (Å) of Driess' complex: Ga-Fe 2.4010(12), Ga-Cl 2.2463(6), $_{ax}$C-O 1.149(3), $_{eq}$C-O 1.168(3), 1.157(2), 1.156(3). Other selected bond distances and angles of **7** are given in **Table 2.2**.*

IR absorption bands for complex **7** ν_{CO} = 2072(w), 1980(s) and 1865(s) cm^{-1}) are slightly more spread out in comparison to that reported by Fischer for [(tmeda)(Cl)Ga—Fe(CO)$_4$] (ν_{CO} = 2011, 1928 and 1881 cm^{-1}). Overall, ν_{CO} absorptions of complex **7** are shifted hypsochromic by ~ 60-80 cm^{-1} in comparison to the chloro and alkyl derivatives of the tmeda complexes (**Table 2.3**). Other metal carbonyl (M = Fe, W, Cr and Mo) complexes of gallium and aluminium have been reported where the carbonyl absorption bands generally range between 1863 and 2050 cm^{-1}.[35–37]

Complex	ν_{CO}
[(L)(CH$_3$)Ga—Fe(CO)$_4$]	1992 (vs), 1905 (s), 1863 (vs)
[(L)(CH$_2$CH$_3$)Ga—Fe(CO)$_4$]	1992 (vs), 1905 (s), 1863 (vs)
[(L)(Cl)Ga—Fe(CO)$_4$]	2011 (vs), 1928 (vs), 1881 b (vs)
[(L')Ga—Fe(CO)$_4$]	2032 (s), 1959 (s), 1941 (vs)
[(L'')Ga—Fe(CO)$_4$]	2037 (s), 1966 (s), 1942 (vs)
[(L''')(Cl)Ga—Fe(CO)$_4$] (**7**)	2072(w), 1980(s) and 1865(s)

Table 2.3. *IR absorptions in the ν_{CO} range of complex **7**, Fischer's tmeda based complexes[35] and Robinson's multi-bonded Fe-Ga complex[38] and Jutzi's Cp*Ga-Fe(CO)$_4$ complex[39]. L = tmeda, L' = 2,6-bis(2,4,6-triisopropylphenyl)-phenyl, L'' = Cp* and L''' = NBn-BZIMPY.*

2.2.3 Computational Studies

Density functional theory calculations (M062X/cc-pVTZ) were performed on simplified models of DIMPY (model **A** with R=R'=H) and BZIMPY (model **B** with G=NH and imidazoles in-place of benzimidazoles) in an effort to help rationalize the electronic differences between the two ligands. Selected molecular orbitals of both simplified ligand sets and their optimized geometries are depicted in **Figure 2.6**. The HOMOs of both ligands are π-type MOs and the energy of this MO is significantly higher for BZIMPY, suggesting that this ligand should be a stronger donor. This conclusion is also consistent with the shorter imidazole N-Ga distances in **1**-**3** (determined crystallographically and reproduced computationally) as compared to the imine N-Ga distances in **5**. It is worthy to note however that the energies of the MOs corresponding to the pyridine "lone pair" are energetically very similar for both ligands. The LUMO of DIMPY is significantly lower in energy than that of BZIMPY (−0.89 eV vs −0.47 eV), which suggests that BZIMPY should be a worse electron-acceptor than DIMPY, which is reputed for its non-innocence. Snapping energies of the [LGaCl$_2$]$^+$ (L = BZIMPY or DIMPY ligands) complexes were calculated from optimized complex models and indicate that BZIMPY forms a stronger complex with the [GaCl$_2$]$^+$ fragment than does DIMPY by approximately 75 kcal/mol. This result suggests that, while DIMPY complexes benefit significantly from kinetic stabilization (as discussed previously), the BZIMPY ligand forms more thermodynamically stable complexes with [GaCl$_2$]$^+$

that are not as sterically cumbersome. We postulate that this combination should facilitate further chemistry at the metal site.
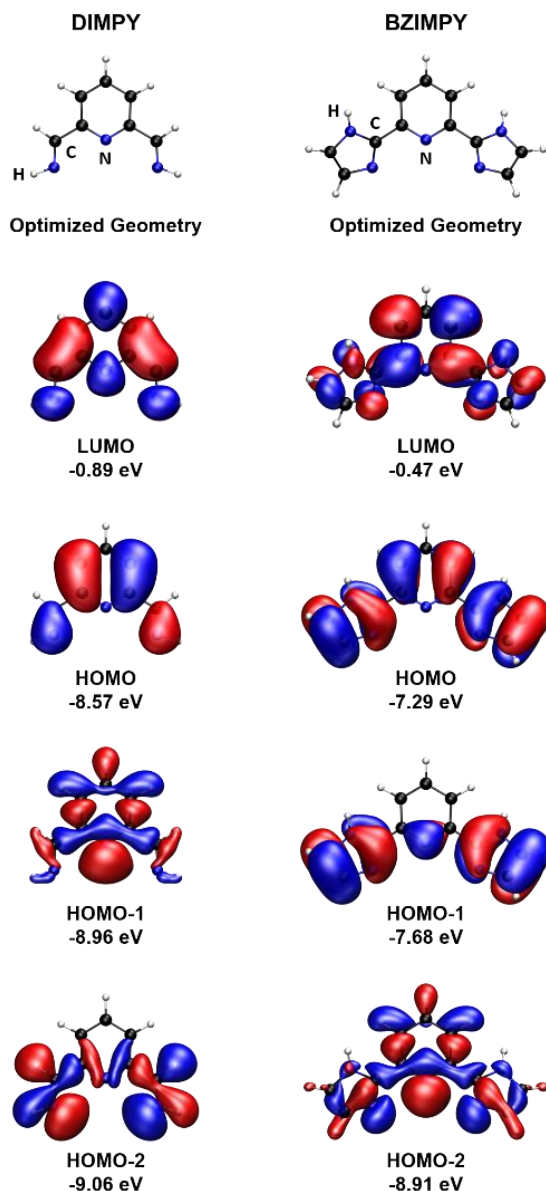
Figure 2.6. *Optimized geometries and selected molecular orbitals of simplified models of DIMPY and BZIMPY (M062X/cc-pVTZ).*

2.3 Conclusions

We report Ga(III) coordination to 2,6-Bis(benzimidazol-2-yl)pyridine (G-BZIMPY, G = NBn, N(3,5-CF$_3$)Bn, N-Allyl and O) ligands. The G-Bzimpy

ligands proved to be more electron-rich and sterically accessible alternatives to 2,6-bis(imino)pyridine (DIMPY) ligands for Group 13 coordination. Compound **1** can be readily reduced to Ga(I) using $K_2[Fe(CO)_4]$ which results in the bimetallic complex NBn-BZIMPYGaClFe(CO)$_4$ (**7**) that contains a rare Ga(I)-Fe(0) linkage with a sterically accessible GaCl that may be available for further chemistry.

2.4 Experimental

2.4.1 General Remarks

All manipulations were carried out using standard inert-atmosphere techniques. All reagents and chemicals were obtained from Sigma-Aldrich. All reagents were used without further purification. MeCN-d_3 was dried over calcium hydride or phosphorus pentoxide, and dichloromethane-d_2 was dried over phosphorus pentoxide. All other solvents were dried on a series of Grubbs-type columns and were degassed prior to use.[40] All glassware was stored in a 170 °C oven for several hours and was degassed prior to use. 2,6-Bis(benzimidazol-2-yl)pyridine (NH-BZIMPY),[41] 2,6-bis(benzoxazol-2-yl)pyridine (O-BZIMPY)[42] and $K_2[Fe(CO)_4]$[43] were all prepared according to the literature procedures.

NMR spectra were recorded at room temperature on Bruker Avance III 500 MHz, Bruker Avance Ultrashield 300 MHz, and Bruker Avance DPX 300 MHz spectrometers. Chemical shifts are reported in parts per million relative to

internal standards for ^{1}H and [13]C (the given deuterated solvent) and external standards for [19]F (CFCl$_3$). Coupling constants |J| are given in hertz. Elemental analysis was performed at the University of Windsor Mass Spectrometry Service Laboratory using a Perkin-Elmer 2400 combustion CHN analyzer. Infrared spectra were recorded using the neat solids on a Bruker ALPHA FT-IR spectrometer using a Platinum ATR sampling module. Stretching frequencies (ν) are reported in cm^{-1} and intensities are reported using the following abbreviations: vw = very weak, w = weak, m = medium, s = strong, vs = very strong.

2.4.2 Synthesis

Alkylation reactions of NH-BZIMPY were carried according to general procedure for the synthesis of NBn-BZIMPY.[55] Similar procedures were carried out to isolate the NAllyl, N(3,5-CF$_3$)Bn derivates:
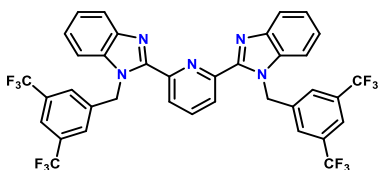
[N(3,5-CF$_3$)Bn-BZIMPY] A 100 mL round bottom flask was charged with NH-BZIMPY (600 mg, 1.93 mmol) and KOH (249 mg, 4.44 mmol) in 30 mL acetone. The reaction mixture was refluxed at 60 °C for one hour before adding 3,5-bis(trifluoromethyl)benzyl bromide (0.78 mL, 4.26 mmol) and was further refluxed for another 12 hours. Volatiles were removed under reduced pressure, and the residue was treated with dichloromethane (20 mL) and filtered.

Filtrate was dried under vacuum and the resulting precipitate was suspended in hexane and collected by filtration to yield N(3,5-CF$_3$)Bn-BZIMPY as an off-white precipitate. Ligand was further dried in a vacuum oven at 60 °C for 16 hours (1.31 g, 89%). ^{1}H NMR (CD$_2$Cl$_2$) δ: 8.44 (d, 2H, $^3J_{HH}$ = 8 Hz), 8.10 (t, 1H, $^3J_{HH}$ = 8 Hz), 7.88 (d, 2H, $^3J_{HH}$ = 8 Hz), 7.78 (b, 2H), 7.38 (s, 6H), 7.30 (m, 2H), 7.18 (d, 2H, $^3J_{HH}$ = 8 Hz), 5.80 (s, 4H). ^{13}C{^{1}H} NMR δ: 150.05, 150.03, 143.46, 140.21, 139.13, 136.41, 132.52 ($^2J_{CF}$ = 33 Hz), 126.96, 126.54, 124.67, 123.78, 123.34 ($^1J_{CF}$ = 272 Hz), 122.23, 120.99, 110.61, 47.88. ^{19}F{^{1}H} NMR δ: −63.47.
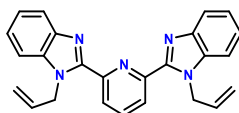
[NAllyl-BZIMPY] A 100 mL round bottom flask was charged with NH-BZIMPY (800 mg, 2.57 mmol) and KOH (331 mg, 5.90 mmol) in 30 mL acetone. The reaction mixture was refluxed at 60 °C for one hour before adding allyl bromide (0.5 mL, 5.77 mmol) and was further refluxed for another 12 hours. Volatiles were removed under reduced pressure, and the residue was treated with dichloromethane (20 mL) and filtered. Filtrate was dried under vacuum and the resulting precipitate was suspended in hexane and collected by filtration to yield NAllyl-BZIMPY as a white precipitate. Ligand was further dried in a vacuum oven at 60 °C for 16 hours (762 g, 76%). ^{1}H NMR (CD$_2$Cl$_2$) δ: 8.40 (d, 2H, $^3J_{HH}$ = 8 Hz), 8.03 (t, 1H, $^3J_{HH}$ = 8 Hz), 7.83 (m, 2H), 7.46 (m, 2H), 7.33 (m, 4H), 5.96 (ddt, 2H, $^3J_{HH}$ = 18 Hz, $^3J_{HH}$ = 10 Hz, $^4J_{HH}$ = 5 Hz), 5.45 (m, 4H), 5.12 (dd, 2H, $^3J_{HH}$ = 10 Hz, $^2J_{HH}$ = 2 Hz), 4.92 (dd, 2H, $^3J_{HH}$ = 18 Hz, $^2J_{HH}$ = 2 Hz). ^{13}C{^{1}H}

NMR δ: 150.29, 143.30, 138.34, 136.98, 133.48, 125.90, 123.82, 123.04, 120.46, 116.96, 111.28, 47.82.
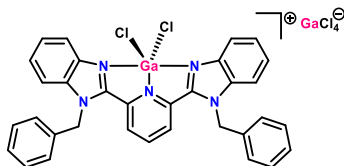
[NBn-BZIMPYGaCl₂][GaCl₄] (**1**) A 100 mL Schlenk flask was charged with NBn-BZIMPY (500 mg, 1.02 mmol) and GaCl₃ (360 mg, 2.04 mmol). To that was added 40 mL of dichloromethane resulting in an immediate formation of a yellow solution. After 2 hours of stirring, the solvent was evaporated under reduced pressure and the resulting solid was suspended in toluene (20 mL), collected and washed with toluene (2×10 mL) yielding **1** as a pale-yellow solid (788 mg, 92%). Slow evaporation from dichloromethane yielded crystals suitable for X-ray Diffraction. ^{1}H NMR (CD₂Cl₂) δ: 8.50 (t, 1H, $^3J_{HH}$ = 8 Hz), 8.33 (d, 2H, $^3J_{HH}$ = 8 Hz), 8.17 (d, 2H, $^3J_{HH}$ = 8 Hz), 7.63 – 7.75 (m, 6H), 7.34 – 7.41 (m, 6H), 7.17 (d, 4H, $^3J_{HH}$ = 8 Hz), 6.01 (s, 4H). ^{13}C{^{1}H} NMR δ: 149.05, 143.01, 140.85, 138.09, 135.56, 132.27, 130.21, 129.51, 128.60, 128.11, 125.76, 125.02, 119.30, 112.21, 49.81. Anal. Calc. for C₃₃H₂₅Cl₆Ga₂N₅ (843.75 g/mol): C, 46.98; H, 2.99; N, 8.30. Found: C, 46.97; H, 3.09; N, 8.06.
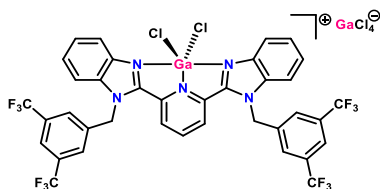
[N(3,5-CF₃)Bn-BZIMPYGaCl₂][GaCl₄] (**2**) A 20 mL vial was charged with N(3,5-CF₃)BnBZIMPY (40 mg, 0.052 mmol) and GaCl₃ (19 mg, 1.04 mmol). 5 mL

of CD$_3$CN was added, resulting in the formation of a yellow solution. The solution was stirred for 1 hr and the solvent was then evaporated under reduced pressure resulting in a yellow solid. Slow evaporation from DCM/CH$_3$CN mix resulted in **2** as yellow crystals suitable for X-ray Diffraction (44 mg, 91%). ^{1}H NMR (CD$_3$CN) δ: 8.53 (t, 1H, $^3J_{HH}$ = 8 Hz), 8.32 (b, 2H), 8.24 (t, 2H, $^3J_{HH}$ = 8 Hz), 8.06 (s, 2H), 7.90 (s, 4H) 7.69-7.77 (m, 6H), 6.18 (s, 4H). ^{13}C{^{1}H} NMR δ: 147.97, 145.15, 144.53, 137.93, 136.62, 131.96 ($^2J_{CF}$ = 33 Hz), 128.04, 127.59, 127.21, 127.15, 124.95, 123.25 ($^1J_{CF}$ = 272 Hz), 122.80, 118.51, 112.79, 48.77. ^{19}F{^{1}H} NMR δ: –63.45. Anal. Calc. for C$_{37}$H$_{21}$Cl$_6$F$_{12}$Ga$_2$N$_5$ (1115.74 g/mol): C; 39.83; H, 1.90; N, 6.28. Found: C; 39.56; H, 1.85; N, 5.97.
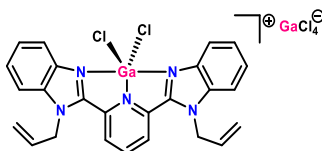
[NAllyl-BZIMPYGaCl$_2$][GaCl$_4$] (**3**) A 20 mL vial was charged with NAllylBZIMPY (30 mg, 0.08 mmol) and GaCl$_3$ (29 mg, 0.16 mmol). 5 mL of CD$_2$Cl$_2$ was added, resulting in the formation of a yellow solution. The solution was allowed to stir overnight and was then left to slowly evaporate resulting in **3** as yellow crystals (50 mg, 85%). ^{1}H NMR (CD$_2$Cl$_2$) δ: 8.83 (t, 1H, $^3J_{HH}$ = 8 Hz), 8.42 (d, 2H, $^3J_{HH}$ = 8 Hz), 8.28 (m, 2H), 7.72 (b, 6H), 6.27 (ddt, 2H, $^3J_{HH}$ = 18 Hz, $^3J_{HH}$ = 10 Hz, $^4J_{HH}$ = 4 Hz), 5.50 (d, 2H, $^3J_{HH}$ = 10 Hz), 5.43 (b, 4H), 5.14 (d, 2H, $^3J_{HH}$ = 18 Hz). ^{13}C{^{1}H} NMR δ: 149.02, 142.88, 141.35, 137.89, 135.77, 129.34, 128.71, 128.23, 125.15, 119.90, 119.20, 112.48, 48.78. Anal. Calc. for

$C_{25}H_{21}Cl_6Ga_2N_5$ (743.63 g/mol): C, 40.38; H, 2.85; N, 9.42. Found: C, 39.62; H, 2.58; N, 9.24.
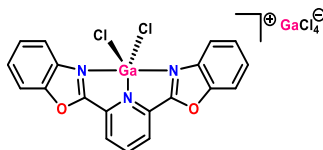
[O-BZIMPYGaCl₂][GaCl₄] (**4**) A 20 mL vial was charged with O-BZIMPY (30 mg, 0.1 mmol) and $GaCl_3$ (36 mg, 0.2 mmol). 5 mL of CH_2Cl_2 was added, and the mixture was sonicated for 24 hours resulting in a yellow suspension and yellow crystals surrounding the inside of the vial, suitable for X-ray diffraction. Upon evaporating DCM, **4** was collected as a yellow solid that is poorly soluble; A dilute solution in CD_3CN however, allowed for NMR analysis (50 mg, 85%). ^1H NMR (CD_3CN) δ: 9.00 (t, 1H, $^3J_{HH}$ = 8 Hz), 8.82 (d, 2H, $^3J_{HH}$ = 8 Hz), 8.17 (b, 2H), 8.05 (b, 2H), 7.83 (b, 4H). $^{13}C\{^1H\}$ NMR δ: 159.93, 154.27, 150.54, 140.42, 134.45, 131.14, 129.74, 127.48, 119.73, 114.37. Anal. Calc. for $C_{19}H_{11}Cl_6Ga_2N_3O_2$ (665.46 g/mol): C, 34.29; H, 1.67; N, 6.31. Found: C, 33.91; H, 1.49; N, 6.29.
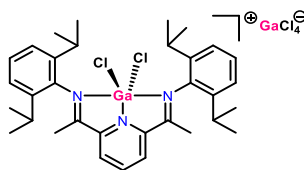
[^{iPr}PDIGaCl₂][GaCl₄] (**5**) A 100 mL Schlenk flask was charged with ^{iPr}PDI (313 mg, 0.65 mmol) and $GaCl_3$ (229 mg, 1.30 mmol). To that was added 40 mL of dichloromethane resulting in an immediate formation of a yellow solution. The reaction was stirred for 16 hours, solvent was then evaporated under reduced pressure and the resulting solid was suspended in Et_2O (20 mL), collected and

washed with Et_2O (2×10 mL) yielding **5** as a yellow solid (430 mg, 81%). Slow evaporation from dichloromethane yielded crystals suitable for X-ray Diffraction. ^{1}H NMR (CD_3CN) δ: 8.96 (t, 1H, $^3J_{HH}$ = 8 Hz), 8.78 (d, 2H, $^3J_{HH}$ = 8 Hz), 7.42 (dd, 2H, $^3J_{HH}$ = 8 Hz), 7.36 (d, 4H, $^3J_{HH}$ = 8 Hz), 2.82 (sept, 4H, $^3J_{HH}$ = 7 Hz), 2.65 (s, 6H), 1.23 (d, 12H, $^3J_{HH}$ = 7 Hz), 1.07 (d, 12H, $^3J_{HH}$ = 7 Hz). $^{13}C\{^1H\}$ NMR δ: 172.19, 149.70, 144.61, 142.29, 137.93, 131.93, 129.86, 125.81, 29.60, 25.25, 24.53, 20.01. Anal. Calc. for $C_{33}H_{43}Cl_6Ga_2N_3$ (833.87g/mol): C, 47.53; H, 5.20; N, 5.04. Found: C, 48.16; H, 4.78; N, 4.64.
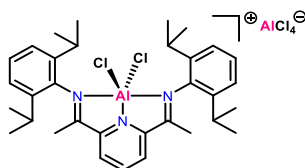
[^{iPr}PDIAlCl$_2$][AlCl$_4$] (**6**) A 100 mL Schlenk flask was charged with ^{iPr}PDI (456 mg, 0.95 mmol) and $AlCl_3$ (252 mg, 1.90 mmol). To that was added 40 mL of dichloromethane resulting in an immediate formation of a yellow solution. The reaction was stirred for 16 hours, solvent was then evaporated under reduced pressure and the resulting solid was suspended in Et_2O (20 mL), collected and washed with Et_2O (2×10 mL) yielding **6** as a yellow solid (680 mg, 96%). Slow evaporation from dichloromethane yielded crystals suitable for X-ray Diffraction. ^{1}H NMR (CD_3CN) δ: 8.93 (t, 1H, $^3J_{HH}$ = 8 Hz), 8.70 (d, 2H, $^3J_{HH}$ = 8 Hz), 7.41 (dd, 2H, $^3J_{HH}$ = 8 Hz), 7.34 (d, 4H, $^3J_{HH}$ = 8 Hz), 2.84 (sept, 4H, $^3J_{HH}$ = 8 Hz), 2.63 (s, 6H), 1.20 (d, 12H, $^3J_{HH}$ = 8 Hz), 1.07 (d, 12H, $^3J_{HH}$ = 8 Hz). $^{13}C\{^1H\}$ NMR δ: 174.66, 148.30, 145.29, 141.43, 137.97, 130.14, 128.73, 124.92, 28.55,

25.25, 24.27, 22.19. Anal. Calc. for $C_{33}H_{43}Cl_6Al_2N_3$ (748.39 g/mol): C, 52.96; H, 5.79; N, 5.61. Found: C, 52.35; H, 6.06; N, 5.46.
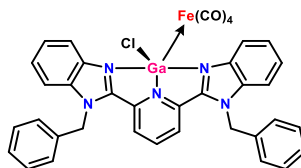
NBn-BZIMPYGaClFe(CO)₄ (**7**) A 20 mL vial was charged with **1** (30 mg, 0.036 mmol) and $K_2[Fe(CO)_4]$ (9 mg, 0.036 mmol). 5 mL of pre-cooled (–40 °C) THF was added resulting in an immediate formation of a dark red/purple solution. The solution stirred for 1 hr before filtration. The filtrate was collected and left at –40 °C for two days to yield (**7**) as deep red crystals suitable for X-ray Diffraction (15 mg, 56%). IR (v_{CO}, cm^{-1}): 2072(w), 1980(s) and 1865(s). ^{1}H NMR (THF-d_8) δ: 8.55 (d, 2H, $^3J_{HH}$ = 8 Hz), 8.28 (t, 1H, $^3J_{HH}$ = 8 Hz), 8.17 (d, 2H, $^3J_{HH}$ = 8 Hz), 7.62 (d, 2H, $^3J_{HH}$ = 8 Hz), 7.47 (m, 4H), 7.33 (m, 6H), 7.22 (d, 4H, $^3J_{HH}$ = 8 Hz), 6.07 (s, 4H). ^{13}C{^{1}H} NMR δ: 220.08, 149.84, 142.70, 138.54, 138.21, 135.78, 130.15, 129.89, 129.19, 128.61, 127.81, 126.50, 125.54, 121.95, 111.55, 48.97. Anal. Calc. for $C_{37}H_{25}ClFeGaN_5O_4$ (765.65 g/mol): C, 58.12; H, 3.30; N, 9.16. Found: C, 56.71; H, 3.46; N, 8.90.

2.4.3 Computational Details

Calculations were performed with the Gaussian 09 suite of programs[44] using Compute Canada's Shared Hierarchical Academic Research Computing Network (SHARCNET). Model complexes were fully optimized with no symmetry constraints using the M06-2X density functional method,[45] in

conjunction with the cc-pVTZ basis set.[46,47] Geometry optimizations were started using models in which the relevant non-hydrogen atoms were placed in positions found experimentally by X-ray crystallography using Gaussview.[48] Frequency calculations were also performed at the same level of theory in order to confirm that the optimized structures were minima on the potential energy hypersurface and to determine thermochemical and vibrational information. Natural bond orbital (NBO) analyses[49] to determine orbital contributions, Wiberg Bond Indices and orbital energies were obtained using the routine included in the Gaussian distributions.[50] Visualizations of the Kohn-Sham orbitals and optimized geometries were made using Gaussview.[48] Snapping energies were calculated by subtracting the sum of the single point energies of the $GaCl_2+$ and ligand fragments (separately) from the energy of their optimized complexes.

2.4.4 X-ray Crystallography

Crystals for investigation were covered in Paratone®, mounted onto a goniometer head, and then rapidly cooled under a stream of cold N_2 of the low-temperature apparatus (Oxford Cryostream) attached to the diffractometer. The data were then collected using the APEXII (Bruker AXS) software suite on a Bruker Photon 100 CMOS diffractometer using a graphite monochromator with MoK_α (λ = 0.71073 Å). For each sample, data were collected at low temperature. APEXII software was used for data reductions and SADABS (Bruker AXS) was used for absorption corrections (multi-scan; semi-empirical

from equivalents). XPREP was used to determine the space group and the structures were solved and refined using the SHELX[51] software suite as implemented in the WinGX[52] or OLEX2[53] program suites. Validation of the structures was conducted using PLATON[54] and the structures have been deposited in the Cambridge Structural Database (CCDC 1857723-1857729).

Compound Name	[NBn-BZIMPYGaCl$_2$] [GaCl$_4$]	[N(3,5-CF$_3$)Bn-BZIMPYGaCl$_2$] [GaCl$_4$]	[NAllyl-BZIMPYGaCl$_2$] [GaCl$_4$]
Label	**1**	**2**	**3**
CCDC ID	1857729	1857726	1857728
Empirical formula	C$_{33}$H$_{27}$Cl$_6$Ga$_2$N$_5$	C$_{37}$H$_{21}$Cl$_6$F$_{12}$Ga$_2$N$_5$	C$_{25}$H$_{20}$Cl$_6$Ga$_2$N$_5$
Formula weight	845.73	1115.73	742.6
Temperature (K)	170	170	169.81
Crystal system	triclinic	triclinic	monoclinic
Space group	P–1	P–1	P2$_1$/n
a (Å)	7.7334(9)	9.0074(7)	9.6466(7)
b (Å)	13.7970(16)	14.0425(10)	18.8631(12)
c (Å)	16.6692(17)	17.2131(14)	16.5594(11)
α (°)	92.736(4)	81.875(2)	90
β (°)	102.861(4)	86.671(3)	102.788(2)
γ (°)	101.348(4)	75.708(2)	90
Volume (Å^3)	1692.2(3)	2088.1(3)	2938.5(3)
Z	2	2	4
ρ$_{calc}$ (g·cm^{-3})	1.66	1.775	1.679
μ (mm^{-1})	2.099	1.765	2.405
F(000)	848	1100	1476
Crystal size (mm^3)	0.34 × 0.2 × 0.2	0.34 × 0.311 × 0.3	0.31 × 0.24 × 0.075
Radiation	MoKα (λ = 0.71073)	MoKα (λ = 0.71073)	MoKα (λ = 0.71073)
2Θ range for data collection (°)	5.622 to 61.204	5.68 to 60.068	5.884 to 60.058
Index ranges	−11 ≤ h ≤ 11 −19 ≤ k ≤ 19 −23 ≤ l ≤ 21	−12 ≤ h ≤ 12 −19 ≤ k ≤ 19 −24 ≤ l ≤ 24	−13 ≤ h ≤ 13 −26 ≤ k ≤ 26 −23 ≤ l ≤ 23
Reflections collected	110801	121980	115507
Independent reflections	10302 R$_{int}$ = 0.0465 R$_{sigma}$ = 0.0236	12167 R$_{int}$ = 0.0356 R$_{sigma}$ = 0.0202	8584 R$_{int}$ = 0.0695 R$_{sigma}$ = 0.0268
Data/restraints /parameters	10302/0/415	12167/40/587	8584/0/359
Goodness-of-fit on F^2	1.079	1.059	1.039
Final R indexes [I>=2σ(I)]	R$_1$ = 0.0579 wR$_2$ = 0.1827	R$_1$ = 0.0458 wR$_2$ = 0.0994	R$_1$ = 0.0268 wR$_2$ = 0.0611
Final R indexes [all data]	R$_1$ = 0.0715 wR$_2$ = 0.1947	R$_1$ = 0.0622 wR$_2$ = 0.1130	R$_1$ = 0.0357 wR$_2$ = 0.0648
Largest diff. peak/hole (e·Å^{-3})	1.72/−1.03	1.69/−0.98	0.65/−0.78
Refinement method	Full-matrix least-squares on F^2		

$$R_1 = \frac{\sum||F_o|-|F_c||}{\sum|F_o|} \qquad wR_2 = \sqrt{\frac{\sum w(F_o{}^2 - F_c{}^2)^2}{\sum w(F_o{}^2)^2}} \qquad R_{int} = \frac{\sum|F_o{}^2 - F_o{}^2(mean)|}{\sum F_o{}^2} \qquad R_{sigma} = \frac{\sum \sigma(F_o{}^2)}{\sum F_o}$$

Table 2.4. *Crystallographic data and structure refinement.*

2,6-Bis(benzimidazol-2-yl)pyridine as More Electron-Rich and Sterically Accessible Alternatives to 2,6-bis(imino)pyridine for Group 13 Coordination Chemistry

Compound Name	[O-BZIMPYGaCl₂] [GaCl₄]	[^{iPr}PDIGaCl₂][GaCl₄] C₄H₈O	[^{iPr}PDIAlCl₂][AlCl₄] CH₂Cl₂
Label	4	5	6
CCDC ID	1857724	1857725	1857727
Empirical formula	C₇₆H₄₄Cl₂₄Ga₈N₁₂O₈	C₃₇H₅₁Cl₆Ga₂N₃O	C₃₄H₄₅Al₂Cl₈N₃
Formula weight	2661.79	905.94	833.29
Temperature (K)	170.08	170	170
Crystal system	monoclinic	monoclinic	monoclinic
Space group	P2₁/c	P2₁/n	P2₁/c
a (Å)	9.692	9.7574(9)	10.3391(10)
b (Å)	9.329	10.4579(9)	31.617(3)
c (Å)	26.919	41.051(4)	13.0556(12)
α (°)	90	90	90
β (°)	99.92	95.473(2)	106.521(2)
γ (°)	90	90	90
Volume (Å³)	2397.6	4169.8(6)	4091.6(7)
Z	1	4	4
ρ_{calc} (g·cm⁻³)	1.844	1.443	1.353
μ (mm⁻¹)	9.119	1.709	0.622
F(000)	1304	1864	1728
Crystal size (mm³)	0.43 × 0.37 × 0.15	0.37 × 0.218 × 0.176	0.37 × 0.34 × 0.33
Radiation	CuKα (λ = 1.54178)	MoKα (λ = 0.71073)	MoKα (λ = 0.71073)
2Θ range for data collection (°)	6.666 to 149.228	5.724 to 58.402	5.9 to 58.444
Index ranges	−12 ≤ h ≤ 12 −11 ≤ k ≤ 11 −33 ≤ l ≤ 33	−13 ≤ h ≤ 13 −14 ≤ k ≤ 14 −56 ≤ l ≤ 56	−14 ≤ h ≤ 13 −43 ≤ k ≤ 43 −17 ≤ l ≤ 17
Reflections collected	38330	111488	80246
Independent reflections	4898 R_{int} = 0.0732 R_{sigma} = 0.0464	11291 R_{int} = 0.0330 R_{sigma} = 0.0178	11071 R_{int} = 0.0327 R_{sigma} = 0.0192
Data/restraints /parameters	4898/162/289	11291/0/452	11071/51/463
Goodness-of-fit on F²	1.166	1.072	1.043
Final R indexes [I>=2σ(I)]	R₁ = 0.0664 wR₂ = 0.1744	R₁ = 0.0380 wR₂ = 0.0818	R₁ = 0.0523 wR₂ = 0.1268
Final R indexes [all data]	R₁ = 0.0670 wR₂ = 0.1752	R₁ = 0.0458 wR₂ = 0.0851	R₁ = 0.0599 wR₂ = 0.1323
Largest diff. peak/hole (e·Å⁻³)	0.91/−1.64	1.07/−0.91	1.59/−1.52
Refinement method	Full-matrix least-squares on F²		

$$R_1 = \frac{\sum||F_o|-|F_c||}{\sum|F_o|} \qquad wR_2 = \sqrt{\frac{\sum w(F_o{}^2-F_c{}^2)^2}{\sum w(F_o{}^2)^2}} \qquad R_{int} = \frac{\sum|F_o{}^2-F_o{}^2(mean)|}{\sum F_o{}^2} \qquad R_{sigma} = \frac{\sum \sigma(F_o{}^2)}{\sum F_o}$$

Table 2.5. *Crystallographic data and structure refinement.*

2,6-Bis(benzimidazol-2-yl)pyridine as More Electron-Rich and Sterically Accessible Alternatives to 2,6-bis(imino)pyridine for Group 13 Coordination Chemistry

Compound Name	[NBn-BZIMPYGa–Fe(CO)$_4$] 2(C$_4$H$_8$O)
Label	7
CCDC ID	1857723
Empirical formula	C$_{45}$H$_{41}$ClFeGaN$_5$O$_6$
Formula weight	908.85
Temperature (K)	170.05
Crystal system	monoclinic
Space group	P2$_1$/c
a (Å)	9.7841(14)
b (Å)	15.069(2)
c (Å)	28.034(4)
α (°)	90
β (°)	92.701(4)
γ (°)	90
Volume (Å^3)	4128.8(10)
Z	4
ρ$_{calc}$ (g·cm^{-3})	1.462
μ (mm^{-1})	1.124
F(000)	1872
Crystal size (mm^3)	0.26 × 0.2 × 0.09
Radiation	MoKα (λ = 0.71073)
2Θ range for data collection (°)	5.856 to 53.466
Index ranges	−12 ≤ h ≤ 12 −19 ≤ k ≤ 19 −35 ≤ l ≤ 35
Reflections collected	64624
Independent reflections	8735 R$_{int}$ = 0.0777 R$_{sigma}$ = 0.0474
Data/restraints /parameters	8735/132/532
Goodness-of-fit on F^2	1.118
Final R indexes [I>=2σ(I)]	R$_1$ = 0.0623 wR$_2$ = 0.1433
Final R indexes [all data]	R$_1$ = 0.0866 wR$_2$ = 0.1568
Largest diff. peak/hole (e·Å^{-3})	0.73/−0.89
Refinement method	Full-matrix least-squares on F^2

$$R_1 = \frac{\sum||F_o|-|F_c||}{\sum|F_o|} \qquad wR_2 = \sqrt{\frac{\sum w(F_o{}^2 - F_c{}^2)^2}{\sum w(F_o{}^2)^2}} \qquad R_{int} = \frac{\sum|F_o{}^2 - F_o{}^2(mean)|}{\sum F_o{}^2} \qquad R_{sigma} = \frac{\sum \sigma(F_o{}^2)}{\sum F_o{}^2}$$

Table 2.6. *Crystallographic data and structure refinement.*

CHAPTER 2
2,6-Bis(benzimidazol-2-yl)pyridine as More Electron-Rich and Sterically Accessible Alternatives to 2,6-
bis(imino)pyridine for Group 13 Coordination Chemistry

2.5 References

(1)   Peris, E.; Crabtree, R. H. *Chem. Soc. Rev.* **2018**, *47*, 1959–1968.

(2)   Gibson, V. C.; Spitzmesser, S. K. *Chem. Rev.* **2003**, *103* (1), 283–315.

(3)   De Bruin, B.; Bill, E.; Bothe, E.; Weyhermüller, T.; Wieghardt, K. *Inorg. Chem.* **2000**, *39* (13), 2936–2947.

(4)   Chirik, P. J.; Wieghardt, K. *Science* **2010**, *327* (5967), 794–795.

(5)   Jurca, T.; Lummiss, J.; Burchell, T. J.; Gorelsky, S. I.; Richeson, D. S. *J. Am. Chem. Soc.* **2009**, *131* (13), 4608–4609.

(6)   Reeske, G.; Cowley, A. H. *Chem. Commun.* **2006**, *372* (16), 1784.

(7)   Martin, C. D.; Ragogna, P. J. *Dalton Trans.* **2011**, *40* (44), 11976.

(8)   Flock, J.; Suljanovic, A.; Torvisco, A.; Schoefberger, W.; Gerke, B.; Pöttgen, R.; Fischer, R. C.; Flock, M. *Chem. Eur. J.* **2013**, *19* (46), 15504–15517.

(9)   Chu, T.; Belding, L.; van der Est, A.; Dudding, T.; Korobkov, I.; Nikonov, G. I. *Angew. Chem. - Int. Ed.* **2014**, *53* (10), 2711–2715.

(10)   Baker, R. J.; Jones, C.; Kloth, M.; Mills, D. P. *New J. Chem.* **2004**, *28*, 207–213.

(11)   Jurca, T.; Dawson, K.; Mallov, I.; Burchell, T.; Yap, G. P. a; Richeson, D. S. *Dalton Trans.* **2010**, *39* (5), 1266–1272.

(12)   Thompson, E. J.; Myers, T. W.; Berben, L. A. *Angew. Chem. - Int. Ed.* **2014**, *53* (51), 14132–14134.

(13)   Myers, T. W.; Berben, L. A. *J. Am. Chem. Soc.* **2013**, *135* (27), 9988–9990.

(14) Myers, T. W.; Berben, L. A. *Chem. Sci.* **2014**, *5* (7), 2771–2777.

(15) Scott, J.; Gambarotta, S.; Korobkov, I.; Knijnenburg, Q.; De Bruin, B.; Budzelaar, P. H. M. *J. Am. Chem. Soc.* **2005**, *127* (49), 17204–17206.

(16) Zhang, Y.; Zhou, Q. F.; Huo, G. F.; Yin, G. Q.; Zhao, X. L.; Jiang, B.; Tan, H.; Li, X.; Yang, H. B. *Inorg. Chem.* **2018**, *57* (7), 3516–3520.

(17) Mansour, A. M.; Shehab, O. R. *Eur. J. Inorg. Chem.* **2017**, (37), 4299–4310.

(18) Zheng, Y.; He, L.; Zhang, D. Y.; Tan, C. P.; Ji, L. N.; Mao, Z. W. *Dalton Trans.* **2017**, *46* (34), 11395–11407.

(19) Günnaz, S.; Özdemir, N.; Dayan, S.; Dayan, O.; Çetinkaya, B. *Organometallics* **2011**, *30* (15), 4165–4173.

(20) Liu, S. G.; Zuo, J. L.; Li, Y. Z.; You, X. Z. *J. Mol. Struct.* **2004**, *705* (1–3), 153–157.

(21) Sheng-Guia, L.; Zi-Lub, C.; Kaic, L.; Xiao-Linga, C. *Chin. J. Struct. Chem.* **2013**, (5) 637–642.

(22) Evans, D. A.; Kozlowski, M. C.; Burgey, C. S.; MacMillan, D. W. C. *J. Am. Chem. Soc.* **1997**, *119* (33), 7893–7894.

(23) Yang, Y.; Li, C. G.; Luo, X. J.; Luo, Z. H.; Liu, R. J.; Jiang, Y. X.; Liang, W. J. *Synth. React. Inorg., Met. -Org., Nano-Met. Chem.* **2016**, *46* (9), 1376–1380.

(24) Morsali, A.; Mahjoub, A. *Inorg. Chem. Commun.* **2004**, *7* (7), 915–918.

(25) Kocherga, M.; Castaneda, J.; Walter, M. G.; Zhang, Y.; Saleh, N.-A.; Wang, L.; Jones, D. S.; Merkert, J. W.; Donovan-Merkert, B.; Li, Y.; Hofmann, T.; Schmedake, T. A.

Chem. Commun. **2018**.

(26) Yu, X.-Y.; Zou, H.-H.; Wei, L.-Q.; Zeng, M.-H. *Inorg. Chem. Commun.* **2010**, *13* (10), 1137–1139.

(27) Wei, L.-Q.; Zeng, M.-H.; Ng, S. W. *Acta Crystallogr., Sect. E: Struct. Rep. Online,* ***2010***, *66, m56–m56.*

(28) Thompson, J. R.; Snider, D.; Wren, J. E. C.; Kroeker, S.; Williams, V. E.; Leznoff, D. B. *Eur. J. Inorg. Chem.* **2017**, (1), 88–98.

(29) Meng, F. Y.; Zhou, Y. L.; Zou, H. H.; Zeng, M. H.; Liang, H. *J. Mol. Struct.* **2009**, *920* (1–3), 238–241.

(30) Swidan, A.; Suter, R.; Macdonald, C. L. B.; Burford, N. *Chem. Sci.* **2018**, *9* (26), 5837–5841.

(31) Suter, R.; Swidan, A.; Macdonald, C. L. B.; Burford, N. *Chem. Commun.* **2018**, *54* (33), 4140–4143.

(32) Suter, R.; Gray, P. A.; Burford, N.; McDonald, R. *Chem. Eur. J.* **2018**, *24* (18), 4718–4723.

(33) Knijnenburg, Q.; Smits, J. M. M.; Budzelaar, P. H. M. *Organometallics* **2006**, *25* (4), 1036–1046.

(34) Tan, G.; Szilvási, T.; Inoue, S.; Blom, B.; Driess, M. *J. Am. Chem. Soc.* **2014**, *136* (27), 9732–9742.

(35) Fischer, R. A.; Schulte, M. M.; Weiss, J.; Zsolnai, L.; Jacobi, A.; Huttner, G.; Frenking, G.; Boehme, C.; Vyboishchikov, S. F. *J. Am. Chem. Soc.* **1998**, *120* (6),

1237–1248.

(36)   Adamczyk, T.; Li, G. M.; Linti, G.; Pritzkow, H.; Seifert, A.; Zessin, T. *Eur. J. Inorg. Chem.* **2011**, (23), 3480–3492.

(37)   Fölsing, H.; Segnitz, O.; Bossek, U.; Merz, K.; Winter, M.; Fischer, R. A. *J. Organomet. Chem.* **2000**, *606* (2), 132–140.

(38)   Su, J.; Li, X.-W.; Crittendon, R. C.; Campana, C. F.; Robinson, G. H. *Organometallics* **1997**, *16* (21), 4511–4513.

(39)   Jutzi, P.; Neumann, B.; Reumann, G.; Stammler, H.-G. *Organometallics* **1998**, *17* (7), 1305–1314.

(40)   Pangborn, A. B.; Giardello, M. A.; Grubbs, R. H.; Rosen, R. K.; Timmers, F. J. *Organometallics* **1996**, *15* (5), 1518–1520.

(41)   Addison, A. W.; Rao, T. N.; Wahlgren, C. G. *J. Heterocycl. Chem.* **1983**, 20, 1481–1484.

(42)   Singh, A.; Das, G.; Mondal, B. *Polyhedron* **2008**, *27* (12), 2563–2568.

(43)   Baby, A.; Brunet, J. J.; Kindela, F. B.; Neibecker, D. *Synth. Commun.* **1994**, *24* (20), 2827–2834.

(44)   Frisch, M. J.; Trucks, G. W.; Schlegel, H. B.; Scuseria, G. E.; Robb, M. A.; Cheeseman, J. R.; Scalmani, G.; Barone, V.; Mennucci, B.; Petersson, G. A.; Nakatsuji, H.; Caricato, M.; Li, X.; Hratchian, H. P.; Izmaylov, A. F.; Bloino, J.; Zheng, G.; Sonnenberg, J. L.; Hada, M.; Ehara, M.; Toyota, K.; Fukuda, R.; Hasegawa, J.; Ishida, M.; Nakajima, T.; Honda, Y.; Kitao, O.; Nakai, H.; Vreven, T.;

Montgomery, J., J. A.; Peralta, J. E.; Ogliaro, F.; Bearpark, M.; Heyd, J. J.; Brothers, E.; Kudin, K. N.; Staroverov, V. N.; Kobayashi, R.; Normand, J.; Raghavachari, K.; Rendell, A.; Burant, J. C.; Iyengar, S. S.; Tomasi, J.; Cossi, M.; Rega, N.; Millam, N. J.; Klene, M.; Knox, J. E.; Cross, J. B.; Bakken, V.; Adamo, C.; Jaramillo, J.; Gomperts, R.; Stratmann, R. E.; Yazyev, O.; Austin, A. J.; Cammi, R.; Pomelli, C.; Ochterski, J. W.; Martin, R. L.; Morokuma, K.; Zakrzewski, V. G.; Voth, G. A.; Salvador, P.; Dannenberg, J. J.; Dapprich, S.; Daniels, A. D.; Farkas, Ö.; Foresman, J. B.; Ortiz, J. V.; Cioslowski, J.; Fox, D. J. *Gaussian 09*; Gaussian, Inc.: Wallingford CT, 2009.

(45) Zhao, Y.; Truhlar, D. G. *Theor. Chem. Acc.* **2008**, *120* (1–3), 215–241.

(46) Dunning, T. H. *J. Chem. Phys.* **1989**, *90* (2), 1007–1023.

(47) Woon, D. E.; Dunning, T. H. *J. Chem. Phys.* **1993**, *98* (2), 1358–1371.

(48) *Gaussview 3.0*; Gaussian Inc: Pittsburgh, 2003.

(49) Reed, A. E.; Curtiss, L. A.; Weinhold, F. *Chem. Rev.* **1988**, *88* (6), 899–926.

(50) Glendening, E. D.; Badenhoop, J. K.; Reed, A. E.; Carpenter, J. E.; Bohmann, J. A.; Morales, C. M.; Landis, C. R.; Weinhold, F. *NBO 6.0*; Theoretical Chemistry Institute, University of Wisconsin: Madison, WI, 2013.

(51) Sheldrick, G. M. *Acta Crystallogr., Sect. A Found. Crystallogr.* **2008**, *64* (1), 112–122.

(52) Farrugia, L. J. *J. Appl. Crystallogr.* **1999**, *32* (4), 837–838.

(53) Dolomanov, O. V.; Bourhis, L. J.; Gildea, R. J.; Howard, J. A. K.; Puschmann, H. *J. Appl. Crystallogr.* **2009**, *42* (2), 339–341.

(54)   Spek, A. L. *J. Appl. Crystallogr.* **2003**, *36* (1), 7–13.

(55)   Inkaya, E.; Gunnaz, S.; Ozdemir, N.; Dayan, O.; Dincer, M.; Cetinkaya, B. *Spectrochim. Acta, Part A,* **2013**, *103*, 255–263.

CHAPTER 3:
2,6-Bis(benzimidazol-2-yl)pyridine Complexes of Group 14 Elements

3.1 Introduction

Neutral trinitrogen donor ligands such as bis(imino)pyridine ($^{R'}$DIMPY, **A**) have played an important role in transition metal chemistry and have generated highly active catalysts[1–3] for ethylene polymerisation.[4] In several instances, variously substituted $^{R'}$DIMPY ligands bound to main group elements have allowed for the isolation of different low valent fragments including: Ge(0)[5], Sn(0) [6], As(I)[7], P(I)[8], and In(I)[9].

E = Ge, Sn   EX = GeCl⁺, SnCl⁺   E = Ge²⁺, Sn²⁺
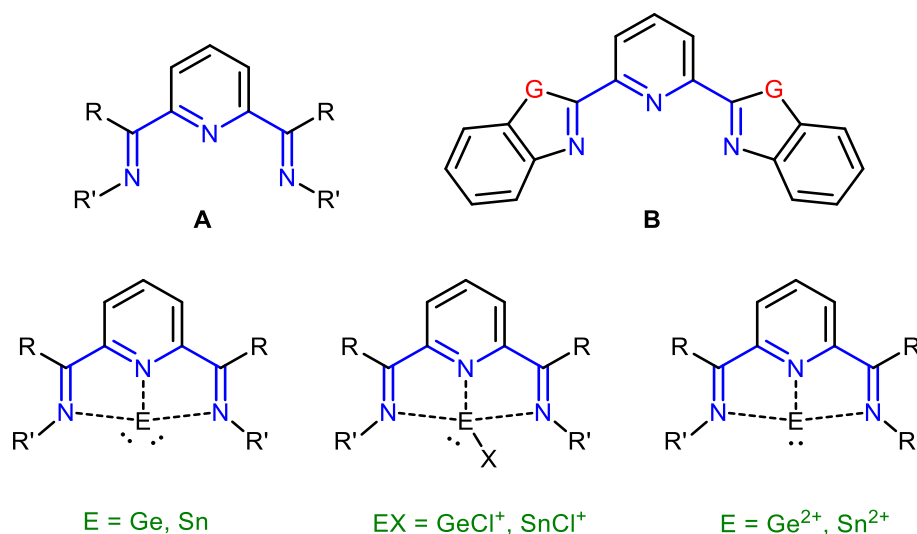
Scheme 3.1. *Top: DIMPY (A) vs G-BZIMPY (G = NH, NBn, N(3,5-CF₃)Bn, NAllyl and O). Bottom: DIMPY complexes of group 14 elements.*

The use of pincer ligands with group 14 elements dates back to 1985 - before the term "pincer" was even adopted - where Archer and co-workers reported the synthesis of a tripyridine tin(II)chloride complexes.[10] Pincer

ligands are very tuneable allowing for the introduction of asymmetry in the ligand producing a chiral catalyst. Evans and co-workers reported the tin(II) chiral Lewis acid shown in **Figure 3.1** that have been used in aldol condensation reactions, resulting in good yields with greater than 90% ee.[11]
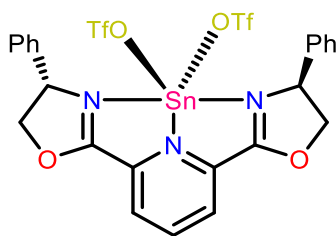
Figure 3.1. *Evans tin(II) chiral Lewis acid catalyst.*

DIMPY ligands have also been important in the development of group 14 low-valent chemistry. Roesky reported the self-ionization products of [iPr]DIMPY with the corresponding $GeCl_2$ and $SnCl_2$[12] to yield [[iPr]DIMPYMCl][MCl_3] (M = Ge, Sn). Nikonov later showed that treating the germanium complex with 2 equivalents of potassium graphite (KC_8) in benzene results in a Ge(0) complex [[iPr]DIMPYGe(0)] as shown in **Scheme 3.2**.[5] Other variants of the [R']DIMPYE(II) (E = Ge, Sn) have also been reported.[13,14]
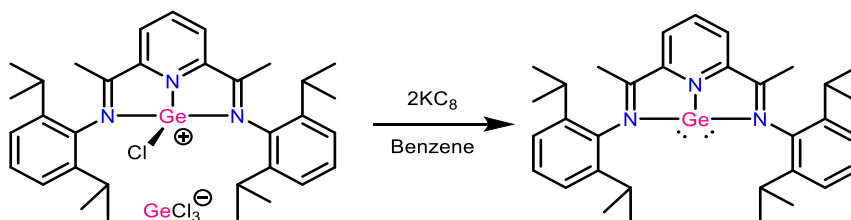
Scheme 3.2. *Nikonov's synthesis of [[iPr]DIMPYGe(0)].*

In this work, we explore the coordination of group 14 elements to different variants of G-BZIMPY (ligands **B**, **Scheme 3.1**). These ligands are

more rigid than their DIMPY analogues and there have been a few examples of complexes reported featuring transition metals.[15-18] We recently reported the coordination of different G-BZIMPY ligands to Ga(III) centres, and determined that G-BZIMPY are electron-rich and sterically accessible alternatives to DIMPY ligands for group 13 coordination chemistry.[19] Complexes of BZIMPY ligands with indium[20,21] and lead have also been investigated.[22-28] Recent work by Schmedake[29] and co-workers reported the synthesis of a Si(BZIMPY)₂ complex (**Scheme 3.3**) as a potential electron transport layer and electroluminescent layer in organic electronic devices.
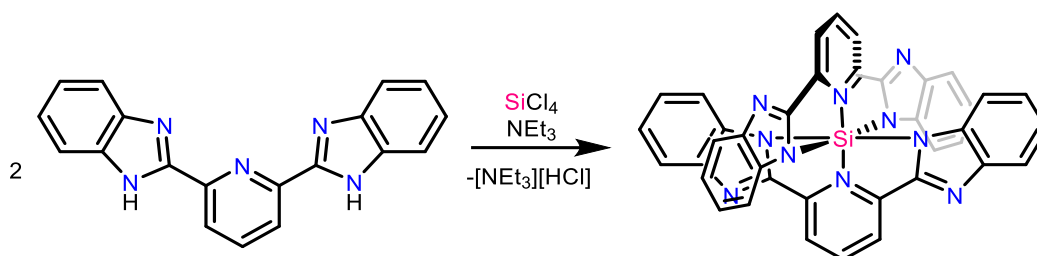
Scheme 3.3. *Synthesis of Si(BZIMPY)₂.*

The parent ligand, NH-BZIMPY can be easily prepared and functionalized at the nitrogen atom of the benzimidazole allowing for tuning of the electronic and steric properties. Analogous imidazole and benzimidazole tripodal ligand coordination to main group elements have also been investigated.[30-34]

3.2 Results and Discussion

3.2.1 Synthesis and Characterization

Treatment of the parent ligand NH-BZIMPY with MCl_2 (M = Ge, Sn) resulted in coloured materials that were insoluble in common organic solvents and thus, further characterisation was not possible. To increase the solubility of the resulting complexes, NH nitrogen sites were substituted using different alkylating agents to introduce allyl, Bn and $(3,5-CF_3)$Bn derivatives. These derivatives allowed for increased solubility and thus, characterisation by means of heteronuclear NMR spectroscopy and X-ray crystallography (**Figure 3.2**).
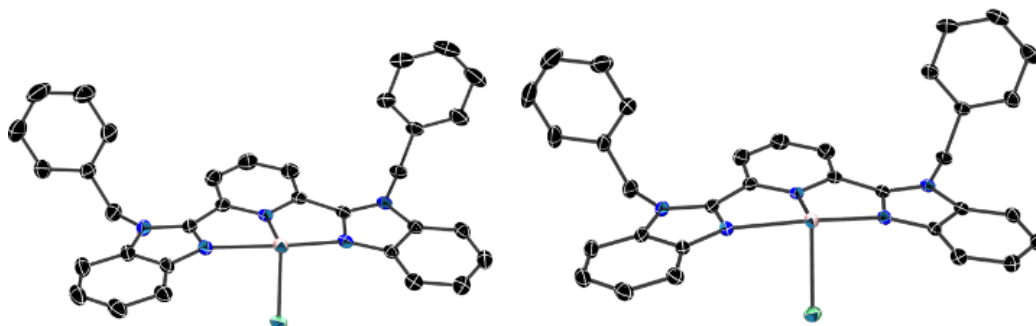
Figure 3.2. Solid state structure of the cations in [NBn-BZIMPYGeCl][GeCl₃] (1, left) and [NBn-BZIMPYSnCl][SnCl₃] (2, right). Thermal ellipsoids are shown at 50% probability level. Hydrogen atoms, solvent molecules and counterions are omitted for clarity. Selected bond distances and angles are listed in Table 3.1.

The self-ionization process (L + 2 MCl_2 → [LMCl][MCl₃]) has been previously reported for the structurally related DIMPY ligands.[12-14] A 1:1 reaction of BZIMPY and MCl_2 results in 50% yield of the self-ionized product, [BZIMPYMCl][MCl₃]; thus, it was necessary to use two equivalents of metal halide for the reaction to go to completion (**Scheme 3.4**). Products **1** and **2**

([NBn-BZIMPYMCl][MCl₃]) were obtained in high yields (>85%) and large scales by treating NBn-BZIMPY with two equivalents of MCl_2 in dichloromethane (DCM), resulting in an immediate intense yellow solution for **1** (M = Ge) and a slower more pale-yellow solution for **2** (M = Sn). Slow evaporation from a DCM solution yields yellow crystals of **1** and **2** suitable for X-ray diffraction. Compounds **3** and **4** ([N(3,5-CF₃)Bn-BZIMPYMCl][MCl₃]) were obtained by treatment of N(3,5-CF₃)Bn-BZIMPY with two equivalents of MCl_2 in CD₃CN. Similarly, reaction with $GeCl_2$ resulted in a faster and more intense yellow colour than $SnCl_2$. Crystals of **3** and **4** suitable for X-ray diffraction were obtained from slow evaporation of CD₃CN solutions.

G-Bzimpy

1: **M** = Ge; **G** = NBn
2: **M** = Sn; **G** = NBn
3: **M** = Ge; **G** = N(3,5-CF₃)Bn
4: **M** = Sn; **G** = N(3,5-CF₃)Bn
5: **M** = Ge; **G** = NAllyl
6: **M** = Ge; **G** = O
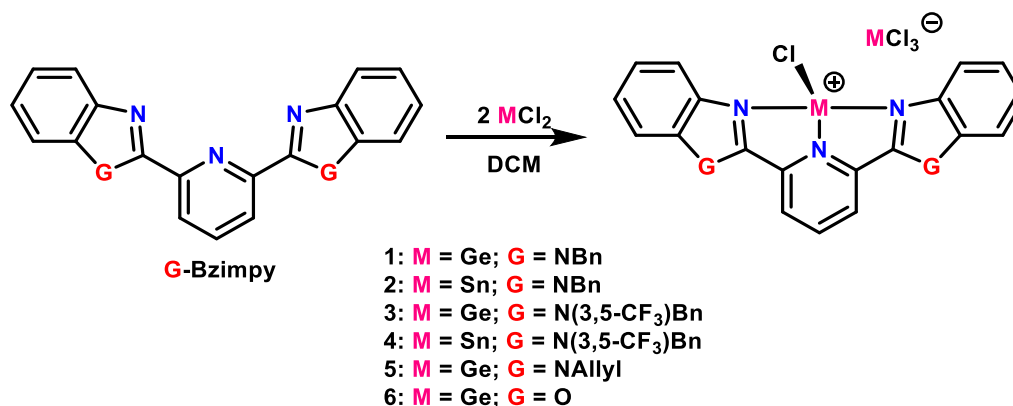
Scheme 3.4. *Self-ionization reactions of MCl₃ (M = Ge, Sn) with G-BZIMPY ligands.*

G-BZIMPY complexes of germanium are more soluble than their tin counterparts. As a result, G-BZIMPY ligands with G = NAllyl and O were very poorly soluble when coordinated to tin and only slightly soluble in the case of germanium. [NAllyl-BZIMPYGeCl][GeCl₃] (**5**) and [O-BZIMPYGeCl][GeCl₃] (**6**) were obtained by treating two equivalents of $GeCl_2$ with the corresponding G-BZIMPY followed by sonication for 24 hours to yield a sparingly soluble yellow

solution. Crystals suitable for X-ray diffraction were obtained by slow evaporation of a dilute solution of **5** and **6**.
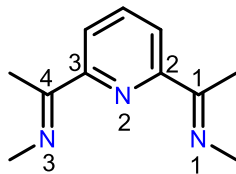
	1	[DIMPY-GeCl]+	2	[DIMPY-SnCl]+	3	4	5	6
M-N1	2.1999(17)	2.2669(14)	2.3335(13)	2.411(2)	2.149(4)	2.356(6)	2.230(2)	2.485(2)
M-N2	2.1373(16)	2.0712(15)	2.3750(13)	2.286(2)	2.169(4)	2.416(5)	2.158(2)	2.196(2)
M-N3	2.2340(16)	2.2548(8)	2.3424(13)	2.404(2)	2.306(3)	2.373(5)	2.231(2)	2.286(1)
M-Cl	2.2871(6)	2.2434(8)	2.4667(4)	2.4359(9)	2.262(1)	2.448(2)	2.279(7)	2.266(6)
N1-C1	1.315(3)	1.277(2)	1.326(2)	1.280(3)	1.327(6)	1.333(7)	1.325(3)	1.294(3)
C1-C2	1.470(3)	1.482(2)	1.470(2)	1.488(4)	1.458(6)	1.456(7)	1.465(3)	1.455(3)
C2-N2	1.355(2)	1.348(2)	1.3526(19)	1.353(3)	1.351(7)	1.352(6)	1.355(3)	1.345(2)
N2-C3	1.355(3)	1.348(2)	1.350(2)	1.343(3)	1.347(5)	1.335(7)	1.349(3)	1.342(2)
C3-C4	1.464(3)	1.481(2)	1.475(2)	1.492(4)	1.470(8)	1.482(7)	1.466(3)	1.446(3)
C4-N3	1.324(2)	1.275(2)	1.3309(19)	1.274(3)	1.318(6)	1.325(7)	1.325(3)	1.302(2)
N1-M-N2	73.14(6)	73.28(7)	67.94(5)	68.79(7)	73.48(13)	67.29(16)	73.03(8)	70.62(6)
N2-M-N3	72.54(6)	73.52(7)	67.25(4)	68.71(7)	71.73(13)	66.51(15)	72.91(8)	73.14(5))
N2-M-N3	142.82(6)	145.99(7)	131.37(5)	136.87(7)	141.72(13)	129.42(15)	144.48(8)	143.33(6)

Table 3.1. *Selected bond distances (Å) and angles (°) of complexes **1-6**, and [iPrDIMPYMCl]+ (M = Ge, Sn)[12].*
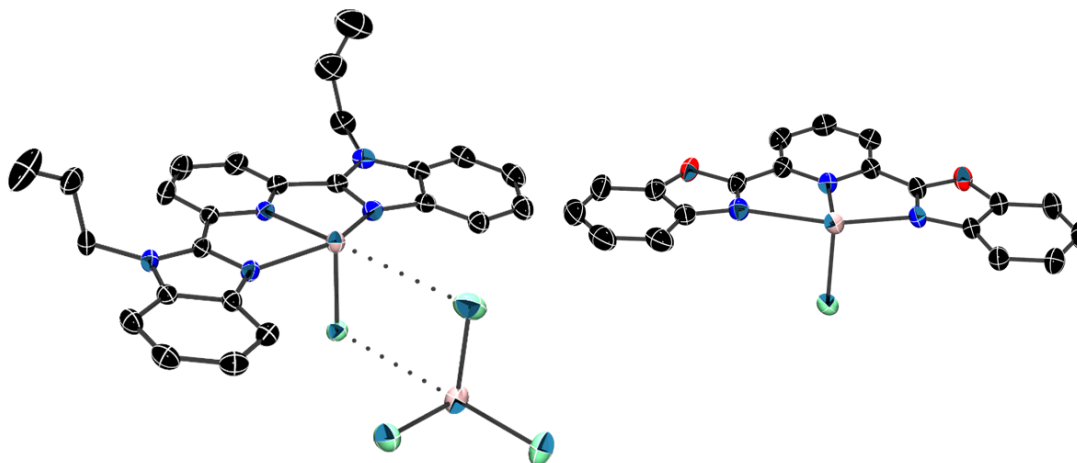
Figure 3.3. *Solid state structure of the cations in [Allyl-BZIMPYGeCl][GeCl$_3$] (**5**, left) and [O-BZIMPYGeCl][GeCl$_3$] (**6**, right). Thermal ellipsoids are shown at 50% probability level. Hydrogen atoms, solvent molecules and counterion are omitted for clarity.*

Next, we were interested in comparing the G-BZIMPY complexes of germanium and tin to those of ^{iPr}DIMPY. [^{iPr}DIMPYMCl][MCl$_3$] complexes of germanium and tin were reported by Roesky as the products of the reaction of ^{iPr}DIMPY with two equivalents of the corresponding GeCl$_2$ and SnCl$_2$.[12] The germanium and tin coordination complexes of ^{iPr}DIMPY have a shorter bond distance to the pyridine (M-N2) than the imine donors (M-N1 and M-N3) (**Table 3.1**). This trend was also observed in group 13 complexes of ^{iPr}DIMPY and is likely due to the steric hindrance of the bulky imine donors.[19] Complexes **1** and **2** contain shorter M-N1 and M-N3 distances (benzimidazole donors) than their ^{iPr}DIMPY counterparts (imine donors) suggesting a stronger BZIMPY donor ligand than ^{iPr}DIMPY. This was also observed and confirmed by computational analysis with group 13 complexes of G-BZIMPY.[19]

Complex **3** shows slight asymmetry in the solid state with the germanium coordinating closer to N1 and N2 (M-N1: 2.149(4)Å and M-N2:

2.169(4)Å) than to N3 (M-N3: 2.306(3)Å). This asymmetry is not observed in the room temperature proton NMR spectrum, which is likely due to the Ge centre exchanging between N1 and N3 at a rate faster than the NMR time scale. This asymmetry could be a result of crystal packing effects in the solid state. Asymmetry in the solid-state structure is also observed in [O-BZIMPYGeCl][GeCl$_3$], complex **6** (**Table 3.1**). Complex **5** shows an intermolecular interaction between the Ge–Cl fragment of the cation and a Ge–Cl fragment of the anion (**Figure 3.3**, left). These interactions (3.3961(7) Å and 3.543(1) Å) are within the Van der Waals radii expected for Ge (2.13 Å) and Cl (1.89 Å) (Ge–Cl= 4.02 Å).[35]

As introduced earlier, Evans' chiral Lewis acid contains a dicationic tin(II) pincer complex with two triflate anions.[11] In an effort to produce a similar Lewis ([G-BZIMPY-M][OTf]$_2$), complex **1** was treated with 1, 2 and 5 equivalents of trimethylsilyl trifluoromethanesulfonate (TMS-OTf) in CD$_3$CN yielding the monocationic complex [NBn-BZIMPYGeCl][OTf] (**7**, **Figure 3.4**, left) where the [GeCl$_3$] anion is exchanged by a triflate anion [OTf]. Treatment of the commercially available Sn(OTf)$_2$ with an equivalent of NBn-BZIMPY in CD$_3$CN results in the dicationic tin complex, [NBn-BZIMPYSn][OTf]$_2$ (**8**, **Figure 3.4**, right). Slow evaporation of both complexes from an acetonitrile solution results in yellow crystals suitable for X-ray diffraction.
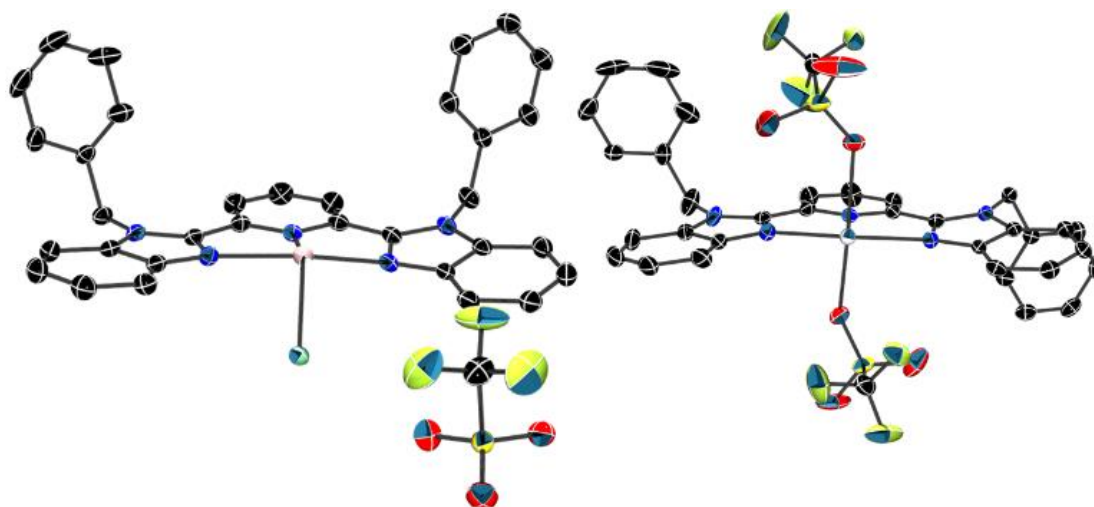
Figure 3.4. *Solid state structure of the cations in [NBn-BZIMPYGeCl][OTf] (**7**, left) and [NBn-BZIMPYSn][OTf]$_2$ (**8**, right). Thermal ellipsoids are shown at 50% probability level. Hydrogen atoms and solvent molecules are omitted for clarity. Selected bond distances and angles are listed in **Table 3.2**.*

The Lewis acidity of the resulting complexes was assessed using the Gutmann-Beckett method.[36,37] A CH$_3$CN solution was prepared containing an equivalent of triethylphosphine oxide and **8**. This solution exhibited a singlet in the ^{31}P{^{1}H} NMR at δ = 76.5 ppm, which is significantly shifted from the free phosphine oxide ($\Delta\delta$ = 35.5 ppm). Using the Gutmann-Beckett method, this shift corresponds to an acceptor number of 78. To put this into perspective, other commonly used boron containing Lewis acids have the following acceptor numbers: B(C$_6$F$_5$)$_3$ (82) < BF$_3$ (89) < BCl$_3$ (106) < BBr$_3$ (109) < BI$_3$ (115).[38] This suggests that the Lewis acidity of **8** is slightly weaker than that of B(C$_6$F$_5$)$_3$ (BCF). As a result of the Lewis acidic tin, the two triflate anions coordinate to the tin centre in the solid state resulting in a pseudo-square pyramidal geometry around tin. Assessing the Lewis acidity of **7** using the same method results in a more significant shift in the ^{31}P{^{1}H} NMR with a singlet at δ

= 91.9 ppm. This shift of $\Delta\delta$ = 50.9 ppm (from free phosphine oxide) yields an acceptor number of 112, suggesting that **7** is a very strong Lewis acid and is comparable to other strong BX_3 (X = Cl, Br, and I) Lewis acids.

Complexes **1** and **7** have similar bond distances around the germanium and within the ligand framework. Complex **1** is more soluble in dichloromethane while complex **7** is more soluble in acetonitrile. In the case of tin, comparing complexes **2** to **8** where the chloride is absent in the latter, the bond distances of the tin centre to the ligand are similar, however, the two triflate anions are now bound to the tin centre forming a pseudo-square pyramidal geometry around the tin centre unlike complex **7** where the triflate was non-coordinating.
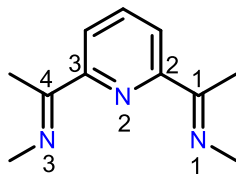
	7	8	9
M-N1	2.1865(13)	2.329(4)	2.095(2)/2.088(3)
M-N2	2.1589(12)	2.401(5)	2.038(2)/2.036(2)
M-N3	2.1947(13)	2.347(5)	2.105(2)/2.079(3)
M-Cl	2.2703(4)	–	–
N1-C1	1.327(2)	1.323(6)	1.324(3)/1.336(3)
C1-C2	1.467(2)	1.482(8)	1.475(3)/1.478(4)
C2-N2	1.355(2)	1.343(7)	1.345(3)/1.348(4)
N2-C3	1.353(2)	1.363(8)	1.345(3)/1.335(4)
C3-C4	1.469(2)	1.476(8)	1.471(3)/1.480(4)
C4-N3	1.327(2)	1.330(7)	1.326(3)/1.333(3)
N1-M-N2	72.84(5)	67.70(15)	77.20(8)/77.74(8)
N2-M-N3	72.40(5)	67.66(15)	77.72(8)/78.16(9)
N2-M-N3	142.67(5)	134.83(16)	154.86(8)/155.82(9)

Table 3.2. *Selected bond distances (Å) and angles (°) of complexes **7-10**.*

3.2.2 UV-vis Studies

UV-vis absorption spectra of complexes **1**-**8** were collected in dichloromethane (DCM). Complex **1** in DCM gives a yellow solution that shows intense absorption band at 322 nm (ε = 23,000 L mol^{-1} cm^{-1}) and a moderate band at 375 nm (ε = 9,700 L mol^{-1} cm^{-1}). Absorption bands are assigned in-accordance with other BZIMPY metal complexes reported in literature where the high-energy intense band is attributed to an intra-ligand (IL) transition, while the low-energy band is assigned to a metal-to-ligand charge-transfer

(MLCT).[39,40] Increasing the polarity of the solvent in **1** (CH_3CN) results in negative solvatochromism of the low-energy band. **Figure 3.5a** illustrates this blue-shift of the CT band resulting in a single overlapping band at 314 nm (ε = 29,000 L mol^{-1} cm^{-1}). The same observation was made in **6** (**Figure 3.5c**) where a DCM solution yielded two bands at 376 nm (ε = 6,200 L mol^{-1} cm^{-1}) and 321 nm (ε = 31,000 L mol^{-1} cm^{-1}); while in CH_3CN, negative solvatochromism of the low-energy band shifts and disappears under the IL band at 316 nm (ε = 37,200 L mol^{-1} cm^{-1}). [NBn-BZIMPYSnCl][$SnCl_3$] (**2**) exhibits a MLCT band at 370 nm with a molar absoritivity of ε = 19,600 L mol^{-1} cm^{-1} that is significantly stronger than its germanium counterparts. Using a more polar solvent (CH_3CN) with **2** does not result in a significant change to the MLCT, 364 nm (ε = 19,400 L mol^{-1} cm^{-1}) as shown in **Figure 3.5b**. IL band of **2** in DCM (318 nm, ε = 23,600 L mol^{-1} cm^{-1}) does not shift upon increasing the polarity of the solvent (317 nm, ε = 24,500 L mol^{-1} cm^{-1}). It is worth noting that the different group-14 element bound to G-BZIMPY not only results in a difference in the intensity of the MLCT band, but it can dictate whether or not negative solvatochromism is observed. In light of the differences between the UV-vis spectra of the germanate (**1**) and triflate (**7**) salts of an identical cation, the solvent effects observed for the germanium-containing complexes are likely primarily a consequence of differing cation-anion-solvent interactions.

For both the germanium and tin complexes, changing the R group in the NR-BZIMPY ligands has a negligible effect on the observed absorbance. Germanium complexes of NR-BZIMPY (**1**, **3** and **5**) have an IL band at 311-322

nm (ε = 20,800-21,200 L mol^{-1} cm^{-1}) and a MLCT band at 375-384 nm (ε = 9,600-12,800 L mol^{-1} cm^{-1}). Tin counterparts (**2** and **4**) have a relatively similar IL band at 318-320 nm (ε = 21,200-23,600 L mol^{-1} cm^{-1}) but a significantly more intense MLCT band at 365-370 nm (ε = 17,900-19,600 L mol^{-1} cm^{-1}).

To study the impact of changing the counter-ion and the abstraction of the chloride on absorption bands, UV-vis spectra of **7** and **8** were collected in DCM. The low-energy band in **7** is likely blue-shifted and not observed, as a result, a single broad absorption is observed at 319 nm with a molar absorptivity of ε = 31,100 L mol^{-1} cm^{-1} (**Figure 3.5a**). The absorption bands in **8** (368 nm, ε = 23,900 L mol^{-1} cm^{-1} and 318 nm, ε = 29,300 L mol^{-1} cm^{-1}) do not shift in comparison to **2**, confirming that Sn(II)-BZIMPY complexes are not sensitive to polarity of the solvent nor the environment surrounding the tin(II) centre.
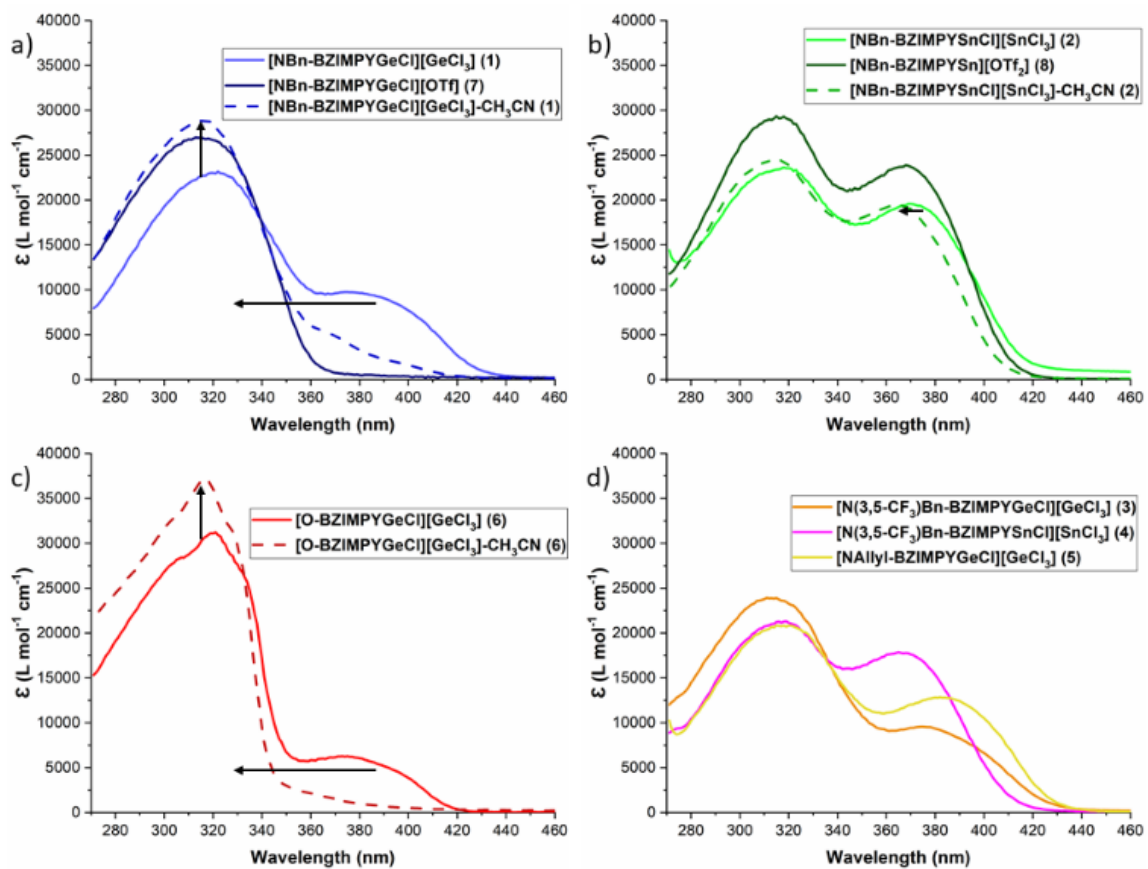
Figure 3.5. *a) UV-vis absoption of 1 in DCM vs CH₃CN along with 7 in DCM. b) UV-vis absoption of 2 in DCM vs CH₃CN along with 8 in DCM. c) UV-vis absoption of 6 in DCM vs CH₃CN. d) UV-vis absoption of 3-5 in DCM. Spectra collected in CH₃CN are indicated by the dashed line.*

3.2.3 Reduction Attempts

Reduction of the [^{iPr}DIMPYGe(II)Cl]$^+$ into the Ge(0) complex was reported by Nikonov as noted above (**Scheme 3.2**).[5] We thus investigated similar reactions in which complexes **1** and **2** were treated with different reducing agents including KC$_8$, potassium, or sodium naphthalide in THF; each of these reactions resulted in the deposition of the main group element and the release of the free NBn-BZIMPY ligand. We recently reported the successful reduction of Ga(III) to Ga(I) BZIMPY complex using Collman's reagent

($K_2[Fe(CO)_4]$) to yield of [(NBn-BZIMPY)(Cl)Ga—Fe(CO)$_4$].[19] Again, attempts to extend this chemistry to group 14 complexes by treating complexes **1** or **2** with an equivalent of $K_2[Fe(CO)_4]$ in THF results in the free NBn-BZIMPY ligand along with an insoluble precipitate. Using an equivalent of [Ni(COD)$_2$], we anticipated the reduction of the main group element and the oxidation of the Ni(0) centre to Ni(II). Although the nickel centre is indeed oxidized, it displaces the main group element to yield [(NBn-BZIMPY)$_2$Ni][MCl$_3$]$_2$ (M = Ge (**9**), Sn (**10**), **Figure 3.6**).
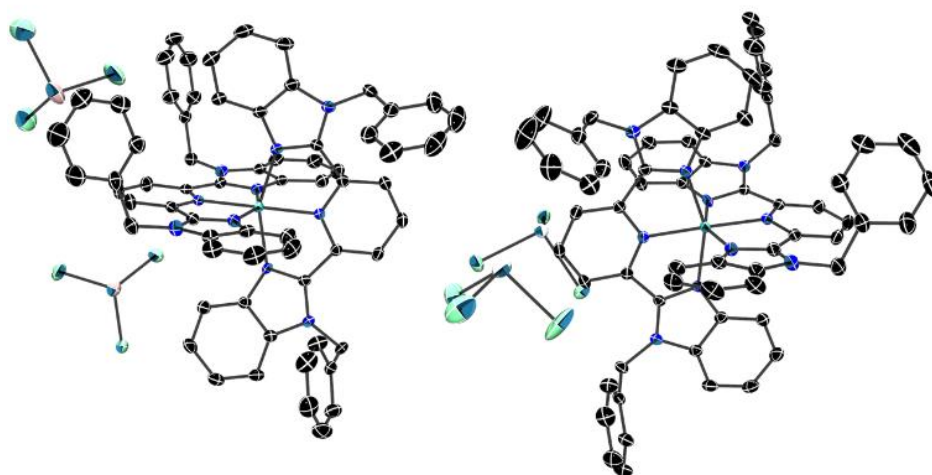
Figure 3.6. *Solid state structure of the cations in [(NBn-BZIMPY)₂Ni][GeCl₃]₂ (**9**, left) and [(NBn-BZIMPY)₂Ni][SnCl₃]₂ (**10**, right). Thermal ellipsoids are shown at 50% probability level. Hydrogen atoms and solvent molecules are omitted for clarity. Selected bond distances and angles are listed in **Table 3.2**.*

These reactions were repeated using half an equivalent of Ni(COD)$_2$ to yield **9** and **10** in 34-37% yields (**Scheme 3.5**). The crystal structures of **9** and **10** are isomorphous, having the same unit cell parameters with the tin replacing the germanium in complex **10**.
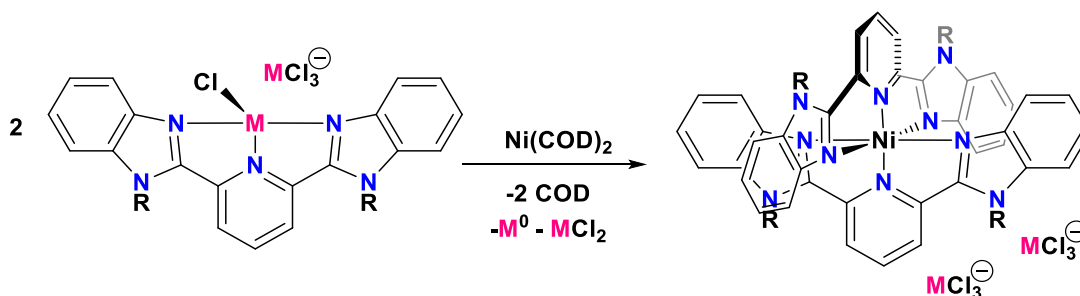
Scheme 3.5. *Reduction attempt of complexes **1** and **2** using Ni(COD)$_2$ to yield complexes **9** and **10** respectively (R = Bz).*

In an effort to elucidate possible reasons for the observed G-BZIMPY ligand behaviour in reducing conditions, cyclic voltammetry experiments of NBn-BZIMPY were undertaken. From the voltammograms (**Figure 3.7**), it was determined that there is a single irreversible reduction that occurs at −0.902 V (*versus* Fc/Fc$^+$).
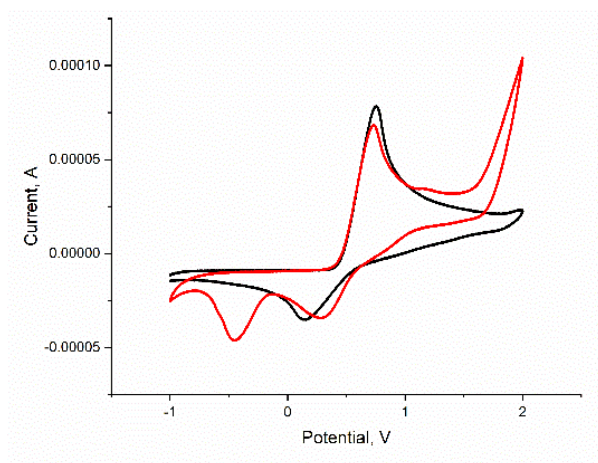
Figure 3.7. *Overlapping CVs of 0.01M solution of ferrocene (Fc/Fc$^+$) in black and 0.01M solution of ferrocene/NBn-BZIMPY in red. Both solutions were prepared in DCM with 0.1M [NBu$_4$][PF$_6$]. Working and counter electrodes were Pt, the reference electrode was Ag/AgCl, and the scan rate was 100 mVs^{-1}.*

3.2.4 Computational Studies

Gas phase geometry optimizations on simplified NH-BZIMPY models (2,6-di(1H-imidazol-1-yl)pyridine) of compound **1** and **2** (**1'** and **2'** corresponding to Ge and Sn complexes of the simplified ligand, respectively) performed at the M062X/cc-pVTZ level of theory result in models with near perfect *Cs* symmetry and metrical parameters that are close to the values determined experimentally using single crystal X-ray diffraction. Inspection of the molecular orbitals of **1'** reveal that the HOMO has significant contributions from germanium, corresponding to the "lone pair". The energy of the HOMO (–10.89 eV) is significantly higher than the HOMO of the model [ClGe(^{H}DIMPY)]$^{1+}$ calculated at the same level of theory (–11.48 eV) and suggests that **1'** should be a superior donor. Interestingly, NBO analyses corroborate the conclusion regarding germanium "lone pair" energies but suggest that the donor abilities of NH-BZIMPY and ^{H}DIMPY are similar. The HOMO−1 and HOMO−2 of **1'** are π-type ligand-based MOs with A'' and A' symmetry, respectively, and the HOMO−3 and HOMO−4, represent the "lone pairs" on the chlorine atom. The LUMO has A' symmetry, but does not exhibit any metal-ligand anti-bonding character and thus does not explain why reduction attempts were unsuccesful. Models of the putative Ge(0) species [Ge(NH-BZIMPY)] and [Ge(^{H}DIMPY)] exhibit similar structural features and HOMO-LUMO energy differences and do not provide any obvious electronic rationale for the instability of the NH-BZIMPY variant. Given the foregoing, it is likely that kinetic instability of the putative reduced compound precludes its isolation.

Compound 1'

| Optimized Geometry | HOMO -10.89 eV | LUMO -5.01 eV |
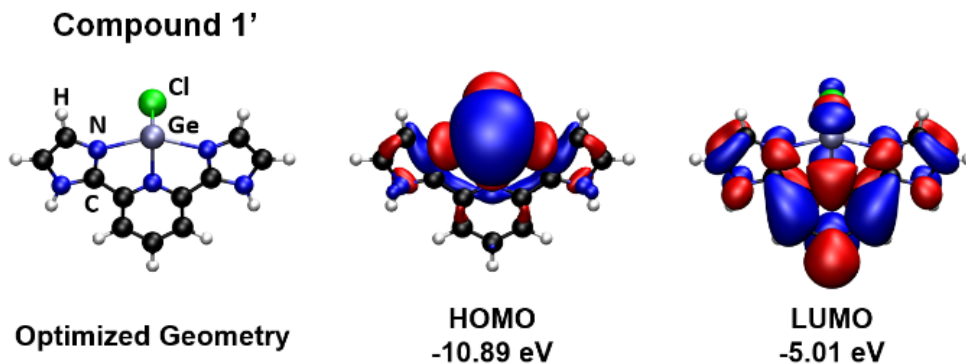
*Figure 3.8. Optimized geometry and selected occupied molecular orbitals of **1'** (M062X/cc-pVTZ).*

3.3 Conclusions

We presented Ge(II) and Sn(II) coordination to 2,6-Bis(benzimidazol-2-yl)pyridine (G-BZIMPY, G = NBn, N(3,5-CF₃)Bn, NAllyl and O) ligands. Some of the salts were assessed to be potent Lewis acids using the Gutman-Beckett method. UV-vis absorption spectra of these complexes feature an intense high-energy intra-ligand band and a moderate low-energy MLCT band. Negative solvatochromism was observed in germanium-containing complexes upon increasing polarity of the solvent, but this was not observed in those of tin. Attempts to reduce these M(II) complexes into low-valent M(0) complexes were not successful; this is likely attributable to kinetic instability of the resulting reduced compounds.

3.4 Experimental

3.4.1 General Remarks

All manipulations were carried out using standard inert-atmosphere techniques. All reagents and chemicals were obtained from Sigma-Aldrich. All reagents were used without further purification. MeCN-d_3 was dried over calcium hydride or phosphorus pentoxide, and dichloromethane-d_2 was dried over phosphorus pentoxide. All other solvents were dried on a series of Grubbs-type columns and were degassed prior to use.[41] All glassware was stored in a 170 °C oven for several hours. 2,6-Bis(benzimidazol-2-yl)pyridine (NH-BZIMPY),[42] 2,6-bis(benzoxazol-2-yl)pyridine (O-BZIMPY),[43] NBn-BZIMPY,[44] N(3,5-CF$_3$)Bn-BZIMPY,[19] NAllyl-BZIMPY,[19] and K$_2$[Fe(CO)$_4$][45] were all prepared according to the literature procedures.

NMR spectrum was recorded at room temperature on Bruker Avance III 500 MHz, Bruker Avance Ultrashield 300 MHz, and Bruker Avance DPX 300 MHz spectrometers. Chemical shifts are reported in parts per million relative to internal standards for ^{1}H and [13]C (the given deuterated solvent) and external standards for [19]F (CFCl$_3$). Coupling constants |J| are given in hertz. Elemental analysis was performed at the University of Windsor Mass Spectrometry Service Laboratory using a Perkin-Elmer 2400 combustion CHN analyzer.

Cyclic voltammetry was performed in dry CH$_2$Cl$_2$ solutions using [NBu$_4$][PF$_6$] (0.1 M) as the electrolyte with analyte concentration of approximately 0.01 M. A platinum electrode, a platinum wire, and 1.0 M

Ag/AgCl electrode were used as the working, auxiliary, and reference electrodes, respectively. The experiments were run with a scan rate of 100 mV/s and a sensitivity of 100 μA/V and the potentials reported are referenced to ferrocene/ferrocenium ($E_{1/2}$ = 0.0 V).

3.4.2 Synthesis
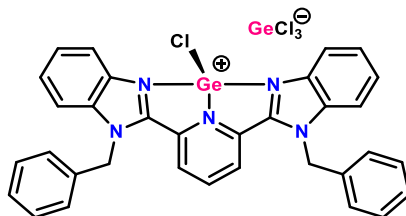
[NBn-BzimpyGeCl][GeCl₃] (**1**) A 100 mL Schlenk flask was charged with NBn-BZIMPY (465 mg, 0.95 mmol) and GeCl$_2$·dioxane (438 mg, 1.9 mmol). To that was added 40 mL of dichloromethane resulting in an immediate formation of a yellow/green solution. After 2 hours of stirring, the solvent was evaporated under reduced pressure and the resulting solid was suspended in toluene (20 mL), collected and washed with toluene (2×10 mL) yielding **1** as a yellow solid (630 mg, 85%). Slow evaporation from dichloromethane yielded yellow crystals suitable for X-ray Diffraction. ^{1}H NMR (CD$_2$Cl$_2$) δ: 8.45 (t, 1H, $^3J_{HH}$ = 8 Hz), 8.20 (b, 4H), 7.65 (m, 4H), 7.37 (b, 4H), 7.24 (b, 8H), 6.02 (s, 4H). ^{13}C{^{1}H} NMR δ: 145.81, 145.38, 144.47, 137.88, 137.31, 133.96, 130.07, 129.18, 127.91, 126.75, 126.23, 125.10, 119.20, 112.32, 50.10. Anal. Calc. for C$_{33}$H$_{25}$Cl$_4$Ge$_2$N$_5$ (778.68 g/mol): C, 50.90; H, 3.24; N, 8.99. Found: C, 50.59; H, 3.12; N, 8.82.
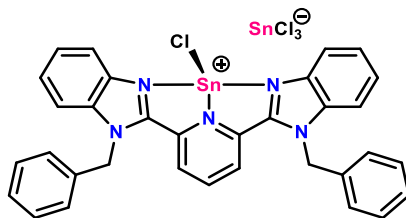
[NBn-BzimpySnCl][SnCl₃] (**2**) A 100 mL Schlenk flask was charged with NBn-BZIMPY (500 mg, 1.0 mmol) and SnCl$_2$ (386 mg, 2.0 mmol). To that was added 40 mL of dichloromethane resulting in an immediate formation of a yellow solution. After allowing the reaction to stir overnight, the solvent was evaporated under reduced pressure and the resulting solid was suspended in toluene (20 mL), collected and washed with toluene (2×10 mL) yielding **2** as a pale-yellow solid (910 mg, 98%). Slow evaporation from dichloromethane yielded yellow crystals suitable for X-ray Diffraction. ^{1}H NMR (CD$_2$Cl$_2$) δ: 8.27 (t, 1H, $^3J_{HH}$ = 8 Hz), 8.16 (d, 2H, $^3J_{HH}$ = 8 Hz), 8.07 (d, 2H, $^3J_{HH}$ = 8 Hz), 7.62 (m, 5H), 7.42 (m, 5H), 7.13 – 7.26 (m, 6H), 6.03 (s, 4H). ^{13}C{^{1}H} NMR δ: 148.32, 144.93, 144.48, 137.89, 134.26, 130.08, 129.09, 127.48, 126.70, 126.55, 126.20, 125.50, 119.11, 112.35, 50.50. Anal. Calc. for C$_{33}$H$_{25}$Cl$_4$Sn$_2$N$_5$(toluene)$_{0.5}$ (916.89 g/mol): C, 47.81; H, 3.19; N, 7.64. Found: C, 48.01; H, 3.25; N, 7.16.
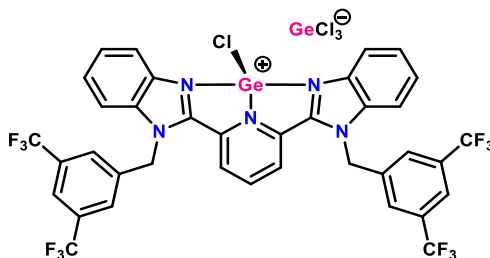
[N(3,5-CF₃)Bn-BzimpyGeCl][GeCl₃] (**3**) A 20 mL vial was charged with N(3,5-CF$_3$)Bn-BZIMPY (40 mg, 0.052 mmol) and GeCl$_2$·dioxane (24 mg, 1.0 mmol). 5 mL of CD$_3$CN was added, resulting in the formation of a yellow solution. The

solution was allowed to stir overnight and was then left to evaporate resulting in **3** as yellow crystals (47 mg, 85%). ^{1}H NMR (CD$_3$CN) δ: 8.46 (t, 1H, $^3J_{HH}$ = 8 Hz), 8.22 (m, 4H), 8.02 (s, 2H), 7.85 (s, 4H), 7.62-7.74 (m, 6H), 6.15 (s, 4H). ^{13}C{^{1}H} NMR δ: 148.04, 146.55, 144.60, 138.32, 137.74, 132.82 ($^2J_{CF}$ = 33 Hz), 128.48, 128.04, 127.97, 127.36, 125.87, 124.20 ($^1J_{CF}$ = 272 Hz), 123.52, 119.55, 113.24, 49.65. ^{19}F{^{1}H} NMR δ: −64.40. Anal. Calc. for C$_{37}$H$_{21}$Cl$_4$F$_{12}$Ge$_2$N$_5$ (1050.65 g/mol): C, 42.30; H, 2.01; N, 6.67. Found: C, 42.08; H, 2.20; N, 6.33.
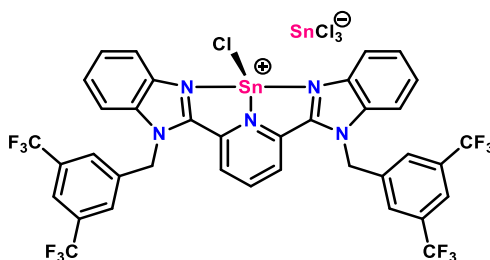
[N(3,5-CF$_3$)Bn-BzimpySnCl][SnCl$_3$] (**4**) A 20mL vial was charged with N(3,5-CF$_3$)Bn-BZIMPY (40 mg, 0.052 mmol) and SnCl$_2$ (20 mg, 1.0 mmol). 5 mL of CD$_3$CN was added to the vial, resulting in the formation of a pale-yellow solution. The solution was allowed to stir overnight and was then left to evaporate resulting in **4** as yellow crystals (58 mg, 97%). ^{1}H NMR (CD$_3$CN) δ: 8.24 (t, 1H, $^3J_{HH}$ = 8 Hz), 8.21 (m, 2H), 8.13 (d, 2H, $^3J_{HH}$ = 8 Hz), 8.03 (s, 2H), 7.85 (s, 4H), 7.62-7.68 (m, 6H), 6.13 (s, 4H). ^{13}C{^{1}H} NMR δ: 147.97, 144.80, 144.25, 137.68, 137.25, 131.90 ($^2J_{CF}$ = 33 Hz), 127.23, 127.15, 127.09, 126.30, 125.38, 123.40 ($^1J_{CF}$ = 272 Hz), 122.58, 118.63, 112.24, 48.94. ^{19}F{^{1}H} NMR δ: −62.63 (s). Anal. Calc. for C$_{37}$H$_{21}$Cl$_4$F$_{12}$Sn$_2$N$_5$ (1142.81 g/mol): C, 38.89; H, 1.85; N, 6.13. Found: C, 39.11; H, 2.12; N, 6.35.
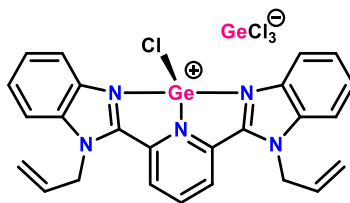
[NAllyl-BZIMPYGeCl][GeCl₃] (**5**) A 20mL vial was charged with NAllyl-BZIMPY (20 mg, 0.051 mmol) and GeCl$_2$·dioxane (24 mg, 0.10 mmol). 5 mL of CD$_3$CN was added to the vial, resulting in the formation of a yellow precipitate. The solution was sonicated overnight to yield a pale-yellow solution with yellow precipitate. Solvent was evaporated to yield **5** as yellow precipitate (26 mg, 75%). Crystals were formed by dissolving a few milligrams of **5** in CH$_3$CN and leaving the solution to slowly evaporate yielding yellow crystals suitable for X-ray diffraction.^{1}H NMR (CD$_2$Cl$_2$) δ: 8.67 (t, 1H, $^3J_{HH}$ = 8 Hz), 8.47 (d, 2H, $^3J_{HH}$ = 8 Hz), 8.13 (d, 2H, $^3J_{HH}$ = 8 Hz), 7.81 (d, 2H, $^3J_{HH}$ = 8 Hz), 7.66 (m, 4H), 6.30 (b, 2H), 5.29 – 5.47 (m, 6H), 5.09 (d, 2H, $^3J_{HH}$ = 18 Hz). Compound is not soluble enough to obtain a ^{13}C NMR. Anal. Calc. for C$_{25}$H$_{21}$Cl$_4$Ge$_2$N$_5$ (678.54 g/mol): C, 44.25; H, 3.12; N, 10.32. Found: C, 43.81; H, 2.96; N, 9.98.
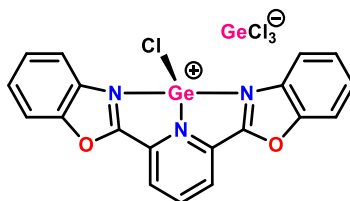
[O-BZIMPYGeCl][GeCl₃] (**6**) A 20mL vial was charged with O-BZIMPY (20 mg, 0.064 mmol) and GeCl$_2$·dioxane (30 mg, 0.13 mmol). 4 mL of CD$_3$CN and 1 mL of CD$_2$Cl$_2$ were added to the vial, resulting in the formation of a yellow solution. The solution was allowed to stir overnight, and slow evaporation of the solvent yielded yellow crystals of **6** (35 mg, 92%). ^{1}H NMR (CD$_2$Cl$_2$/CD$_3$CN (1:4)) δ: 8.69

(m, 3H), 8.08 (d, 2H, $^3J_{HH}$ = 8 Hz), 7.91 (d, 2H, $^3J_{HH}$ = 8 Hz), 7.76 (t, 2H, $^3J_{HH}$ = 8 Hz), 7.66 (t, 2H, $^3J_{HH}$ = 8 Hz). $^{13}C\{^1H\}$ NMR δ: 159.88, 152.01, 145.02, 143.55, 137.90, 129.56, 127.90, 127.47, 120.57, 113.06.; Anal. Calc. for $C_{19}H_{11}Cl_4Ge_2N_3O_2(CH_3CN)_{0.33}$ (613.89 g/mol): C, 38.46; H, 1.97; N, 7.59. Found: C, 38.83; H, 1.85; N, 7.28.
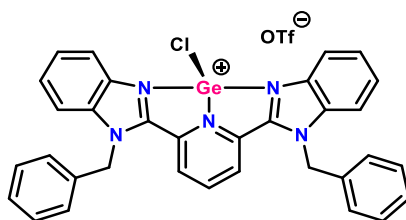
[NBn-BzimpyGeCl][OTf] (**7**) A 20 mL vial was charged compound **1** (50 mg, 0.064 mmol). 5 mL of CD_3CN was added, followed by excess TMSOTf (0.035 mL, 0.19 mmol). The solution was stirred for an hour and left to slowly evaporate yielding **7** as yellow crystals (45 mg, 94%). ^1H (CD_3CN) δ: 8.39 (t, 1H, $^3J_{HH}$ = 8 Hz), 8.25 (d, 2H, $^3J_{HH}$ = 8 Hz), 8.18 (m, 2H), 7.62 (m, 4H), 7.76 (m, 2H), 7.66 (m, 2H), 7.33 – 7.40 (m, 6H), 7.20 (d, 2H, $^3J_{HH}$ = 8 Hz), 6.01 (s, 4H). $^{13}C\{^1H\}$ NMR δ: 146.21, 145.64, 144.26, 142.12, 138.16, 137.47, 134.74, 130.06, 128.18, 127.07, 126.57, 123.72 ($^1J_{CF}$ = 313 Hz), 119.17, 112.99, 49.94. $^{19}F\{^1H\}$ NMR δ: −77.83 Anal. Calc. for $C_{34}H_{25}F_3N_5O_3SGe$ (748.74 g/mol): C, 54.54; H, 3.37; N, 9.35. Found: C, 54.09; H, 3.10; N, 9.22.
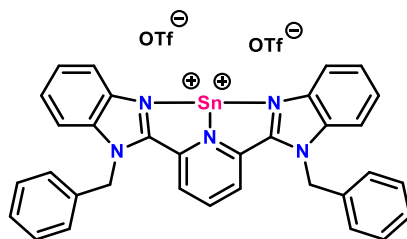
[NBn-BzimpySn][OTf]₂ (8) A 20 mL vial was charged with NBn-BZIMPY (40 mg, 0.082 mmol) and Sn(OTf)₂ (35 mg, 0.084 mmol). 5 mL of CD₃CN was added, resulting in the formation of a yellow solution. The solution was allowed to stir overnight and was then left to evaporate resulting in **8** as yellow crystals (59 mg, 80%). ^{1}H NMR (CD₃CN) δ: 8.31 (t, 1H, $^3J_{HH}$ = 8 Hz), 8.22 (d, 2H, $^3J_{HH}$ = 8 Hz), 8.19 (d, 2H, $^3J_{HH}$ = 8 Hz), 7.74 (d, 2H, $^3J_{HH}$ = 8 Hz), 7.62 (m, 4H), 7.35 (m, 6H), 7.17 (d, 4H, $^3J_{HH}$ = 8 Hz), 6.03 (s, 4H). ^{13}C{^{1}H} NMR δ: 149.42, 145.40, 144.79, 138.61, 138.36, 135.15, 130.32, 129.39, 127.95, 127.23, 126.99, 126.33, 122.07 ($^1J_{CF}$ = 316 Hz), 119.40, 113.39, 50.32. ^{19}F{^{1}H} NMR δ: –79.50 Anal. Calc. for C₃₅H₂₅F₆N₅O₆S₂Sn (908.43 g/mol): C, 46.28; H, 2.77; N, 7.71. Found: C, 45.88; H, 3.02; N, 7.59.

9,   M = Ge, R = Bz
10, M = Sn, R = Bz
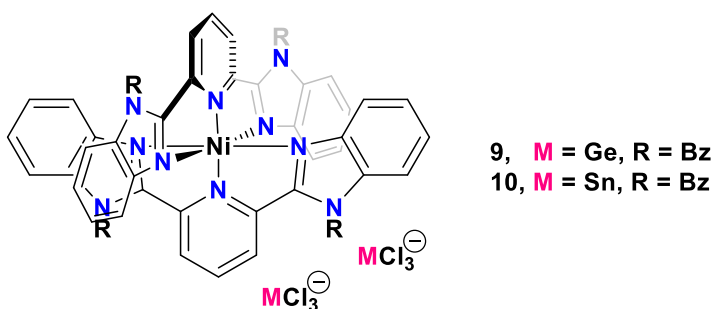
[(NBn-BZIMPY)₂Ni][GeCl₃]₂ (9) A 20 mL vial was charged with compound **1** (36 mg, 0.046 mmol) and Ni(COD)₂ (7 mg, 0.025 mmol). 5 mL of THF (precooled to –40 °C) was added resulting in a colour change from yellow to deep brown/red solution. The reaction was allowed to warm up to room

temperature and stir for 1 hr before filtering. 1 mL of hexane was added to the filtrate and was allowed to sit are room temperature overnight, resulting in deep brown crystals of **9** (12 mg, 37%). Anal. Calc. for $C_{66}H_{50}Cl_6Ge_2N_{10}Ni$ (1399.85 g/mol): C, 56.63; H, 3.81; N, 10.01. Found: C, 56.60; H, 3.81; N, 9.75.

[(NBn-BZIMPY)₂Ni][SnCl₃]₂ (10) A 20 mL vial was charged with compound **2** (48 mg, 0.055 mmol) and Ni(COD)₂ (8 mg, 0.029 mmol). 5 mL of THF (precooled to –40 °C) was added resulting in a colour change from yellow to a deep brown solution. The reaction was allowed to warm up to room temperature and stir for 1 hr before filtering. 1 mL of hexane was added to the resulting filtrate and was allowed to sit are room temperature overnight, resulting in light brown crystals of **10** (14 mg, 34%). Anal. Calc. for $C_{66}H_{50}Cl_6Sn_2N_{10}Ni$ (1492.20 g/mol): C, 53.13; H, 3.38; N, 9.39. Found: C, 49.81; H, 3.23; N, 8.68.

Gutmann-Beckett method:

Reaction of **7** with OPEt₃; A 20mL vial was charged with **7** (14 mg, 0.019 mmol) and OPEt₃ (3 mg, 0.022 mmol) in 1 mL CH₃CN. Reaction mixture was stirred for 30 minutes before collecting phosphorus NMR. ³¹P{¹H} NMR (CH₃CN) δ: 91.9.

Reaction of **8** with OPEt₃; A 20mL vial was charged with **8** (34 mg, 0.037 mmol) and OPEt₃ (5 mg, 0.037 mmol) in 1 mL CH₃CN. Reaction mixture was stirred for 30 minutes before collecting phosphorus NMR. ³¹P{¹H} NMR (CH₃CN) δ: 76.5.

3.4.3 Computational Details

Calculations were performed with the Gaussian 09 suite of programs[46] using Compute Canada's Shared Hierarchical Academic Research Computing Network (SHARCNET). Model complexes were fully optimized with no symmetry constraints using the M06-2X density functional method,[47] in conjunction with the cc-pVTZ basis set.[48,49] The cc-pVQZ-PP basis set employing a relativistic small-core pseudopotential was used for tin.[50] Geometry optimizations were started using models in which the relevant non-hydrogen atoms were placed in positions found experimentally by X-ray crystallography using Gaussview.[51] Frequency calculations were also performed at the same level of theory in order to confirm that the optimized structures were minima on the potential energy hypersurface and to determine thermochemical and vibrational information. Natural bond orbital (NBO) analyses[52] to determine orbital contributions, Wiberg Bond Indices and orbital energies were obtained using the routine included in the Gaussian distributions.[53] Visualizations of the Kohn-Sham orbitals and optimized geometries were made using Gaussview.[51]

3.4.4 X-ray Crystallography

Crystals for investigation were covered in Paratone®, mounted onto a goniometer head, and then rapidly cooled under a stream of cold N_2 of the low-temperature apparatus (Oxford Cryostream) attached to the diffractometer. The data were then collected using the APEXIII (Bruker AXS) software suite on

a Bruker Photon 100 CMOS diffractometer using a graphite monochromator with MoK$_\alpha$ (λ = 0.71073 Å). For each sample, data were collected at low temperature. APEXIII software was used for data reductions and SADABS (Bruker AXS) was used for absorption corrections (multi-scan; semi-empirical from equivalents). XPREP was used to determine the space group and the structures were solved and refined using the SHELX[54] software suite as implemented in the WinGX[55] or OLEX2[56] program suites. Validation of the structures was conducted using PLATON[57] and the structures have been deposited in the Cambridge Structural Database (CCDC 1895464-1895473).

Compound Name	[NBn-BZIMPYGeCl][GeCl$_3$] 0.5(CH$_2$Cl$_2$)	[NBn-BZIMPYSnCl][SnCl$_3$]	[N(3,5-CF$_3$)Bn-BzimpyGeCl][GeCl$_3$]
Label	1	2	3
CCDC ID	1895464	1895465	1895466
Empirical formula	C$_{133}$H$_{102}$Cl$_{18}$Ge$_8$N$_{20}$	C$_{33}$H$_{27}$Cl$_4$N$_5$Sn$_2$	C$_{37}$H$_{21}$Cl$_4$F$_{12}$Ge$_2$N$_5$
Formula weight	3199.16	872.77	1050.57
Temperature (K)	170	170	170
Crystal system	triclinic	triclinic	triclinic
Space group	P–1	P–1	P–1
a (Å)	14.1393(9)	7.4012(4)	8.9182(8)
b (Å)	15.1768(9)	13.5942(8)	14.4073(13)
c (Å)	16.3072(11)	16.4392(9)	16.3208(14)
α (°)	86.094(2)	80.1799(19)	73.936(3)
β (°)	74.051(2)	87.4275(19)	80.147(3)
γ (°)	76.567(2)	79.968(2)	75.525(3)
Volume (Å^3)	3272.6(4)	1604.65(16)	1939.4(3)
Z	1	2	2
ρ_{calc} (g·cm^{-3})	1.623	1.806	1.799
μ (mm^{-1})	2.238	1.923	1.921
F(000)	1602	856	1036
Crystal size (mm^3)	0.21 × 0.21 × 0.135	0.25 × 0.17 × 0.12	0.47 × 0.2 × 0.1
Radiation	MoKα (λ = 0.71073)	MoKα (λ = 0.71073)	MoKα (λ = 0.71073)
2Θ range for data collection (°)	5.872 to 61.186	5.912 to 61.176	5.664 to 58.45
Index ranges	−20 ≤ h ≤ 20 −21 ≤ k ≤ 21 −23 ≤ l ≤ 23	−10 ≤ h ≤ 10 −19 ≤ k ≤ 19 −23 ≤ l ≤ 22	−12 ≤ h ≤ 12 −19 ≤ k ≤ 19 −22 ≤ l ≤ 22
Reflections collected	224637	107568	88406
Independent reflections	20073 R$_{int}$ = 0.0470 R$_{sigma}$ = 0.0236	9854 R$_{int}$ = 0.0273 R$_{sigma}$ = 0.0119	10430 R$_{int}$ = 0.0474 R$_{sigma}$ = 0.0255
Data/restraints/parameters	20073/24/820	9854/0/397	10430/72/569
Goodness-of-fit on F^2	1.07	1.192	1.073
Final R indexes [I>=2σ(I)]	R$_1$ = 0.0375 wR$_2$ = 0.0839	R$_1$ = 0.0220 wR$_2$ = 0.0526	R$_1$ = 0.0632 wR$_2$ = 0.1738
Final R indexes [all data]	R$_1$ = 0.0598 wR$_2$ = 0.0973	R$_1$ = 0.0256 wR$_2$ = 0.0553	R$_1$ = 0.0707 wR$_2$ = 0.1787
Largest diff. peak/hole (e·Å^{-3})	1.36/−1.11	0.47/−1.11	1.67/−1.17
Refinement method	Full-matrix least-squares on F^2		

$$R_1 = \frac{\sum ||F_o| - |F_c||}{\sum |F_o|} \qquad wR_2 = \sqrt{\frac{\sum w(F_o^2 - F_c^2)^2}{\sum w(F_o^2)^2}} \qquad R_{int} = \frac{\sum |F_o^2 - F_o^2(mean)|}{\sum F_o^2} \qquad R_{sigma} = \frac{\sum \sigma(F_o^2)}{\sum F_o^2}$$

Table 3.3. *Crystallographic data and structure refinement.*

Compound Name	[N(3,5-CF₃)Bn-BzimpySnCl][SnCl₃]	[NAllyl-BZIMPYGeCl][GeCl₃]	[O-BZIMPYGeCl][GeCl₃]
Label	4	5	6
CCDC ID	1895467	1895468	1895469
Empirical formula	$C_{37}H_{21}Cl_4F_{12}N_5Sn_2$	$C_{25}H_{21}Cl_4Ge_2N_5$	$C_{19}H_{11}Cl_4Ge_2N_3O_2$
Formula weight	1142.77	678.45	600.29
Temperature (K)	170.2	220	170
Crystal system	triclinic	monoclinic	monoclinic
Space group	P–1	P2₁/c	P2₁/n
a (Å)	9.1861(13)	10.4681(7)	10.4493(7)
b (Å)	13.4274(18)	16.4860(9)	12.5471(7)
c (Å)	17.478(2)	15.2025(9)	16.9264(10)
α (°)	75.357(4)	90	90
β (°)	80.979(4)	94.718(2)	96.429(2)
γ (°)	79.243(4)	90	90
Volume (Å³)	2035.5(5)	2614.7(3)	2205.2(2)
Z	2	4	4
ρcalc (g·cm⁻³)	1.865	1.723	1.808
μ (mm⁻¹)	1.581	2.734	3.233
F(000)	1108	1352	1176
Crystal size (mm³)	0.325 × 0.31 × 0.305	0.25 × 0.22 × 0.07	0.48 × 0.44 × 0.13
Radiation	MoKα (λ = 0.71073)	MoKα (λ = 0.71073)	MoKα (λ = 0.71073)
2Θ range for data collection (°)	5.93 to 55	5.918 to 61.998	5.824 to 58.414
Index ranges	−11 ≤ h ≤ 11 −17 ≤ k ≤ 17 −22 ≤ l ≤ 22	−15 ≤ h ≤ 15 −22 ≤ k ≤ 23 −22 ≤ l ≤ 21	−14 ≤ h ≤ 14 −17 ≤ k ≤ 16 −23 ≤ l ≤ 23
Reflections collected	99263	128096	73857
Independent reflections	9248 Rint = 0.0393 Rsigma = 0.0177	8324 Rint = 0.0602 Rsigma = 0.0283	5953 Rint = 0.0320 Rsigma = 0.0142
Data/restraints/parameters	9248/150/597	8324/0/341	5953/0/271
Goodness-of-fit on F²	1.098	1.144	1.049
Final R indexes [I>=2σ(I)]	R₁ = 0.0617 wR₂ = 0.1484	R₁ = 0.0415 wR₂ = 0.0824	R₁ = 0.0268 wR₂ = 0.0635
Final R indexes [all data]	R₁ = 0.0715 wR₂ = 0.1594	R₁ = 0.0796 wR₂ = 0.1009	R₁ = 0.0322 wR₂ = 0.0673
Largest diff. peak/hole (e·Å⁻³)	2.62/−2.03	0.97/−0.91	0.92/−0.72
Refinement method	Full-matrix least-squares on F²		

$$R_1 = \frac{\sum||F_o|-|F_c||}{\sum|F_o|} \quad wR_2 = \sqrt{\frac{\sum w(F_o^2-F_c^2)^2}{\sum w(F_o^2)^2}} \quad R_{int} = \frac{\sum|F_o^2-F_o^2(mean)|}{\sum F_o^2} \quad R_{sigma} = \frac{\sum \sigma(F_o^2)}{\sum F_o}$$

Table 3.4. *Crystallographic data and structure refinement.*

Compound Name	[NBn-BzimpyGeCl] [OTf]	[NBn-BzimpySn] [OTf]$_2$	[(NBn-BZIMPY)$_2$Ni] [GeCl$_3$]$_2$ 1.5(C$_4$H$_4$O)
Label	7	8	9
CCDC ID	1895470	1895471	1895472
Empirical formula	C$_{34}$H$_{25}$ClF$_3$GeN$_5$O$_3$S	C$_{35}$H$_{25}$F$_6$N$_5$O$_6$S$_2$Sn	C$_{72}$H$_{62}$Cl$_6$Ge$_2$N$_{10}$NiO$_{1.5}$
Formula weight	748.69	908.41	1507.9
Temperature (K)	170	169.94	170
Crystal system	triclinic	monoclinic	triclinic
Space group	P–1	P2$_1$	P–1
a (Å)	8.9152(4)	14.776(11)	13.6605(8)
b (Å)	13.6048(6)	12.477(11)	14.1678(9)
c (Å)	14.3903(7)	20.178(16)	19.8848(14)
α (°)	117.3640(10)	90	82.572(2)
β (°)	95.9400(10)	111.21(2)	76.130(2)
γ (°)	90.1870(10)	90	62.991(2)
Volume (Å^3)	1539.21(12)	3468(5)	3327.9(4)
Z	2	4	2
ρ$_{calc}$ (g·cm^{-3})	1.615	1.74	1.505
μ (mm^{-1})	1.214	0.945	1.473
F(000)	760	1816	1540
Crystal size (mm^3)	0.3 × 0.23 × 0.168	0.28 × 0.2 × 0.18	0.35 × 0.22 × 0.22
Radiation	MoKα (λ = 0.71073)	MoKα (λ = 0.71073)	MoKα (λ = 0.71073)
2Θ range for data collection (°)	5.862 to 61.268	5.916 to 51.904	5.642 to 55.754
Index ranges	−12 ≤ h ≤ 12 −19 ≤ k ≤ 19 −20 ≤ l ≤ 20	−18 ≤ h ≤ 18 −15 ≤ k ≤ 15 −24 ≤ l ≤ 24	−17 ≤ h ≤ 17 −18 ≤ k ≤ 18 −26 ≤ l ≤ 26
Reflections collected	107376	84848	44388
Independent reflections	9453 R$_{int}$ = 0.0257 R$_{sigma}$ = 0.0130	13043 R$_{int}$ = 0.0449 R$_{sigma}$ = 0.0293	15560 R$_{int}$ = 0.0270 R$_{sigma}$ = 0.0316
Data/restraints /parameters	9453/0/433	13043/1/991	15560/174/893
Goodness-of-fit on F^2	1.04	1.125	1.031
Final R indexes [I>=2σ(I)]	R$_1$ = 0.0312 wR$_2$ = 0.0776	R$_1$ = 0.0294 wR$_2$ = 0.0666	R$_1$ = 0.0403 wR$_2$ = 0.0919
Final R indexes [all data]	R$_1$ = 0.0382 wR$_2$ = 0.0828	R$_1$ = 0.0322 wR$_2$ = 0.0676	R$_1$ = 0.0599 wR$_2$ = 0.1055
Largest diff. peak/hole (e·Å^{-3})	1.25/−0.64	0.95/−0.48	0.88/−1.02
Refinement method	Full-matrix least-squares on F^2		

$$R_1 = \frac{\sum||F_o|-|F_c||}{\sum|F_o|} \qquad wR_2 = \sqrt{\frac{\sum w\left(F_o{}^2-F_c{}^2\right)^2}{\sum w\left(F_o{}^2\right)^2}} \qquad R_{int} = \frac{\sum|F_o{}^2-F_o{}^2(mean)|}{\sum F_o{}^2} \qquad R_{sigma} = \frac{\sum \sigma\left(F_o{}^2\right)}{\sum F_o{}^2}$$

Table 3.5. *Crystallographic data and structure refinement.*

Compound Name	[(NBn-BZIMPY)$_2$Ni] [SnCl$_3$]$_2$ 1.5(C$_4$H$_8$O)
Label	10
CCDC ID	1895473
Empirical formula	C$_{72}$H$_{59}$Cl$_6$N$_{10}$NiO$_{1.5}$Sn$_2$
Formula weight	1597.08
Temperature (K)	170
Crystal system	triclinic
Space group	P–1
a (Å)	13.7350(7)
b (Å)	14.0932(8)
c (Å)	19.9403(12)
α (°)	82.180(2)
β (°)	76.134(2)
γ (°)	63.862(2)
Volume (Å^3)	3362.1(3)
Z	2
ρ$_{calc}$ (g·cm^{-3})	1.578
μ (mm^{-1})	1.307
F(000)	1606
Crystal size (mm^3)	0.17 × 0.14 × 0.04
Radiation	MoKα (λ = 0.71073)
2Θ range for data collection (°)	5.566 to 61.016
Index ranges	−19 ≤ h ≤ 19 −20 ≤ k ≤ 20 −28 ≤ l ≤ 28
Reflections collected	223779
Independent reflections	20496 R$_{int}$ = 0.0465 R$_{sigma}$ = 0.0243
Data/restraints /parameters	20496/183/893
Goodness-of-fit on F^2	1.099
Final R indexes [I>=2σ(I)]	R$_1$ = 0.0378 wR$_2$ = 0.0781
Final R indexes [all data]	R$_1$ = 0.0607 wR$_2$ = 0.0917
Largest diff. peak/hole (e·Å^{-3})	1.09/−1.41
Refinement method	Full-matrix least-squares on F^2

$$R_1 = \frac{\sum||F_o|-|F_c||}{\sum|F_o|} \qquad wR_2 = \sqrt{\frac{\sum w(F_o^2-F_c^2)^2}{\sum w(F_o^2)^2}} \qquad R_{int} = \frac{\sum|F_o^2-F_o^2(mean)|}{\sum F_o^2} \qquad R_{sigma} = \frac{\sum \sigma(F_o^2)}{\sum F_o^2}$$

Table 3.6. *Crystallographic data and structure refinement.*

3.5 References

(1) Peris, E.; Crabtree, R. H. *Chem. Soc. Rev.* **2018**, *47*, 1959–1968.

(2) De Bruin, B.; Bill, E.; Bothe, E.; Weyhermüller, T.; Wieghardt, K. *Inorg. Chem.* **2000**, *39* (13), 2936–2947.

(3) Chirik, P. J.; Wieghardt, K. *Science* **2010**, *327* (5967), 794–795.

(4) Gibson, V. C.; Spitzmesser, S. K. *Chem. Rev.* **2003**, *103* (1), 283–315.

(5) Chu, T.; Belding, L.; van der Est, A.; Dudding, T.; Korobkov, I.; Nikonov, G. I. *Angew. Chem. - Int. Ed.* **2014**, *53* (10), 2711–2715.

(6) Flock, J.; Suljanovic, A.; Torvisco, A.; Schoefberger, W.; Gerke, B.; Pöttgen, R.; Fischer, R. C.; Flock, M. *Chem. Eur. J.* **2013**, *19* (46), 15504–15517.

(7) Reeske, G.; Cowley, A. H. *Chem. Commun.* **2006**, *372* (16), 1784.

(8) Martin, C. D.; Ragogna, P. J. *Dalton Trans.* **2011**, *40* (44), 11976.

(9) Jurca, T.; Lummiss, J.; Burchell, T. J.; Gorelsky, S. I.; Richeson, D. S. *J. Am. Chem. Soc.* **2009**, *131* (13), 4608–4609.

(10) Archer, S. J.; Koch, K. R.; Nassimbeni, L. R. *J. Crystallogr. Spectrosc. Res.* **1986**, *16* (4), 449–458.

(11) Evans, D. A.; MacMillan, D. W. C.; Campos, K. R. *J. Am. Chem. Soc.* **1997**, *119* (44), 10859–10860.

(12) Singh, A. P.; Roesky, H. W.; Carl, E.; Stalke, D.; Demers, J. P.; Lange, A. *J. Am. Chem. Soc.* **2012**, *134* (10), 4998–5003.

(13) Jurca, T.; Hiscock, L. K.; Korobkov, I.; Rowley, C. N.; Richeson, D. S. *Dalton Trans.* **2014**, *43* (2), 690–697.

(14) Magdzinski, E.; Gobbo, P.; Workentin, M. S.; Ragogna, P. J. *Inorg. Chem.* **2013**, *52* (19), 11311–11319.

(15) Zhang, Y.; Zhou, Q. F.; Huo, G. F.; Yin, G. Q.; Zhao, X. L.; Jiang, B.; Tan, H.; Li, X.; Yang, H. B. *Inorg. Chem.* **2018**, *57* (7), 3516–3520.

(16) Zheng, Y.; He, L.; Zhang, D. Y.; Tan, C. P.; Ji, L. N.; Mao, Z. W. *Dalton Trans.* **2017**, *46* (34), 11395–11407.

(17) Mansour, A. M.; Shehab, O. R. *Eur. J. Inorg. Chem.* **2017**, (37), 4299–4310.

(18) Günnaz, S.; Özdemir, N.; Dayan, S.; Dayan, O.; Çetinkaya, B. *Organometallics* **2011**, *30* (15), 4165–4173.

(19) Swidan, A.; Binder, J. F.; St. Onge, P. B.; Suter, R.; Burford, N.; Macdonald, C. *Dalton Trans.* **2019**, *48*, 1284–1291.

(20) Liu, S. G.; Zuo, J. L.; Li, Y. Z.; You, X. Z. *J. Mol. Struct.* **2004**, *705* (1–3), 153–157.

(21) Sheng-Guia, L.; Zi-Lub, C.; Kaic, L.; Xiao-Linga, C. *Chinese J. Struct. Chem.* **2013**, (5,) 637–642.

(22) Evans, D. A.; Kozlowski, M. C.; Burgey, C. S.; MacMillan, D. W. C. *J. Am. Chem. Soc.* **1997**, *119* (33), 7893–7894.

(23) Yang, Y.; Li, C. G.; Luo, X. J.; Luo, Z. H.; Liu, R. J.; Jiang, Y. X.; Liang, W. J. *Synth. React. Inorganic, Met. Nano-Metal Chem.* **2016**, *46* (9), 1376–1380.

(24) Morsali, A.; Mahjoub, A. *Inorg. Chem. Commun.* **2004**, *7* (7), 915–918.

(25) Yu, X.-Y.; Zou, H.-H.; Wei, L.-Q.; Zeng, M.-H. *Inorg. Chem. Commun.* **2010**, *13* (10), 1137–1139.

(26) Wei, L.-Q.; Zeng, M.-H.; Ng, S. W. *Acta Crystallogr. Sect. E Struct. Reports Online* **2010**, *66* (1), m56–m56.

(27) Thompson, J. R.; Snider, D.; Wren, J. E. C.; Kroeker, S.; Williams, V. E.; Leznoff, D. B. *Eur. J. Inorg. Chem.* **2017**, No. 1, 88–98.

(28) Meng, F. Y.; Zhou, Y. L.; Zou, H. H.; Zeng, M. H.; Liang, H. *J. Mol. Struct.* **2009**, *920* (1–3), 238–241.

(29) Kocherga, M.; Castaneda, J.; Walter, M. G.; Zhang, Y.; Saleh, N.-A.; Wang, L.; Jones, D. S.; Merkert, J.; Donovan-Merkert, B.; Li, Y.; Hofmann, T.; Schmedake, T. A. *Chem. Commun.* **2018**, *54* (100), 14073–14076.

(30) Suter, R.; Gray, P. A.; Burford, N.; McDonald, R. *Chem. Eur. J.* **2018**, *24* (18), 4718–4723.

(31) Chadwick, F. M.; McKay, A. I.; Martinez-Martinez, A. J.; Rees, N. H.; Krämer, T.; Macgregor, S. A.; Weller, A. S. *Chem. Sci.* **2017**, *8* (9), 5.

(32) Suter, R.; Swidan, A.; Macdonald, C. L. B.; Burford, N. *Chem. Commun.* **2018**, *54* (33), 4140–4143.

(33) Suter, R.; Swidan, A.; Zijlstra, H. S.; Macdonald, C. L. B.; McIndoe, J. S.; Burford, N. *Dalton Trans.* **2018**, *47* (46), 16729–16736.

(34) Swidan, A.; Suter, R.; Macdonald, C. L. B.; Burford, N. *Chem. Sci.* **2018**, *9* (26), 5837–5841.

(35) Batsanov, S. S. *Inorg. Mater.* **2001**, *37* (9), 871–885.

(36) Welch, G. C.; Cabrera, L.; Chase, P. A.; Hollink, E.; Masuda, J. D.; Wei, P.; Stephan, D. W. *Dalton Trans.* **2007**, (31) 3407–3414.

(37) Britovsek, G. J. P.; Ugolotti, J.; White, A. J. P. *Organometallics* **2005**, *24* (7), 1685–1691.

(38) Beckett, M. A.; Strickland, G. C.; Holland, J. R.; Sukumar Varma, K. *Polymer (Guildf).* **1996**, *37* (20), 4629–4631.

(39) Yam, V. W.-W.; Wong, K. M.-C.; Zhu, N. *J. Am. Chem. Soc.* **2002**, *124* (23), 6506–6507.

(40) Tam, A. Y. Y.; Lam, W. H.; Wong, K. M. C.; Zhu, N.; Yam, V. W. W. *Chem. Eur. J.* **2008**, *14* (15), 4562–4576.

(41) Pangborn, A. B.; Giardello, M. A.; Grubbs, R. H.; Rosen, R. K.; Timmers, F. J. *Organometallics* **1996**, *15* (5), 1518–1520.

(42) Addison, A. W.; Rao, T. N.; Wahlgren, C. G. *J. Heterocycl. Chem.* **1983**, 20, 1481–1484.

(43) Singh, A.; Das, G.; Mondal, B. *Polyhedron* **2008**, *27* (12), 2563–2568.

(44) Inkaya, E.; Gunnaz, S.; Ozdemir, N.; Dayan, O.; Dincer, M.; Cetinkaya, B. *Spectrochim Acta A Mol Biomol Spectrosc* **2013**, *103*, 255–263.

(45) Baby, A.; Brunet, J. J.; Kindela, F. B.; Neibecker, D. *Synth. Commun.* **1994**, *24* (20), 2827–2834.

(46) Frisch, M. J.; Trucks, G. W.; Schlegel, H. B.; Scuseria, G. E.; Robb, M. A.; Cheeseman, J. R.; Scalmani, G.; Barone, V.; Mennucci, B.; Petersson, G. A.; Nakatsuji, H.; Caricato, M.; Li, X.; Hratchian, H. P.; Izmaylov, A. F.; Bloino, J.; Zheng, G.; Sonnenberg, J. L.; Hada, M.; Ehara, M.; Toyota, K.; Fukuda, R.; Hasegawa, J.; Ishida, M.; Nakajima, T.; Honda, Y.; Kitao, O.; Nakai, H.; Vreven, T.; Montgomery, J., J. A.; Peralta, J. E.; Ogliaro, F.; Bearpark, M.; Heyd, J. J.; Brothers, E.; Kudin, K. N.; Staroverov, V. N.; Kobayashi, R.; Normand, J.; Raghavachari, K.; Rendell, A.; Burant, J. C.; Iyengar, S. S.; Tomasi, J.; Cossi, M.; Rega, N.; Millam, N. J.; Klene, M.; Knox, J. E.; Cross, J. B.; Bakken, V.; Adamo, C.; Jaramillo, J.; Gomperts, R.; Stratmann, R. E.; Yazyev, O.; Austin, A. J.; Cammi, R.; Pomelli, C.; Ochterski, J. W.; Martin, R. L.; Morokuma, K.; Zakrzewski, V. G.; Voth, G. A.; Salvador, P.; Dannenberg, J. J.; Dapprich, S.; Daniels, A. D.; Farkas, Ö.; Foresman, J. B.; Ortiz, J. V.; Cioslowski, J.; Fox, D. J. *Gaussian 09*; Gaussian, Inc.: Wallingford CT, 2009.

(47) Zhao, Y.; Truhlar, D. G. *Theor. Chem. Acc.* **2008**, *120* (1–3), 215–241.

(48) Dunning, T. H. *J. Chem. Phys.* **1989**, *90* (2), 1007–1023.

(49) Woon, D. E.; Dunning, T. H. *J. Chem. Phys.* **1993**, *98* (2), 1358–1371.

(50) Peterson, K. A. *J. Chem. Phys.* **2003**, *119* (21), 11099–11112.

(51) *Gaussview 3.0*; Gaussian Inc: Pittsburgh, 2003.

(52) Reed, A. E.; Curtiss, L. A.; Weinhold, F. *Chem. Rev.* **1988**, *88* (6), 899–926.

(53) Glendening, E. D.; Badenhoop, J. K.; Reed, A. E.; Carpenter, J. E.; Bohmann, J. A.; Morales, C. M.; Landis, C. R.; Weinhold, F. *NBO 6.0*; Theoretical Chemistry Institute, University of Wisconsin: Madison, WI, 2013.

(54) Sheldrick, G. M. *Acta Crystallogr. Sect. A Found. Crystallogr.* **2008**, *64* (1), 112–122.

(55) Farrugia, L. J. *J. Appl. Crystallogr.* **1999**, *32* (4), 837–838.

(56) Dolomanov, O. V.; Bourhis, L. J.; Gildea, R. J.; Howard, J. A. K.; Puschmann, H. *J. Appl. Crystallogr.* **2009**, *42* (2), 339–341.

(57) Spek, A. L. *J. Appl. Crystallogr.* **2003**, *36* (1), 7–13.

CHAPTER 4:
2,6-Bis(benzimidazol-2-yl)pyridine Complexes of Group 15 Elements

4.1 Introduction

Trinitrogen donors have played an important role in the development of recent main group chemistry.[1–11] Among these notable ligands is the redox-active bis(imino)pyridine (DIMPY) that is useful in preparing highly active transition metal catalysts.[12–14] Cowley and Reeske reported that treatment of DIMPY to a mixture of AsCl$_3$ with SnCl$_2$ generates the arsenic(I)-DIMPY complex shown in **Scheme 4.1**, right.[4] Later work by Ragogna resulted in the isolation of a P(I) cation using PI$_3$ and DIMPY (**Scheme 4.1**, left).[3,5]
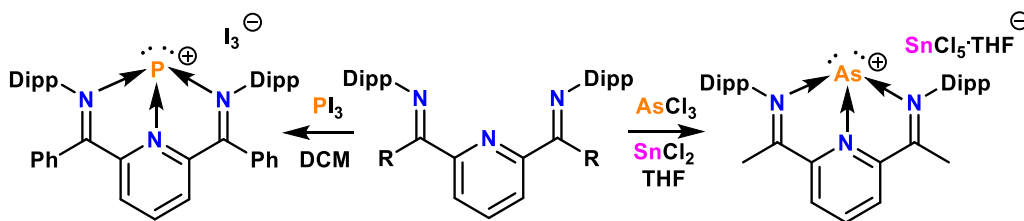
Scheme 4.1. *Low valent P(I) and As(I) complexes of DIMPY. Dipp = 2,6-diisopropylphenyl.*

Stephan and co-workers reported the synthesis of a P(III) dicationic complex of tripyridine that can be prepared as shown in **Scheme 4.2**.[15] The resulting Lewis acid has proven to be useful in catalytic hydrodefluorination (HDF) of unactivated fluoroalkanes.
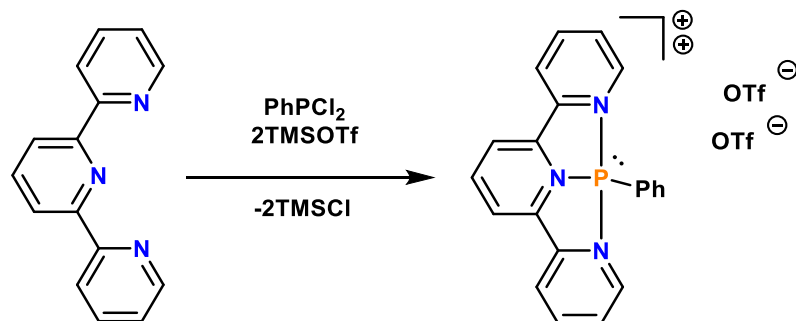
Scheme 4.2. *Stephan's dicationic P(III) catalyst.*

Tridentate ligands, in general, have led to many interesting pnictogen containing compounds.[16–32] In particular, early work by Arduengo presented new and unusual bonding in 10-P-3 ADPO allowing for the idea of a shape-shifting compound.[33] Recently, work by Radosevich and co-workers illustrated that such compounds with distorted tricoordinate phosphorus result in an active phosphorus centre capable of transfer hydrogenation and small molecule activation.[34,35] An example containing a trinitrogen ligand (**Figure 4.1**) can readily activate E-H (O-H and N-H) bonds to yield a phosphorus(V) centre that is reversible to the phosphorus(III) centre at elevated temperatures.[36]
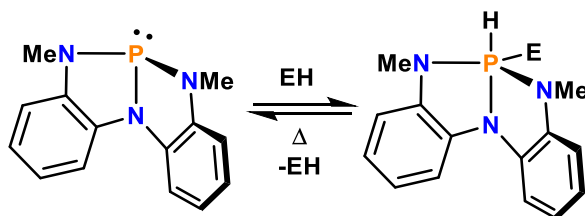
Figure 4.1. *Arduengo's 10–P–3 (T-shaped) and 8–P–3 (bent) phosphines.*

In this work, we explore the coordination of group 15 elements to bisbenzimidazole (BZIMPY) ligands **B** shown in **Figure 4.2** with G = NBn. These

BZIMPY ligands are more rigid than their DIMPY counterparts and have been used to a much lesser extent with transition metals.[37–40] We have recently reported that BZIMPY ligands are more electron-rich and sterically accessible alternatives to DIMPY ligands for group 13 and 14 coordination chemistry.[9,41] Other literature main group complexes of BZIMPY contain indium,[42,43] lead,[44–50] and silicon.[51] Parent NH-BZIMPY ligand allows for the introduction of different substituents to tune the electronic and steric properties. Analogous imidazole and benzimidazole tripodal ligand coordination to MG elements have also been investigated.[52–56]
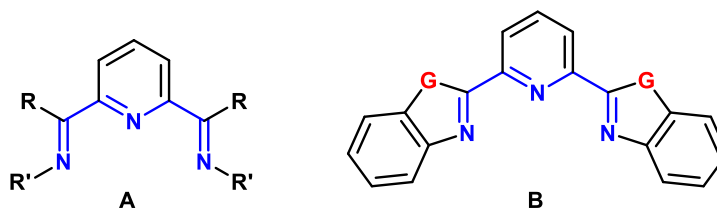
Figure 4.2. *A: DIMPY ligand, B: BZIMPY ligand (G = NH, NBn, N(3,5-CF₃)Bn, N-Allyl and O).*

4.2 Results and Discussion

4.2.1 Synthesis and Characterization

Coordination of group 13 and 14 elements to G-BZIMPY has proven to be successful by treatment of G-BZIMPY with two equivalents of group 13 or 14 metal halides (MCl_3 and MCl_2) yielding the self-ionized products: [G-BZIMPYMCl₂][MCl₄] and [G-BZIMPYMCl][MCl₃], respectively. Extending this approach to group 15 metal halides, MCl_3 (M = P, As and Sb), does not result in any reactivity or any indication of coordination to G-BZIMPY.

As noted above, Cowley[4] and Ragogna[5] were successful in isolating the As(I) and P(I) complexes of DIMPY using $AsCl_3/SnCl_2$ and PI_3, respectively. Attempts to implement this method with NBn-BZIMPY resulted in grey insoluble materials with $PCl_3/SnCl_2$ and orange insoluble materials with PI_3. The only materials collected and characterized from these reactions were those of free NBn-BZIMPY ligand.

On the other hand, following Stephan's[15] work, the introduction of excess TMS-OTf to a solution containing NBn-BZIMPY and PCl_3 in DCM/CH_3CN results in an immediate intense yellow colour (**Scheme 4.3**). After allowing the reaction mixture to stir overnight, solvents were removed under reduced pressure and the resulting solid was suspended in toluene, filtered and dried under vacuum to yield [NBn-BZIMPYPCl][OTf]$_2$ (**1**) as a yellow solid in good yield (79%). Slow evaporation from a DCM/CH_3CN mixture yields yellow crystals of **1** suitable for X-ray diffraction (**Figure 4.3**). A similar procedure was carried out to prepare and isolate [NBn-BZIMPYAsCl][OTf]$_2$ (**2**) and [NBn-BZIMPYSbCl][OTf]$_2$ (**3**) in decent yields (65-83%).
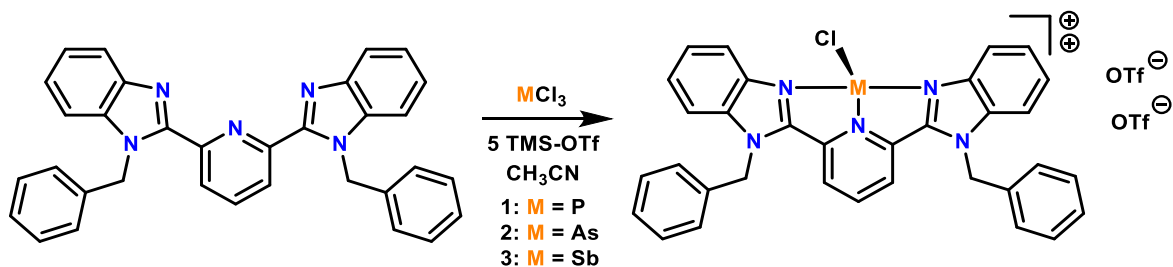
Scheme 4.3. *Reaction of MCl_3 (M = P, As, Sb) with Bn-BZIMPY to yield complexes **1**, **2** and **3**.*
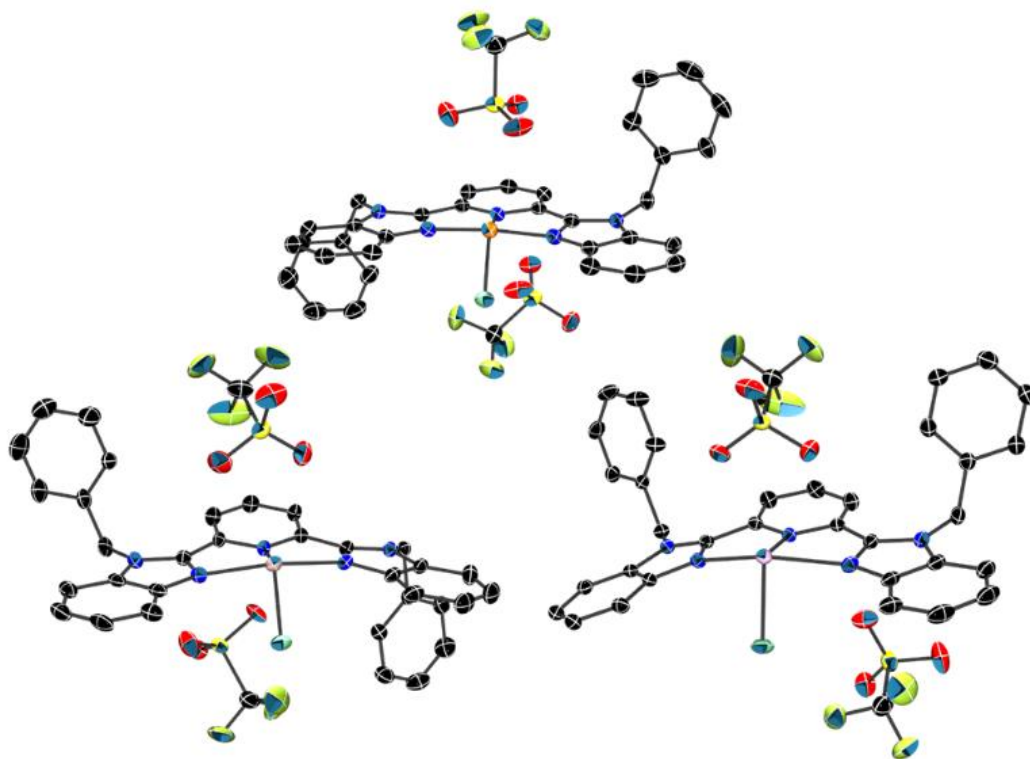
Figure 4.3. *Solid state structure of the [NBn-BZIMPYPCl][OTf]₂ (**1**, top), [NBn-BZIMPYAsCl][OTf]₂ (**2**, left), and [NBn-BZIMPYSbCl] [OTf]₂ (**3**, right). Thermal ellipsoids are shown at 50% probability level. Hydrogen atoms and solvent molecules are omitted for clarity. Selected bond distances and angles of complexes **1-3** are in **Table 4.1**.*

The phosphorus centre in **1** is binding symmetrically to both benzimidazole donors with P-N bond distances of 1.913(2) and 1.916(2) Å. The P-N bond distance to the pyridine nitrogen (1.855(2) Å) is significantly shorter, which is different from that observed in group 13 and 14 complexes where the M-N bond distances to pyridine nitrogen are longer than M-N bond distances to benzimidazole nitrogens. To assess the planarity of complex **1**, the pyridine para-carbon, pyridine nitrogen and phosphorus angle is examined. For complex **1**, C5-N2-P angle is 175.8(1)°, which is close to 180°, suggesting a planar complex. As the binding element increases in size going to As and Sb, this angle decreases as the main group element sits slightly above the plane of

the ligand, resulting in slight distortion to the planarity and the C5-N2-M angles being 164.0(4)° for arsenic and 166.2(1)° for antimony.

As a result of this distortion in planarity, the solid-state structure is not symmetric, resulting in differences in the M-N bond distances to the two benzimidazole arms. In arsenic, the As-N bond distances to benzimidazoles are 2.089(7) and 2.130(7) Å, while the As-N bond distance to the pyridine nitrogen is 2.002(7) Å, consistent with the observation made in **1**, having a shorter M-N bond distance to pyridine. Similarly, antimony binding results in slight distortion in the planarity of the ligand with the antimony centre sitting closer to N1 and N2 (2.253(2) and 2.260(2) Å, respectively) compared to N3 (2.292(2) Å).
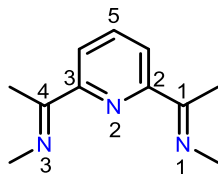
	1	**2**	**3**
M-N1	1.913(2)	2.089(7)	2.253(2)
M-N2	1.855(2)	2.002(7)	2.260(2)
M-N3	1.916(2)	2.130(7)	2.292(2)
M-Cl	2.0549(11)	2.168(2)	2.3585(9)
N1-C1	1.326(4)	1.317(11)	1.335(3)
C1-C2	1.452(4)	1.455(11)	1.462(4)
C2-N2	1.366(3)	1.363(10)	1.357(3)
N2-C3	1.367(3)	1.353(10)	1.358(3)
C3-C4	1.451(4)	1.455(11)	1.469(3)
C4-N3	1.326(4)	1.313(10)	1.331(3)
N1-M-N2	79.83(9)	76.4(3)	70.54(8)
N2-M-N3	80.08(9)	76.5(3)	70.16(7)
N2-M-N3	156.89(10)	149.5(3)	136.10(8)
C5-N2-M	175.8(1)	164.0(4)	166.2(1)

Table 4.1. *Selected bond distances (Å) and angles (°) of complexes **1**, **2** and **3**.*

While the reaction has a distinct colour change from colourless to yellow upon the addition of TMS-OTf, the ^{1}H NMR spectrum exhibits a clear downfield shift of the ligand protons upon binding of the metal centre which can be used as a handle to confirm coordination. The C5-H proton in particular is very sensitive to pnictogen binding and this sensitivity is dependent on the main group element bound. The downfield shift, Δδ, observed increases going from Sb to As to P as shown in **Figure 4.4**. Thus, going up the periodic table results in greater influence on the shift of the ligand protons.

CH$_3$CN solutions were prepared containing an equivalent of triethylphosphine oxide with **1**, **2** and **3**. These solutions exhibited a significant shift ($\Delta\delta$ ~51 ppm) in the ^{31}P{^{1}H} NMR spectrum from the free phosphine oxide (δ= 41.0 ppm). Using the Gutmann-Beckett method, these shifts correspond to acceptor numbers of 112-113 for complexes **1**-**3**. To put this into perspective, other commonly used boron containing Lewis acids have the following acceptor numbers: B(C$_6$F$_5$)$_3$ (82) <BF$_3$ (89) < BCl$_3$ (106) < BBr$_3$ (109) < BI$_3$ (115). This suggests that complexes **1**-**3** are very strong Lewis acid and are comparable to other strong BX$_3$ (X = Cl, Br, and I) Lewis acids.
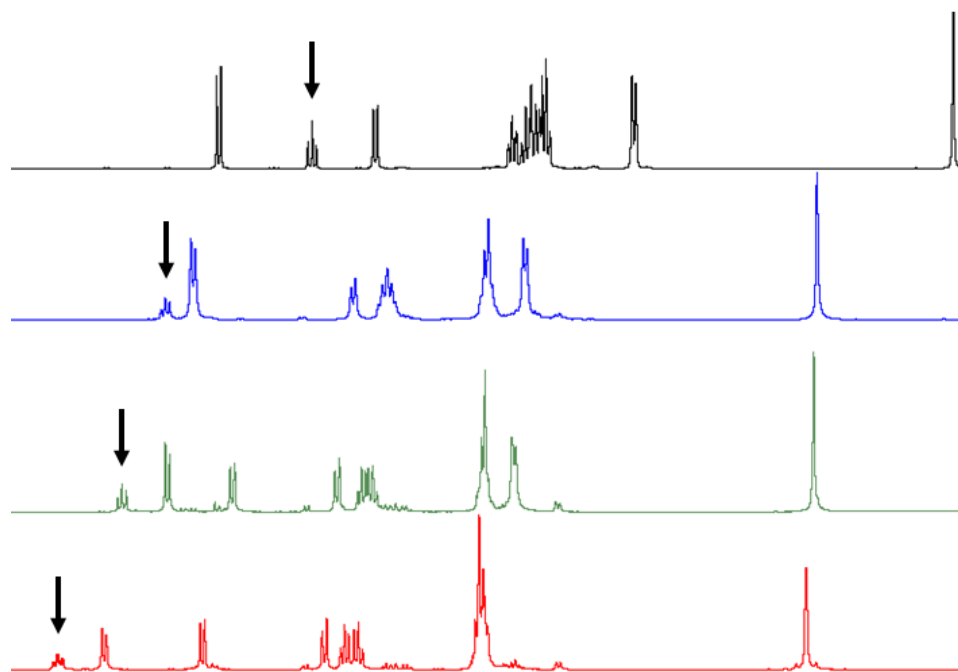
Figure 4.4. ^{1}H NMR of **1** (red), **2** (green), **3** (blue), and free NBn-BZIMPY ligand (black).

4.3 Conclusions

We present group 15 (P, As, and Sb) coordination to 2,6-Bis(benzimidazol-2-yl)pyridine (NBn-BZIMPY) ligand. The resulting complexes are characterized by FT-

NMR and SC X-ray Diffraction. Further chemistry and reactivity are currently under way.

4.4 Experimental

4.4.1 General Remarks

All manipulations were carried out using standard inert-atmosphere techniques. All reagents and chemicals were obtained from Sigma-Aldrich. All reagents were used without further purification. MeCN-d_3 was dried over calcium hydride or phosphorus pentoxide, and dichloromethane-d_2 was dried over phosphorus pentoxide. All other solvents were dried on a series of Grubbs-type columns and were degassed prior to use.[57] All glassware was stored in a 170 °C oven for several hours and was degassed prior to use. 2,6-Bis(benzimidazol-2-yl)pyridine (NH-BZIMPY),[58] and the alkylation of NBn-BZIMPY[59] were prepared according to literature procedures. Alkylation reactions of NH-BZIMPY were carried according to general procedure reported.[9,59]

NMR spectra were recorded at room temperature on Bruker Avance III 500 MHz, Bruker Avance Ultrashield 300 MHz, and Bruker Avance DPX 300 MHz spectrometers. Chemical shifts are reported in parts per million relative to internal standards for ^{1}H and ^{13}C (the given deuterated solvent) and external standards for ^{19}F (CFCl$_3$) and ^{31}P (85% H$_3$PO$_4$). Coupling constants |J| are given in hertz. Elemental analysis was performed at the University of Windsor Mass

Spectrometry Service Laboratory using a Perkin-Elmer 2400 combustion CHN analyzer.

4.4.2 Synthetic Information
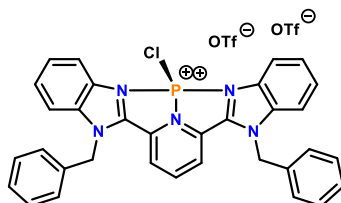
[NBn-BZIMPYPCl][OTf]₂ (1) To 100 mL Schlenk flask charged with NBn-Bzimpy (305 mg, 0.62 mmol) in 40 mL CH$_3$CN, PCl$_3$ (56 μL, 0.62 mmol) was added followed by TMSOTf (0.45 mL, 2.5 mmol). This resulted in an immediate formation of a yellow solution that was allowed to stir for 18 hours. Solvents were removed under reduced pressure and the resulting solid was suspended in Et$_2$O (20 mL), collected and washed with Et$_2$O (2×10 mL) yielding **1** as a yellow solid (420 mg, 79%). Slow evaporation from dichloromethane yielded crystals suitable for X-ray Diffraction. ^{1}H NMR (CD$_3$CN) δ: 8.99 (t, 1H, $^3J_{HH}$ = 8 Hz), 8.82 (d, 2H, $^3J_{HH}$ = 8 Hz), 8.45 (d, 2H, $^3J_{HH}$ = 8 Hz), 7.99 (d, 2H, $^3J_{HH}$ = 8 Hz), 7.88 (m, 4H), 7.40 (m, 10H), 6.18 (s, 4H). ^{13}C{^{1}H} NMR δ: 152.62 (d, J_{CP} = 5 Hz) 141.63, 140.77 (d, J_{CP} = 13 Hz) 138.62 (d, J_{CP} = 8 Hz), 133.61, 132.63, 130.75, 130.41, 129.94 (d, J_{CP} = 13 Hz), 127.83, 127.72, 127.26 (d, J_{CP} = 7 Hz), 119.75 (q, $^1J_{CF}$ = 315 Hz), 118.48, 115.08, 50.89. ^{19}F{^{1}H} NMR δ: –78.56. Anal. Calc. for C$_{35}$H$_{25}$ClF$_6$N$_5$O$_6$PS$_2$ (856.15g/mol): C, 49.10; H, 2.94; N, 8.18. Found: C, 48.91; H, 3.23; N, 8.05.
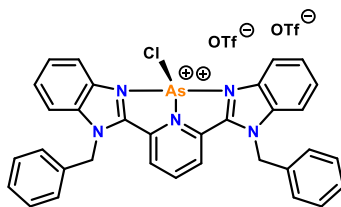
[NBn-BZIMPYAsCl][OTf]₂ (**2**) To a 20 mL vial was charged with NBn-Bzimpy (30 mg, 0.06 mmol) in 5 mL CD_3CN, $AsCl_3$ (5.3 µL, 0.06 mmol) was added followed by TMSOTf (44 µL, 0.24 mmol). This resulted in an immediate formation of a yellow solution that was allowed to stir for 18 hours. The solution was then slowly evaporated to yield **2** as yellow crystals (36 mg, 65%). ¹H NMR (CD_3CN) δ: 8.75 (t, 1H, $^3J_{HH}$ = 8 Hz), 8.58 (d, 2H, $^3J_{HH}$ = 8 Hz), 8.33 (d, 2H, $^3J_{HH}$ = 8 Hz), 7.94 (d, 2H, $^3J_{HH}$ = 8 Hz), 7.84 (m, 4H, $^3J_{HH}$ = 8 Hz), 7.38 (m, 6H), 7.27 (d, 4H, $^3J_{HH}$ = 8 Hz), 6.15 (s, 4H). ¹³C{¹H} NMR δ: 151.10, 143.75, 142.45, 138.57, 135.02, 133.81, 130.44, 130.16, 130.03, 129.80, 129.55, 127.60, 127.20, 119.98 (q, $^1J_{CF}$ = 318 Hz), 118.70, 114.50, 50.66. ¹⁹F{¹H} NMR δ: –78.58. Anal. Calc. for $C_{35}H_{25}ClF_6N_5O_6AsS_2$ (900.10g/mol): C, 46.70; H, 2.80; N, 7.78. Found: C, 47.26; H, 3.12; N, 7.76.
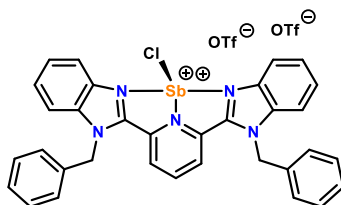
[NBn-BZIMPYSbCl][OTf]₂] (**3**) To a 20 mL vial was charged with NBn-Bzimpy (30 mg, 0.06 mmol) in 5 mL CD_3CN, $SbCl_3$ (14 mg, 0.06 mmol) was added followed by TMSOTf (44 µL, 0.24 mmol). This resulted in an immediate formation of a yellow solution that was allowed to stir for 18 hours. The solution was then slowly evaporated to yield **3** as yellow crystals (48 mg, 83%).

^{1}H NMR (CD$_3$CN) δ: 8.59 (t, 1H, $^3J_{HH}$ = 8 Hz), 8.48 (d, 4H, $^3J_{HH}$ = 8 Hz), 7.88 (d, 2H, $^3J_{HH}$ = 8 Hz), 7.75 (p, 4H, $^3J_{HH}$ = 8 Hz), 7.38 (m, 6H), 7.23 (d, 4H, $^3J_{HH}$ = 8 Hz), 6.14 (s, 4H). ^{13}C{^{1}H} NMR δ: 148.63, 146.93, 142.55, 138.46, 136.56, 134.06, 130.44, 129.70, 129.52, 128.92, 127.85, 127.06, 119.58 (q, $^1J_{CF}$ = 317 Hz), 119.20, 114.04, 50.79. ^{19}F{^{1}H} NMR δ: –78.46. Anal. Calc. for C$_{35}$H$_{25}$ClF$_6$N$_5$O$_6$SbS$_2$ (946.94 g/mol): C, 44.39; H, 2.66; N, 7.40. Found: C, 44.34; H, 2.97; N, 7.29.

Gutmann-Beckett method:

General Method; A 20mL vial was charged with **1**, **2** or **3** (0.02 mmol) and OPEt$_3$ (0.02 mmol) in 1 mL CH$_3$CN. Reaction mixture was stirred for 30 minutes before collecting phosphorus NMR spectrum. ^{31}P{^{1}H} NMR (**1** + OPEt$_3$) (CH$_3$CN) δ: 110.2 (P-Cl), 92.0 (OPEt$_3$). ^{31}P{^{1}H} NMR (**2** + OPEt$_3$) (CH$_3$CN) δ: 92.0. ^{31}P{^{1}H} NMR (**3** + OPEt$_3$) (CH$_3$CN) δ: 91.9.

4.4.3 X-ray Crystallography

Crystals for investigation were covered in Paratone®, mounted onto a goniometer head, and then rapidly cooled under a stream of cold N$_2$ of the low-temperature apparatus (Oxford Cryostream) attached to the diffractometer. The data were then collected using the APEXIII (Bruker AXS) software suite on a Bruker Photon 100 CMOS diffractometer using a graphite monochromator with MoK$_\alpha$ (λ = 0.71073 Å). For each sample, data were collected at low temperature. APEXIII software was used for data reductions and SADABS (Bruker AXS) was used for absorption corrections (multi-scan; semi-empirical from equivalents). XPREP was used to determine the

space group and the structures were solved and refined using the SHELX[60] software

suite as implemented in the WinGX[61] or OLEX2[62] program suites. Validation of the

structures was conducted using PLATON[63] and the structures have been deposited in

the Cambridge Structural Database (CCDC 1900124-1900126).

Compound Name	[NBn-BzimpyPCl][OTf]$_2$	[NBn-BzimpyAsCl][OTf]$_2$	[NBn-BzimpySbCl][OTf]$_2$
Label	1	2	3
CCDC ID	1900124	1900125	1900126
Empirical formula	C$_{37}$H$_{28}$ClF$_6$N$_6$O$_6$PS$_2$	C$_{35}$H$_{25}$AsClF$_6$N$_5$O$_6$S$_2$	C$_{35}$H$_{25}$ClF$_6$N$_5$O$_6$S$_2$Sb
Formula weight	897.19	900.09	946.92
Temperature (K)	170	170.02	170
Crystal system	triclinic	triclinic	monoclinic
Space group	P–1	P–1	P2$_1$/c
a (Å)	10.868(3)	10.3092(10)	10.468(3)
b (Å)	12.773(4)	12.1838(12)	38.097(11)
c (Å)	14.929(5)	15.3923(16)	8.951(3)
α (°)	113.309(10)	75.358(3)	90
β (°)	90.838(10)	86.818(4)	96.418(7)
γ (°)	92.882(9)	75.649(4)	90
Volume (Å^3)	1899.6(9)	1812.1(3)	3547.4(18)
Z	2	2	4
ρ$_{calc}$ (g·cm^{-3})	1.569	1.65	1.773
μ (mm^{-1})	0.339	1.212	1.058
F(000)	916	908	1888
Crystal size (mm^3)	0.33 × 0.19 × 0.1	0.12 × 0.1 × 0.08	0.3 × 0.27 × 0.24
Radiation	MoKα (λ = 0.71073)	MoKα (λ = 0.71073)	MoKα (λ = 0.71073)
2Θ range for data collection (°)	6.39 to 53.46	5.744 to 55.136	5.784 to 59.15
Index ranges	−10 ≤ h ≤ 13 −16 ≤ k ≤ 16 −18 ≤ l ≤ 18	−13 ≤ h ≤ 13 −15 ≤ k ≤ 15 −20 ≤ l ≤ 20	−13 ≤ h ≤ 14 −49 ≤ k ≤ 52 −12 ≤ l ≤ 12
Reflections collected	23186	83558	27892
Independent reflections	7973 R$_{int}$ = 0.0529 R$_{sigma}$ = 0.0646	8292 R$_{int}$ = 0.1186 R$_{sigma}$ = 0.0531	9818 R$_{int}$ = 0.0369 R$_{sigma}$ = 0.0399
Data/restraints/parameters	7973/0/533	8292/0/505	9818/0/505
Goodness-of-fit on F^2	1.017	1.129	1.091
Final R indexes [I>=2σ(I)]	R$_1$ = 0.0482 wR$_2$ = 0.1135	R$_1$ = 0.1030 wR$_2$ = 0.2660	R$_1$ = 0.0391 wR$_2$ = 0.0917
Final R indexes [all data]	R$_1$ = 0.0817 wR$_2$ = 0.1287	R$_1$ = 0.1262 wR$_2$ = 0.2785	R$_1$ = 0.0461 wR$_2$ = 0.0947
Largest diff. peak/hole (e·Å^{-3})	1.08/−0.39	3.04/−0.87	0.84/−1.41
Refinement method	Full-matrix least-squares on F^2		

$$R_1 = \frac{\sum ||F_o| - |F_c||}{\sum |F_o|} \qquad wR_2 = \sqrt{\frac{\sum w(F_o{}^2 - F_c{}^2)^2}{\sum w(F_o{}^2)^2}} \qquad R_{int} = \frac{\sum |F_o{}^2 - F_o{}^2(mean)|}{\sum F_o{}^2} \qquad R_{sigma} = \frac{\sum \sigma(F_o{}^2)}{\sum F_o}$$

Table 4.2. *Crystallographic data and structure refinement.*

4.5 References

(1)   Chu, T.; Belding, L.; van der Est, A.; Dudding, T.; Korobkov, I.; Nikonov, G. I. *Angew. Chem. - Int. Ed.* **2014**, *53* (10), 2711–2715.

(2)   Flock, J.; Suljanovic, A.; Torvisco, A.; Schoefberger, W.; Gerke, B.; Pöttgen, R.; Fischer, R. C.; Flock, M. *Chem. Eur. J.* **2013**, *19* (46), 15504–15517.

(3)   Reeske, G.; Cowley, A. H. *Chem. Commun.* **2006**, *372* (16), 1784.

(4)   Martin, C. D.; Ragogna, P. J. *Dalton Trans.* **2011**, *40* (44), 11976.

(5)   Jurca, T.; Lummiss, J.; Burchell, T. J.; Gorelsky, S. I.; Richeson, D. S. *J. Am. Chem. Soc.* **2009**, *131* (13), 4608–4609.

(6)   Archer, S. J.; Koch, K. R.; Nassimbeni, L. R. *J. Crystallogr. Spectrosc. Res.* **1986**, *16* (4), 449–458.

(7)   Singh, A. P.; Roesky, H. W.; Carl, E.; Stalke, D.; Demers, J. P.; Lange, A. *J. Am. Chem. Soc.* **2012**, *134* (10), 4998–5003.

(8)   Swidan, A.; Binder, J. F.; St. Onge, P. B.; Suter, R.; Burford, N.; Macdonald, C. *Dalton Trans.* **2019**, *48*, 1284–1291.

(9)   Ferraz, K. S. O.; Silva, N. F.; Jeferson, G.; Miranda, L. F. De; Romeiro, C. F. D.; Souza-fagundes, E. M.; Mendes, I. C.; Beraldo, H. *Eur. J. Med. Chem.* **2012**, *53* (2), 98–106.

(10)   Battaglia, L. P.; Corradi, A. B.; Pelosi, G.; Cantoni, A.; Alonzo, G.; Bertazzi, N. *J. Chem. Soc. Dalton Trans.* **1991**, (11), 3153–3155.

(11)   Magdzinski, E.; Gobbo, P.; Martin, C. D.; Workentin, M. S.; Ragogna, P. J. *Inorg.*

Chem. **2012**, *51* (15), 8425–8432.

(12)   De Bruin, B.; Bill, E.; Bothe, E.; Weyhermüller, T.; Wieghardt, K. *Inorg. Chem.* **2000**, *39* (13), 2936–2947.

(13)   Chirik, P. J.; Wieghardt, K. *Science (80-.).* **2010**, *327* (5967), 794–795.

(14)   Gibson, V. C.; Spitzmesser, S. K. *Chem. Rev.* **2003**, *103* (1), 283–315.

(15)   Chitnis, S. S.; Krischer, F.; Stephan, D. W. *Chem. Eur. J.* **2018**, *24*, 6543–6546.

(16)   Herbert, D. E.; Miller, A. D.; Ozerov, O. V. *Chem. Eur. J.* **2012**, *18* (25), 7696–7704.

(17)   Stewart, C. A.; Calabrese, J. C.; Arduengo, A. J. *J. Am. Chem. Soc.* **1985**, *107* (11), 3397–3398.

(18)   Robinson, T. P.; De Rosa, D. M.; Aldridge, S.; Goicoechea, J. M. *Angew. Chem. - Int. Ed.* **2015**, *54* (46), 13758–13763.

(19)   Arduengo, A. J.; Culley, S. A. *J. Am. Chem. Soc.* **1985**, *107* (4), 1089–1090.

(20)   Culley, S. A.; Arduengo, A. J. *J. Am. Chem. Soc.* **1984**, *106* (4), 1164–1165.

(21)   Arduengo, A. J.; Stewart, C. A.; Davidson, F. *J. Am. Chem. Soc.* **1986**, *108* (2), 322–323.

(22)   Hyvl, J.; Yoshida, W. Y.; Moore, C. E.; Rheingold, A. L.; Cain, M. F. *Polyhedron* **2018**, *143*, 99–104.

(23)   Svoboda, T.; Jambor, R.; Růžička, A.; Padělková, Z.; Erben, M.; Jirásko, R.; Dostál, L. *Eur. J. Inorg. Chem.* **2010**, *2010* (11), 1663–1669.

(24)   Vránová, I.; Jambor, R.; Růžička, A.; Hoffmann, A.; Herres-Pawlis, S.; Dostál, L.

Dalton Trans. **2015**, *44* (1), 395–400.

(25)   Robinson, T. P.; Lo, S.-K.; De Rosa, D.; Aldridge, S.; Goicoechea, J. M. *Chem. Eur. J.* **2016**, *22* (44), 15712–15724.

(26)   Strîmb, G.; Pöllnitz, A.; Raţ, C. I.; Silvestru, C. *Dalton Trans.* **2015**, *44* (21), 9927–9942.

(27)   Cui, J.; Li, Y.; Ganguly, R.; Kinjo, R. *Chem. Eur. J.* **2016**, *22* (29), 9976–9985.

(28)   Kilian, P.; Slawin, A. M. Z. *Dalton Trans.* **2007**, No. 30, 3289–3296.

(29)   Bezombes, J.-P.; Carré, F.; Chuit, C.; Corriu, R. J. P.; Mehdi, A.; Reyé, C. *J. Organomet. Chem.* **1997**, *535* (1), 81–90.

(30)   Cui, J.; Li, Y.; Ganguly, R.; Inthirarajah, A.; Hirao, H.; Kinjo, R. *J. Am. Chem. Soc.* **2014**, *136* (48), 16764–16767.

(31)   Day, G. S.; Pan, B.; Kellenberger, D. L.; Foxman, B. M.; Thomas, C. M. *Chem. Commun.* **2011**, *47* (12), 3634–3636.

(32)   Robinson, T. P.; De Rosa, D.; Aldridge, S.; Goicoechea, J. M. *Chem. Eur. J.* **2017**, *23* (61), 15455–15465.

(33)   Arduengo, A. J.; Stewart, C. A. *Chem. Rev.* **1994**, *94* (5), 1215–1237.

(34)   McCarthy, S. M.; Lin, Y. C.; Devarajan, D.; Chang, J. W.; Yennawar, H. P.; Rioux, R. M.; Ess, D. H.; Radosevich, A. T. *J. Am. Chem. Soc.* **2014**, *136* (12), 4640–4650.

(35)   Dunn, N. L.; Ha, M.; Radosevich, A. T. *J. Am. Chem. Soc.* **2012**, *134* (28), 11330–11333.

(36) Zhao, W.; McCarthy, S. M.; Lai, T. Y.; Yennawar, H. P.; Radosevich, A. T. *J. Am. Chem. Soc.* **2014**, *136* (50), 17634–17644.

(37) Zhang, Y.; Zhou, Q. F.; Huo, G. F.; Yin, G. Q.; Zhao, X. L.; Jiang, B.; Tan, H.; Li, X.; Yang, H. B. *Inorg. Chem.* **2018**, *57* (7), 3516–3520.

(38) Zheng, Y.; He, L.; Zhang, D. Y.; Tan, C. P.; Ji, L. N.; Mao, Z. W. *Dalton Trans.* **2017**, *46* (34), 11395–11407.

(39) Mansour, A. M.; Shehab, O. R. *Eur. J. Inorg. Chem.* **2017**, (37), 4299–4310.

(40) Günnaz, S.; Özdemir, N.; Dayan, S.; Dayan, O.; Çetinkaya, B. *Organometallics* **2011**, *30* (15), 4165–4173.

(41) Swidan, A.; St. Onge, P. B.; Binder, J. F.; Suter, R.; Burford, N.; Macdonald, C. *Dalton Trans.* **2019**, *48*, 7835-7843.

(42) Liu, S. G.; Zuo, J. L.; Li, Y. Z.; You, X. Z. *J. Mol. Struct.* **2004**, *705* (1–3), 153–157.

(43) LIU Sheng-Guia, CHEN Zi-Lub, LIANG Kaic, C. X.-L. *Chinese J. Struct. Chem.* **2013**, No. 5, 637–642.

(44) Evans, D. A.; Kozlowski, M. C.; Burgey, C. S.; MacMillan, D. W. C. *J. Am. Chem. Soc.* **1997**, *119* (33), 7893–7894.

(45) Yang, Y.; Li, C. G.; Luo, X. J.; Luo, Z. H.; Liu, R. J.; Jiang, Y. X.; Liang, W. J. *Synth. React. Inorganic, Met. Nano-Metal Chem.* **2016**, *46* (9), 1376–1380.

(46) Morsali, A.; Mahjoub, A. *Inorg. Chem. Commun.* **2004**, *7* (7), 915–918.

(47) Yu, X.-Y.; Zou, H.-H.; Wei, L.-Q.; Zeng, M.-H. *Inorg. Chem. Commun.* **2010**, *13* (10), 1137–1139.

(48)   Wei, L.-Q.; Zeng, M.-H.; Ng, S. W. *Acta Crystallogr. Sect. E Struct. Reports Online* **2010**, *66* (1), m56–m56.

(49)   Thompson, J. R.; Snider, D.; Wren, J. E. C.; Kroeker, S.; Williams, V. E.; Leznoff, D. B. *Eur. J. Inorg. Chem.* **2017**, *2017* (1), 88–98.

(50)   Meng, F. Y.; Zhou, Y. L.; Zou, H. H.; Zeng, M. H.; Liang, H. *J. Mol. Struct.* **2009**, *920* (1–3), 238–241.

(51)   Kocherga, M.; Castaneda, J.; Walter, M. G.; Zhang, Y.; Saleh, N.-A.; Wang, L.; Jones, D. S.; Merkert, J. W.; Donovan-Merkert, B.; Li, Y.; Hofmann, T.; Schmedake, T. A. *Chem. Commun.* **2018**.

(52)   Swidan, A.; St. Onge, P. B.; Binder, J. F.; Suter, R.; Burford, N.; Macdonald, C. *Dalton Trans.* **2019**, *48*, 7835-7843.

(53)   Suter, R.; Swidan, A.; Zijlstra, H. S.; Macdonald, C. L. B.; McIndoe, J. S.; Burford, N. *Dalton Trans.* **2018**, *47* (46), 16729–16736.

(54)   Suter, R.; Swidan, A.; Macdonald, C. L. B.; Burford, N. *Chem. Commun.* **2018**, *54* (33), 4140–4143.

(55)   Swidan, A.; Suter, R.; Macdonald, C. L. B.; Burford, N. *Chem. Sci.* **2018**, *9* (26), 5837–5841.

(56)   Suter, R.; Gray, P. A.; Burford, N.; McDonald, R. *Chem. Eur. J.* **2018**, *24* (18), 4718–4723.

(57)   Pangborn, A. B.; Giardello, M. A.; Grubbs, R. H.; Rosen, R. K.; Timmers, F. J. *Organometallics* **1996**, *15* (5), 1518–1520.

(58)   Addison, A. W.; Rao, T. N.; Wahlgren, C. G. *J. Heterocycl. Chem*. **1983**, *20*, 1481–1484.

(59)   Inkaya, E.; Gunnaz, S.; Ozdemir, N.; Dayan, O.; Dincer, M.; Cetinkaya, B. *Spectrochim Acta A Mol Biomol Spectrosc* **2013**, *103*, 255–263.

(60)   Sheldrick, G. M. *Acta Crystallogr. Sect. A Found. Crystallogr.* **2008**, *64* (1), 112–122.

(61)   Farrugia, L. J. *J. Appl. Crystallogr.* **1999**, *32* (4), 837–838.

(62)   Dolomanov, O. V.; Bourhis, L. J.; Gildea, R. J.; Howard, J. A. K.; Puschmann, H. *J. Appl. Crystallogr.* **2009**, *42* (2), 339–341.

(63)   Spek, A. L. *J. Appl. Crystallogr.* **2003**, *36* (1), 7–13.

CHAPTER 5:
Tris(benzoimidazol)amine (L) complexes of pnictogen(III) and pnictogen(V) cations and the [LP]$^{3+}$/[LPF$_2$]$^{3+}$ redox couple

5.1 Introduction

Phosphorus(III) centres can undergo reversible oxidative addition of N-H and O-H bonds and have potential application as catalysts in organic transformations. This traditional Lewis basic reactivity extends to pnictogen(III) centres in general, but has been challenged by the realization of the Lewis acid "umpolung" made possible by the introduction of a cationic charge.[2] A variety of pnictogen(III) based cations have been synthesized by halide abstraction from PnX$_3$ derivatives in the presence of various ligands and weakly coordinating anions.[3] The cationic charge not only lowers the energy of the pnictogen based LUMO but also lowers the energy of the HOMO, so that oxidation is impeded. Consequently, examples of redox couples of the type [Pn(III)]$^{3+}$: [Pn(V)R$_2$]$^{3+}$ have not been reported. The fluorophilicity of phosphenium cations[4] and dications[5] is well established and has led to the discovery of effective catalysts for hydrofluorination reactions.[6] The Lewis acidity of [LPR]$^{2+}$ with L = terpyridine is an active catalyst for dehydrofluorination of fluoroalkanes, suggesting a substantial fluoride affinity.[7]

We have recently shown that the multidentate BIMEt$_3$ ligand encapsulates a germanium dication that is readily oxidized to [BIMEt$_3$GeF$_2$][OTf]$_2$, and have now exploited the versatility of this ligand to synthesise [P(BIMEt$_3$)][OTf]$_3$.[8] As an analogue of the Verkade superbases (**I**),[9] the trication adopts a proazaphosphatrane

127

CHAPTER 5
Tris(benzoimidazol)amine (L) complexes of pnictogen(III) and pnictogen(V) cations and the
[LP]3+/[LPF2]3+ redox couple

type cage structure, and is oxidized by XeF_2 to give $[P(BIMEt_3)F_2][OTf]_3$, which

represents a rare example of a cationic Pn(V) centre with a charge > +2.[10] (e.g. for +2

charge $[Ph_3PnL_x][OTf]_2$, Pn = As[11], Sb, Bi[12]; and +3 charge $[Ph_2SbL_x][OTf]_3$[13]). The

synthesis and characterization of the heavier tricationic pnictogen salts

$[BIMEt_3Pn][OTf]_3$ (Pn = As, Sb) are also reported.
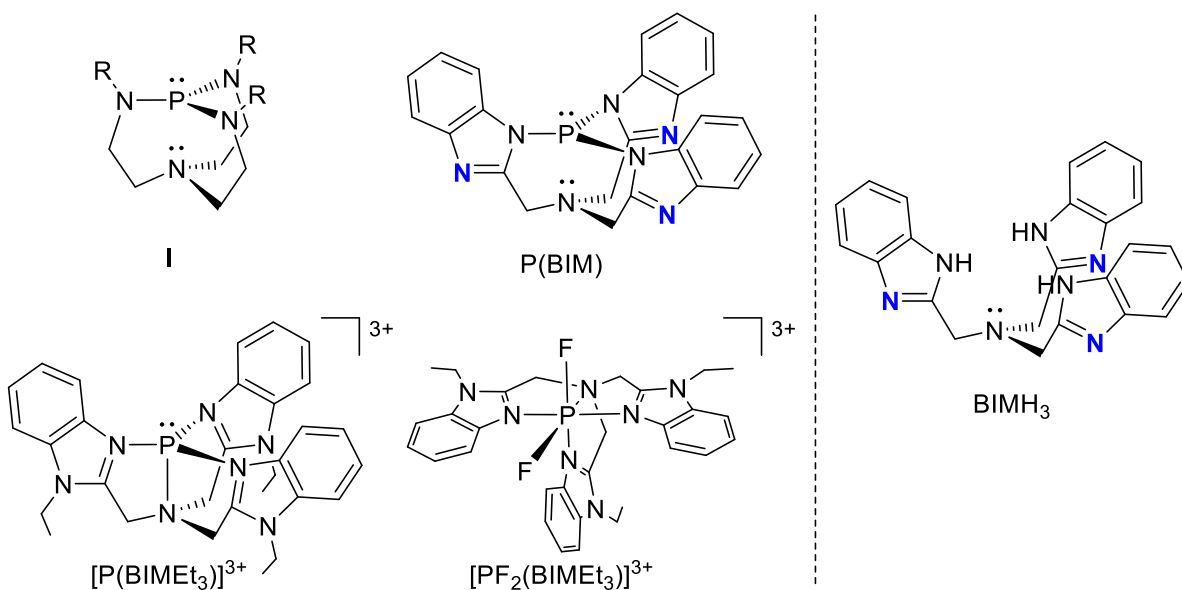
Figure 5.1. *Highlight of the phosphorus containing compounds synthesized (left), BIMH₃ ligand (right).*

5.2 Results and Discussion

P(BIM) was synthesized from the reaction of BIMH₃[14] (**Figure 5.1**) and PCl_3

in the presence of a slight excess of NaH in THF at room temperature. Quantitative

formation of P(BIM) was evidenced by a single peak in the ³¹P NMR spectrum (³¹P δ

= 44.7 ppm). Crystals of P(BIM) were obtained by slow evaporation of the solvent

from a DCM/MeCN solution. In the solid state structure (**Figure 5.2a**), two

enantiomers are present in the unit cell, with the benzoimidazole groups arranged

CHAPTER 5
Tris(benzoimidazol)amine (L) complexes of pnictogen(III) and pnictogen(V) cations and the
[LP]3+/[LPF2]3+ redox couple

either in their S or R enantiomer. The geometry at N1 is essentially planar (319.48°

and 317.75°, respectively) and features a pre-ordered N1 --- P bond with an average

distance of 2.925 Å. The P – N3 bonds (1.721 Å) are significantly longer than those

observed in **I** (e.g. 1.694 Å for $N(CH_2\text{-}CH_2\text{-}NR)_3P$ with R = CH(Me)Ph).[15] The

nucleophilic behaviour of P(BIM) was explored by reactions involving a variety of

stoichiometric ratios of methyl triflate. In each case the ^{31}P-NMR spectrum of the

reaction mixture indicated the formation of several products which we speculate to

result from simultaneous methylation of the nitrogen and phosphorus atoms. We

have modelled the energetic profile of the reactions using DFT calculations at the

PBEPBE/6-311+G(d,p) level of theory.[16] Structure optimizations for each complex

imply that methylation is favoured at the imino nitrogen atoms (coloured blue). In

the gas phase each methylation of an imino centre is exergonic. Similar results were

obtained with MeCN as a solvent model but an energetic minimum was not evident

for $[PMe(BIMMe_3)]^{4+}$ (**Table 4.1** and SI), and consistently, complicated reaction

mixtures are observed for MeOTf and P(BIM). Nevertheless, addition of excess MeOTf

resulted in a colourless precipitate (insoluble in common organic solvents) which

suggests for the potential formation of $[PMe(BIMMe_3)]^{4+}$.
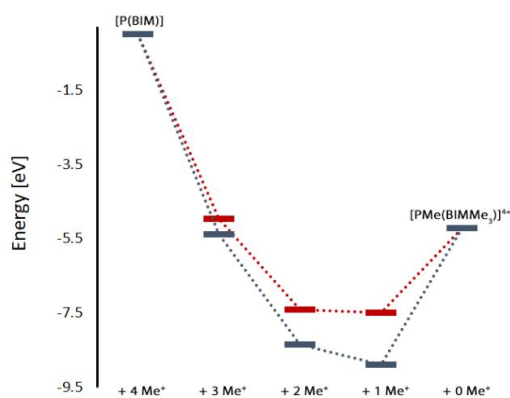
N-methylation	eV	P-methylation	eV
P(BIM) + 4 Me$^+$	0	P(BIM) + 4 Me$^+$	0
[P(BIMMe)]$^+$ + 3 Me$^+$	−5.38	[PMe(BIM)]$^+$ + 3 Me$^+$	−4.96
[P(BIMMe$_2$)]$^{2+}$ + 2 Me$^+$	−8.34	[PMe(BIMMe)]$^{2+}$ + 2 Me$^+$	−7.40
[P(BIMMe$_3$)]$^{3+}$ + 1 Me$^+$	−8.90	[PMe(BIMMe$_2$)]$^{3+}$ + 1 Me$^+$	−7.49
[PMe(BIMMe$_3$)]$^{4+}$	−5.21	[PMe(BIMMe$_3$)]$^{4+}$	−5.21

Table 5.1. *Summary of Gibbs free energies for optimized gas phase structures for the stepwise methylation of [P(BIM)] at the PBEPBE/6-311+G(d,p) level of theory. N-methylation in blue and P-methylation in red.*

Based on the modelled stability of [P(BIMMe$_3$)]$^{3+}$, we examined the reaction of BIMEt$_3$ [17] with "P(OTf)$_3$" by mixing PCl$_3$ and AgOTf acetonitrile in the presence of BIMEt$_3$. A singlet at δ = 56.1 ppm in the ^{31}P NMR spectrum indicates the quantitative formation of [P(BIMEt$_3$)][OTf]$_3$, which has been separated from the AgCl by filtration, and crystallized by layering the reaction mixture with diethyl ether. As TMSOTf is a relatively weak halide abstracting agent, reactions of AsCl$_3$ with BIMEt$_3$ and excess TMSOTf formed primarily [AsCl(BIMEt$_3$)][OTf]$_2$, which has been isolated in small quantities. The heavier analogue [SbF(BIMEt$_3$)][OTf]$_2$ can be formed quantitatively by reaction with SbF$_3$ and two equivalents of TMSOTf. The dications in derivatives of

CHAPTER 5
Tris(benzoimidazol)amine (L) complexes of pnictogen(III) and pnictogen(V) cations and the
[LP]3+/[LPF2]3+ redox couple

[MX(BIMEt3)][OTf]2 exhibit one set of signals for the benzoimidazole groups in the

^{1}H-NMR spectrum consistent with a labile ligand in solution, as observed for

analogous germanium complexes.[8] Salts of the trications [As(BIMEt3)][OTf]3 and

[Sb(BIMEt3)][OTf]3 were isolated in a similar fashion to the phosphorus analogue

using three equivalents of AgOTf as the halide abstractor.
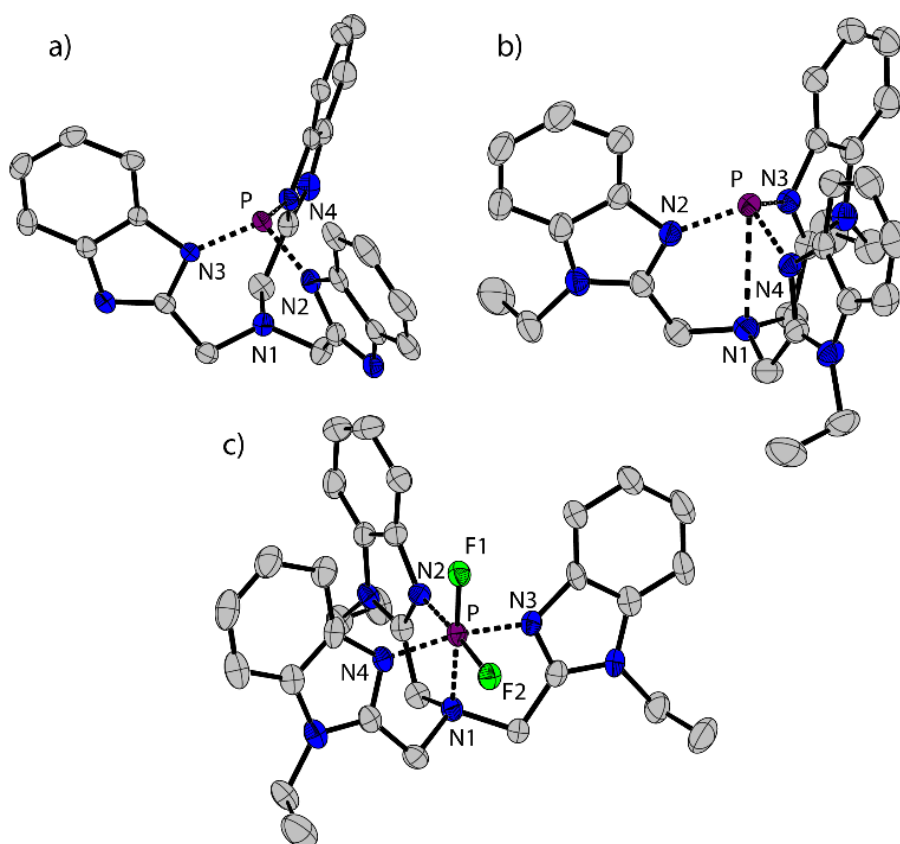
Figure 5.2. *(a) Solid state structure of one of two independent molecules of P(BIM). (b) Solid state structure of the cation in [P(BIMEt3)][OTf]3•(MeCN)2. (c) Solid state structure of the cation in [PF2(BIMEt3)][OTf]3•MeCN. Thermal ellipsoids are shown at a 50% probability level. Hydrogen atoms, solvent molecules and triflate anions are omitted for clarity. Inter-atomic distances and angles are summarized in **Table 5.2**.*

[P(BIMEt3)][OTf]3• (MeCN)2 crystallizes in the space group P–1 (See **Figure**

5.2b). The three triflate anions are remote from the phosphorus centre (3.58 - 3.92

Å). The unique apex nitrogen atom (°Σ$_{N1}$ = 350.5) is significantly bent out of plane

CHAPTER 5
Tris(benzoimidazol)amine (L) complexes of pnictogen(III) and pnictogen(V) cations and the
[LP]3+/[LPF2]3+ redox couple

towards the phosphorus centre consistent with a cross ring bonding interaction. Nevertheless, N1---P(2.866(2) Å) is only slightly shorter than those in P(BIM) (2.912(2) and 2.938(2) Å). In the solid state, [As(BIMEt$_3$)][OTf]$_3$ and [Sb(BIMEt$_3$)][OTf]$_3$ (**Figure 5.3c,d**) exhibit a significantly different geometry around the pnictogen centre. The polygon described by the ligands is best described as a pentagonal bipyramid with three nitrogen atoms (N1, N2 and N3), one triflate oxygen atom and the lone pair in the plane. A second triflate oxygen atom and one nitrogen (N4) atom occupy the axial positions. This geometry enables significantly shorter Pn-N1 bond (As-N1 2.104(4) and Sb-N1 2.389(2) and 2.370(2) Å, respectively) compared to that in [P(BIMEt$_3$)][OTf]$_3$ (P-N1 2.879 Å). Two of the three triflate anions have a weak interaction with the pnictogen centre (**Table 5.3**). The mono-halide derivatives [SbF(BIMEt$_3$)][OTf]$_2$ and [AsCl(BIMEt$_3$)][OTf]$_2$ crystallise as dimeric structures. The antimony fluoride is linked by two triflate anions and the arsenic chloride is linked by chlorine substituents (As-Cl 2.3342(7) and 3.913(2) Å)). The antimony centre adopts a tetragonal pyramidal geometry with two oxygen atoms from the triflate anions (Sb --- OTf 2.551(2) and 2.793(2) Å) and two nitrogen atoms (Sb-N 2.214(2) and 2.165(2) Å) with the antimony 0.486 Å above this plane.

CHAPTER 5
Tris(benzoimidazol)amine (L) complexes of pnictogen(III) and pnictogen(V) cations and the
[LP]3+/[LPF2]3+ redox couple
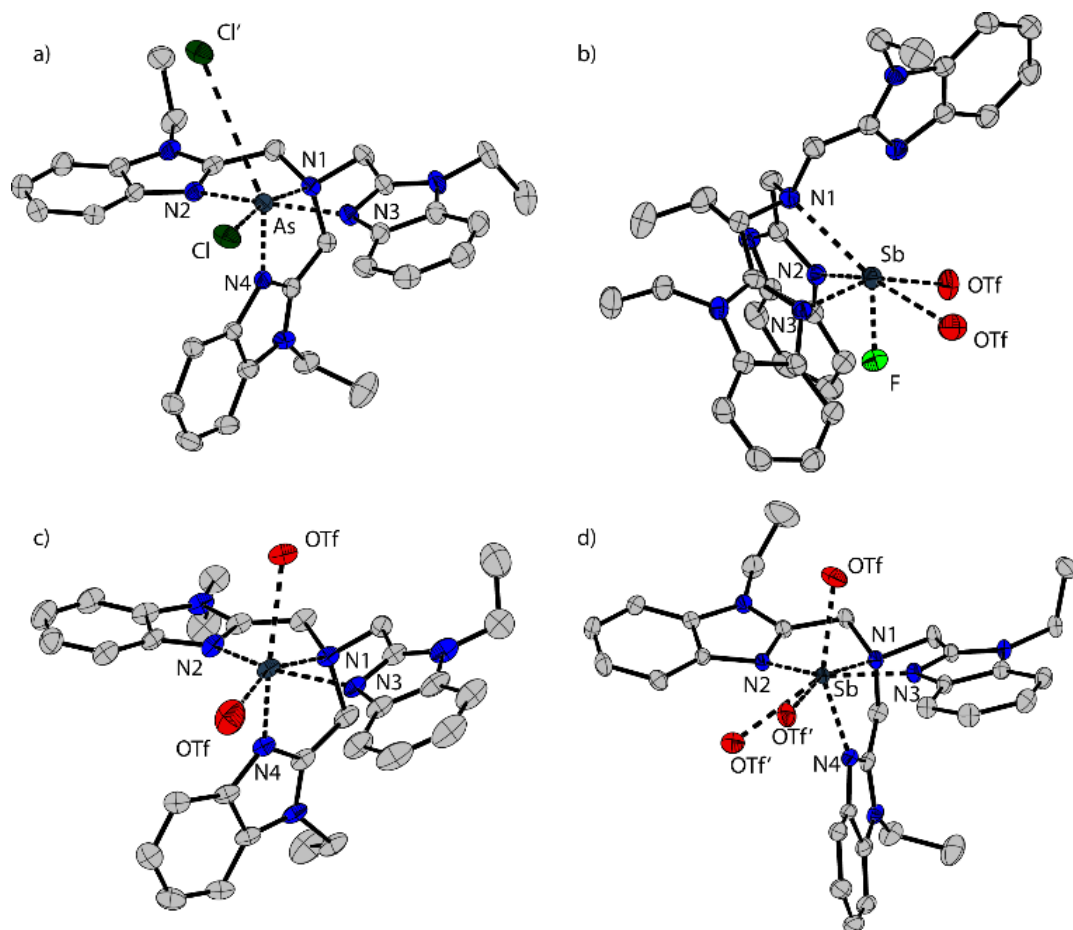
Figure 5.3. *Solid state structure of (a) [AsCl(BIMEt₃)]²⁺, (b) [SbF(BIMEt₃)]²⁺, (c) [As(BIMEt₃)]³⁺ and (d) [Sb(BIMEt₃)]³⁺. Thermal ellipsoids are shown at a 50% probability level. Oxygen atoms of the triflate anions that interact with the pnictogen centres are shown, but the other atoms of the anions are omitted for clarity as well as the hydrogen atoms and solvent molecules. Interatomic distances and angles are summarized in* ***Table 5.3****.*

Equimolar mixtures of PCl₅ and BIMEt₃ with three equivalents of AgOTf give a mixture of products as evidenced by the ³¹P NMR spectrum of the reaction mixture. Isolation of [P(BIMEt₃)][OTf]₃ from this mixture implicates formation of [PCl₂(BIMEt₃)][OTf]₃, which is subsequently reduced. In this context, we have studied the oxidation of [P(BIMEt₃)][OTf]₃ with the expectation to form cationic compounds analogous to [PPh₃I][I₃][18] or [Ph₃P-I-I][19] However, reaction of addition of [P(BIMEt₃)][OTf]₃ with a large excess of I₂ caused only a small chemical shift in the

CHAPTER 5
Tris(benzoimidazol)amine (L) complexes of pnictogen(III) and pnictogen(V) cations and the
[LP]3+/[LPF2]3+ redox couple

^{31}P NMR spectrum and a product could not be isolated. Nevertheless, Stephan's approach for oxidation of phosphenium cations[4] was applied using equimolar mixtures of [P(BIMEt$_3$)][OTf]$_3$ and XeF$_2$ in acetonitrile to yield a mixture of products with a prominent doublet of doublets resonance in the ^{31}P-NMR spectrum ([31]P δ = –127.8 ppm; $^1J_{PF}$ = 899.3 and 849.7 Hz) and consistently, two doublet of doublet resonances in the ^{19}F NMR spectrum (δ = –65.5 and –33.9 ppm; $^2J_{FF}$ = 52.0 Hz). Attempts to scale up the reaction yielded several different fluorinated phosphorus species. Rapid crystallization from a saturated acetonitrile solution at –35 °C layered with diethyl ether yielded small amounts of fragile crystals, that have been characterized as [PF$_2$(BIMEt$_3$)][OTf]$_3$. Consistent with the solution NMR spectra (**Figure 5.4**), the solid state structure reveals, inequivalent fluorine substituents at phosphorus (**Figure 5.2c**) and two different benzoimidazole environments.

CHAPTER 5
Tris(benzoimidazol)amine (L) complexes of pnictogen(III) and pnictogen(V) cations and the
[LP]3+/[LPF2]3+ redox couple

^{31}P-NMR spectrum of [(BIMEt$_3$)PF$_2$]$^{3+}$

^{19}F-NMR spectrum of [(BIMEt$_3$)PF$_2$]$^{3+}$

Figure 5.4. *NMR spectra for [PF$_2$(BIMEt$_3$)][OTf]$_3$ in CD$_3$CN.*

The N1-P distance (1.893(13) Å) is significantly shorter than that in [P(BIMEt$_3$)][OTf]$_3$. The P-F1 bond *trans* to the tertiary amine is longer [1.577(9) Å] than P-F2 [1.604(9) Å]. Consequently, the pseudo C$_{3v}$-geometry of the cation in [P(BIMEt$_3$)][OTf]$_3$ adjusts to C$_s$ symmetry in the octahedral frame in [PF$_2$(BIMEt$_3$)][OTf]$_3$. Moreover, P-N1 in [PF$_2$(BIMEt$_3$)][OTf]$_3$ is shorter than that in [P(BIMEt$_3$)][OTf]$_3$ and the other P – N bonds are longer (**Table 5.2**). This substantive change in geometry is also evidenced by ^{31}P NMR spectroscopy ([PF$_2$(BIMEt$_3$)]$^{3+}$ δ = –127.8 ppm) with a chemical shift difference of 184 ppm upon oxidation. There are no close interactions of the phosphorus centre with any of the triflate anions, so that the cation in [PF$_2$(BIMEt$_3$)][OTf]$_3$ represents the first fully characterized tricationic P(V)$^{3+}$ species.

Tris(benzoimidazol)amine (L) complexes of pnictogen(III) and pnictogen(V) cations and the [LP]3+/[LPF2]3+ redox couple

	P(BIM)	$[P(BIMEt_3)]^{3+}$	$[PF_2(BIMEt_3)]^{3+}$
P N2	1.7281(11)	1.7279(16)	1.791(13)
	1.7159(11)	1.7352(16)	1.798(13)
	1.7201(11)	1.7364(16)	1.773(13)
	1.7246(12)		
	1.7137(11)		
	1.7242(12)		
P N1	2.912(2)	2.866(2)	1.893(13)
	2.938(2)		
P OTf	---	3.591(2)	---
		3.922(2)	
		3.584(2)	
P F	---	---	1.604(9)
			1.577(9)
^{31}P δ	44.7 (s)	56.1 (s)	–127.8 (dd)
°Σ$_P$	319.48	320.2	---
	317.75		
°Σ$_{N1}$	353.77	350.5	328.0
	355.85		

Table 5.2. *Selected bond distances in Å, angles in ° and ^{31}P NMR chemical shifts in ppm for P(BIM), [P(BIMEt₃)][OTf]₃ and [PF₂(BIMEt₃)][OTf]₃*

	$[AsCl(BIMEt_3)]^{3+}$	$[As(BIMEt_3)]^{3+}$	$[SbF(BIMEt_3)]^{2+}$	$[Sb(BIMEt_3)]^{3+}$	
Pn N2	1.964(2)	1.918(4)	2.214(2)	2.193(2)	2.168(2)
	2.078(2)	2.085(4)	2.165(3)	2.233(2)	2.246(2)
	2.251(2)	2.195(4)		2.335(2)	2.346(2)
Pn N1	2.268(2)	2.104(4)	2.635(3)	2.389(2)	2.370(2)
Pn OTf	---	2.646(4)	2.551(2)	2.421(2)	2.485(2)
		2.796(4)	2.793(2)	3.181(2)	3.171(2)
				2.833(2)	2.820(2)
				3.258(2)	3.313(2)
Pn X	2.3342(7)		1.9344(19) X = F		
	3.913(2) X = Cl				

Table 5.3. *Selected bond distances in Å for [AsCl(BIMEt₃)][OTf]₂, [SbF(BIMEt₃)][OTf]₂, [As(BIMEt₃)][OTf]₃ and [Sb(BIMEt₃)][OTf]₃.*

CHAPTER 5
Tris(benzoimidazol)amine (L) complexes of pnictogen(III) and pnictogen(V) cations and the
[LP]3+/[LPF2]3+ redox couple

5.3 Conclusions

We have presented a versatile and facile synthetic approach to a number of pnictogen(III) cations in the BIMEt$_3$ ligand scaffold. The phosphorus derivative [P(BIMEt$_3$)][OTf]$_3$ can be readily oxidized to form the first tricationic phosphorus(V) complex, [LP^{V}F$_2$]$^{3+}$. A fundamental study for general use of such pnictogen salts in Lewis acid catalysis, small molecule activation or as catalytic fluorination agents is ongoing.

5.4 Experimental

5.4.1 General Remarks

All air- and moisture-sensitive manipulations were carried out using standard vacuum line Schlenk techniques or in an MBraun Labmaster inert atmosphere dry-box containing an atmosphere of purified nitrogen. THF-d_8, CD$_2$Cl$_2$ and C$_6$D$_6$ were purchased from Sigma Aldrich. CD$_2$Cl$_2$ was dried over CaH$_2$ and distilled, THF-d_8 and C$_6$D$_6$ were distilled over potassium. All glassware was stored in a 170 °C oven for several hours and was degassed prior to use. Solvents were distilled over the appropriate drying agent. Anhydrous grade MeCN was obtained from Sigma-Aldrich and used without distillation but stored over 3 Å molecular sieves. Solvents were additionally tested using a ketyl test to guarantee oxygen and moisture free

CHAPTER 5
Tris(benzoimidazol)amine (L) complexes of pnictogen(III) and pnictogen(V) cations and the
[LP]3+/[LPF2]3+ redox couple

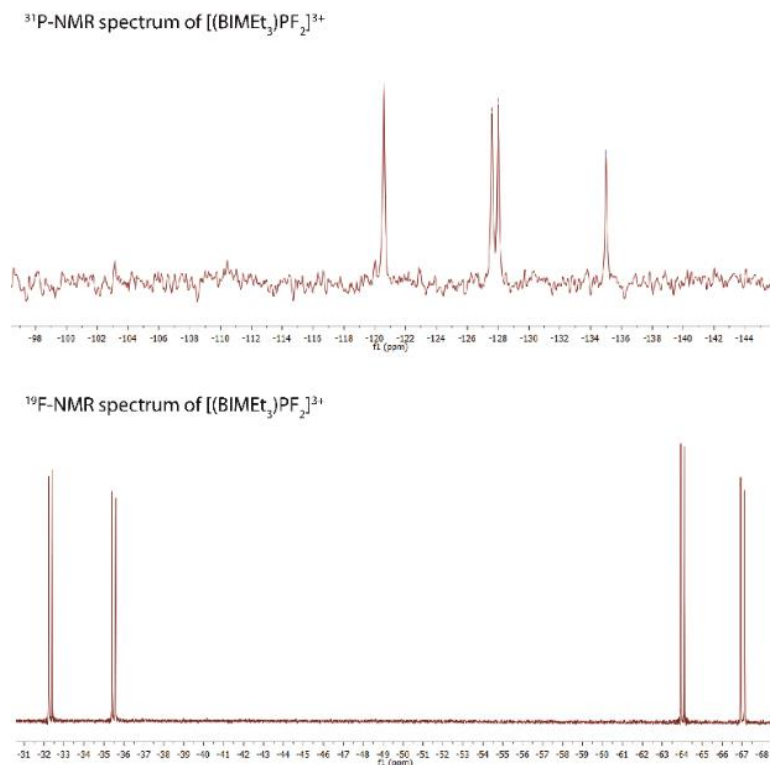conditions. TMSOTf (99%) was distilled before use. BIMH$_3$[20] and BIMEt$_3$[21] were

synthesized following literature procedures.

NMR tubes fitted with J-Young valves were charged and sealed inside the

glovebox. ^{1}H NMR spectra were recorded on Bruker spectrometers operating at 300,

360 MHz, ^{13}C NMR at 76 MHz. ^{31}P NMR at 121.6 MHz, ^{19}F NMR at 282.5 MHz. All ^{1}H

and ^{13}C NMR chemical shifts are reported relative to SiMe$_4$ using the ^{1}H (residual) and

^{13}C chemical shifts of the solvent as a secondary standard.

Infrared spectra were obtained on a Perkin Elmer Frontier instrument.

Elemental analysis was performed at the University of Windsor Mass Spectrometry

Service Laboratory using a Perkin Elmer 2400 combustion CHN analyser. All quantum

chemical calculations were carried out using Gaussian 16. [22]

5.4.2 Synthesis
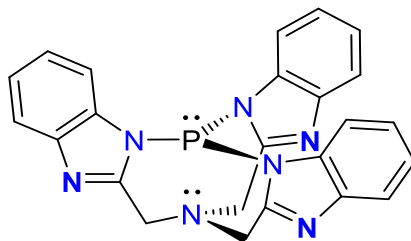
P(BIM): A 100 mL Schlenk flask was charged with BIMH$_3$ (500 mg, 1.23 mmol) and

NaH (90 mg, 3.74 mmol) in 30 mL THF at room temperature. After bubbling stops,

the reaction was left to stir for 30 mins followed by the addition of PCl$_3$ (0.117 mL,

1.28 mmol) yielding in white precipitate. The reaction mixture was allowed to stir for

24 hours before solvent was removed under reduced pressure. DCM (30 mL) was

added and the resulting suspension was filtered through Celite® and washed with DCM (2 x 10 mL). Solvent from the filtrate was removed under reduced pressure to result in P(BIM) as a colourless solid, 0.367 g (69 %). Slow evaporation from THF or acetonitrile yields colourless crystals suitable for X-ray diffraction $C_{24}H_{18}N_7P \bullet$ THF, MW = 507.53 g/mol, MP = 185 (dec.), EA [calc.]: C, 66.26; H, 5.16; N, 19.32 EA [found.]: C, 66.23; H, 5.04; N,18.87. ^{1}H NMR (300 MHz, CDCl$_3$) δ = 8.00 (d, 3H, $^3J_{HH}$ = 6.6 Hz), 7.70 (d, 3H, $^3J_{HH}$ = 7.8 Hz), 7.37 (m, 6H), 4.59 (s, 6H). ^{13}C{^{1}H} NMR (75.5 MHz, CDCl$_3$) δ = 154.42 (d, J_{CP} = 8.7 Hz), 144.23 (d, J_{CP} = 7.2 Hz), 137.59 (d, J_{CP} = 36.9 Hz), 128.7 (d, J_{CP} = 61.2 Hz), 124.36 (d, J_{CP} = 9.2 Hz), 120.31 (s), 111.41 (d, J_{CP} = 24.5 Hz), 51.16 (s). ^{31}P{^{1}H} NMR (121.5 MHz, CDCl$_3$) δ = 44.74 (s).
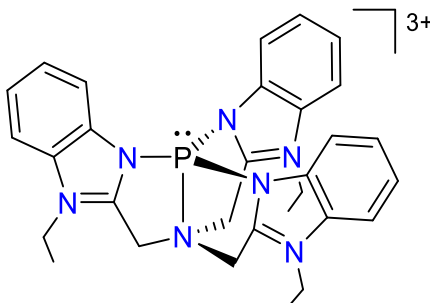
[P(BIMEt₃)][OTf]₃: To a rapidly stirred suspension of PCl$_3$ (0.2 mmol, 18 µL) and BIMEt$_3$ (0.2 mmol, 100 mg) in 3 mL of MeCN, TMSOTf (0.50 mmol, 100 µL) was added to yield a blue solution. The solution was left to stir for 10 mins. AgOTf (0.6 mmol, 154 mg) was added, producing a cloudy blue mixture due to precipitation of AgCl. The mixture was then filtered and the clear solution was layered with 6 mL of diethyl ether and placed in the freezer at –35 °C. Colourless blocks were isolated from after 72 hours. Yield: 204 mg (94 %) of the composition $C_{33}H_{33}F_9N_7O_9PS_3$ (MeCN)$_3$ MW = 1093.0 g/mol, MP = 184 °C (brown) – 241 °C (black) (dec.) EA [calc.] $C_{33}H_{33}F_9N_7O_9PS_3$:

C, 40.86; H, 3.43; N, 9.99 EA [found.]: C, 40.10; H, 3.89 ; N, 9.99 ^{1}H NMR (300 MHz, MeCN-d3) δ = 8.68 (*pseudo-d* (broad), *J* = 8.59 Hz, 3H), 7.92 (*pseudo-d* (broad), *J* = 8.20 Hz, 3H), 7.84 (ddd, *J* = 1.2, 7.2, 8.4 Hz, 3H), 7.75 (ddd, *J* = 0.9, 7.4, 8.2 Hz, 3H). 5.38 (d, *J*$_{P,H}$ =0.7 Hz, 6H), 4.47 (quart, *J* = 7.4 Hz, 6H), 1.53 (t, *J* = 7.4 Hz, 9H). ^{19}F{^{1}H} NMR (283 MHz, CD$_3$CN): δ = −79.6 (s). ^{13}C{^{1}H} NMR (75.5 MHz CD$_3$CN): δ = 155.18 (d, *J* = 9.2 Hz, 1C), 134.67 (d, *J* = 40.6 Hz, 1C), 132.92 (d, *J* = 5.8 Hz, 1C), 128.26 (d, *J* = 1.9 Hz, 1C), 128.09 (d, *J* = 1.6 Hz, 1C), 114.39 (d, *J* = 27.8 Hz, 1C), 113.6 (s), 54.9 (s), 42.3 (s), 12.3 (s). ^{31}P{^{1}H} NMR (121.4 MHz , CD$_3$CN): δ = 56.1 (s)
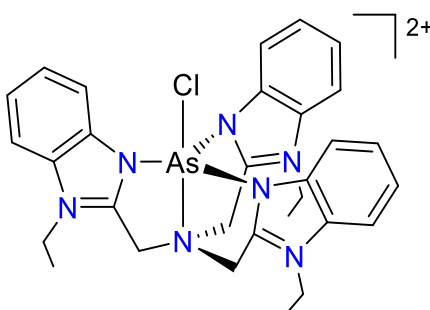
[AsCl(BIMEt₃)][OTf]₂: To a suspension of AsCl$_3$ (1 mmol, 83 μL) and BIMEt$_3$ (1 mmol, 500 mg) in 6 mL of MeCN, TMSOTf (5 mmol, 470 μL) was slowly added to yield a clear yellow solution. The solution was left at room temperature for 30 minutes. The mixture was then filtered over a glass filter and the light yellow solution was layered with 6 mL of diethyl ether and placed in the freezer at −35 °C. A crystalline colourless solid was isolated from the solution within 2 days. Yield: 310 mg (32 %) of the composition C$_{32}$H$_{33}$ClF$_6$N$_7$O$_6$AsS$_2$•MeCN$_2$, MW = 982.25 g/mol MP = 112 °C (dec.). EA [calc.] C$_{32}$H$_{33}$ClF$_6$N$_7$O$_6$AsS$_2$: C, 42.70; H, 3.70; N, 10.89. EA [found.]: C, 42.72; H, 3.95; N 10.79. ^{1}H NMR (300 MHz, CD$_3$CN) δ = 8.29 (*pseudo-d* (broad), *J* = 7.1 Hz, 3H), 7.70 (*pseudo-d* (broad), *J* = 7.1 Hz, 3H), 7.6 – 7.4 (m, 6H), 5.35 (s, 6H), 4.31 (quart, *J* = 7.21

CHAPTER 5
Tris(benzoimidazol)amine (L) complexes of pnictogen(III) and pnictogen(V) cations and the
[LP]3+/[LPF2]3+ redox couple

Hz, 6H), 1.38 (t, *J* = 7.21 Hz, 9H). $^{19}F\{^1H\}$ NMR (283 MHz, CD$_3$CN): δ = −79.28 (s).

$^{13}C\{^1H\}$ NMR (75.5 MHz, CD$_3$CN): δ = 150.9 (s), 136.2 (s), 134.2 (s), 125.8 (s), 125.5

(s), 117.9 (s), 112.2 (s), 55.5 (s), 40.9 (s), 13.5 (s).
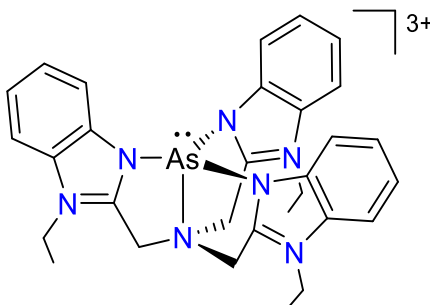
[As(BIMEt$_3$)][OTf]$_3$: To a suspension of AsCl$_3$ (0.2 mmol, 16.6 μL) and BIMEt$_3$ (0.2

mmol, 100 mg) in 3 mL of MeCN, TMSOTf (1 mmol, 200 μL) was slowly added to yield

a clear yellow solution. The solution was left at room temperature for 30 minutes.

AgOTf (0.375 mmol, 96 mg) was added, producing a cloudy yellow mixture due to

precipitation of AgCl. The mixture was then filtered through Celite. The volatiles were

removed under reduced pressure to yield a yellow oily precipitate, which was

titurated with 1 mL of DCM and 4 mL of diethyl ether. The leftover colourless solid

was dried under reduced pressure to isolate 148 mg of a colourless solid. Single

crystals for X-ray diffraction analysis were grown from MeCN solutions layered with

diethyl ether at −35 °C. Yield: 148 mg (68 %) of the composition

C$_{33}$H$_{33}$F$_9$N$_7$O$_9$AsS$_3$•MeCN$_2$, MW = 1095.9 g/mol MP = 161 °C (dec.). EA [calc.]: C, 40.55;

H, 3.59; N, 11.50. EA [found.]: C, 38.80; H, 3.52; N 9.69. ^1H NMR (300 MHz, CD$_3$CN) δ =

8.30 – 8.18 (*m,* 3H), 7.81 – 7.72 (*m,* 3H), 7.68 – 7.53 (*m,* 6H), 5.87 (s, 6H), 4.38 (quart,

J = 7.32 Hz, 6H), 1.48 (t, *J* = 7.32 Hz, 9H). $^{19}F\{^1H\}$ NMR (283 MHz, CD$_3$CN): δ = −79.3.

$^{13}C\{^1H\}$ NMR (75.5 MHz, CD$_3$CN): δ = 149.5 (s, C$_{arom}$), 134.7 (s, C$_{arom}$), 133.4 (s, C$_{arom}$),

CHAPTER 5
Tris(benzoimidazol)amine (L) complexes of pnictogen(III) and pnictogen(V) cations and the
[LP]3+/[LPF2]3+ redox couple

126.3 (s, C$_{arom}$), 126.2 (s, C$_{arom}$), 116.0 (s, C$_{arom}$), 112.64 (s, C$_{arom}$), 61.2 (s, CH$_2$), 41.5 (s,

CH$_2$), 13.0 (s, CH$_3$).
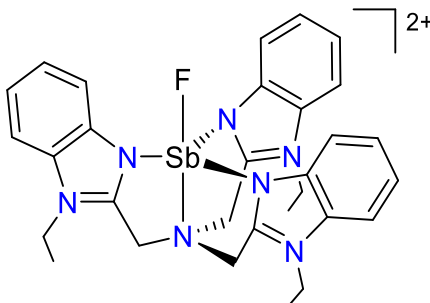
[SbF(BIMEt$_3$)][OTf]$_2$: To a solution of SbF(OTf)$_2$ (0.2 mmol, 88 mg) in 3 mL of MeCN,

BIMEt$_3$ (0.2 mmol, 100 mg) was added as a solid. The solution was left to stir for 16

hours at room temperature, then the mixture was layered with 4 mL of diethyl ether

and placed in the freezer at –35 °C. Colourless crystals suitable for X-ray

crystallography were isolated. Yield: 192 mg (92 %), C$_{32}$H$_{33}$F$_7$N$_7$O$_6$S$_2$Sb•(MeCN)$_2$, MW

= 1012.6 g/mol, MP = 183 °C (grey) – 220 °C (black), EA [calc.] for C$_{32}$H$_{33}$F$_7$N$_7$O$_6$S$_2$Sb:

C, 41.30; H, 3.57; N, 10.54; EA [found.]: C, 40.69; H, 3.56; N, 10.18; ^{1}H NMR (300 MHz,

CD$_3$CN) δ = 8.17 – 8.0 (*m,* 3H), 7.70 – 7.55 (*m,* 3H), 7.52 – 7.3 (*m,* 6H), 5.1 (s, 6H), 4.25

(quart, *J* = 7.32 Hz, 6H), 1.35 (t, *J* = 7.32 Hz, 9H). ^{19}F{^{1}H} NMR (283 MHz, CD$_3$CN): δ =

–79.25 (s). ^{13}C{^{1}H} NMR (75.5 MHz, CD$_3$CN): δ = 151.0 (s, C$_{arom}$), 134.6 (s, C$_{arom}$), 126.0

(s, C$_{arom}$), 125.8 (s, C$_{arom}$), 116.0 (s, C$_{arom}$), 112.3 (s, C$_{arom}$), 58.6 (s, CH$_2$), 40.6 (s, CH$_2$),

13.2 (s, CH$_3$).

CHAPTER 5
Tris(benzoimidazol)amine (L) complexes of pnictogen(III) and pnictogen(V) cations and the
[LP]3+/[LPF2]3+ redox couple
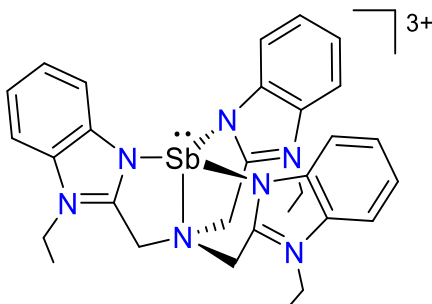
[Sb(BIMEt₃)][OTf]₃: To a solution of SbFOTf₂ (0.2 mmol, 88 mg) in 4 mL of MeCN, BIMEt₃ (0.2 mmol, 100 mg) was added. To the light yellow solution an excess TMSOTf (0.5 mmol, 100 µL) was added. The solution was left to stir for 30 minutes. ^{19}F NMR spectroscopy showed no presence of remaining fluoride bound antimony. The mixture was filtered and the clear yellow solution was layered with 2 mL of diethyl ether and was placed in the freezer at −25 °C for 16 hours. Colourless blocks suitable for X-ray crystallography were isolated by decantation of the solvent. The mother liquor was concentrated and layered with 8 mL of ether to isolate another crop of microcrystalline product. $C_{33}H_{33}F_9N_7O_9S_3Sb$, Yield: 188 mg (89 %) MW = 1060.6 g/mol. MP = 204 °C (melt and dec.). EA [calc.]: C, 37.37; H, 3.14; N, 9.24. EA [found.]: C, 37.71; H, 3.34; N, 9.23. ^{1}H NMR (300 MHz, CD₃CN) δ = 8.27 – 8.17 (*m,* 3H), 7.75 – 7.65 (*m*, 3H), 7.44 – 7.55 (*m,* 6H), 5.45 (s, 6H), 4.28 (quart, *J* = 7.34 Hz, 6H), 1.38 (t, *J* = 7.34 Hz, 9H). ^{19}F{^{1}H} NMR (283 MHz, CD₃CN): δ = −79.25 (s). ^{13}C{^{1}H} NMR (75.5 MHz, CD₃CN): δ = 151.0 (s, C_arom), 134.6 (s, C_arom), 126.0 (s, C_arom), 125.8 (s, C_arom), 116.0 (s, C_arom), 112.3 (s, C_arom), 58.6 (s, CH₂), 40.6 (s, CH₂), 13.2 (s, CH₃).
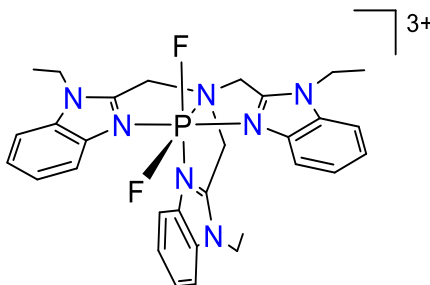
[PF₂(BIMEt₃)][OTf]₃: To a solution of [P(BIMEt₃)][OTf]₃ (0.1 mmol, 109 mg) in 3 mL of MeCN XeF₂ (0.1 mmol, 17 mg) was added to yield a light yellow solution. After stirring for 30 minutes a colourless precipitate was formed, the reaction mixture was filtered and another equivalent of XeF₂ (0.1 mmol, 17 mg) was added, the mixture was layered with 4 mL of diethyl ether and was placed in the freezer for 16 hours to isolate 55 mg of colourless crystals. Total yield: 55 mg (53 %) of the composition $C_{33}H_{33}F_{11}N_7O_9PS_3$ • MeCN. MW = 1048.9 g/mol, MP = 251 °C (dec.) EA [calc.]: C, 39.33; H, 3.30; N, 9.73. EA [found.]: C, 39.38; H, 3.10; N, 9.63. ^{1}H NMR (300 MHz, MeCN-d3) δ = 8.88 – 8.76 (m, 1H, CH$_{arom}$), 8.27 – 8.07 (m, CH$_{arom}$, 2H), 8.27 – 8.07 (m, 2H, CH$_{arom}$), 8.04 – 7.81 (m, 3H, CH$_{arom}$), 7.81 – 7.58 (m, 6H, CH$_{arom}$), 6.45 (dd, J = 17.1, 20.2 Hz, 2H, , CH₂), 6.01 (pseudo-t, J = 8.0 Hz, 4H, , CH₂), 4.55 (dq, J = 1.4, 7.4 Hz, 4H, , CH₂), 4.17 (q, J = 7.4 Hz, 2H, CH₂), 1.60 (t, J = 7.4 Hz, 6H, CH₃), 1.36 (t, J = 7.4 Hz, 3H, CH₃). ^{19}F{^{1}H} NMR (283 MHz, CD₃CN): δ = –79.3 (s), –65.5 (dd, J_{PF} = 849.7, J_{FF} = 52.0), –33.9 (dd, J_{PF} = 899.3, J_{FF} = 52.0). ^{13}C{^{1}H} NMR (75.5 MHz CD₃CN): δ = 144.0 (s, C_{arom}), 143.5 (s, C_{arom}), 134.7 (d, J = 9.2 Hz, C_{arom}), 134.1 (d, J = 7.0 Hz, C_{arom}) 128.6 (s, C_{arom}), 128.4 (s, C_{arom}), 128.1 (s, C_{arom}), 127.9 (s, C$_{arom}$), 115.0 (d, J = 9.2 Hz, C$_{arom}$), 114.2 (d, J = 7.6 Hz, C$_{arom}$), 114.1 (s, C_{arom}), 113.9 (s, C_{arom}), 60.5 (s, CH₂), 60.13 (s, CH₂), 42.7 (s, CH₂), 42.38 (s, CH₂), 12.97 (s, CH₃), 11.93 (s, CH₃). ^{31}P{^{1}H} NMR (121.4 MHz , CD₃CN): δ = –127.8 (dd, J_{PF} = 899.3, 849.7 Hz)

CHAPTER 5
Tris(benzoimidazol)amine (L) complexes of pnictogen(III) and pnictogen(V) cations and the
[LP]3+/[LPF2]3+ redox couple

Traces of moisture leads to decomposition of the product and the formation of [HBIMEt$_3$][PF$_6$] indicated by the formation of a *septed*-resonance in the ^{31}P-NMR spectrum for the PF$_6$-anion (−144.6 ppm, $^1J_{P,F}$ = 706.3 Hz). Scaling up the reaction only yielded several side products. Decomposition of the product in solution was observed if left in MeCN overnight, crystallization has to be initiated right after addition of XeF$_2$ to isolate crystalline material of the [PF$_2$(BIMEt$_3$)][OTf]$_3$.

5.4.3 X-ray Crystallography

Crystals for investigation were covered in Paratone®, mounted onto a goniometer head, and then rapidly cooled under a stream of cold N$_2$ of the low-temperature apparatus (Oxford Cryostream) attached to the diffractometer. The data were then collected using the APEXII (Bruker AXS) software suite on a Bruker Photon 100 CMOS diffractometer using a graphite monochromator with MoK$_\alpha$ (λ = 0.71073 Å). For each sample, data were collected at low temperature. APEXII software was used for data reductions and SADABS (Bruker AXS) was used for absorption corrections (multi-scan; semi-empirical from equivalents). XPREP was used to determine the space group and the structures were solved and refined using the SHELX[23] software suite as implemented in the WinGX[24] or OLEX2[25] program suites. Validation of the structures was conducted using PLATON and the structures have been deposited in the Cambridge Structural Database (CCDC 1578584-1578587).[26]

Tris(benzoimidazol)amine (L) complexes of pnictogen(III) and pnictogen(V) cations and the [LP]3+/[LPF2]3+ redox couple

Compound Name	[BIMEt₃AsCl][OTf]₂	[BIMP]	[BIMEt₃Sb][OTf]₃
Label			
CCDC ID	1578584	1578585	1578586
Empirical formula	$C_{36}H_{36}AsClF_6N_9O_6S_2$	$C_{50}H_{39}N_{15}P_2$	$C_{76}H_{81}F_{18}N_{19}O_{18}S_6Sb_2$
Formula weight	979.23	911.90	2326.49
Temperature (K)	150.0	140.0	150.01
Crystal system	monoclinic	monoclinic	triclinic
Space group	$P2_1/c$	$P2_1/n$	P–1
a (Å)	14.2067(6)	13.0553(5)	12.726(5)
b (Å)	15.9799(8)	25.1646(12)	18.899(8)
c (Å)	18.6556(10)	14.6359(6)	20.823(8)
α (°)	90	90	102.659(14)
β (°)	94.050(2)	114.6194(15)	97.475(14)
γ (°)	90	90	99.315(14)
Volume (Å³)	4224.6(4)	4371.2(3)	4750(3)
Z	4	4	2
ρ_{calc} (g·cm⁻³)	1.540	1.386	1.6264
μ (mm⁻¹)	1.049	0.157	0.810
F(000)	1996.0	1896.0	2348.5
Crystal size (mm³)	0.24 × 0.2 × 0.18	0.29 × 0.23 × 0.2	0.29 × 0.28 × 0.13
Radiation	MoKα (λ = 0.71073)	MoKα (λ = 0.71073)	Mo Kα (λ = 0.71073)
2Θ range for data collection (°)	5.548 to 63.11	5.742 to 56.646	5.44 to 55
Index ranges	−18 ≤ h ≤ 20 −23 ≤ k ≤ 23 −27 ≤ l ≤ 27	−17 ≤ h ≤ 17 −33 ≤ k ≤ 33 −19 ≤ l ≤ 19	−17 ≤ h ≤ 18 −26 ≤ k ≤ 26 −29 ≤ l ≤ 29
Reflections collected	210673	206509	133890
Independent reflections	13753 R_{int} = 0.0748 R_{sigma} = 0.0464	10847 R_{int} = 0.0485 R_{sigma} = 0.0152	21371 R_{int} = 0.0637 R_{sigma} = 0.0576
Data/restraints /parameters	13753/0/527	10847/0/605	21371/6/1263
Goodness-of-fit on F²	1.090	1.094	1.063
Final R indexes [I>=2σ(I)]	R_1 = 0.0512 wR_2 = 0.1096	R_1 = 0.0385 wR_2 = 0.0899	R_1 = 0.0368 wR_2 = 0.0846
Final R indexes [all data]	R_1 = 0.1031 wR_2 = 0.1381	R_1 = 0.0495 wR_2 = 0.0988	R_1 = 0.0582 wR_2 = 0.0993
Largest diff. peak/hole (e·Å⁻³)	0.81/−0.68	0.32/−0.40	2.19/−1.25
Refinement method	Full-matrix least-squares on F²		

$$R_1 = \frac{\sum||F_o|-|F_c||}{\sum|F_o|} \qquad wR_2 = \sqrt{\frac{\sum w(F_o^2-F_c^2)^2}{\sum w(F_o^2)^2}} \qquad R_{int} = \frac{\sum|F_o^2-F_o^2(mean)|}{\sum F_o^2} \qquad R_{sigma} = \frac{\sum \sigma(F_o^2)}{\sum F_o}$$

Table 5.4. *Crystallographic data and structure refinement.*

Tris(benzoimidazol)amine (L) complexes of pnictogen(III) and pnictogen(V) cations and the
[LP]3+/[LPF2]3+ redox couple

Compound Name	[BIMEt₃P][OTf]₃	[BIMEt₃As][OTf]₃	[BIMEt₃SbF][OTf]₂
Label			
CCDC ID	1578587	1581022	1581023
Empirical formula	$C_{39}H_{42}F_9N_{10}O_9PS_3$	$C_{37}H_{39}AsF_9N_9O_9S_3$	$C_{36}H_{39}F_7N_9O_6S_2Sb$
Formula weight	1092.99	1095.87	1012.63
Temperature (K)	150.0	173.15	193.15
Crystal system	triclinic	monoclinic	triclinic
Space group	P–1	P2₁/c	P–1
a (Å)	10.8599(7)	14.0065(3)	13.1877(6)
b (Å)	10.9646(8)	15.9167(3)	13.3482(7)
c (Å)	20.3805(14)	21.8331(5)	13.4824(7)
α (°)	81.217(2)	90	79.6653(7)
β (°)	83.234(2)	107.9657(13)	63.0215(6)
γ (°)	89.295(2)	90	84.7868(7)
Volume (Å³)	2381.6(3)	4630.08(17)	2080.63(18)
Z	2	4	2
ρ_calc (g·cm⁻³)	1.5240	1.572	1.616
μ (mm⁻¹)	0.288	3.138	0.851
F(000)	1125.7	2232.0	1024.0
Crystal size (mm³)	0.26 × 0.2 × 0.06	0.57 × 0.259 × 0.223	0.227 × 0.183 × 0.133
Radiation	Mo Kα (λ = 0.71073)	CuKα (λ = 1.54178)	MoKα (λ = 0.71073)
2Θ range for data collection (°)	5.64 to 61.22	6.634 to 136.478	3.102 to 55.13
Index ranges	−15 ≤ h ≤ 14 −15 ≤ k ≤ 15 −29 ≤ l ≤ 29	−14 ≤ h ≤ 16 −19 ≤ k ≤ 19 −26 ≤ l ≤ 25	−17 ≤ h ≤ 17 −17 ≤ k ≤ 17 −17 ≤ l ≤ 17
Reflections collected	112259	25884	18546
Independent reflections	14440 [R_int = 0.0634, R_sigma = 0.0474]	8479 [R_int = 0.0804, R_sigma = 0.0654]	9603 [R_int = 0.0385, R_sigma = 0.0608]
Data/restraints /parameters	14440/0/646	8479/0/615	9603/0/552
Goodness-of-fit on F²	1.069	1.057	1.039
Final R indexes [I>=2σ(I)]	R₁ = 0.0539 wR₂ = 0.1264	R₁ = 0.0898 wR₂ = 0.2548	R₁ = 0.0434 wR₂ = 0.1033
Final R indexes [all data]	R₁ = 0.0940 wR₂ = 0.1480	R₁ = 0.0989 wR₂ = 0.2635	R₁ = 0.0586 wR₂ = 0.1125
Largest diff. peak/hole (e·Å⁻³)	1.21/−1.17	3.21/−2.02	1.21/−0.60
Refinement method	Full-matrix least-squares on F²		

$$R_1 = \frac{\sum||F_o|-|F_c||}{\sum|F_o|} \qquad wR_2 = \sqrt{\frac{\sum w(F_o{}^2-F_c{}^2)^2}{\sum w(F_o{}^2)^2}} \qquad R_{int} = \frac{\sum|F_o{}^2-F_o{}^2(mean)|}{\sum F_o{}^2} \qquad R_{sigma} = \frac{\sum \sigma(F_o{}^2)}{\sum F_o}$$

Table 5.5. *Crystallographic data and structure refinement.*

Tris(benzoimidazol)amine (L) complexes of pnictogen(III) and pnictogen(V) cations and the [LP]3+/[LPF2]3+ redox couple

Compound Name	[[BIMEt₃PF₂][OTf]₃
Label	
CCDC ID	1819912
Empirical formula	$C_{37}H_{39}F_{11}N_9O_9PS_3$
Formula weight	1089.92
Temperature (K)	170.02
Crystal system	triclinic
Space group	P–1
a (Å)	13.753(7)
b (Å)	14.060(7)
c (Å)	14.321(7)
α (°)	109.504(13)
β (°)	98.444(13)
γ (°)	111.998(9)
Volume (Å³)	2300.1(19)
Z	2
ρ_{calc} (g·cm⁻³)	1.574
μ (mm⁻¹)	0.304
F(000)	1116.0
Crystal size (mm³)	0.24 × 0.14 × 0.06
Radiation	MoKα (λ = 0.71073)
2Θ range for data collection (°)	5.802 to 49.424
Index ranges	−16 ≤ h ≤ 16
	−16 ≤ k ≤ 16
	−16 ≤ l ≤ 16
Reflections collected	55372
Independent reflections	7797
	R_{int} = 0.1024
	R_{sigma} = 0.0674
Data/restraints /parameters	7797/0/636
Goodness-of-fit on F²	1.083
Final R indexes [I>=2σ(I)]	R_1 = 0.1889
	wR_2 = 0.5278
Final R indexes [all data]	R_1 = 0.2467
	wR_2 = 0.5690
Largest diff. peak/hole (e·Å⁻³)	1.42/−1.01
Refinement method	Full-matrix least-squares on F²

$$R_1 = \frac{\sum ||F_o|-|F_c||}{\sum |F_o|} \qquad wR_2 = \sqrt{\frac{\sum w(F_o{}^2-F_c{}^2)^2}{\sum w(F_o{}^2)^2}} \qquad R_{int} = \frac{\sum |F_o{}^2-F_o{}^2(mean)|}{\sum F_o{}^2} \qquad R_{sigma} = \frac{\sum \sigma(F_o{}^2)}{\sum F_o{}^2}$$

Table 5.6. *Crystallographic data and structure refinement.*

5.5 References

(1)   a) Arduengo, A. J.; Stewart, C. A.; Davidson, F.; Dixon, D. A.; Becker, J. Y.; Culley, S. A.; Mizen, M. B. *J. Am. Chem. Soc.* **1987**, *109*, 627-647; b) Zhao, W.; McCarthy, S. M.; Lai, T. Y.; Yennawar, H. P.; Radosevich, A. T. *J. Am. Chem. Soc.* **2014**, *136*, 17634-17644; c) Martin, D.; Soleilhavoup, M.; Bertrand, G. *Chem. Sci.* **2011**, *2*, 389-399; d) McCarthy, S. M.; Lin, Y. -C.; Devarajan, D.; Chang, J. W.; Yennawar, H. P.; Rioux, R. M.; Ess, D. H.; Radosevich, A. T. *J. Am. Chem. Soc.* **2014**, *136*, 4640-4650; e) Dunn, N. L.; Ha, M.; Radosevich, A. T. *J. Am. Chem. Soc.* **2012**, *134*, 11330-11333; f) Cui, J.; Li, Y.; Ganguly, R.; Inthirarajah, A.; Hirao, H.; Kinjo, R. *J. Am. Chem. Soc.* **2014**, *136*, 16764-16767; g) Robinson, T. P.; De Rosa, D. M.; Aldridge, S.; Goicoechea, J. M. *Angew. Chem. - Int. Ed.* **2015**, *54*, 13758-13763.

(2)   a) Chitnis, S. S.; Robertson, A. P. M.; Burford, N.; Patrick, B. O.; McDonald, R.; Ferguson, M. J. *Chem. Sci.* **2015**, *6*, 6545-6555; b) Chitnis, S. S.; Vos, K. A.; Burford, N.; McDonald, R.; Ferguson, M. J. *Chem. Commun.* **2016**, *52*, 685-688; c) Henne, F. D.; Dickschat, A. T.; Hennersdorf, F.; Feldmann, K. O.; Weigand, J. J. *Inorg. Chem.* **2015**, *54*, 6849-6861; d) Petuskova, J.; Patil, M.; Holle, S.; Lehmann, C. W.; Thiel, W.; Alcarazo, M. *J. Am. Chem. Soc.* **2011**, *133*, 20758-20760; e) Carreras, J.; Patil, M.; Thiel, W.; Alcarazo, M. *J. Am. Chem. Soc.* **2012**, *134*, 16753-16758; f) Weigand, J. J.; Feldmann, K. O.; Echterhoff, A. K. C.; Ehlers, A. W.; Lammertsma, K. *Angew. Chem. - Int. Ed.* **2010**, *49*, 6178-6181.

CHAPTER 5
Tris(benzoimidazol)amine (L) complexes of pnictogen(III) and pnictogen(V) cations and the
[LP]3+/[LPF2]3+ redox couple

(3)   a) Engesser, T. A.; Lichtenthaler, M. R.; Schleep, M.; Krossing, I. *Chem. Soc. Rev.* **2016**, *45*, 789-899; b) Robertson, A. P. M.; Gray, P. A.; Burford, N. *Angew. Chem. - Int. Ed.* **2014**, *53*, 6050-6069; c) Sinclair, H.; Suter, R.; Burford, N.; McDonald, R.; Ferguson, M. J. *Can. J. Chem.* **2018**, 1-5; d) Suter, R.; Gray, P. A.; Burford, N.; McDonald, R. *Chem. Eur. J.* **2018**, *24*, 4718-4723.

(4)   a) Mehta, M.; Holthausen, M. H.; Mallov, I.; Pérez, M.; Qu, Z. W.; Grimme, S.; Stephan, D. W. *Angew. Chem. - Int. Ed.* **2015**, *54*, 8250-8254; b) Holthausen, M. H.; Mehta, M.; Stephan, D. W. *Angew. Chem. - Int. Ed.* **2014**, *53*, 6538-6541.

(5)   Kozma, Á.; Rust, J.; Alcarazo, M. *Chem. Eur. J.* **2015**, *21*, 10829-10834.

(6)   a) Caputo, C. B.; Hounjet, L. J.; Dobrovetsky, R.; Stephan, D. W. *Science* **2013**, *341*, 1374-1377; b) Bayne, J. M.; Stephan, D. W. *Chem. Soc. Rev.* **2016**, *45*, 765-774.

(7)   Chitnis, S. S.; Krischer, F.; Stephan, D. W. *Chem. Eur. J.* **2018**, *24*, 6543–6546.

(8)   Suter, R.; Swidan, A.; Macdonald, C. L. B.; Burford, N. *Chem. Commun.* **2018**, 10.1039/C1038CC01799A.

(9)   a) Schmidt, H.; Lensink, C.; Xi, S. K.; Verkade, J. G. *Z. Anorg. Allg. Chem.* **1989**, *578*, 75-80; b) Tang, J.; Dopke, J.; Verkade, J. G. *J. Am. Chem. Soc.* **1993**, *115*, 5015-5020; c) Tang, J. S.; Verkade, J. G. *J. Am. Chem. Soc.* **1993**,

CHAPTER 5
Tris(benzoimidazol)amine (L) complexes of pnictogen(III) and pnictogen(V) cations and the
[LP]3+/[LPF2]3+ redox couple

115, 1660-1664; d) Kisanga, P. B.; Verkade, J. G. *Tetrahedron* **2001**, *57*, 467-475; e) Mummadi, S.; Kenefake, D.; Diaz, R.; Unruh, D. K.; Krempner, C. *Inorg. Chem.* **2017**, *56*, 10748-10759.

(10)   Gray, P. A.; Burford, N. *Coord. Chem. Rev.* **2016**, *324*, 1-16.

(11)   Donath, M.; Bodensteiner, M.; Weigand, J. J. *Chem. Eur. J.* **2014**, *20*, 17306-17310.

(12)   Robertson, A. P. M.; Burford, N.; McDonald, R.; Ferguson, M. J. *Angew. Chem. - Int. Ed.* **2014**, *53*, 3480-3483.

(13)   Frazee, C.; Burford, N.; McDonald, R.; Ferguson, M. J.; Decken, A.; Patrick, B. O. *Chem. Eur. - J.* **2018**, *24*, 4011-4013.

(14)   a) Zhang, S.-R.; Du, D.-Y.; Qin, J.-S.; Bao, S.-J.; Li, S.-L.; He, W.-W.; Lan, Y.-Q.; Shen, P.; Su, Z.-M. *Chem. Eur. J.* **2014**, *20*, 3589-3594; b) Liu, X.; Bai, Y.; Verkade, J. G. *J. Organomet. Chem.* **1999**, *582*, 16-24; c) Shutov, P. L.; Karlov, S. S.; Harms, K.; Tyurin, D. A.; Churakov, A. V.; Lorberth, J.; Zaitseva, G. S. *Inorg. Chem.* **2002**, *41*, 6147-6152.

(15)   Liu, X.; Ilankumaran, P.; Guzei, I. A.; Verkade, J. G. *J. Org. Chem.* **2000**, *65*, 701-706.

(16)   Frisch, M. J. *, et al. Gaussian 16., Revision. A.03., Gaussian, Inc., Wallingford CT,* **2016**.

(17)   Lonnon, D. G.; Craig, D. C.; Colbran, S. B. *Dalton Trans.* **2006**, 3785-3797.

(18)   Cotton, F. A.; Kibala, P. A. *J. Am. Chem. Soc.* **1987**, *109*, 3308-3312.

CHAPTER 5
Tris(benzoimidazol)amine (L) complexes of pnictogen(III) and pnictogen(V) cations and the
[LP]3+/[LPF2]3+ redox couple

(19)   a) Godfrey, S. M.; Kelly, D. G.; McAuliffe, C. A.; Mackie, A. G.; Pritchard, R. G.; Watson, S. M. *J. Chem. Soc., Chem. Commun.* **1991**, 1163-1164; b) Robinson, T. P.; De Rosa, D.; Aldridge, S.; Goicoechea, J. M. *Chemistry* **2017**, *23*, 15455-15465.

(20)   Zhang, S.-R.; Du, D.-Y.; Qin, J.-S.; Bao, S.-J.; Li, S.-L.; He, W.-W.; Lan, Y.-Q.; Shen, P.; Su, Z.-M. *Chem. Eur. J.* **2014**, *20*, 3589-3594.

(21)   Lonnon, D. G.; Craig, D. C.; Colbran, S. B. *Dalton Trans.* **2006**, 3785-3797.

(22)   Frisch, M. J. *et al. Gaussian 16., Revision. A.03., Gaussian, Inc., Wallingford CT,* **2016**.

(23)   Sheldrick, G. *Acta Cryst. A* **2008**, *64*, 112-122.

(24)   Farrugia, L. *J. Appl. Crystallogr.* **1999**, *32*, 837-838.

(25)   Dolomanov, O. V.; Bourhis, L. J.; Gildea, R. J.; Howard, J. A. K.; Puschmann, H. *J. Appl. Crystallogr.* **2009**, *42*, 339-341.

(26)   Spek, A. *J. Appl. Crystallogr.* **2003**, *36*, 7-13.

CHAPTER 6:
Towards the Synthesis of an Anionic Carbon(0)

6.1 Introduction

Carbon contains four valence electrons and is most stable in the +4 oxidation state. Carbon in the +2 oxidation state (carbenes) has played an important role in transient intermediates of organic and organometallic chemistry since the 1950s. The first stable carbene (**Scheme 6.1**) was in the form of a stable *N*-hetercyclic carbene (NHC) reported in 1991 by Arduengo and co-workers.[1] Carbenes can exist in the singlet state with two non-bonding electrons having an opposite spin or in the triplet state where the two non-bonding electrons have the same spin. Knowing the multiplicity of the ground-state is important in determining the reactivity of the carbene.[2]
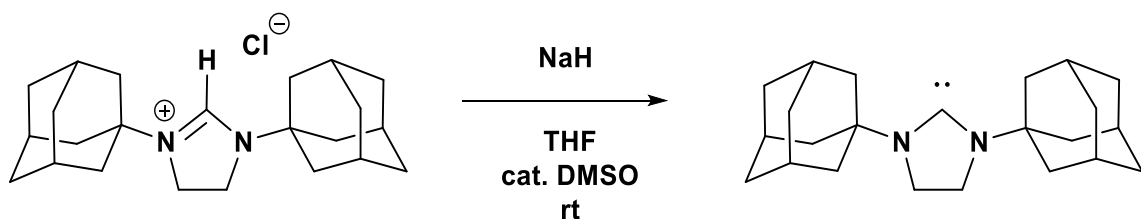
Scheme 6.1. *Synthesis of the first stable N-heterocyclic carbene.*

After their discovery, carbenes and alkylidenes (a carbon(II) without a heteroatom substituent on the alpha carbon) have played a significant role in metal catalysts. Among these notable examples is the second-generation Grubbs' catalyst (**Figure 6.1**) that is used for olefin metathesis.[3] Robert H. Grubbs was a co-recipient of the 2005 Nobel Prize in Chemistry for his work on olefin metathesis. *N*-heterocyclic

153

carbenes were necessary for recent developments in the field of main group chemistry; some notable examples include some of the first examples of low valent group 13-15 complexes (**Figure 6.1**).[3–6]
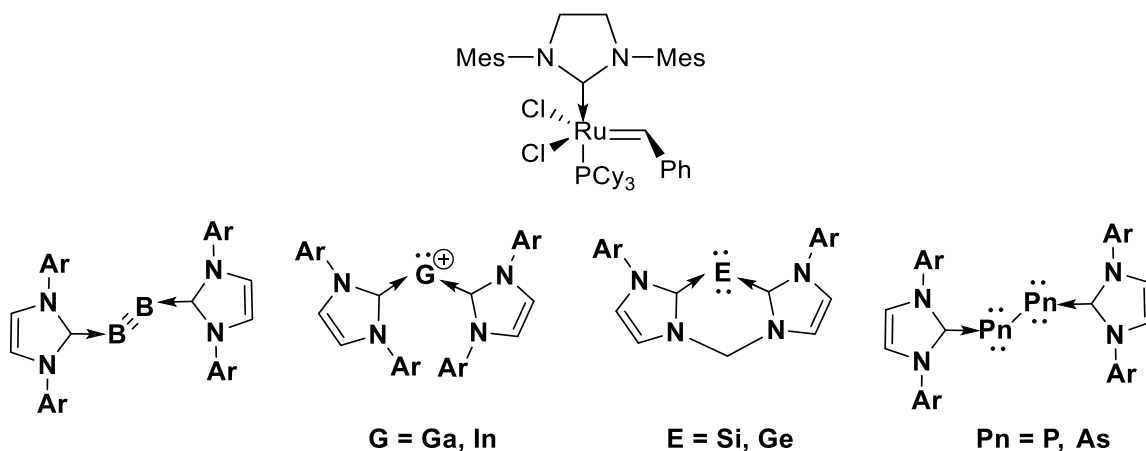
Figure 6.1. *Grubbs' second-generation catalyst (top), and some notable examples of the use of N-heterocyclic carbenes in the stabilization of low-valent group 13-15 elements.*

Carbon in the zero-oxidation state contains four non-bonding electrons (i.e. all of the carbon's four valence electrons). **Figure 6.2** illustrates the difference in electron configuration between a C(IV), C(II) and C(0); this method of oxidation state assignment has been introduced in section **1.2** of Chapter 1.
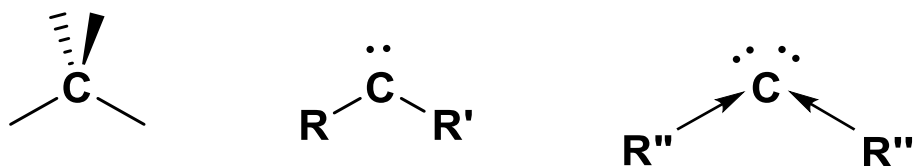
Figure 6.2. *Depiction of carbon centres in the +4 (left), +2 (centre) and 0 (right) oxidation states.*

A crucial difference between a carbon(+2) and a carbon(0) is in the degenerate p-type orbitals, p_x and p_y. In carbenes, one of the two p-orbitals contains a pair of

electrons (singlet carbenes) making it a σ-donor, while the orthogonal p-orbital is empty and serves as a π-acceptor. A carbon(0) on the other hand, contains a lone pair of electrons in each of the two p-orbitals, resulting in both p-orbitals as electron donors.
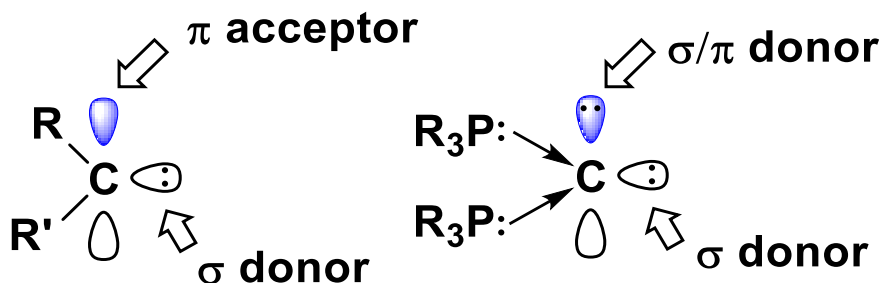
Figure 6.3. *Frontier orbital difference between a carbon(+2) (left) and a carbon(0) (right). The carbon(+2) shown is assuming a singlet state.*

Having two lone pairs would allow for one lone pair to be a σ-type donor while the other can either be σ- or π-donating, depending on the type of complex formed. **Figure 6.4** demonstrates the two different binding modes of a carbon(0) centre with σ- and π-donors and with two σ- donors.

Alcarazo and co-workers[7] reported that the use of a carbodiphosphorane as a donor ligand revealed the capability of simultaneous σ- and a π-donation. This was evident by the stabilization observed in the reactive dihydrido borenium cation shown in **Figure 6.4** (left). With the B–C bond distance (1.5030 Å) being closer to a B=C double bond (1.35–1.45 Å) than a B–C single bond (1.58–1.62 Å), it can be deduced that this is a clear indication of the π-type contribution from the second lone pair of electrons into the B–C bond bringing stabilization to the reactive borenium centre.[7] Additionally, Alcarazo reported the chiral heterobimetallic complex shown in

Figure 6.4 (right) that demonstrates the capability of a carbon(0) centre to serve as

a two σ-donor site.[8]
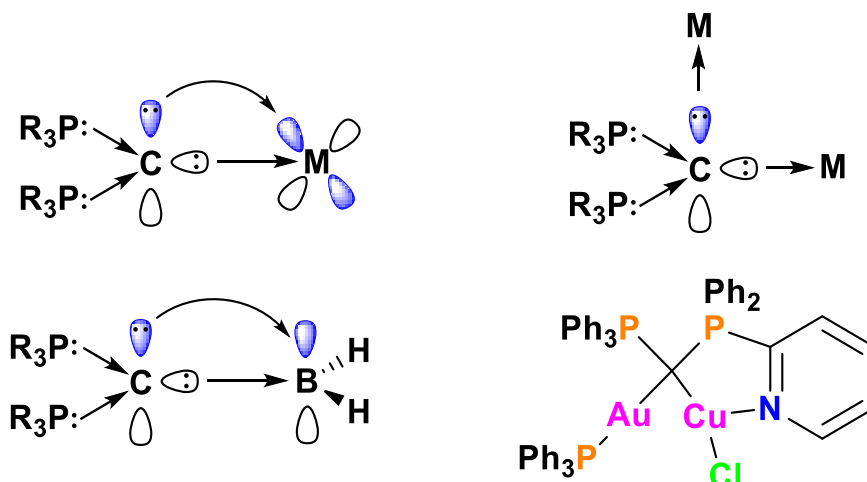
Figure 6.4. *An example of carbon(0) with a σ and a π-donor (left), with two σ-donor orbitals (right).*

The first carbon(0) was reported in 1961, which was a carbodiphosphorane

(CDP) of the form, $Ph_3P{:}{\rightarrow}C{\leftarrow}{:}PPh_3$.[9] It was not until recently that further studies of

these compounds gained interest as ligands for transition metals and main group

elements.[10–17] **Figure 6.5** highlights a few examples of these carbodiphosphorane

coordination complexes.
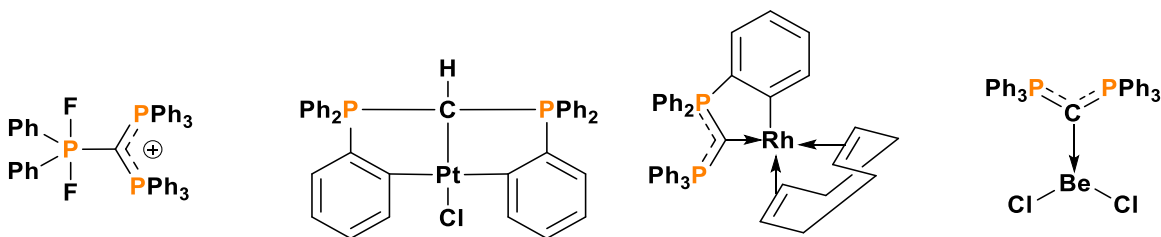
Figure 6.5. *Selected examples of carbodiphosphorane complexes of transition metals and main group elements.*

Carbodiphosphoranes are supported by two phosphine donors coordinating to the carbon(0) centre. Another form of carbon(0) ligands is those stabilized by carbene donors resulting in a carbodicarbene compound. Carbodicarbenes (CDC) were theoretically studied by Frenking in 2006[18,19] and synthesized a year later by Bertrand and co-workers as shown in **Scheme 6.2**.[20]
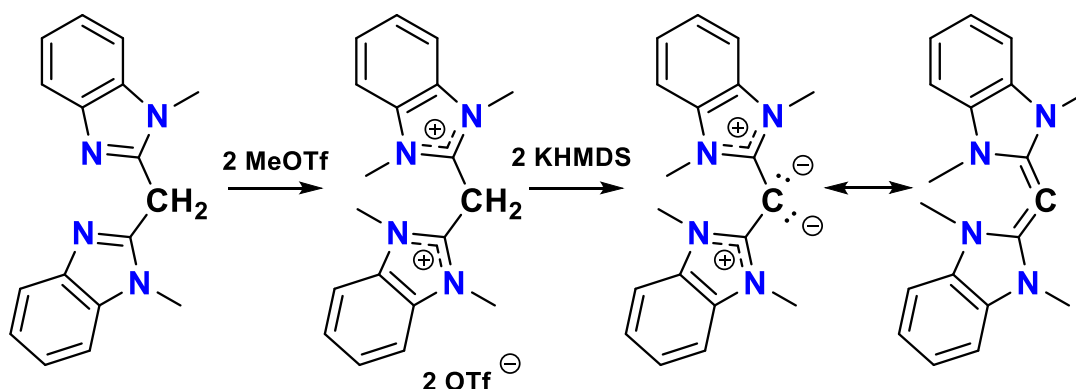
Scheme 6.2. Bertrand's synthesis of the first carbodicarbene.

Despite the fact that the first stable carbon(0) was reported three decades before Arduengo's work on stable carbenes, carbenes gained larger popularity and have been investigated to a much greater extent than carbon(0) ligands.[18] Carbodicarbenes, in particular, were predicted to be better donors than either carbenes or phosphines solely based on v_{CO} stretching frequencies of *cis*-[RhCl(CO)$_2$(L)] as reported by Bertrand (**Table 6.1**).[20]

L	PR$_3$	NHC	CDC
v_{CO} **(cm^{-1})**	2070–2090	2036–2058	2014

Table 6.1. v_{CO} stretching frequencies cis-[RhCl(CO)$_2$(L)] complexes where L = PR$_3$, NHC and CDC.

In hopes of creating better carbon(0) donors, we propose that an anionic carbon(0) ligand would be a better σ- and π- donor than its neutral counterpart making it more attractive as a ligand for coordination chemistry. This would be feasible by having an anionic bisphosphine ligand bind a carbon(0) centre giving it an overall negative charge. To this end, Jonas Peters ligand (**Scheme 6.4**, JCP-Li, JCP⁻) was predicted to be a good candidate to investigate the isolation of an anionic carbon(0) ligand.[21] JCP⁻ ligands have been previously employed in the isolation of heavier group 14 elements as illustrated in **Scheme 6.3**.[6] JCP⁻ ligand has also been used as a new class of ligand for metal catalysts due to its strong σ- donation ability demonstrated by carbonyl frequency studies compared to other phosphines.[22] In-addition, metal complexes of JCP⁻ ligand have proven to be useful in co-polymerization reactions of CO and ethylene (in the case of JCP-Pd)[23] and the activation of C–H bonds of benzene (using JCP-Pt).[22]
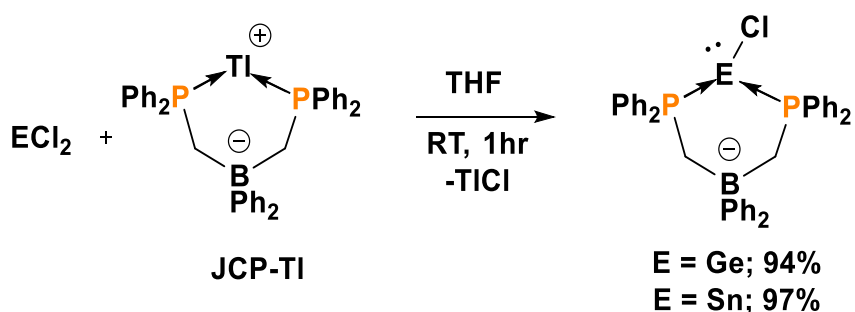
Scheme 6.3. *JCP-Tl ligand reactivity with heavier group 14 elements (Ge and Sn).*

6.2 Results and Discussion

6.2.1 Attempted Synthesis of an Anionic Carbodiphosphorane

The overall synthetic steps to obtain JCP-Li are shown in **Scheme 6.4**. Phosphine reagent, **I**, is prepared by the deprotonation of methyldiphenylphosphine using ^{n}BuLi and TMEDA (tetramethylethylenediamine).[24] **II** is prepared by heating the neat reaction mixture of tribromoborane with two equivalents of trimethyl(phenyl)silane to yield diphenylbromoborane (**II**).[25] The desired bis(phosphino)borate is prepared by mixing two equivalents of **I** with an equivalent of **II** in diethylether at –78 °C, yielding JCP-Li.[22]
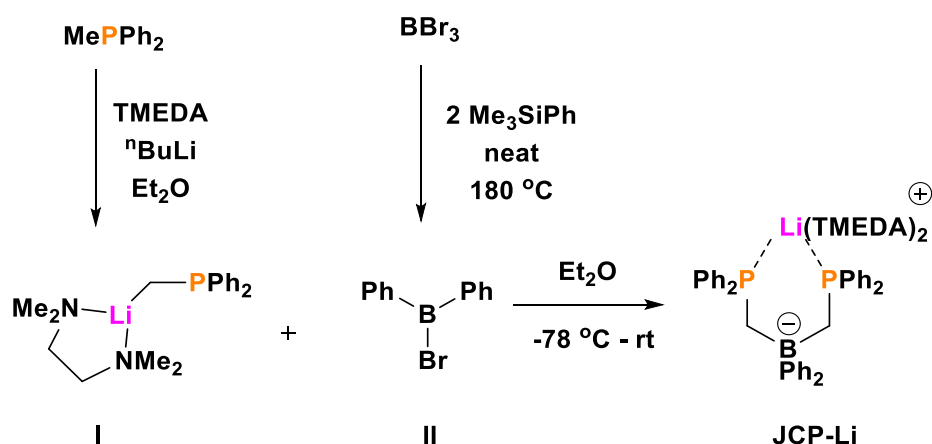
Scheme 6.4. *Synthesis of Peters' ligand, JCP-Li.*

We postulate that the treatment of JCP-Li in neat CH_2Br_2 should liberate LiBr salt and yield the fragment [JCPCH$_2$][Br] (**IV**) as shown in **Scheme 6.5**. **IV** would then be treated with two equivalents of a base to doubly deprotonate the methylene bridge resulting in an overall anionic carbodiphosphorane, [K][JCP(C)] (**V**) as shown in the scheme below.
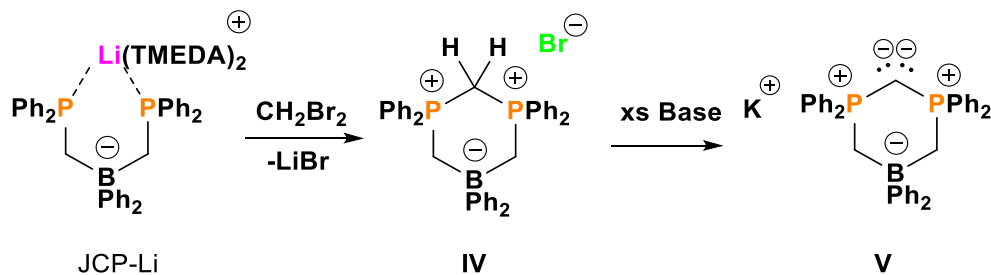
Scheme 6.5. *Proposed synthesis of an anionic carbodicarbene using JCP-Li as the starting ligand.*

Experimentally, treatment of JCP-Li with CH_2Br_2 results in a mixture of products in the $^{31}P\{^1H\}$ NMR and characterization of the resulting products was not successful. It is likely that the presence of Li^+ or TMEDA results in side reactions with the anticipated product and/or resulting intermediates. As a result, finding another cation was desirable and can be achieved by salt metathesis reactions. One option is to prepare the thallium(I) salt of JCP that was used by Ragogna and co-workers for their heavier group 14 complexes introduced earlier (**Scheme 6.3**).[6] While this cation might be a good candidate considering its success with heavier group 14 analogues, due to the toxicity of thallium, we were inclined to find another counterion to experiment with. Among the other variants reported by Peters, one particular example is JCP-ASN[22] (ASN = 5-Azoniaspiro[4.4]nonane), which can be easily prepared by the salt metathesis reaction of JCP-Li with ASNBr in methanol to yield JCP-ASN in high yields (>90%).

Upon preparing the ASN salt of JCP, treatment of JCP-ASN with dibromomethane results in clean reactivity with a single product peak observed in the $^{31}P\{^1H\}$ NMR (+25 ppm). The resulting peak decomposes over time, however, and thus, subsequent deprotonation of **IV** was performed *in situ*. Addition of excess (2.5

equivalents) NaNH$_2$ to a THF solution of **IV** results in immediate bubbling of

ammonia. Filtration through Celite and removal of solvent from the filtrate under

reduced pressure results in an off-white solid. Dissolving the resulting crude

materials in THF and allowing for slow evaporation results in colourless crystals

suitable for X-ray diffraction. The resulting structure was that of the singly

deprotonated neutral product, JCP-CH (**1**, **Scheme 6.6**).
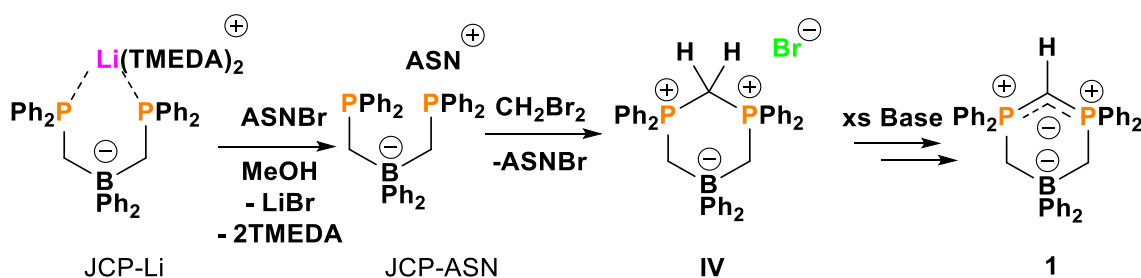
Scheme 6.6. *Synthetic route to isolate neutral compound **1**. Base = NaNH$_2$*

Compound **1** (**Figure 6.6**) is overall neutral with the geometry at the carbon

being sp^2 hybridized. The $^{31}P\{^1H\}$ NMR shows a single peak at +20 ppm. **Scheme 6.6**

illustrates the overall scheme of the reaction and the base used in the deprotonation

to **1** is sodium amide (NaNH$_2$). Irrespective of the stoichiometry used (1-5 equivalents

of base), the only product observed and isolated in all cases is **1**. Other bases have

been employed in an attempt to deprotonate the remaining proton to yield an anionic

carbodiphosphorane but were not successful. Bases liked NaNH$_2$, ^{n}BuLi, ^{t}BuLi,

KHMDS, NaH and LiAlH$_4$ have all resulted in no reactivity towards **1**. Transition metal

complexes like Zr(Bn)$_4$, Ag(OAc), Pd(OAc)$_2$ and Cu(OAc) are known to abstract

protons (internal bases) by activating C-H bonds and yielding organometallic

complexes.[26] Attempts to generate the anionic carbodiphosphorane and coordinating

it to a transition metal in-situ did not work in all of these cases; no reactivity was observed.
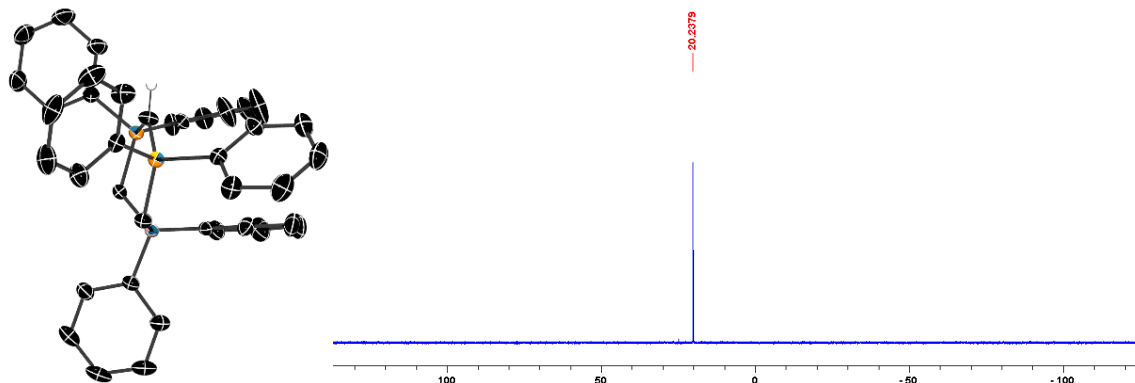
Figure 6.6. *Solid state structure of **1** (left). Thermal ellipsoids are shown at 50% probability level. Hydrogen atoms and solvent molecules are omitted for clarity. Selected bond distances and angles are given in **Table 6.2**. $^{31}P\{^{1}H\}$ NMR of **1** (right).*

Deprotonation of **1** has proven to be a challenge and thus, an alternative method to arrive at the anionic carbodiphosphorane was desired. A C–Br fragment in-place of C–H would, in theory, be easier to break as a C–Br bond (~285 kJ/mol) is significantly weaker than a C–H bond (~411 kJ/mol)[27] making it a good candidate to undergo reduction of the C(II) centre using mild reducing conditions.

Treating JCP-ASN with CBr$_4$, it was anticipated that ASNBr would be eliminated resulting in the product [JCP-CBr$_2$][Br]; this was not observed, and the $^{31}P\{^{1}H\}$ NMR spectrum showed a mixture of at least 10 different phosphorus containing fragments. This is likely due to the generation of free bromine molecules in solution reacting with the product and intermediates leading to the different side products. To avoid this, excess of zinc powder was added to the reaction mixture prior to the addition of CBr$_4$ to abstract free bromine molecules as they are generated

during the course of the reaction. The reaction mixture was stirred for 2 days in THF, followed by filtration through Celite. The filtrate was dried under reduced pressure to yield **2** as a colourless solid (**Scheme 6.7**).
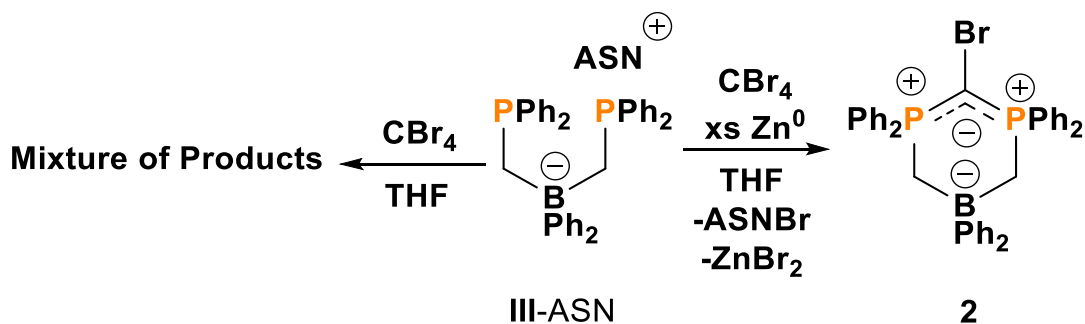
Scheme 6.7. *Synthetic route to isolate JCP-CBr (**2**) with and without the presence of Zn^0 powder.*

Dissolving **2** in THF and allowing it to slowly evaporate yields crystals suitable for X-ray diffraction (**Figure 6.7**). Next, we were interested in reducing **2** to the anionic carbodiphosphorane using various reducing agents like Mg^0, Zn^0, $Ni(COD)_2$ and ^nBuLi. All of these reagents did not yield any reactivity towards **2**, and the use of stronger reducing agents like KC_8, Na^0 and K^0 result in decomposition of **2**, determined by observing multiple peaks in the ^{31}P NMR spectrum.
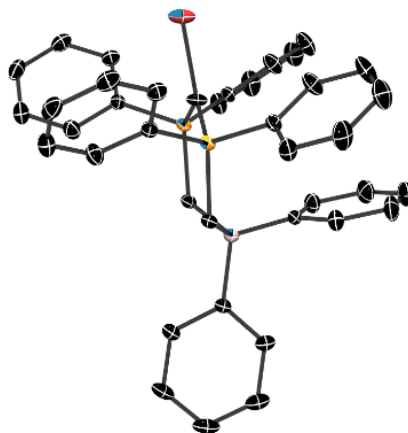
Figure 6.7. *Solid state structure of **2**. Thermal ellipsoids are shown at 50% probability level. Hydrogen atoms and solvent molecules are omitted for clarity. Selected bond distances and angles are given in **Table 6.2**.*

Both **1** and **2** are similar crystallographically in-terms of the internal bond distances within the phosphine ligand. Both structures assume a half-chair conformation with the bridging carbon (C1) in plane with the ligand and the boron sitting out of plane. This is due to having the carbon's lone pair delocalized in the P-C bonds and not localized on the carbon centre (C1). The sum of angles around C1 in **2** add-up to $°\Sigma_{C1}$: 358.35°; which is very close to 360° (for a planar system). This is very different compared to Ragogna's germanium and tin complexes of JCP where the sum of angles around the germanium and tin are $°\Sigma_{Ge}$: 280.15° and $°\Sigma_{Sn}$: 272.94° respectively. This is a result of the lone pair being delocalized on germanium and tin centres resulting in the chloride pointing out of plane as shown in **Figure 6.8**. This is further illustrated by examining the P-C1 bond distances in **1** and **2** (~1.71 Å) being significantly shorter than that expected for a P-C single bond (~ 1.80–1.85 Å) and more consistent with a P-C double bond (~ 1.6–1.7 Å) supporting the idea of a delocalized lone pair making an ylide in **1** and **2**.[28]
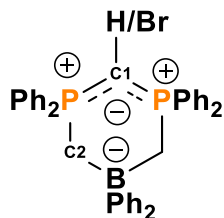
	[Ph₂B(CH₂PPh₂)₂ CH] (1)	[Ph₂B(CH₂PPh₂)₂ CBr] (2)	[Ph₂B(CH₂PPh₂)₂ GeCl]	[Ph₂B(CH₂PPh₂)₂ SnCl]
C1-X	-	1.9211(19)	2.2895(9)	2.460(1)
P-C1	1.7053(13); 1.7070(13)	1.7134(9)	P-Ge: 2.4567(9); 2.4565(9)	P-Sn: 2.672(1); 2.7005(9)
P-C2	1.7899(14); 1.7747(13)	1.7891(13)	1.812(3); 1.809(3)	1.811(4); 1.799(3)
B-C2	1.6664(19); 1.6732(18)	1.6710(19)	1.680(4); 1.673(5)	1.687(7); 1.675(5)
P-C1-P	125.55(8)	126.67(11)	P-Ge-P: 85.50(3)	P-Sn-P:81.74(3)
P-C1-Br	-	115.84(6)	P-Ge-Cl: 99.77(3); 94.88(3)	P-Sn-Cl: 97.43(4); 93.77(4)
°Σ	-	°Σ$_{C1}$: 358.35	°Σ$_{Ge}$: 280.15	°Σ$_{Sn}$: 272.94

Table 6.2. *Selected bond distances (Å) and angles (°) of compounds **1** and **2** along with Ragogna's [Ph₂B(CH₂PPh₂)₂MCl] (M = Ge, Sn).*
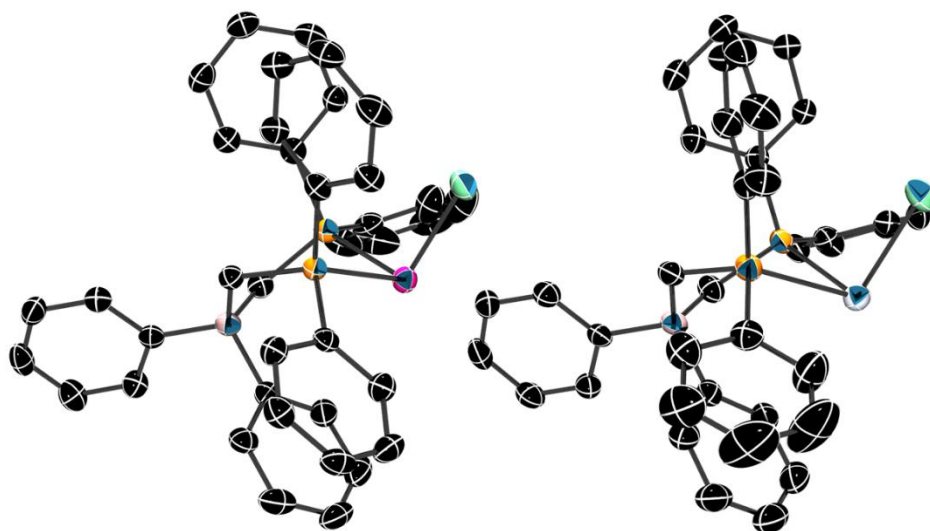
Figure 6.8. *Solid state structure of Ragogna's [Ph₂B(CH₂PPh₂)₂GeCl] (left) and Ragogna's [Ph₂B(CH₂PPh₂)₂SnCl] (right). Thermal ellipsoids are shown at 50% probability level. Hydrogen atoms and solvent molecules are omitted for clarity. Selected bond distances and angles are given in **Table 6.2**.*

6.2.2 Attempted Synthesis of an Anionic Carbodicarbene

The resulting decomposition from the reduction attempts raised the question

of whether or not JCP ligand is a suitable candidate for the isolation of an anionic

carbodiphosphorane. Our group previously reported the triphosphenium salt

depicted in **Scheme 6.8**, which contains a phosphorus(I) centre stabilized by a dppe

(1,2-Bis(diphenylphosphino)ethane) donor ligand.[29] Having phosphine donors to

stabilize the P(I) centre did not provide enough support and stabilization for the P(I)

centre to undergo further reactivity without decomposition. Work performed during

my master's research (**Scheme 6.8**) consisted of introducing a carbene donor to

displace the weaker dppe ligand, resulting in a P(I) centre that is stabilized by two

carbenes. This change gave rise to a more stable P(I) centre that can undergo further

chemistry without decomposition.[30–33]
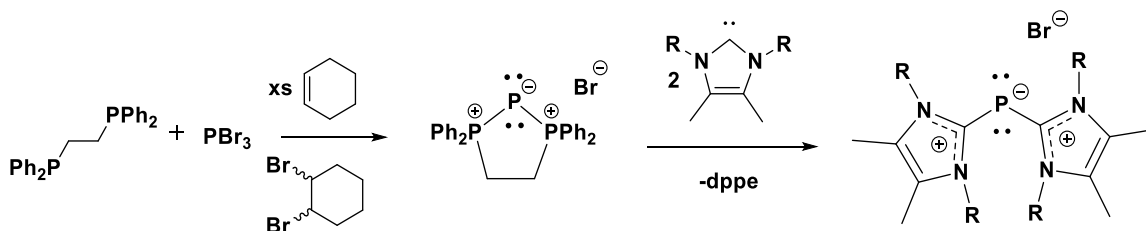
Scheme 6.8. Reaction scheme showing the synthesis of triphosphenium P(I) cation and the subsequent ligand exchange reaction with N-heterocyclic carbenes.

Carbodicarbenes have been first reported by Bertrand and co-workers as

mentioned previously, following the synthetic route shown in **Scheme 6.2**.[20] Carbene

donors are stronger and more stabilizing than phosphines, therefore, we became

interested in synthesizing an anionic carbodicarbene (as an alternative to an anionic

carbodiphosphorane) in hopes of obtaining a stable anionic carbon(0) centre. Using

the same starting ligand as Bertrand's, (**VI**, **Scheme 6.9**), we attempted to add a

negative overall charge by adding a dialkylbromoborane to **VI** in THF, which resulted

in the formation of white precipitate that is insoluble in solvents like DCM, THF and

CH_3CN. The precipitate was collected by filtration and washed with ether to yield **3**

and **4** ([(NMeBz)$_2$CH$_2$BR$_2$][Br]) in great yields (82% and 85% respectively).
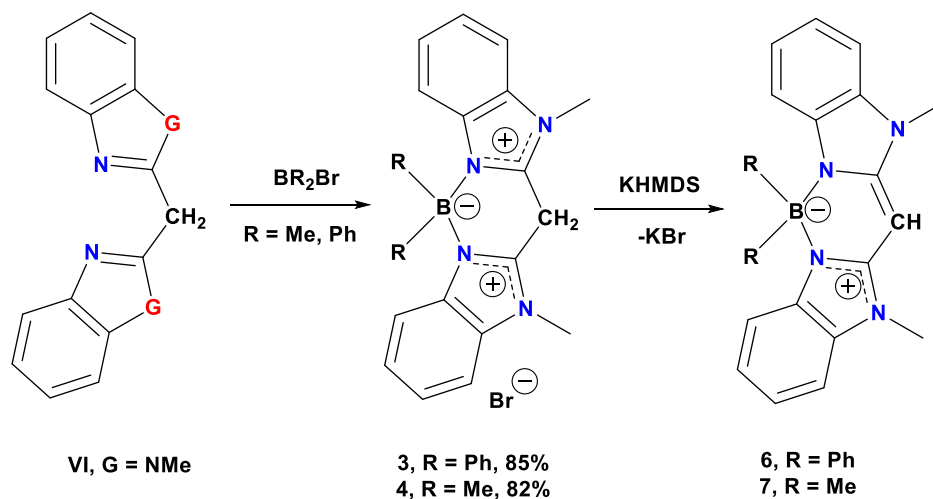
Scheme 6.9. *Synthesis of compounds **3**, **4**, **6**, and **7**. G = NR, S or O, for **VI**, G = NMe.*

Compounds **3** and **4** were treated with 2.5 equivalents of KHMDS (potassium

hexamethyldisilazide) in THF and were allowed to stir for 16 hours yielding pale-

yellow solutions and yellow precipitate (**Scheme 6.9**). The resulting compounds have

poor solubility, but slow evaporation of the dilute yellow solutions resulted in yellow

crystals suitable for X-ray diffraction. Structures of **6** and **7** were obtained (**Figure

6.9**); both structures show planar geometry throughout the compound with the

boryl-R groups pointing above and below the plane of the compound. Unlike the half

chair confirmation adapted by compounds **1** and **2**, compounds **6** and **7** have a planar

core with C1-N1-N2-C2 dihedral angles of 1.01° in **6** and 0.00° in **7**.
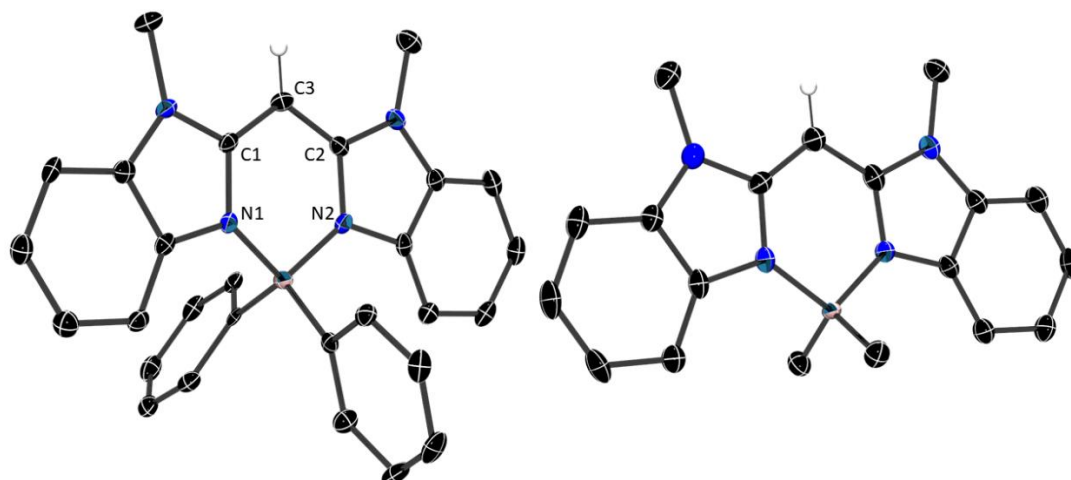
Figure 6.9. *Solid state structure of **6** (left) and **7** (right). Thermal ellipsoids are shown at 50% probability level. Hydrogen atoms and solvent molecules are omitted for clarity. Selected bond distances and angles are given in **Table 6.3**.*
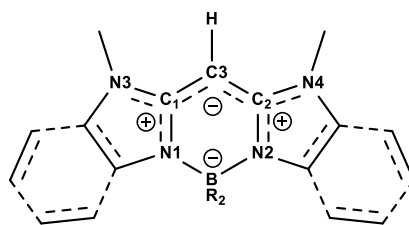
	(NMeBz)$_2$CH$_2$ (VI)	(NMeBz)$_2$CH BPh$_2$ (6)	(NMeBz)$_2$CH BMe$_2$ (7)	(SBz)$_2$CH$_2$BMe$_2$ (8)
C1-C3 (C3-C2)	1.501(2); 1.489(2)	1.394(4); 1.399(4)	1.389(6); 1.388(6)	1.462(11); 1.492(11)
C1-N1 (C2-N2)	1.318(2); 1.315(2)	1.357(4); 1.356(4)	1.359(6); 1.356(7)	1.318(9); 1.324(10)
C1-N3 (C2-N4)	1.368(2); 1.369(2)	1.370(4); 1.370(4)	1.372(6); 1.372(6)	C1-S: 1.712(8); 1.699(8)
N1-B (N2-B)	-	1.587(4); 1.577(4)	1.584(6); 1.589(6)	1.625(11); 1.601(11)
C1-C3-C2	-	116.1(2)	115.9(5)	114.5(7)
C1-N1-N2-C2	55.12	1.01	0.00	1.72
N1-B-N2	-	102.8(2)	103.0(4)	104.3(6)

Table 6.3. *Selected bond distances (Å) and angles (°) of compounds VI and **6-8**.*

CHAPTER 6
Towards the Synthesis of an Anionic Carbon(0)

Other variants of the Ligand have been investigated ([(**G**Bz)$_2$CH$_2$BR$_2$][Br]) where G = NR, S and O (**Scheme 6.9**). In cases where G = NR, compounds **3** and **4** were isolated, but as mentioned above, poor solublility did not allow for characterization by NMR spectroscopy or X-ray crystallography. Ligands with G = O or S were insoluble in common organic solvents; however, counter-ion exchange using TMSOTf resulted in increased solubility of the ligand with G = S to yield [(SBz)$_2$CH$_2$BR$_2$][OTf] (**5**) as shown in **Scheme 6.10**.

After isolating the neutral compounds **6** and **7**, attempts to further deprotonate the compounds were not successful. A similar library of bases as used with **1** and **2** was employed but no reactivity was observed. Despite the failed attempt to obtain an anionic carbodicarbene, compounds **6** and **7** have dye like properties (**Figure 6.10,** right) with a core similar to that of boron-dipyrromethene (BODIPY, **Figure 6.10**, left) that are useful fluorescent dyes.[34]

Figure 6.10. *Core structure of BODIPY (left) and a suspension of compound **6** in dark (middle) and under UV-light (right).*
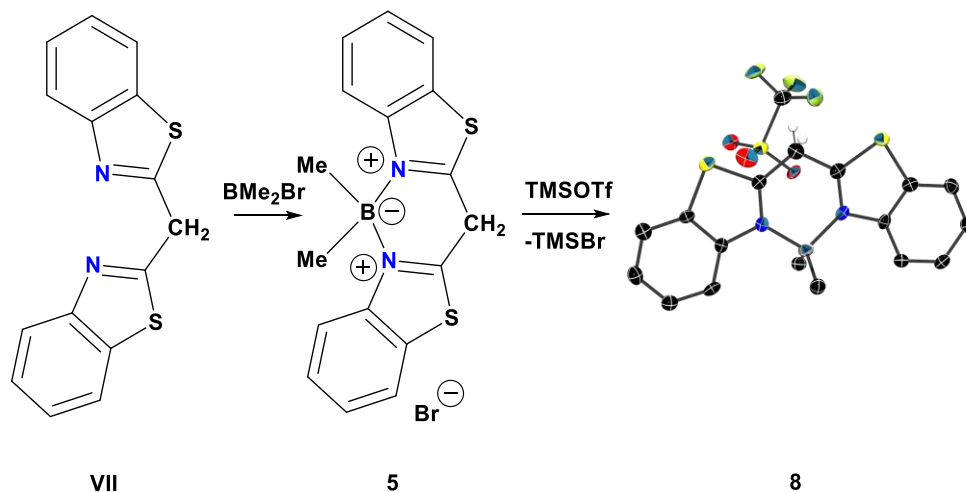
Scheme 6.10. *Reaction scheme showing synthesis of **8**.*

Although carbodicarbenes have been predicted to be better donors solely based on v_{CO} stretching frequencies of cis-[RhCl(CO)$_2$(L)] as mentioned earlier;[20] recent work by Grubbs and co-workers show that carbodicarbenes are weaker donors than carbenes.[35] **Figure 6.11** displays a series of ruthenium-based olefin metathesis catalysts where the catalyst on the left is Grubbs second generation that generally has higher activity and stability than Grubbs first generation catalyst. The middle catalyst contains a bis(NHC) ruthenium catalyst that is slow to initiate due to the strong NHC donors making it harder for ligand dissociation to take place and result in an active catalyst. The bis(NHC) ruthenium catalyst only showed modest reactivity at elevated temperatures.[35] Lastly, a mixed system of NHC–CDC ruthenium catalyst was prepared by Grubbs and it was anticipated to be an even slower reaction due to the strong donor ability of CDC. To their surprise and mine, the CDC ligand was the labile ligand, readily dissociating to yield an active catalyst at room temperature. This illustrates that the donor ability of a ligand is not the only factor in play and that

ν_{CO} stretching frequencies can be used to predict donor strengths of similar systems, but cannot be reliable to compare different systems.
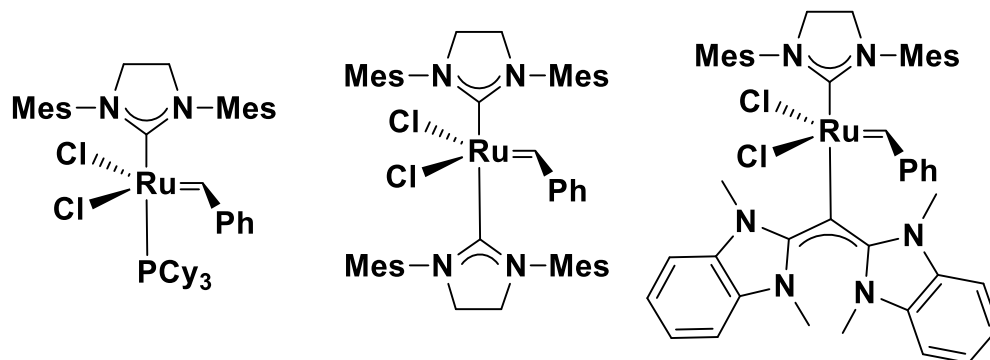
Figure 6.11. *A series of ruthenium-based catalysts reported by Grubbs.*

6.3 Conclusions

We successfully synthesized compounds **1** and **2** that represent the first examples of six-membered ring systems with this specific arrangement of atoms. Although further deprotonation was not successful, these compounds show the different behaviour adopted by the carbon in comparison to heavier group-14 analogues of the same ligand. Compounds **6** and **7** have interesting features and the central arrangement resembles that of BODIPY making it a potential fluorescent dye.

6.4 Experimental

6.4.1 General Remarks

All manipulations were carried out using standard inert-atmosphere techniques. All reagents and chemicals were obtained from Sigma-Aldrich. All reagents were used without further purification. MeCN-*d*₃ was dried over calcium

hydride or phosphorus pentoxide, and dichloromethane-d_2 was dried over phosphorus pentoxide. All other solvents were dried on a series of Grubbs-type columns and were degassed prior to use.[36] All glassware was stored in a 170 °C oven for several hours and was degassed prior to use. **I**[24], **II**[25], JCP-Li[22], JCP-ASN[22], **VI**[37], and [(SBz)$_2$CH$_2$BR$_2$] (**VII**)[38] were all prepared according to the literature procedures.

NMR spectra were recorded at room temperature on Bruker Avance III 500 MHz, Bruker Avance Ultrashield 300 MHz, and Bruker Avance DPX 300 MHz spectrometers. Chemical shifts are reported in parts per million relative to internal standards for ^{1}H and ^{13}C (the given deuterated solvent) and external standards for external standards (85% H$_3$PO$_4$ for ^{31}P). Coupling constants |J| are given in hertz. Elemental analysis was performed at the University of Windsor Mass Spectrometry Service Laboratory using a Perkin-Elmer 2400 combustion CHN analyzer.

6.4.2 Synthesis
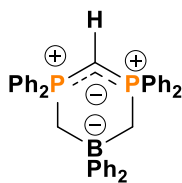
[Ph$_2$B(CH$_2$PPh$_2$)$_2$CH] (1) A 100 mL Schlenk flask was charged with JCP-ASN (600 mg, 0.87 mmol) in 3 mL CH$_2$Br$_2$. After 5 minutes of stirring, all the precipitate disappeared and solvents were removed under reduced pressure. THF (40 mL) was added followed by NaNH$_2$ (170 mg, 4.34 mmol) resulting in bubbling of NH$_3$. The mixture was refluxed for 4 hours, cooled down to room temperature and filtered through Celite. Solvents were removed from the filtrate under reduced pressure to yield **1** as

an off-white precipitate (280 mg, 56%). ^{1}H NMR (d$_8$-THF) δ: 7.67 (t, 8H, $^3J_{HH}$ = 9 Hz), 7.34 (m, 12H), 6.86 (b, 4H), 6.62 (m, 6H), 1.94 (d, 4H, $^2J_{PH}$ = 16 Hz), 1.24 (t, 1H, $^2J_{PH}$ = 4 Hz). ^{13}C{^{1}H} NMR δ: 136.93 (vt, J_{PC} = 84 Hz), 133.45, 131.92 (vt, J_{PC} = 10 Hz), 131.08, 128.95 (vt, J_{PC} = 11 Hz), 126.52, 123.33, 16.93 (b), 1.63 (m). ^{31}P{^{1}H} NMR δ: 20.24 (s). ^{11}B{^{1}H} NMR δ: –13.41 (s). Anal. Calc. for C$_{39}$H$_{35}$BP$_2$ (576.47 g/mol): C, 81.26; H, 6.12; N, 0.00. Found: C, 80.76; H, 5.85; N, 0.04.
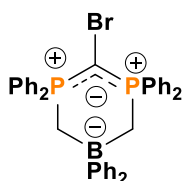
[Ph$_2$B(CH$_2$PPh$_2$)$_2$CBr] (**2**) A 100 mL Schlenk flask was charged with JCP-ASN (2.0 g, 2.90 mmol), CBr$_4$ (962 mg, 2.90 mmol) and zinc powder (240 mg, 3.7 mmol) in THF. The reaction mixture was refluxed for 2 days before cooling down to room temperature and filtering through Celite. Solvents were removed from the filtrate under reduced pressure resulting in **2** as an off-white solid. (800 mg, 44%). ^{31}P{^{1}H} NMR δ: 22.58 (s). Anal. Calc. for C$_{39}$H$_{34}$BBrP$_2$ (655.36 g/mol): C, 71.48; H, 5.23; N, 0.00. Found: C, 71.56; H, 5.01; N, 0.10.

3, G = NMe, R = Ph
4, G = NMe, R = Me
5, G = S,   R = Me
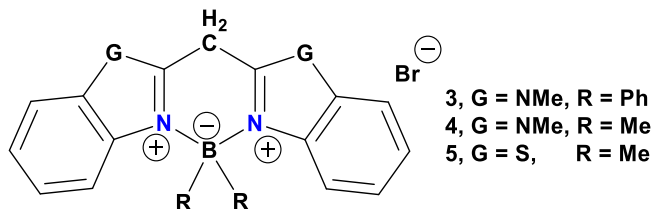
General synthesis of **[(NMeBz)$_2$CH$_2$BPh$_2$][Br]** (**3**), **[(NMeBz)$_2$CH$_2$BMe$_2$][Br]** (**4**) and **[(SBz)$_2$CH$_2$BMe$_2$][Br]** (**5**) To a 100 mL Schlenk flask charged with **VI** (450 mg, 1.63 mmol) in 40 mL Et$_2$O, (400 mg, 1.63 mmol) of BPh$_2$Br was added resulting in a

white suspension. After allowing the reaction mixture to stir for 18 hours, the corresponding product was collected by filtration to yield **3** (712 mg, 85%) as a colourless solid. Similar procedure was carried out using (230 mg, 0.83 mmol) of **VI** and (0.081 mL, 0.83 mmol) BMe_2Br to yield **4** (270 mg, 82%) as a colourless solid; **VII** (247 mg, 0.87 mmol) and BMe_2Br (0.085 mL, 0.87 mmol) to yield **5** (338 mg, 99%) as a yellow solid. Poor solubility of these compounds did not allow for characterization via NMR or the formation of crystals suitable for X-ray diffraction.

6, R = Ph
7, R = Me
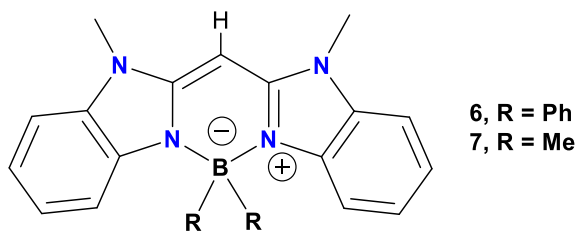
General synthesis of **[(NMeBz)₂CHBPh₂]** (**6**) and **[(NMeBz)₂CHBMe₂]** (**7**) A 100 mL Schlenk flask charged with 0.27 mmol of **3** or **4** and KHMDS (106 mg, 0.53 mmol) in 40 mL THF was sonicated for 18 hours to result in yellow precipitate and small yellow crystals on the glass walls. These crystals were suitable for X-ray diffraction and allowed for the identification of the resulting structures of **6** and **7**. These compounds are very poorly soluble that no NMR data was collected for either compound.
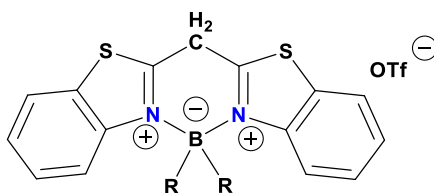
[(SBz)₂CH₂BMe₂][OTf] (**8**) **5** (40 mg, 0.10 mmol) was suspended in a in CH_3CN in a 20 mL vial followed by the addition of TMSOTf (0.036 mL, 0.20 mmol). The reaction mixture was allowed to stir for 18 hours before decanting the dilute solution to

another vial to slowly crystalize yielding yellow crystals of **8** suitable for X-ray diffraction. The resulting product is poorly soluble to obtain NMR data.

6.4.3 X-ray Crystallography

Crystals for investigation were covered in Paratone®, mounted onto a goniometer head, and then rapidly cooled under a stream of cold N_2 of the low-temperature apparatus (Oxford Cryostream) attached to the diffractometer. The data were then collected using the APEXII (Bruker AXS) software suite on a Bruker Photon 100 CMOS diffractometer using a graphite monochromator with MoK_α (λ = 0.71073 Å). For each sample, data were collected at low temperature. APEXII software was used for data reductions and SADABS (Bruker AXS) was used for absorption corrections (multi-scan; semi-empirical from equivalents). XPREP was used to determine the space group and the structures were solved and refined using the SHELX[39] software suite as implemented in the WinGX[40] or OLEX2[41] program suites. Validation of the structures was conducted using PLATON[42].

Compound Name	JCP-CH	JCP-CBr	[(NMeBz)$_2$CHBPh$_2$]
Label	1	2	6
CCDC ID	N/A	N/A	N/A
Empirical formula	C$_{39}$H$_{35}$BP$_2$	C$_{39}$H$_{34}$BBrP$_2$	C$_{29}$H$_{25}$BN$_4$
Formula weight	576.42	655.32	448.36
Temperature (K)	173.2	130.02	104.99
Crystal system	monoclinic	monoclinic	monoclinic
Space group	C2/c	P2$_1$/m	P2$_1$/c
a (Å)	33.5185(12)	10.9367(6)	11.6667(18)
b (Å)	11.4085(5)	14.9347(8)	9.9803(14)
c (Å)	17.5461(6)	10.9789(5)	19.924(3)
α (°)	90	90	90
β (°)	112.3982(13)	116.601(2)	105.021(6)
γ (°)	90	90	90
Volume (Å^3)	6203.4(4)	1603.43(15)	2240.7(6)
Z	8	2	4
ρ_{calc} (g·cm^{-3})	1.234	1.357	1.329
μ (mm^{-1})	0.167	1.409	0.26
F(000)	2432	676	928
Crystal size (mm^3)	0.441 × 0.241 × 0.171	0.435 × 0.13 × 0.04	0.3 × 0.1 × 0.1
Radiation	MoKα (λ = 0.71073)	MoKα (λ = 0.71073)	MoKα (λ = 0.71073)
2Θ range for data collection (°)	5.888 to 61.146	6.856 to 58.382	5.882 to 52.896
Index ranges	−45 ≤ h ≤ 47 −16 ≤ k ≤ 16 −25 ≤ l ≤ 23	−15 ≤ h ≤ 14 −20 ≤ k ≤ 20 −15 ≤ l ≤ 13	−14 ≤ h ≤ 14 −12 ≤ k ≤ 12 −24 ≤ l ≤ 24
Reflections collected	139391	65838	57858
Independent reflections	9506 R$_{int}$ = 0.0534 R$_{sigma}$ = 0.0232	4485 R$_{int}$ = 0.0428 R$_{sigma}$ = 0.0177	4594 R$_{int}$ = 0.2237 R$_{sigma}$ = 0.0834
Data/restraints /parameters	9506/0/379	4485/0/211	4594/0/309
Goodness-of-fit on F^2	1.05	1.065	1.105
Final R indexes [I>=2σ(I)]	R$_1$ = 0.0441 wR$_2$ = 0.1013	R$_1$ = 0.0285 wR$_2$ = 0.0627	R$_1$ = 0.0716 wR$_2$ = 0.1340
Final R indexes [all data]	R$_1$ = 0.0636 wR$_2$ = 0.1131	R$_1$ = 0.0399 wR$_2$ = 0.0687	R$_1$ = 0.1193 wR$_2$ = 0.1538
Largest diff. peak/hole (e·Å^{-3})	0.36/−0.35	0.33/−0.40	0.31/−0.34
Refinement method	Full-matrix least-squares on F^2		

$$R_1 = \frac{\sum ||F_o| - |F_c||}{\sum |F_o|} \qquad wR_2 = \sqrt{\frac{\sum w(F_o{}^2 - F_c{}^2)^2}{\sum w(F_o{}^2)^2}} \qquad R_{int} = \frac{\sum |F_o{}^2 - F_o{}^2(mean)|}{\sum F_o{}^2} \qquad R_{sigma} = \frac{\sum \sigma(F_o{}^2)}{\sum F_o{}^2}$$

Table 6.4. *Crystallographic data and structure refinement.*

Compound Name	[NMeBzCHBMe₂]	[SBzCH₂BMe₂][OTf]
Label	7	8
CCDC ID	N/A	NA
Empirical formula	$C_{19}H_{21}BN_4$	$C_{18}H_{16}BF_3N_2O_3S_3$
Formula weight	314.21	438.16
Temperature (K)	118.98	130
Crystal system	monoclinic	orthorhombic
Space group	$P2_1/m$	$Pna2_1$
a (Å)	8.4744(13)	7.774
b (Å)	6.8215(11)	15.237
c (Å)	14.0742(18)	16.729
α (°)	90	89.83
β (°)	91.053(5)	89.97
γ (°)	90	89.86
Volume (Å³)	813.5(2)	1981.6
Z	2	1
ρ_{calc} (g·cm⁻³)	1.283	0.367
μ (mm⁻¹)	0.076	1.235
F(000)	334	221
Crystal size (mm³)	0.37 × 0.12 × 0.04	0.45 × 0.269 × 0.2
Radiation	MoKα (λ = 0.71073)	CuKα (λ = 1.54184)
2Θ range for data collection (°)	5.658 to 58.6	7.836 to 150.32
Index ranges	−11 ≤ h ≤ 11 −9 ≤ k ≤ 9 −19 ≤ l ≤ 18	−9 ≤ h ≤ 9 −19 ≤ k ≤ 19 −20 ≤ l ≤ 20
Reflections collected	24742	46828
Independent reflections	2389 R_{int} = 0.0707 R_{sigma} = 0.0360	3998 R_{int} = 0.1720 R_{sigma} = 0.0792
Data/restraints /parameters	2389/0/146	3998/1/281
Goodness-of-fit on F²	1.071	1.121
Final R indexes [I>=2σ(I)]	R_1 = 0.0991 wR_2 = 0.2783	R_1 = 0.0660 wR_2 = 0.1037
Final R indexes [all data]	R_1 = 0.1160 wR_2 = 0.2961	R_1 = 0.0968 wR_2 = 0.1143
Largest diff. peak/hole (e·Å⁻³)	0.70/−0.46	0.46/−0.50
Refinement method	Full-matrix least-squares on F²	

$$R_1 = \frac{\sum||F_o|-|F_c||}{\sum|F_o|} \qquad wR_2 = \sqrt{\frac{\sum w(F_o{}^2-F_c{}^2)^2}{\sum w(F_o{}^2)^2}} \qquad R_{int} = \frac{\sum|F_o{}^2-F_o{}^2(mean)|}{\sum F_o{}^2} \qquad R_{sigma} = \frac{\sum \sigma(F_o{}^2)}{\sum F_o{}^2}$$

Table 6.5. *Crystallographic data and structure refinement.*

6.5 References

(1)   Arduengo, A. J.; Harlow, R. L.; Kline, M. *J. Am. Chem. Soc.* **1991**, *113* (1), 361–363.

(2)   Bourissou, D.; Guerret, O.; Gabbaï, F. P.; Bertrand, G. *Chem. Rev.* **2000**, *100* (1), 39–92.

(3)   Scholl, M.; Trnka, T. M.; Morgan, J. P.; Grubbs, R. H. *Tetrahedron Lett.* **1999**, *40* (12), 2247–2250.

(4)   Xiong, Y.; Yao, S.; Tan, G.; Inoue, S.; Driess, M. *J. Am. Chem. Soc.* **2013**, *135* (13), 5004–5007.

(5)   Thirumoorthi, R.; Chivers, T.; Gendy, C.; Vargas-Baca, I. *Organometallics* **2013**, *32* (19), 5360–5373.

(6)   Weicker, S. A.; Dube, J. W.; Ragogna, P. J. *Organometallics* **2013**, *32* (22), 6681–6689.

(7)   Inés, B.; Patil, M.; Carreras, J.; Goddard, R.; Thiel, W.; Alcarazo, M. *Angew. Chem. - Int. Ed.,* **2011***, 50,* 8400–8403.

(8)   Alcarazo, M.; Radkowski, K.; Mehler, G.; Goddard, R.; Fürstner, A. *Chem. Commun.* **2013**, *49* (30), 3140–3142.

(9)   Ramirez, F.; Desai, N. B.; Hansen, B.; McKelvie, N. *J. Am. Chem. Soc.* **1961**, *83* (16), 3539–3540.

(10)   Yogendra, S.; Hennersdorf, F.; Bauzá, A.; Frontera, A.; Fischer, R.; Weigand, J. J. *Dalton Trans.* **2017**, *46* (44), 15503–15511.

(11)   Petz, W.; Neumüller, B. *Polyhedron* **2011**, *30* (11), 1779–1784.

(12)   Kubo, K.; Jones, N. D.; Ferguson, M. J.; McDonald, R.; Cavell, R. G. *J. Am. Chem. Soc.* **2005**, *127* (15), 5314–5315.

(13) Petz, W.; Kutschera, C.; Neumüller, B. *Organometallics* **2005**, *24* (21), 5038–5043.

(14) El-Hellani, A.; Monot, J.; Tang, S.; Guillot, R.; Bour, C.; Gandon, V. *Inorg. Chem.* **2013**, *52* (19), 11493–11502.

(15) Petz, W.; Neumüller, B.; Klein, S.; Frenking, G. *Organometallics* **2011**, *30* (12), 3330–3339.

(16) Pranckevicius, C.; Iovan, D. A.; Stephan, D. W. *Dalton Trans.* **2016**, *45* (42), 16820–16825.

(17) Petz, W.; Dehnicke, K.; Holzmann, N.; Frenking, G.; Neumüller, B. *Zeitschrift für Anorg. und Allg. Chem.* **2011**, *637* (12), 1702–1710.

(18) Tonner, R.; Öxler, F.; Neumüller, B.; Petz, W.; Frenking, G. *Angew. Chem. - Int. Ed.* **2006**, *45* (47), 8038–8042.

(19) Tonner, R.; Frenking, G. *Chem. Eur. J.* **2008**, *14* (11), 3260–3272.

(20) Dyker, C. A.; Lavallo, V.; Donnadieu, B.; Bertrand, G. *Angew. Chem. - Int. Ed.* **2008**, *47* (17), 3206–3209.

(21) Thomas, J. C.; Peters, J. C. *J. Am. Chem. Soc.* **2001**, *123* (21), 5100–5101.

(22) Thomas, J. C.; Peters, J. C. *J. Am. Chem. Soc.* **2003**, *125* (29), 8870–8888.

(23) Lu, C. C.; Peters, J. C. *J. Am. Chem. Soc.* **2002**, *124* (19), 5272–5273.

(24) Schore, N. E.; Benner, L. S.; LaBelle, B. E. *Inorg. Chem.* **1981**, *20* (10), 3200–3208.

(25) Dorkó, É.; Varga, E.; Gáti, T.; Holczbauer, T.; Pápai, I.; Mehdi, H.; Soós, T. *Synlett* **2014**, *25* (11), 1525–1528.

(26) Yang, Y.; Lan, J.; You, J. *Chem. Rev.* **2017**, *117* (13), 8787–8863.

(27) Darwent, B. deB. U.S. National Bureau of Standards. LCCN 70602101:

Washington, DC. 1970.

(28)   Schmidbaur, H.; Paschalidis, C.; Steigelmann, O.; Müller, G. *Angew. Chem. - Int. Ed. English* **1990**, *29* (5), 516–517.

(29)   Norton, E. L.; Szekely, K. L. S.; Dube, J. W.; Bomben, P. G.; Macdonald, C. L. B. *Inorg. Chem.* **2008**, *47* (3), 1196–1203.

(30)   Binder, J. F.; Swidan, Alaaeddeen, Macdonald, C. L. B. *Inorg. Chem.* **2018**, *57* (I), 11717–11725.

(31)   Macdonald, C. L. B.; Binder, J. F.; Swidan, A.; Nguyen, J. H.; Kosnik, S. C.; Ellis, B. D. *Inorg. Chem.* **2016**, *55* (14), 7152–7166.

(32)   Kosnik, S. C.; Binder, J. F.; Nascimento, M. C.; Swidan, A.; Macdonald, C. L. B. *Chem. Eur. J.* **2018**, chem.201805711.

(33)   Binder, J. F.; Swidan, A.; Tang, M.; Nguyen, J. H.; Macdonald, C. L. B. *Chem. Commun.* **2015**, *51* (36), 7741–7744.

(34)   Schmitt, A.; Hinkeldey, B.; Wild, M. *J. Fluoresc* **2009**, 19, 755–758.

(35)   Liberman-Martin, A. L.; Grubbs, R. H. *Organometallics* **2017**, *36* (21), 4091–4094.

(36)   Pangborn, A. B.; Giardello, M. A.; Grubbs, R. H.; Rosen, R. K.; Timmers, F. J. *Organometallics* **1996**, *15* (5), 1518–1520.

(37)   Braussaud, N.; Thomas, R.; Cavell, K. J.; Skelton, B. W.; White, H. *Synthesis* **2001**, 626–632.

(38)   Forlani, L.; Boga, C.; Vecchio, E. Del; Padovani, M. *ARKIVOC* **2003**, 15 (xv), 75–91.

(39)   Sheldrick, G. M. *Acta Crystallogr. Sect. A Found. Crystallogr.* **2008**, *64* (1), 112–

122.

(40)   Farrugia, L. J. *J. Appl. Crystallogr.* **1999**, *32* (4), 837–838.

(41)   Dolomanov, O. V.; Bourhis, L. J.; Gildea, R. J.; Howard, J. A. K.; Puschmann, H. *J. Appl. Crystallogr.* **2009**, *42* (2), 339–341.

(42)   Spek, A. L. *J. Appl. Crystallogr.* **2003**, *36* (1), 7–13.

CHAPTER 7:
Conclusions and Future Work

7.1 Dissertation Overview

This dissertation revolves around the idea of using chelating ligands to coordinate group 13-15 elements to create new and unique complexes. Three types of ligands have been discussed, a bidentate ligand in the attempted synthesis of an anionic carbon(0), a tridentate (pincer) ligand in the coordination to group 13-15 elements[1], and a tetradentate (tripod) ligand used for group 15 elements,[2] and with our collaborators, we have been successful in expanding this ligand system to group 14 as well.[3,4] The outlook for these new complexes is to be able to create new systems capable of activating small molecules and carrying out different catalytic transformations.

7.2 Bidentate Ligands

7.2.1 Bidentate Ligands Toward the synthesis of an Anionic Carbon(0)

As highlighted in Chapter 6, the attempted synthesis of an anionic carbon(0) involved two types of bidentate ligands, an anionic bisphosphine (JCP-ASN) and an anionic biscarbene. In both cases, the ligands did not yield the anticipated anionic carbon(0); however, new interesting materials were created and characterized in the process.

The JCP ligand has been used by Ragogna's group for the coordination of group 14-15 elements as mentioned earlier.[5–7] Our group illustrated that using a different anionic bisphosphine ligand can result in the zwitterionic triphosphenium compound shown in **Scheme 7.1**.[8,9] In cases where R = PPh$_2$, further reactivity at the P(I) centre was hindered by the presence of a backbone phosphine that readily reacts before the P(I) centre. Introducing a ^{t}Bu group instead allowed for further chemistry and coordination at the P(I) centre.
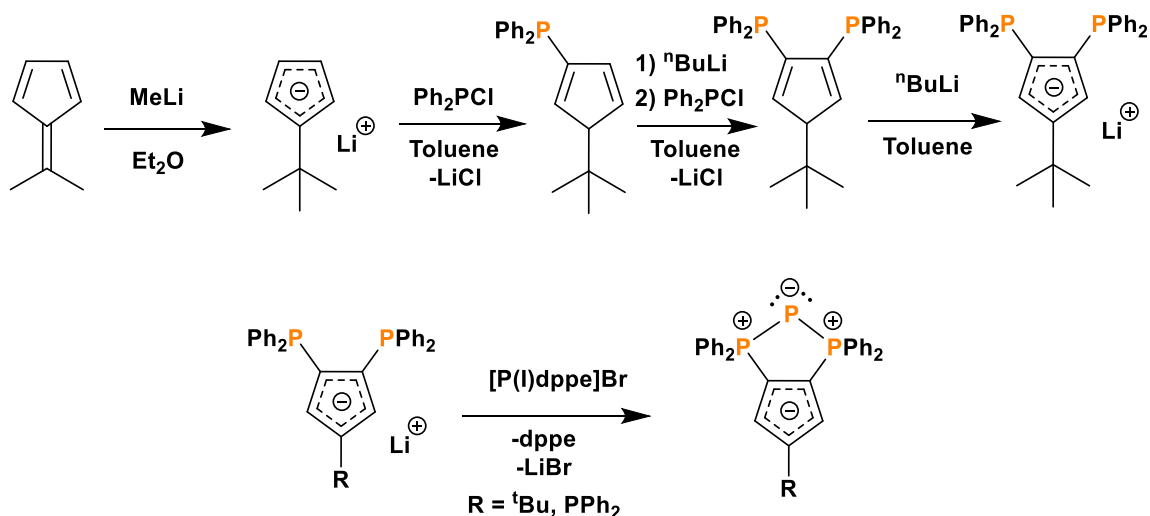
Scheme 7.1. *Synthetic route for zwitterionic triphosphenium compound.*

The presence of a Cp ring in the backbone of the anionic bisphosphine would bring further rigidity and stability to the overall donor ligand and would be a more suitable choice in comparison to the anionic JCP ligand. **Scheme 7.2** depicts the two different pathways that can lead to the anionic carbodiphosphorane using this Cp based ligand instead. Treatment of [Li][^{t}BuCp(PPh$_2$)$_2$] with CH$_2$Br$_2$ followed by excess base (like KHMDS) or treatment with tetrabromomethane followed by a reducing

agent like KC$_8$ would have the potential in yielding the anionic carbodiphosphorane compound **1** as shown in **Scheme 7.2**.

Scheme 7.2. A proposed reaction scheme to attain an anionic carbodiphosphorane.

7.2.2 Bidentate Ligands for Group 13 and 14 Coordination – Part 1

Our group has investigated the coordination of [Li][^{t}BuCp(PPh$_2$)$_2$] to phosphorus,[8,9] but to the best of our knowledge, there have been no reports of the coordination of this ligand (or similar framework) to other main group elements. To this end, we propose the use of these ligands as suitable XL-type donor ligands for group 13 and 14 elements as shown in **Scheme 7.3**.

Scheme 7.3. The proposed reaction of [Li][R-Cp(PPh$_2$)$_2$] with group 13 and 14 metal halides.

Initial reactivity studies of [Li][R-Cp(PPh$_2$)$_2$] with group 14 metal halides were successful. Treatment of [Li][^{t}BuCp(PPh$_2$)$_2$] with either GeCl$_2$ or SnCl$_2$ in THF results in an immediate yellow solution yielding ^{t}BuCp(PPh$_2$)$_2$GeCl (**2**) and ^{t}BuCp(PPh$_2$)$_2$SnCl (**3**), respectively. The ^{31}P{^{1}H} of [Li][^{t}BuCp(PPh$_2$)$_2$] shows a singlet at –20.7 ppm, and upon treatment with an equivalent of GeCl$_2$ or SnCl$_2$, the ^{31}P{^{1}H} shows a new singlet at 5.9 ppm for **2** and 4.1 ppm for **3**. Recrystallization of these products by means of slow evaporation from a THF solution yield yellow crystals of **2** and **3** suitable for X-ray diffraction (**Figure 7.1**).
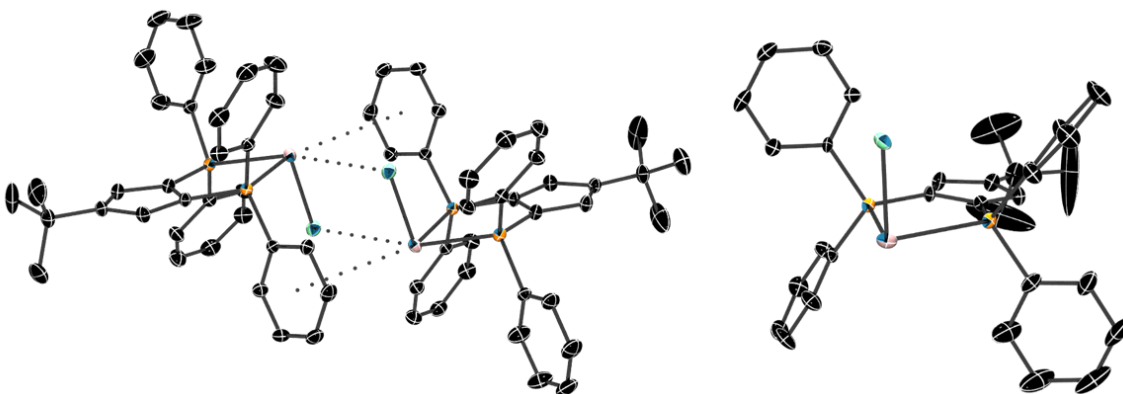
*Figure 7.1. Solid state structure of ^{t}BuCp(PPh$_2$)$_2$GeCl (2, left) and ^{t}BuCp(PPh$_2$)$_2$SnCl (3, right). Thermal ellipsoids are shown at 50% probability level. Hydrogen atoms and solvent molecules are omitted for clarity. Selected bond distances and angles are listed in **Table 7.1**.*

Compounds **2** and **3** were a result of using [Li][R-Cp(PPh$_2$)$_2$] with R = ^{t}Bu. The use of a ligand with R = PPh$_2$ with an equivalent of GeCl$_2$·dioxane results in the backbone phosphine coordinating to a second GeCl$_2$ (**4**, **Figure 7.2**). This is consistent with the observations made by our group with P(I) coordination where having a backbone phosphine results in the backbone phosphine being readily open to reactivity and coordination. Selected bond distances and angles of **4** are in **Table 7.1**.
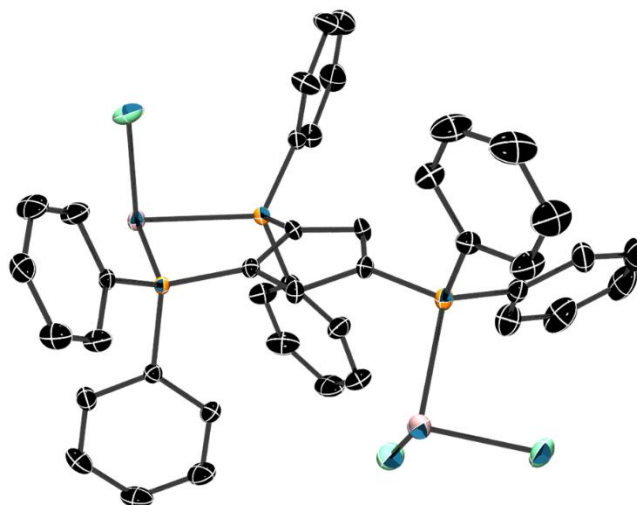
Figure 7.2. *Solid state structure of (GeCl$_2$)PPh$_2$Cp(PPh$_2$)$_2$GeCl (**4**). Thermal ellipsoids are shown at 50% probability level. Hydrogen atoms and solvent molecules are omitted for clarity.*
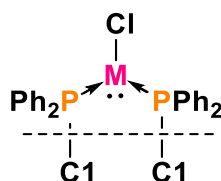
	^{t}BuCp(PPh$_2$)$_2$ GeCl (2)	GeCl$_2$PPh$_2$Cp (PPh$_2$)$_2$GeCl (4)	[Ph$_2$B(CH$_2$PP h$_2$)$_2$GeCl]	^{t}BuCp(PPh$_2$) $_2$SnCl (3)	[Ph$_2$B(CH$_2$PP h$_2$)$_2$SnCl]
M-Cl	2.259(1)	2.2646(9)	2.2895(9)	2.461(2)	2.460(1)
M-P	2.2467(1); 2.2480(1)	2.4840(7); 2.4851(7)	2.4567(9); 2.4565(9)	2.672(2); 2.698(2)	2.672(1); 2.7005(9)
P-C1	1.755(5); 1.757(4)	1.761(2); 1.760(2)	1.812(3); 1.809(3)	1.755(9); 1.755(7)	1.811(4); 1.799(3)
P-M-P	81.99(3)	80.17(2)	85.50(3)	76.97(6)	81.74(3)
P-M-Cl	92.92(4); 91.96(4)	92.36(3); 97.33(3)	99.77(3); 94.88(3)	88.74(6); 76.97(6)	97.43(4); 93.77(4)
°Σ$_M$	266.87	269.86	280.15	242.68	272.94

Table 7.1. *Selected bond distances (Å) and angles (°) of compounds **2**, **3**, and **4** along with Ragogna's [Ph$_2$B(CH$_2$PPh$_2$)$_2$MCl] (M = Ge, Sn).*

The chloride in compounds **2**-**4** is pointing away from the plane of the ligand, similar to structures reported by Ragogna of JCP-GeCl and JCP-SnCl (discussed in chapter 6).[7] Compounds **2** and **4** have very similar bond distances and angles; however, it is noteworthy that in compound **4** the Ge-P bond distance of the P-GeCl$_2$

backbone (2.4666(7)) is slightly shorter than the Ge-P bond distance of the GeCl bond

to the bisphosphine (2.4840(7) and 2.4851(7)). The sum of angles around the Ge and

Sn centres (266.87 and 242.68° respectively) are smaller than those observed in JCP-

GeCl (280.15°) and JCP-SnCl (272.94°) which is likely due to the R-Cp(PPh$_2$)$_2$-MCl

ligand forming a 5-membered ring with the main group element compared to the

cyclohexyl chair confirmation adapted by JCP-MCl. The packing of compounds **2** and

4 are similar in the sense that both compounds have intermolecular interactions of

the M-Cl fragments resulting in packing of these compounds as dimers in the solid

state. These interactions are on the order of 3.3776(9)/3.4235(9) Å in **2**, and

3.236(2)/3.236(2) Å in **4**; the germanium and tin centres also interact with the phenyl

ring of the adjacent compound (**Figure 7.1**) with an M-η^6-Ph distance of 3.851 Å in **2**

and 3.705 Å in **4**. These intermolecular interactions are not observed in Ragogna's

structures, [Ph$_2$B(CH$_2$PPh$_2$)$_2$MCl] (M = Ge, Sn), which is likely due to the bulky

phosphine donors that make these group 14 centres sterically inaccessible for

intermolecular interactions. Compound **3** contains intermolecular interaction

between a GeCl of one compound and the backbone GeCl$_2$ of the neighbouring

compound (3.4226(8) Å) as shown in **Figure 7.3**.
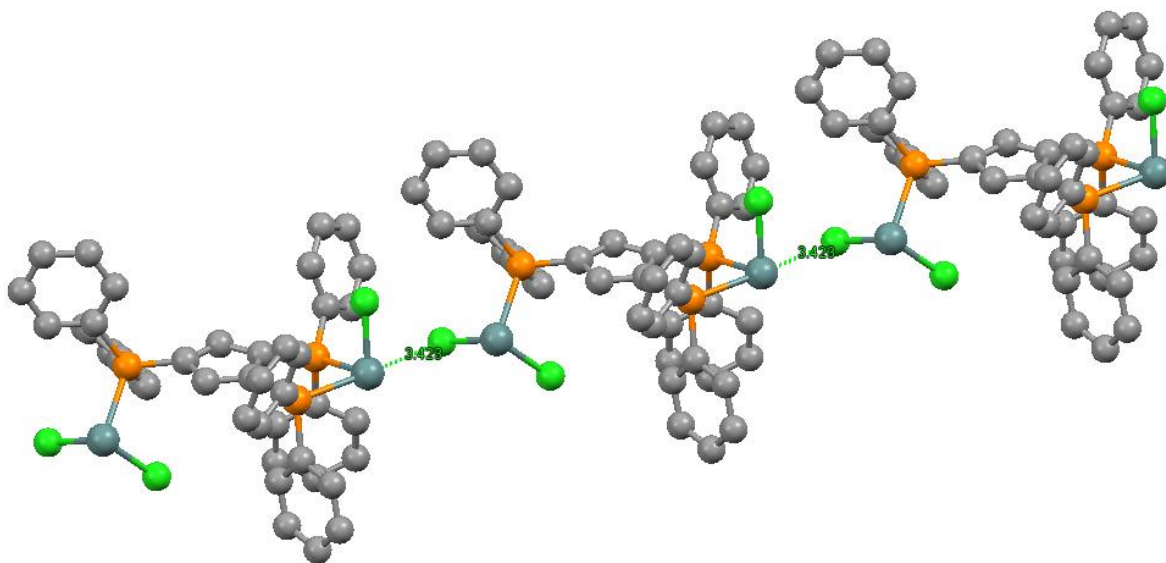
Figure 7.3. *Grown structure of* ***3*** *showing the intermolecular interaction present between the GeCl fragment and the neighbouring GeCl$_2$ fragment.*

7.2.3 Bidentate Ligands for Group 13 and 14 Coordination – Part 2

Another bidentate ligand we propose for coordination of group 14 elements is the ligand used towards the synthesis of anionic carbodicarbenes in chapter 6 ((NMeBz)$_2$CH$_2$). Deprotonation of the ligand yields a [(GBz)$_2$CH]$^-$ (G = NMe, O, or S) anion that is structurally similar to that of NacNac (**Figure 7.4**, left). The use of NacNac ligands with group 13 and 14 elements have lead to many interesting and unique results.[10–24] Coordination of [(GBz)$_2$CH]$^-$ ligand (**Figure 7.4**, right) with group 13 have been recently studied by Stalke and co-workers using different ligand varients that include G = NR, S, and O.[25–27] To the best of our knowledge there has been no reports of the coordination of this ligand to group 14 elements.

R = alkyl; R' = alkyl, aryl   **G = NMe, O, S**
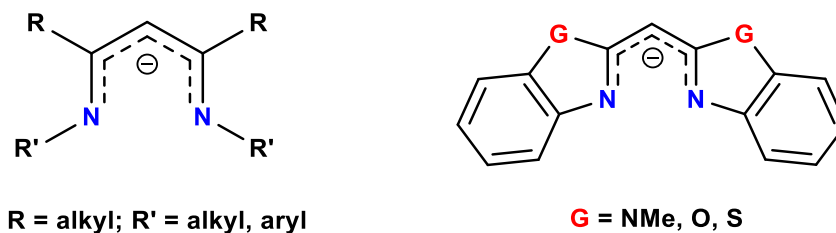
Figure 7.4. *NacNac ligand (left) and [(GBz)₂CH]⁻ (right).*

Our proposal is to treat $(GBz)_2CH_2$ with an equivalent of base followed by the addition of $GeCl_2 \cdot$dioxane or $SnCl_2$ to yield $(GBz)_2CHMCl$ (M = Ge, or Sn) as shown in **Scheme 7.4**. Initial reactivity studies involved the reaction of $(NMeBz)_2CH_2$ with KHMDS followed by $SnCl_2$ in THF to result in a deep brown solution. Upon filtration of the solution and slow evaporation of the filtrate, orange/brown crystals suitable for X-ray diffraction were isolated of $(NMeBz)_2CH_2SnCl$ (**5**, **Figure 7.5**) in low yields (<20%). Selected bond distances and angles of **5** are in **Table 7.2**.
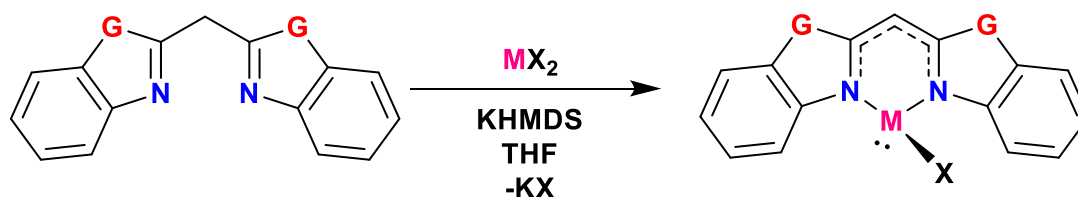
Scheme 7.4. *Proposed reaction of $(GBz)_2CH_2$ with group 14 metal halides (MX_2, M = Ge, or Sn; X = F, Cl, Br or I) to yield $(GBz)_2CHMX$.*

When comparing compound **5** to compounds discussed in chapter 6 with BR_2 backbone, $[(NMeBz)_2CHBPh_2]$ and $[(NMeBz)_2CHBMe_2]$, the internal bond distances within the ligand do not change, regardless if the bound element is boron or tin. This ligand is very rigid in nature, yet very accessible, allowing the metal centre to be open for further reactivity. Full characterization of this compound, synthesis of the

germanium adducts, and studies of the potential reactivity are all part of the future

work proposal.
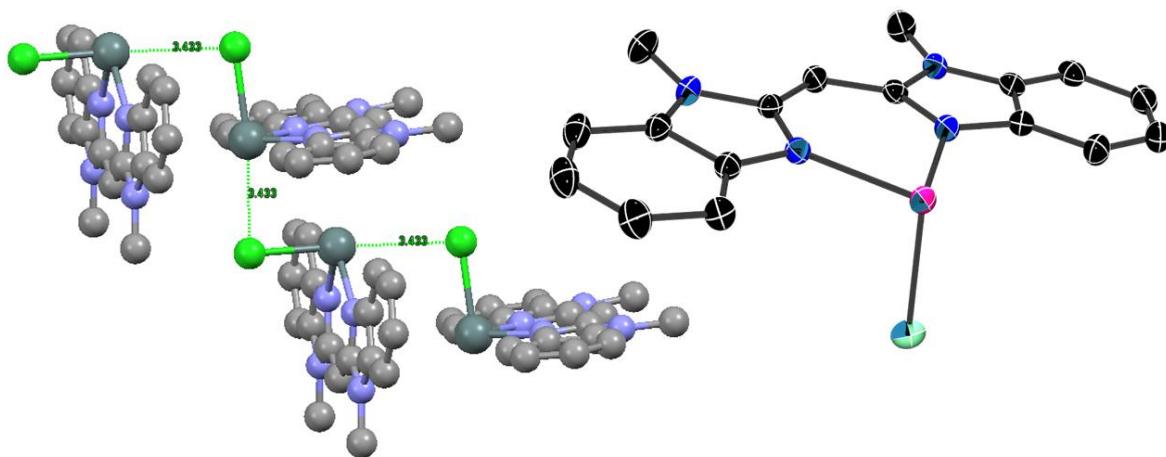
Figure 7.5. *Left: Packing of **5** showing the intermolecular interactions present in the solid state. Right: Solid state structure of (NMeBz)$_2$CH$_2$SnCl (**5**). Thermal ellipsoids are shown at 50% probability level. Hydrogen atoms and solvent molecules are omitted for clarity.*
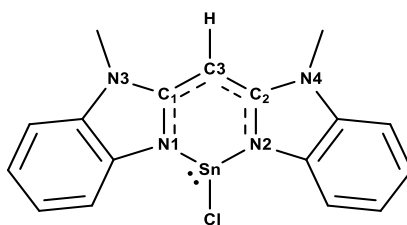
	(NMeBz)$_2$CH$_2$SnCl (**5**)	(NMeBz)$_2$CHBPh$_2$	(NMeBz)$_2$CHBMe$_2$
Sn-Cl	2.5526(7)		
Sn-N	2.168(2); 2.181(2)		
C1-C3 (C3-C2)	1.392(3); 1.398(3)	1.394(4); 1.399(4)	1.389(6); 1.388(6)
C1-N1 (C2-N2)	1.361(3); 1.360(3)	1.357(4); 1.356(4)	1.359(6); 1.356(7)
C1-N3 (C2-N4)	1.375(3); 1.370(3)	1.370(4); 1.370(4)	1.372(6); 1.372(6)
C1-C3-C2	123.1(2)	116.1(2)	115.9(5)
C1-N1-N2-C2	3.1(2)	1.01	0.00
N-Sn-N	82.55(6)		
N-Sn-N	96.25(5); 88.61(5)		
°Σ$_{Sn}$	267.41		

Table 7.2. *Selected bond distances (Å) and angles (°) of **5** and (NRBz)$_2$CHBPh$_2$ (from Chapter 6).*

7.3 Neutral Pincer (Tridentate) Ligand Donor for Groups 13-15

In chapter 4, we reported group 15 adducts of the form, [NBn-BZIMPYMCl][OTf]$_2$ (M = P, As, and Sb). Unfortunately, these compounds are air sensitive and decompose when covered in Paratone® on the microscope slide (going from yellow crystals to colourless non-crystalline material) over the course of a few hours. Stephan's work with the tripyridine donor[28] (**Scheme 7.5**) yielded an air-stable Lewis acid useful for catalytic hydrodefluorination (HDF) of unactivated fluoroalkanes as mentioned earlier.
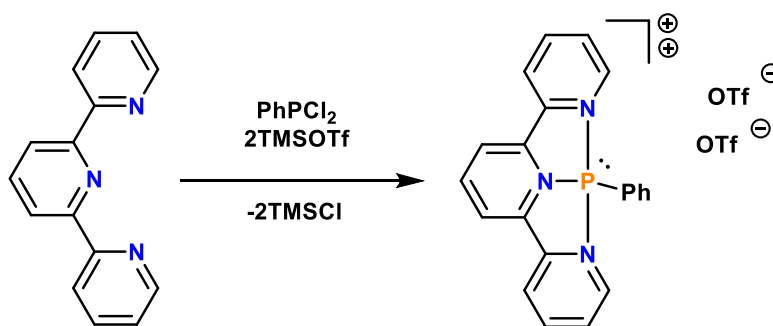
Scheme 7.5. *Stephan's dicationic P(III) catalyst.*

In chapter 3, we discussed Evans work on a Sn(II) chiral Lewis acid (**Figure 7.6**) that has been used in aldol condensation reactions in good yields with greater than 90% ee.[29]
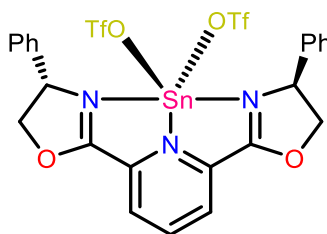
Figure 7.6. *Evans tin(II) chiral Lewis acid catalyst.*

191

For this part of chapter 7, we propose combining Stephan's work discussed in chapter 4 with Evans' ligand discussed in chapter 3 to yield the catalyst shown in **Scheme 7.6**. These ligands are commercially available, bis(oxazoline) ligands (BOX) with CH_2 (BOX) or Py (PYBOX) linkers. Treatment of R-PYBOX with PCl_3 or $PhPCl_2$ and excess TMSOTf should yield R-PYBOX-PX (X = Cl, Ph). The resulting complex would serve as a chrial catalyst that can be useful in substrate selectivity.
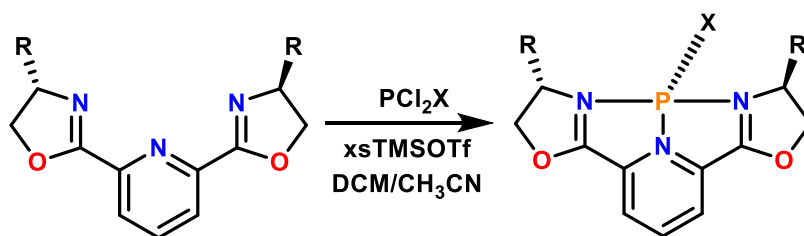
Scheme 7.6. *Proposed complex using R-PYBOX with PCl_2X (X = Cl, Ph) and excess TMSOTf to yield R-PYBOX-PX.*

7.4 Trianionic Pincer (Tridentate) Ligand Donor for Phosphorus

Aside from working with neutral tridentate ligands, we became interested in investigating trianionic nitrogen donor ligands similar to those used by Arduengo and Radosevich.[30–32] Radosevich have shown that such ligands containing phosphorus as the central atom are capable of small molecule activation. Thus, to this end, we propose the use of the BZIM ligand (**Figure 7.7**) that contains two benzimidazole donors as with the parent NH-BZIMPY ligand, but with the difference here is in the central donor nitrogen being NH rather than pyridine. This key difference would allow for a more flexible ligand, permitting for the distortion needed to create an active phosphorus centre and for an anionic nitrogen to give an overall trianionic ligand.
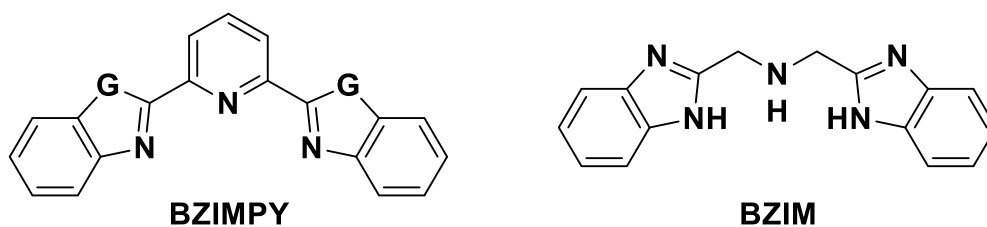
Figure 7.7. *Structure of BZIMPY (left) and BZIM (right).*

In terms of introducing the phosphorus centre, we first attempted a transamination reaction between BZIM and $(Et_2N)_2PCl$ to promote the release of two molecules of Et_2NH and the coordination of phosphorus to BZIM creating a cation similar to the one shown in **Scheme 7.7**. In theory, this reaction is similar to the transamination work reported by Verkade and co-workers in their synthesis of the superbase depicted in **Scheme 7.7**.[33]
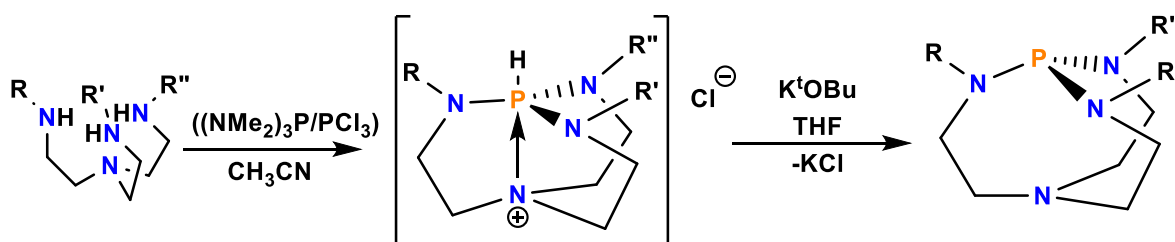
Scheme 7.7. *Synthesis of Verkade's superbase.*

This transamination process would be equivalent to deprotonation of the proton followed by the introduction of the phosphorus centre. The BZIM ligand is very poorly soluble, creating a suspension in DCM until the addition of $(Et_2N)_2PCl$ that results in an immediate uptake of the precipitate into the DCM solution. Allowing the reaction mixture to stir for an hour at room temperature results in a pale-yellow solution. The $^{31}P\{^1H\}$ NMR shows a singlet at 96 ppm that is believed to correspond to the cationic phosphorus shown in **Scheme 7.8**.
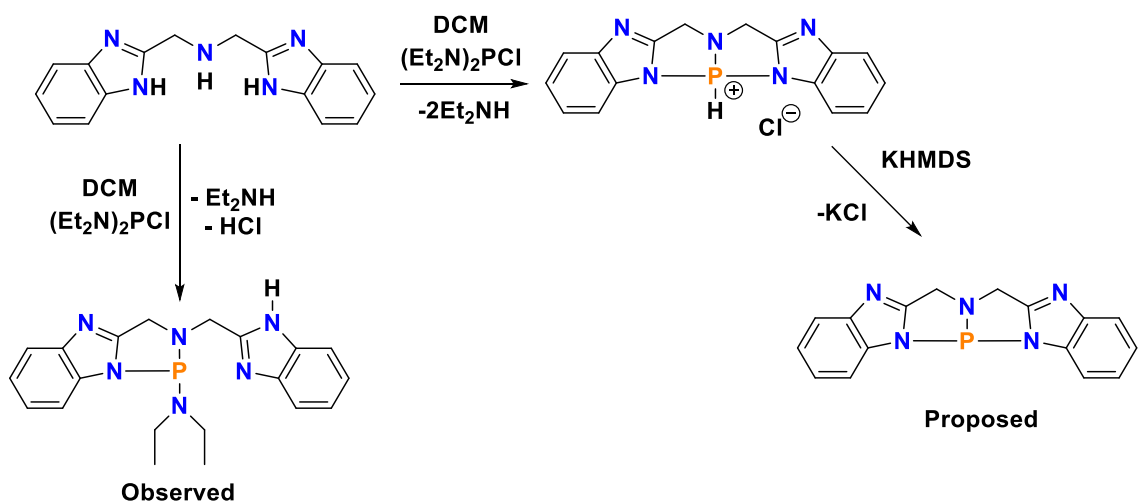
Scheme 7.8. *Proposed outcome of reacting BZIM with (Et₂N)₂PCl followed by KHMDS (right) vs. actual product isolated (left).*

Dissolving the collected materials in DCM and allowing the solvent to slowly evaporate results in colourless crystals suitable for X-ray diffraction. The resulting structure, H-BZIMP(Et₂N) (**6**, **Figure 7.8**), is a result of BZIM reacting with (Et₂N)₂PCl releasing an equivalent of Et₂NH and an HCl. The protonated arm of the ligand is flexible and should have the ability to freely rotate and interact with the amide to form a diethylamine and the pincer phosphine; however, this was not observed at room temperature and was not made possible at elevated temperatures.
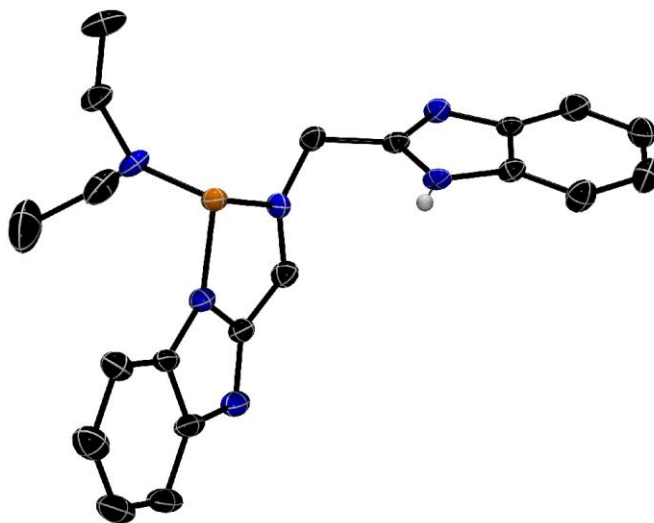
Figure 7.8. *Solid state structure of the H-BZIMP(Et$_2$N) (**6**). Thermal ellipsoids are shown at 50% probability level. Hydrogen atoms and solvent molecules are omitted for clarity.*

The transamination approach showed an interesting result, however, to generate the compound of interest (BZIMP) other means of reactivity were investigated. In particular, deprotonation of the ligand followed by the introduction of PCl$_3$ to yield the desired phosphine was carried out. Treatment of BZIM with 3 equivalents of NaH in THF results in the immediate evolution of H$_2$ gas. Addition of PCl$_3$ to the resulting mixture results in a pale-yellow solution with white precipitate that was separated by centrifugation. The solvent of the filtrate (supernatant) was removed under reduced pressure to result in colourless precipitate. ^{31}P{^{1}H} of the starting material (Et$_2$N)$_2$PCl, consists of a singlet at 155 ppm, compound **6** shows a singlet at 96 ppm and the materials resulting from this reaction gave rise to a singlet at 126 ppm. The proton-coupled NMR spectrum results in a pentet with a ^{3}J$_{CP}$ of 25 Hz that is likely due to the phosphorus centre coupling to the two CH$_2$ methylenes of the BZIM ligand framework. This shift in the phosphorus NMR spectrum is believed to correspond to the compound of interest, BZIMP (**7**). Attempts to crystallize **7** to

obtain crystals suitable for X-ray diffraction were not successful and the ^{1}H and ^{13}C

NMR spectra show the presence of other non-phosphorus containing fragments. To

this end, we hope to pursue further chemistry, first by making compound **7** cleanly

and fully characterizing it, secondly, by testing out its reactivity towards small

molecules.
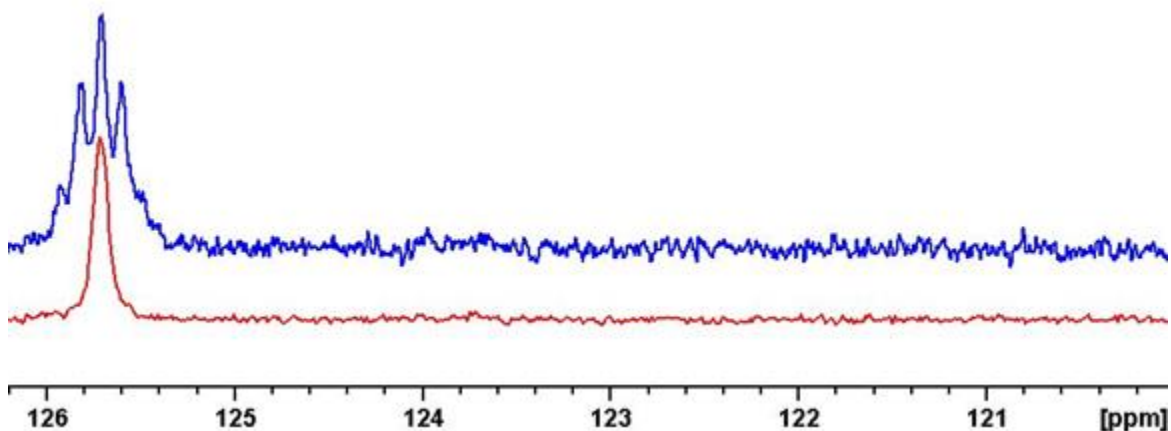
Figure 7.9. *Stacked NMR spectra of BZIMP (**7**) showing ^{31}P{^{1}H} in red and ^{31}P in blue.*

7.5 Conclusions

This dissertation consists of the use of various chelating ligand towards the

coordination of group 13-15 main group elements. In principle, these coordination

reactions are successful and create new complexes with unique physical and chemical

properties. The next step is to use these complexes in applications geared towards

small molecule activations and other chemical transformations that are of importance

to organic and inorganic chemists.

7.6 Experimental

7.6.1 General Remarks

All manipulations were carried out using standard inert-atmosphere techniques. All reagents and chemicals were obtained from Sigma-Aldrich. All reagents were used without further purification. MeCN-d_3 was dried over calcium hydride or phosphorus pentoxide, and dichloromethane-d_2 was dried over phosphorus pentoxide. All other solvents were dried on a series of Grubbs-type columns and were degassed prior to use.[34] All glassware was stored in a 170 °C oven for several hours and was degassed prior to use. $[K][PPh_2Cp(PPh_2)_2]$[35], $[Li][^tBuCp(PPh_2)_2]$[8,36], $(NMeBz)_2CH_2$,[37] and N,N-bis(1H-benzimidazol-2-ylmethyl)- N-amine (BZIM)[38] were all prepared according to the literature procedures.

NMR spectra were recorded at room temperature on Bruker Avance III 500 MHz, Bruker Avance Ultrashield 300 MHz, and Bruker Avance DPX 300 MHz spectrometers. Chemical shifts are reported in parts per million relative to internal standards for ^1H and ^{13}C (the given deuterated solvent) and external standards for ^{19}F ($CFCl_3$) and ^{31}P (85% H_3PO_4). Coupling constants |J| are given in hertz. Elemental analysis was performed at the University of Windsor Mass Spectrometry Service Laboratory using a Perkin-Elmer 2400 combustion CHN analyzer.

7.6.2 Synthesis
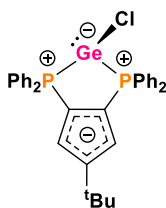
$^tBuCp(PPh_2)_2GeCl$ (2) A 100 mL Schlenk flask was charged with [Li][$^tBuCp(PPh_2)_2$] (400 mg, 0.73 mmol) and $GeCl_2$·dioxane (169 mg, 0.73 mmol). 30 mL Toluene was added to result in a yellow solution. The resulting mixture was allowed to stir for overnight before filtering through Celite to result in a clear pale-yellow solution. Solvents were removed under reduced pressure to yield **2** as a yellow solid (350 mg, 81%). Slow evaporation from dichloromethane yielded crystals suitable for X-ray Diffraction. $^{31}P\{^1H\}$ NMR δ: 5.91.
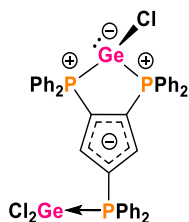
$(GeCl_2)PPh_2Cp(PPh_2)_2GeCl$ (3) A 20 mL vial was charged with [K][$PPh_2Cp(PPh_2)_2$] (31 mg, 0.047 mmol) and $GeCl_2$·dioxane (11 mg, 0.047 mmol). 5 mL of DCM was added, resulting in the formation of a yellow solution. The solution was stirred for 1 hr, filtered through a pipette stuffed with cotton/kimwipes and the filtrate was then slowly evaporated to result in **3** as yellow crystals suitable for X-ray Diffraction. $^{31}P\{^1H\}$ NMR δ: 6.62 (s, 1P), −14.21 (s, 2P).
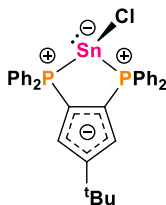
^{t}BuCp(PPh$_2$)$_2$SnCl (**4**) A 20 mL vial was charged with [Li][^{t}BuCp(PPh$_2$)$_2$] (40 mg, 0.073 mmol) and SnCl$_2$ (14 mg, 0.073 mmol). 5 mL of DCM was added, resulting in the formation of a yellow solution. The solution was stirred for 1 hr, filtered through a pipette stuffed with cotton/kimwipes and the filtrate was then slowly evaporated to result in **4** as yellow crystals suitable for X-ray Diffraction. ^{31}P{^{1}H} NMR δ: 4.13.

(NMeBz)$_2$CH$_2$SnCl (**5**) A 20 mL vial was charged with (NMeBz)$_2$CH$_2$ (40 mg, 0.14 mmol), SnCl$_2$ (34 mg, 0.15 mmol) and KHMDS (58 mg, 0.29 mmol). 5 mL of THF was added, resulting in the formation of an orange solution. The solution was stirred for overnight, 5 mL of DCM was added, and the resulting suspension was centrifuged with the resulting filtrate/supernatant slowly evaporated to yield **5** as deep orange/brown crystals suitable for X-ray Diffraction.
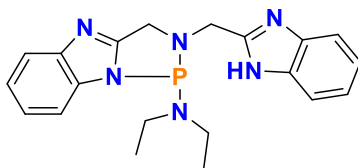
H-BZIMP(Et$_2$N) (**6**). A 20 mL vial was charged with BZIM (40 mg, 0.14 mmol) in 5 mL CH$_3$CN. (Et$_2$N)$_2$PCl (32 μL, 0.15 mmol) was added using a microsyringe resulting in a clear solution as the insoluble BZIM ligand goes in solution. The solution was allowed

to slowly evaporate to yield 6 as colourless crystals suitable for X-ray diffraction. $^{31}P\{^1H\}$ NMR (CDCl$_3$) δ: 93.21 (s). ^{31}P NMR (CDCl$_3$) δ: 93.13 (b).
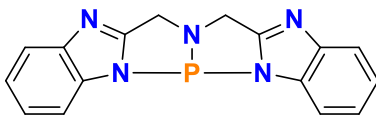
BZIMP (**7**) A 20 mL vial was charged with BZIM (40 mg, 0.14 mmol) and NaH (11 mg, 0.45 mmol). 5 mL of THF was added resulting in the evolution of H$_2$ gas. After allowing the reaction mixture to stir for 15 minutes, PCl$_3$ (16 μL, 0.17 mmol) was added via a microsyringe resulting in a yellow cloudy solution. The solution was centrifuged, and the supernatant was slowly evaporated to yield off-white microcrystalline materials. $^{31}P\{^1H\}$ NMR (CDCl$_3$) δ: 125.17. ^{31}P NMR (CDCl$_3$) δ: 125.70 (q, $^3J_{PH}$ = 25 Hz).

7.6.3 X-ray Crystallography

Crystals for investigation were covered in Paratone®, mounted onto a goniometer head, and then rapidly cooled under a stream of cold N$_2$ of the low-temperature apparatus (Oxford Cryostream) attached to the diffractometer. The data were then collected using the APEXII (Bruker AXS) software suite on a Bruker Photon 100 CMOS diffractometer using a graphite monochromator with MoK$_\alpha$ (λ = 0.71073 Å). For each sample, data were collected at low temperature. APEXII software was used for data reductions and SADABS (Bruker AXS) was used for absorption corrections (multi-scan; semi-empirical from equivalents). XPREP was used to determine the space group and the structures were solved and refined using the SHELX[39] software suite as implemented in the WinGX[40] or OLEX2[41] program suites. Validation of the structures was conducted using PLATON.[42]

Compound Name	$^tBuCp(PPh_2)_2GeCl$	$^tBuCp(PPh_2)_2SnCl$	$Ph_2Cp(PPh_2)_2GeCl$
Label	2	3	4
CCDC ID			
Empirical formula	$C_{66}H_{62}Cl_2Ge_2P_4$	$C_{33}H_{31}ClP_2Sn$	$C_{41}H_{32}Cl_3Ge_2P_3$
Formula weight	1195.11	643.66	869.1
Temperature (K)	170	169.99	170
Crystal system	monoclinic	monoclinic	monoclinic
Space group	$P2_1$	$P2_1/c$	$P2_1/c$
a (Å)	10.134	10.6956(5)	12.1187(5)
b (Å)	27.961	28.1328(15)	32.5341(14)
c (Å)	10.739	10.2273(5)	9.4859(4)
α (°)	90	90	90
β (°)	111.23	110.953(2)	93.837(2)
γ (°)	90	90	90
Volume (Å³)	2836.7	2873.9(3)	3731.6(3)
Z	2	4	4
ρ_{calc} (g·cm⁻³)	1.399	1.488	1.547
μ (mm⁻¹)	1.308	1.114	1.985
F(000)	1232	1304	1752
Crystal size (mm³)	0.25 × 0.23 × 0.18	0.29 × 0.27 × 0.26	0.26 × 0.25 × 0.15
Radiation	MoKα (λ = 0.71073)	MoKα (λ = 0.71073)	MoKα (λ = 0.71073)
2Θ range for data collection (°)	5.828 to 66.548	5.96 to 66.464	5.714 to 65.274
Index ranges	−15 ≤ h ≤ 15 −43 ≤ k ≤ 43 −16 ≤ l ≤ 16	−16 ≤ h ≤ 16 −43 ≤ k ≤ 43 −15 ≤ l ≤ 15	−18 ≤ h ≤ 18 −49 ≤ k ≤ 49 −11 ≤ l ≤ 14
Reflections collected	120387	137724	127338
Independent reflections	21830 R_{int} = 0.0465 R_{sigma} = 0.0426	11014 R_{int} = 0.0403 R_{sigma} = 0.0210	13605 R_{int} = 0.0425 R_{sigma} = 0.0300
Data/restraints /parameters	21830/1/673	11014/30/337	13605/0/442
Goodness-of-fit on F²	1.023	1.453	1.148
Final R indexes [I>=2σ(I)]	R_1 = 0.0444 wR_2 = 0.1079	R_1 = 0.1100 wR_2 = 0.2787	R_1 = 0.0504 wR_2 = 0.1063
Final R indexes [all data]	R_1 = 0.0530 wR_2 = 0.1117	R_1 = 0.1150 wR_2 = 0.2807	R_1 = 0.0678 wR_2 = 0.1116
Largest diff. peak/hole (e·Å⁻³)	4.19/−1.76	3.20/−3.33	1.09/−1.47
Refinement method	Full-matrix least-squares on F²		

$$R_1 = \frac{\sum||F_o|-|F_c||}{\sum|F_o|} \qquad wR_2 = \sqrt{\frac{\sum w(F_o{}^2-F_c{}^2)^2}{\sum w(F_o{}^2)^2}} \qquad R_{int} = \frac{\sum|F_o{}^2-F_o{}^2(mean)|}{\sum F_o{}^2} \qquad R_{sigma} = \frac{\sum \sigma(F_o{}^2)}{\sum F_o}$$

Table 7.3. *Crystallographic data and structure refinement.*

Compound Name	(NMeBz)$_2$CH$_2$SnCl	H-BZIMP(Et$_2$N)
Label	5	6
CCDC ID		
Empirical formula	C$_{68}$H$_{60}$Cl$_4$N$_{16}$Sn$_4$	C$_{21}$H$_{26}$Cl$_2$N$_6$P
Formula weight	1717.88	464.35
Temperature (K)	170	170
Crystal system	orthorhombic	orthorhombic
Space group	P2$_1$2$_1$2$_1$	Pca2$_1$
a (Å)	8.4405(3)	9.9991(4)
b (Å)	12.8765(6)	10.3741(4)
c (Å)	14.7120(7)	21.3526(7)
α (°)	90	90
β (°)	90	90
γ (°)	90	90
Volume (Å^3)	1598.96(12)	2214.94(14)
Z	1	4
ρ$_{calc}$ (g·cm^{-3})	1.784	1.392
μ (mm^{-1})	1.769	0.387
F(000)	848	972
Crystal size (mm^3)	0.33 × 0.175 × 0.125	0.255 × 0.168 × 0.04
Radiation	MoKα (λ = 0.71073)	MoKα (λ = 0.71073)
2Θ range for data collection (°)	5.772 to 66.31	5.972 to 54.314
Index ranges	−12 ≤ h ≤ 12 −19 ≤ k ≤ 19 −22 ≤ l ≤ 22	−12 ≤ h ≤ 12 −13 ≤ k ≤ 13 −27 ≤ l ≤ 27
Reflections collected	41380	20256
Independent reflections	6084 R$_{int}$ = 0.0262 R$_{sigma}$ = 0.0186	4887 R$_{int}$ = 0.0348 R$_{sigma}$ = 0.0322
Data/restraints /parameters	6084/0/210	4887/1/273
Goodness-of-fit on F^2	1.164	1.037
Final R indexes [I>=2σ(I)]	R$_1$ = 0.0194 wR$_2$ = 0.0436	R$_1$ = 0.0567 wR$_2$ = 0.1504
Final R indexes [all data]	R$_1$ = 0.0230 wR$_2$ = 0.0456	R$_1$ = 0.0680 wR$_2$ = 0.1588
Largest diff. peak/hole (e·Å^{-3})	0.56/−0.76	0.27/−0.80
Refinement method	Full-matrix least-squares on F^2	

$$R_1 = \frac{\Sigma||F_o|-|F_c||}{\Sigma|F_o|} \qquad wR_2 = \sqrt{\frac{\Sigma w(F_o{}^2 - F_c{}^2)^2}{\Sigma w(F_o{}^2)^2}} \qquad R_{int} = \frac{\Sigma|F_o{}^2 - F_o{}^2(mean)|}{\Sigma F_o{}^2} \qquad R_{sigma} = \frac{\Sigma \sigma(F_o{}^2)}{\Sigma F_o}$$

Table 7.4. *Crystallographic data and structure refinement.*

7.7 References

(1)   a) Swidan, A.; Binder, J. F.; St. Onge, B. J.; Suter, R.; Burford, N.; Macdonald, C. L. B. *Dalton Trans.* **2019**, *48* (4), 1284–1291. b) Swidan, A.; St. Onge, P. B.; Binder, J. F.; Suter, R.; Burford, N.; Macdonald, C. *Dalton Trans.* **2019**, *48*, 7835-7843.

(2)   Swidan, A.; Suter, R.; Macdonald, C. L. B.; Burford, N. *Chem. Sci.* **2018**, *9* (26), 5837–5841.

(3)   Suter, R.; Swidan, A.; Macdonald, C. L. B.; Burford, N. *Chem. Commun.* **2018**, *54* (33), 4140–4143.

(4)   Suter, R.; Swidan, A.; Zijlstra, H. S.; Macdonald, C. L. B.; McIndoe, J. S.; Burford, N. *Dalton Trans.* **2018**, *47* (46), 16729–16736.

(5)   Bertrand, G. *Chem. Rev.* **2010**, *110* (7), 3851.

(6)   Lu, C. C.; Peters, J. C. *J. Am. Chem. Soc.* **2002**, *124* (19), 5272–5273.

(7)   Weicker, S. A.; Dube, J. W.; Ragogna, P. J. *Organometallics* **2013**, *32* (22), 6681–6689.

(8)   Kosnik, S. C.; Nascimento, M. C.; Binder, J. F.; Macdonald, C. L. B. *Dalton Trans.* **2017**, *46* (48), 17080–17092.

(9)   Kosnik, S. C.; Macdonald, C. L. B. *Dalton Trans.* **2016**, *45* (14), 6251–6258.

(10)   Stoelzel, M.; Präsang, C.; Inoue, S.; Enthaler, S.; Driess, M. *Angew. Chem. - Int. Ed.* **2012**, *51* (2), 399–403.

(11)   Dove, A. P.; Gibson, V. C.; Marshall, E. L.; Rzepa, H. S.; White, A. J. P.; Williams, D. J. *J. Am. Chem. Soc.* **2006**, *128* (30), 9834–9843.

(12)   Hill, M. S.; Hitchcock, P. B. *Chem. Commun.* **2004**, No. 16, 1818–1819.

(13)   Peng, Y.; Fan, H.; Zhu, H.; Roesky, H. W.; Magull, J.; Hughes, C. E. *Angew. Chem. - Int. Ed.* **2004**, *43* (26), 3443–3445.

(14)   Zhao, N.; Zhang, J.; Yang, Y.; Chen, G.; Zhu, H.; Roesky, H. W. *Organometallics* **2013**, *32* (3), 762–769.

(15)   Li, X.; Cheng, X.; Song, H.; Cui, C. *Organometallics* **2007**, *26* (4), 1039–1043.

(16)   Nie, P.; Li, Y.; Yu, Q.; Li, B.; Zhu, H.; Wen, T.-B. *Eur. J. Inorg. Chem.* **2017**, (33), 3892–3899.

(17)   Jana, A.; Ghoshal, D.; Roesky, H. W.; Objartel, I.; Schwab, G.; Stalke, D. *J. Am. Chem. Soc.* **2009**, *131* (3), 1288–1293.

(18)   Hardman, N. J.; Power, P. P. *Chem. Commun.* **2001**, (13) 1184–1185.

(19)   Yang, Z.; Zhong, M.; Ma, X.; De, S.; Anusha, C.; Parameswaran, P.; Roesky, H. W. *Angew. Chem. - Int. Ed.* **2015**, *54* (35), 10225–10229.

(20)   Ganesamoorthy, C.; Krüger, J.; Wölper, C.; Nizovtsev, A. S.; Schulz, S. *Chem. Eur. J.* **2017**, *23* (10), 2461–2468.

(21)   Yang, Z.; Zhong, M.; Ma, X.; Nijesh, K.; De, S.; Parameswaran, P.; Roesky, H. W. *J. Am. Chem. Soc.* **2016**, *138* (8), 2548–2551.

(22)   Cui, C.; Köpke, S.; Herbst-Irmer, R.; Roesky, H. W.; Noltemeyer, M.; Schmidt, H.-G.; Wrackmeyer, B. *J. Am. Chem. Soc.* **2001**, *123* (37), 9091–9098.

(23)   Ekkert, O.; White, A. J. P.; Toms, H.; Crimmin, M. R. *Chem. Sci.* **2015**, *6* (10), 5617–5622.

(24)   Yang, Y.; Zhao, N.; Wu, Y.; Zhu, H.; Roesky, H. W. *Inorg. Chem.* **2012**, *51* (4), 2425–2431.

(25)   Dauer, D.-R.; Koehne, I.; Herbst-Irmer, R.; Stalke, D. *Eur. J. Inorg. Chem.* **2017**, (13), 1966–1978.

(26)   Dauer, D.-R.; Stalke, D. *Dalton Trans.* **2014**, *43* (38), 14432–14439.

(27)   Dauer, D.-R.; Flügge, M.; Herbst-Irmer, R.; Stalke, D. *Dalton Trans.* **2016**, *45* (14), 6149–6158.

(28)   Chitnis, S. S.; Krischer, F.; Stephan, D. W. *Chem. Eur. J.* **2018**, *24*, 6543–6546.

(29)   Evans, D. A.; MacMillan, D. W. C.; Campos, K. R. *J. Am. Chem. Soc.* **1997**, *119* (44), 10859–10860.

(30)   Arduengo, A. J.; Stewart, C. A. *Chem. Rev.* **1994**, *94* (5), 1215–1237.

(31)   McCarthy, S. M.; Lin, Y. C.; Devarajan, D.; Chang, J. W.; Yennawar, H. P.; Rioux, R. M.; Ess, D. H.; Radosevich, A. T. *J. Am. Chem. Soc.* **2014**, *136* (12), 4640–4650.

(32)   Dunn, N. L.; Ha, M.; Radosevich, A. T. *J. Am. Chem. Soc.* **2012**, *134* (28), 11330–11333.

(33)   Verkade, J. G. *Acc. Chem. Res.* **1993**, *26* (9), 483–489.

(34)   Pangborn, A. B.; Giardello, M. A.; Grubbs, R. H.; Rosen, R. K.; Timmers, F. J. *Organometallics* **1996**, *15* (5), 1518–1520.

(35)   Smaliy, R. V; Beaupérin, M.; Mielle, A.; Richard, P.; Cattey, H.; Kostyuk, A. N.; Hierso, J.-C. *Eur. J. Inorg. Chem.* **2012**, (9), 1347–1352.

(36)   Broussier, R.; Bentabet, E.; Mellet, P.; Blacque, O.; Boyer, P.; Kubicki, M. M.; Gautheron, B. *J. Organomet. Chem.* **2000**, *598* (2), 365–373.

(37)   Braussaud, N.; Thomas, R.; Cavell, K. J.; Skelton, B. W.; White, H. *Synthesis* **2001**, 626–632.

(38)   Cariou, R.; Chirinos, J. J.; Gibson, V. C.; Jacobsen, G.; Tomov, A. K.; Britovsek, G. J. P.; White, A. J. P. *Dalton Trans.* **2010**, *39* (38), 9039–9045.

(39)   Sheldrick, G. M. *Acta Crystallogr. Sect. A Found. Crystallogr.* **2008**, *64* (1), 112–122.

(40)   Farrugia, L. J. *J. Appl. Crystallogr.* **1999**, *32* (4), 837–838.

(41)   Dolomanov, O. V.; Bourhis, L. J.; Gildea, R. J.; Howard, J. A. K.; Puschmann, H. *J. Appl. Crystallogr.* **2009**, *42* (2), 339–341.

(42)   Spek, A. L. *J. Appl. Crystallogr.* **2003**, *36* (1), 7–13.

VITA AUCTORIS

NAME:	Alaaeddeen Swidan
PLACE OF BIRTH:	Amman, Jordan
YEAR OF BIRTH:	1989
EDUCATION:	J. L. Forster S. S., High School, Windsor, ON, 2007
	University of Windsor, B.Sc., Windsor, ON, 2011
	University of Windsor, M.Sc., Windsor, ON, 2013 -Dr. Charles L. B. Macdonald
	Cornell University, Grad. Studies, Ithaca, NY, 2015 -Dr. Peter T. Wolczanski
	University of Windsor, Ph.D. Windsor, ON, 2019 -Dr. Charles L. B. Macdonald

LIST OF PUBLICATIONS

1. "2,6-Bis(benzimidazol-2-yl)pyridine Complexes of Group 14 Elements" **Swidan, A**.; Binder, J. F.; St. Onge, P. B. J.; Suter, R.; Burford, N; Macdonald, C. L. B. *Dalton Trans.*, **2019**, Published.

2. "Halogen and sulfur oxidation of germanium and tin dications" Suter, R.; **Swidan, A.**; Macdonald, C. L. B.; Burford, N.; Ferguson, M. *Inorg. Chem.* **2019**, *58* (9), 6238-6245.

3. "2,6-Bis(benzimidazol-2-yl)pyridine as More Electron-Rich and Sterically Accessible Alternatives to 2,6-bis(imino)pyridine for Group 13 Coordination Chemistry" **Swidan, A**.; Binder, J. F.; St. Onge, P. B. J.; Suter, R.; Burford, N; Macdonald, C. L. B. *Dalton Trans.*, **2019**, 48, 1284-1291.

4. "Phosphonium-Templated Iodoplumbates" Omahen, E. H., Binder, J. F., Jacobs, B. F.; **Swidan, A.**; Macdonald, C. L. B., *ACS Omega,* **2018**, *3* (12), 17077-17082.

5. "Diphosphoniodiphosphene Formation by Transition Metal Insertion into a Triphosphenium Zwitterion" Kosnik, S. C.; Binder, J. F.; Nascimento, M. C.; **Swidan, A.**; Macdonald, C. L. B. *Chem. Eur. J.* **2019**, 25, 1208.

6. "Synthesis, characterization and mass-spectrometric analysis of [LSn(IV)F$_{4-x}$]$^{x+}$ salts [L = tris ((1-ethyl-benzoimidazol-2-yl)methyl)amine, x = 1-4]" Suter, R.; **Swidan, A.**; Zijlstra, H.S.; Macdonald, C.L.B; McIndoe, J. S.; Burford, N., *Dalton Trans.* **2018**, *47* (46), 16729–16736.

7. "Synthesis of Heteroleptic Phosphorus(I) Cations by P$^+$ Transfer" Binder, J. F.; **Swidan, A.**; Macdonald, C. L. B., *Inorg. Chem.* **2018**, 57(18), 11717–11725.

8. "Tris(benzoimidazol)amine (L) complexes of pnictogen(III) and pnictogen(V) cations and assessment of the [LP]$^{3+}$/[LPF$_2$]$^{3+}$ redox couple" **Swidan, A**.; Suter, R.; Macdonald, C. L. B.; Burford, N., *Chem. Sci.*, **2018**, 9, 5837-5841.

9. "Oxidation of a germanium(II) dication to access cationic germanium(IV) fluorides" Suter, R.; **Swidan, A**.; Macdonald, C. L. B.; Burford, N., *Chem. Commun.*, **2018**, 54, 4140.

10. "Synthesis and structural characterization of new polyether complexes of germanium(II) and tin(II)" Secara, A. M.; Binder, J. F.; **Swidan, A.,** Macdonald, C. L. B., *Can. J. Chem.*, **2018**, 96(6): 570-577.

11. "Convenient Preparation and Detailed Analysis of a Series of NHC-Stabilized Phosphorus(I) Dyes and Their Derivatives" Macdonald, C. L. B., Binder, J. F.; **Swidan, A.,** Nguyen, J. H., Kosnik, S. C., Ellis, B. D., *Inorg. Chem.*, **2016**, 55 (14), 7152–7166.

12. "Polyether complexes of groups 13 and 14" **Swidan, A.**; Macdonald, C. L. B., *Chem. Soc. Rev.*, **2016**, 45, 3883-3915.

13. "Fe(IV) alkylidenes via protonation of Fe(II) vinyl chelates and a comparative Mössbauer spectroscopic study" Lindley, B. M.; **Swidan, A.;** Lobkovsky, E. B.; Wolczanski, P. T.; Adelhardt, M.; Jörg Sutter, J.; Meyer, K., *Chem. Sci.* **2015**, 6, 4730-4736.

14. "Remarkably stable chelating bis-N-heterocyclic carbene adducts of phosphorus(I) cations" Binder, J. F.; **Swidan, A.;** Tang, M.; Nguyen, J. H.; Macdonald, C. L. B., *Chem. Commun.*, **2015**, 51, 7741.

15. "Water and Ammonia Complexes of Germanium(II) Dications" Bandyopadhyay, R.; Nguyen, J. H.; **Swidan, A.;** Macdonald, C. L. B., *Angew. Chem. - Int. Ed.*, **2013**, 52, 3469-3472.

16. "Low-Oxidation-State Main Group Compounds" Macdonald, C. L. B.; Ellis, B. D.; **Swidan, A.** In the Encyclopedia of Inorganic and Bioinorganic Chemistry; John Wiley & Sons, Ltd: **2012**.

CONFERENCE PRESENTATIONS

1. CSC2018 (101st Canadian Chemistry Conference and Exhibition), Oral Presentation, May 2018, Edmonton, AB, Swidan, A.; St. Ong, B. P., Macdonald, C. L. B. "Novel Pincer Complexes of Group 13-15 Main Group Elements"

2. CSC2017 (100th Canadian Chemistry Conference and Exhibition), poster presentation, May 2017, Toronto, ON. Swidan, A.; St. Ong, B. P., "Pincer Ligand Complexation to Various Main Group Metals"

3. CSC2016 (99th Canadian Chemistry Conference and Exhibition), poster presentation, June 2016; Halifax, NS. Swidan, A.; Schröder, J.; Macdonald, C. L. B.; "Towards The Synthesis of Anionic Carbodiphosphoranes"

4. IRIS-13 (13th International Symposium on Inorganic Ring Systems), poster presentation July 2012; Victoria, BC. Swidan, A.; Nguyen, J.; Ellis, B. D.; Macdonald, C. L. B.; "Synthesis and Characterization of N-heterocyclic carbene adducts of PI cations."

5. CERM2012 (43rd ACS Central Regional Meeting), poster presentation, June 2012; Dearborn, MI. Swidan, A.; Nguyen, J.; Ellis, B. D.; Macdonald, C. L. B.; "Synthesis and Characterization of N-heterocyclic carbene adducts of PI cations."